CONTRAST MATCHING AND DISCRIMINATION IN HUMAN VISION

KAISA MARIA TIIPPANA

Doctor of Philosophy

THE UNIVERSITY OF ASTON IN BIRMINGHAM

June 1995

University of Aston in Birmingham

CONTRAST MATCHING AND DISCRIMINATION IN HUMAN VISION

Kaisa Maria Tiippana
Doctor of Philosophy 1995

SUMMARY

The aim of this work was to investigate human contrast perception at various contrast levels ranging from detection threshold to suprathreshold levels by using psychophysical techniques. The work consists of two major parts. The first part deals with contrast matching, and the second part deals with contrast discrimination.

Contrast matching technique was used to determine when the perceived contrasts of different stimuli were equal. The effects of spatial frequency, stimulus area, image complexity and chromatic contrast on contrast detection thresholds and matches were studied. These factors influenced detection thresholds and perceived contrast at low contrast levels. However, at suprathreshold contrast levels perceived contrast became directly proportional to the physical contrast of the stimulus and almost independent of factors affecting detection thresholds.

Contrast discrimination was studied by measuring contrast increment thresholds which indicate the smallest detectable contrast difference. The effects of stimulus area, external spatial image noise and retinal illuminance were studied. The above factors affected contrast detection thresholds and increment thresholds measured at low contrast levels. At high contrast levels, contrast increment thresholds became very similar so that the effect of these factors decreased.

Human contrast perception was modelled by regarding the visual system as a simple image processing system. A visual signal is first low-pass filtered by the ocular optics. This is followed by spatial high-pass filtering by the neural visual pathways, and addition of internal neural noise. Detection is mediated by a local matched filter which is a weighted replica of the stimulus whose sampling efficiency decreases with increasing stimulus area and complexity.

According to the model, the signals to be compared in a contrast matching task are first transferred through the early image processing stages mentioned above. Then they are filtered by a restoring transfer function which compensates for the low-level filtering and limited spatial integration at high contrast levels. Perceived contrasts of the stimuli are equal when the restored responses to the stimuli are equal.

According to the model, the signals to be discriminated in a contrast discrimination task first go through the early image processing stages, after which signal dependent noise is added to the matched filter responses. The decision made by the human brain is based on the comparison between the responses of the matched filters to the stimuli, and the accuracy of the decision is limited by pre- and post-filter noises.

The model for human contrast perception could accurately describe the results of contrast matching and discrimination in various conditions.

KEY WORDS: Model of human contrast perception, Perceived contrast, Contrast increment threshold

ACKNOWLEDGEMENTS

I would like take the opportunity to thank the people who have assisted me during my research in many ways.

I am grateful to the Head of Department, Mr. Derek Barnes, and to the staff at the Department of Vision Sciences for enabling me to carry out my research.

Sincere thanks to my supervisor, Dr. Jyrki Rovamo, whose enthusiasm and inexhaustible flow of ideas have helped me immensely with my work. I am also very grateful to Dr. Risto Näsänen for sharing with me his vast knowledge of various issues ranging from technical to theoretical.

I want to thank to my colleagues Mr. Timo Koljonen, Dr. Heljä Kukkonen, Mr. Rasko Leinonen, Mr. Olavi Luntinen, Ms. Juvi Mustonen, Dr. Pia Mäkelä, Ms. Heli Räikkönen, and Ms. Seija Uusinarkaus who served as observers. Special thanks to Dr. Outi Ukkonen for her support during the writing up of the thesis.

This work was financially supported by the Association of Finnish Ophthalmic Opticians, Society of Ophthalmic Opticians in Finland, and the Finnish National Agency for Health and Welfare.

Finally, warm thanks to my family in Finland for their support during my years of study, and to Dr. Cordner Peacocke for his invaluable assistance.

Kaisa Tiippana

June 1995

CONTENTS

LIST OF FIGURES

LIST OF TABLES

1. INTRODUCTION

Human contrast vision is the subject of study in this thesis. The main interest is suprathreshold contrast perception which was studied using two psychophysical techniques, contrast matching and contrast discrimination. Contrast perception was investigated for stationary cosine gratings in foveal vision.

Contrast detection threshold refers to the lowest contrast that can be detected. Detection thresholds are used to study factors limiting vision. For example, the modulation transfer functions of the visual system can be inferred from detection thresholds measured as a function of spatial frequency (Rovamo, Mustonen & Näsänen, 1994b). Detection thresholds seem to influence perceived contrast in many situations, as described below. This is because they reflect the influence of the visual mechanisms underlying contrast perception. Therefore, in order to be able to describe human contrast perception, it is important to combine findings obtained at both threshold and suprathreshold contrast levels.

Detection thresholds for cosine gratings have been widely studied. It is well known how they depend on various factors such as spatial frequency, stimulus area, retinal illuminance, and external spatial noise. Detection thresholds are lowest at spatial frequencies around 4 c/deg, and they increase towards lower and higher frequencies (Campbell & Robson, 1968). They decrease as grating area is increased up to a certain size (Hoekstra, van der Goot, van den Brink & Bilsen, 1974). Detection thresholds are lowest at high luminance levels, and they increase as luminance is decreased (van Nes & Bouman, 1967). Detection thresholds increase as the spectral density of external noise is increased above a certain level (Nagaraja, 1964).

Human contrast perception at detection threshold has been described by a model developed by Rovamo, Näsänen and coworkers (e.g. Rovamo, Luntinen & Näsänen, 1993; Rovamo, Mustonen & Näsänen, 1994a; Rovamo, Ukkonen, Thompson & Näsänen, 1994). They have modelled the human visual system as a simple image processor comprising four successive stages. First, the visual signal is low-pass filtered by the optics of the eye which causes the high spatial frequency rise in detection thresholds. Then follows high-pass filtering by the neural visual pathways which explains the low spatial frequency increase in thresholds. Next, internal neural noise is added to the signal. The spectral density of internal noise determines when light-dependent or external spatial noise start to affect detection thresholds. Finally, the signal is detected by a filter whose efficiency decreases with increasing stimulus extent and complexity.

Even though detection thresholds can yield a wealth of useful information, normally stimuli in the visual environment are clearly visible, that is, they are suprathreshold in contrast. The importance of suprathreshold contrast perception in everyday life is thus obvious. Nevertheless, suprathreshold contrast perception has not been as widely studied as detection thresholds. This may be because the phenomena associated with suprathreshold vision have proved to be even more complex than the threshold phenomena. This thesis aims to investigate human contrast perception at a wide range of contrast levels extending from just detectable to the highest obtainable.

The first part of this thesis deals with contrast matching. Contrast matching technique yields information on the relative apparent contrast of different stimuli. In contrast matching, an observer is shown two stimuli which differ in contrast and in most cases also in other aspects such as size, and his task is normally to adjust one of them in contrast until the stimuli appear to have equal contrast. When the two stimuli are identical in size and other such aspects, contrast matches are always physically correct. This means that when the perceived contrasts of the stimuli are equal, their physical contrasts are also equal. However, when the two stimuli are different, matches are not always physically correct. Instead, at low contrast levels matching contrasts depend on detection thresholds so that if the detection threshold of the adjustable stimulus is high, the matching contrast is also high. But as contrast level is increased, matches gradually become physically correct. This is the result found in many studies where contrast matching is done for example with cosine gratings of various spatial frequencies (Watanabe, Mori, Nagata & Hiwatashi, 1968) or areas (Takahashi & Ejima, 1984), or with gratings whose mean luminances are different (see Peli, 1995, for a review).

In the experiments presented in this thesis the effects of spatial frequency, grating area, image complexity and chromaticity on perceived contrast were studied using contrast matching technique. Contrast matching technique has not been previously used with isoluminant chromatic gratings. The results obtained with chromatic gratings of various spatial frequencies were compared with those obtained with the normal achromatic luminance modulated gratings. In addition, perceived contrast of various other achromatic grating stimuli was investigated. A model combining the Rovamo and coworkers' contrast detection model with the idea of signal restoration in the form of a restoring transfer function is introduced in Chapter 4 to account for the results of contrast matching.

The second part of this thesis deals with contrast discrimination. Contrast discrimination yields information on the smallest detectable contrast differences. In a contrast discrimination task, an observer is shown two stimuli which are otherwise identical but they differ in contrast, and he his normally asked to indicate which stimulus has a higher

contrast. The contrast difference is reduced until a threshold is found. The smallest detectable contrast difference is called the contrast increment threshold. When increment thresholds are measured at various contrast levels, the resulting curve is called the contrast discrimination function.

Contrast discrimination functions are dipper-shaped (Nachmias & Sansbury, 1974). This means that as contrast level is increased slightly above zero, extremely small contrast differences are detected so that increment thresholds are first lower than the detection threshold. But at high contrast levels contrasts differences have to be increased so that increment thresholds start to increase with increasing contrast level. When measured for different stimuli, contrast discrimination functions are displaced by an amount proportional to the difference in detection thresholds. That is, increment thresholds are higher for stimuli with high detection thresholds. However, at high contrast levels the differences in increment thresholds decrease so that increment thresholds become very similar for different stimuli (Bradley & Ohzawa, 1986).

There have been several attempts to account for the shape of the contrast discrimination function. The decrease in increment thresholds below detection threshold at low contrasts has been explained for example by an accelerating contrast transducer function (Legge & Foley, 1980), and by a reduction in uncertainty at suprathreshold contrasts (Pelli, 1985). The subsequent increase in increment thresholds can be explained for example by a decelerating contrast transducer function (Legge & Foley, 1980), or by signal dependent noise (e.g. Legge, Kersten & Burgess, 1987).

Previously the effect of spatial frequency on increment thresholds has been thoroughly studied (Legge, 1979). However, the dependence of increment thresholds on grating area, retinal illuminance and external spatial noise has not been systematically investigated, and therefore extended research was carried out here. A new model based on Rovamo and coworkers' contrast detection model, combined with the calculation of a difference-signal for the two stimuli to be discriminated, and the addition of signal dependent noise, is introduced in Chapter 5 to account for the results of contrast discrimination.

2. VISUAL PSYCHOPHYSICS

2.1 Psychophysics in vision research

The responses of a visual system to stimulation can be studied with many techniques, for example neurophysiological single-cell recordings, electrophysiological measurements such as electroencephalography (EEG), various brain scanning techniques such as computed tomography, and psychophysics.

Neurophysiological measurements are used to record responses from individual cells or cell groups for example on the retina or in the visual cortex. Electrophysiological measurements and brain scanning techniques are used to examine which regions of the brain are activated by various stimuli. These techniques give information about the neural activity in various parts of the visual system during stimulation.

Psychophysics is defined as the scientific study of the relation between stimulus and sensation. With psychophysical methods it is possible both to investigate the visual system's responses to various stimuli and to study visual perception.

Psychophysics can be used to record how the strength of sensation changes with changes in the physical stimulus. Let us take a simple experiment as an example. An observer is shown a spot of light whose intensity is varied, and he gives an estimate of the brightness of the light at each intensity level. When the observer's estimates of the brightness are plotted as a function of light intensity, as shown in Figure 2.1, it can be seen that the estimates of brightness do not increase linearly. Instead, when light intensity is increased, perceived brightness increases initially rapidly but then gradually more and more slowly (Stevens, 1961).

Hypotheses about the nature of anatomical and physiological mechanisms underlying sensory experience can be tested with psychophysics. It is assumed that responses to stimuli are directly related to neural activity. The fundamental assumption is that identical neural events give rise to identical perceptual events.

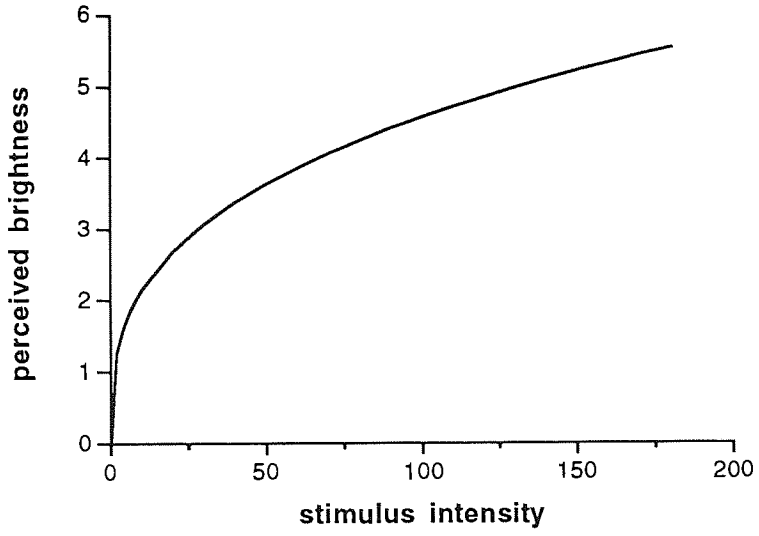

Figure 2.1 Dependence of perceived brightness on stimulus intensity.

2.2 *Sensory thresholds*

The concept of sensory thresholds is essential to psychophysics. Threshold is defined as the smallest stimulus intensity, or other parameter, that can be detected. In the following, contrast is taken as an example even though visual thresholds can be measured for various different parameters.

In biological systems there is no exact limit below which a signal is never detected and above which it is always detected. Instead, if a stimulus is presented several times at various contrast levels, and the observer reports whether he saw the stimulus or not ("yes" or "no"), the resulting function is as shown in Figure 2.2(A) where the proportion of "yes"-responses is plotted as a function of stimulus contrast. The function shows how often the stimulus was seen at various contrasts, and it is called a psychometric function. When a psychometric function is measured, the threshold is often taken as the stimulus contrast which is detected 50 percent of the time, but other values may be used as well.

Psychometric functions are generally not linear. As stimulus strength is increased, the proportion of "yes"-responses increases first slowly, then faster and finally slowly again. This behaviour produces the S-shaped function which is called an ogive. The ogive curve is a cumulative plot of a normal distribution, shown in Figure 2.2(B). Variation in biological systems and psychological measurements tends to be normally distributed.

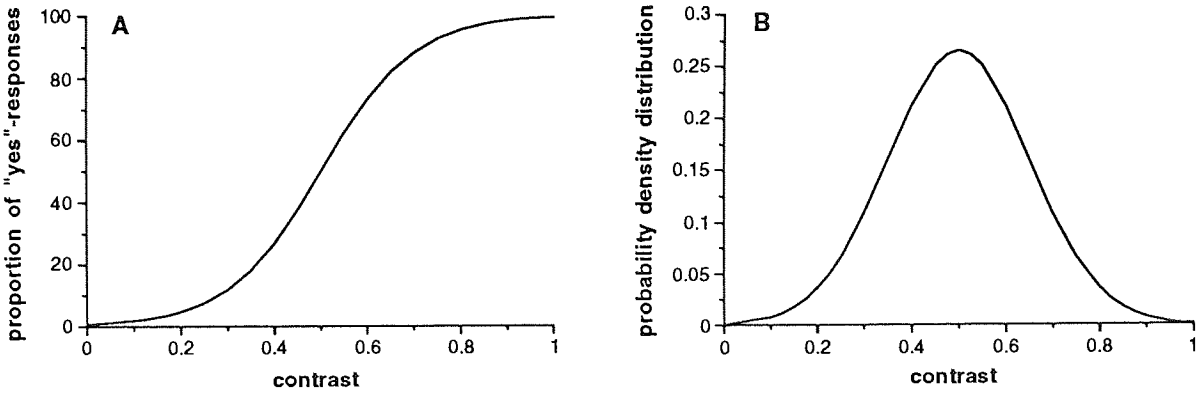

Figure 2.2 An example of a psychometric function in (A) and a normal distribution in (B).

Sensory thresholds can be determined by constructing psychometric functions with a yes-no procedure as described above. This technique is called the method of constant stimuli. The other techniques for measuring thresholds are called the method of adjustment and the method of limits.

In the method of adjustment the observer adjusts the contrast of the stimulus, and his task is to set the stimulus at threshold. If the stimulus is so weak initially that it cannot be seen, the observer increases its contrast until it is just detected. And if the stimulus is initially visible, the observer decreases its contrast until it just disappears. Normally the observer makes a large number of ascending and descending settings, and the threshold is taken as the mean of these settings. The problem with this technique is that the percent correct to which the threshold obtained corresponds on the psychometric function is not known. This is because the observer is allowed to choose his own criterion for "seen" and "not seen".

The method of limits is perhaps the most frequently used technique for determining sensory thresholds. It is similar to the method of adjustment in that a large number of ascending and descending series are made. However, stimulus contrast is changed in small, discrete steps, and the observer reports whether he saw the stimulus or not: "yes" or "no". In an ascending series, the stimulus is initially subthreshold, and its contrast is increased until it is seen, at which point the contrast is recorded. In a descending series, stimulus contrast is decreased starting from a suprathreshold level until the observer says "no" at which point the contrast is recorded. The mean of the transition points from "no" to "yes", and from "yes" to "no", is taken as the threshold.

There are also variations of the method of limits. In the staircase method, after a "yes"-response in an ascending series, the stimulus contrast is recorded, and the direction of the stimulus sequence is reversed into a descending series, and vice versa. This method saves time since stimuli that are much above or below threshold are never presented.

In the forced choice method, the observer is shown two or more alternatives, only one of which contains the stimulus. His task is to report which alternative contained the stimulus. "Not seen" responses are not accepted. Threshold is defined as the contrast corresponding to a specified performance level, for example 75% correct responses.

Threshold responses can be considered identical because the same criterion of performance is always used in a single experiment. For example, if threshold is defined as the amount of contrast at which stimulus is detected 50 percent of the time, and thresholds are measured for many different stimuli, it can be stated that at threshold all stimuli evoke equal signal-to-noise ratios. If the thresholds for the stimuli differ, that is, higher contrast is needed for detection in one stimulus than in another, it can be deduced that the visual system is more sensitive to the latter stimulus than to the former.

2.3 *Psychophysical methods for investigating suprathreshold visual perception*

The threshold described above is called the absolute or detection threshold. There is also another type of threshold, called the discrimination threshold, which is defined as the smallest detectable intensity, contrast or other difference between two stimuli. Discrimination thresholds can be measured for example at various contrast levels ranging from subthreshold to suprathreshold with the same techniques as detection thresholds.

Thresholds are by no means the only psychophysical technique for measuring sensory responses. Other widely used techniques are stimulus matching and magnitude estimation. In the following text, contrast is again taken as an example.

Equal sensation contours can be constructed by using the stimulus matching technique. In a matching experiment, the observer is shown two stimuli. One of them, the standard stimulus, has a constant contrast which is set by the experimenter. The other, the test stimulus, may differ from the standard in contrast and in other respects such as size. The observer's task is to adjust the contrast of the test stimulus to apparently match the contrast of the standard. An equal sensation contour is achieved when the matching contrasts of the test are plotted for example as a function of the area of the test stimulus. The contour

shows the physical contrasts needed to produce a constant perceived contrast for stimuli of various areas. The experiment can be repeated at various standard stimulus contrasts, and contours can be constructed for each contrast level. Equal sensation contours can also be called matching curves.

The method of constant stimuli can also be used as an alternative to the method of adjustment in stimulus matching experiments. The stimulus contrast at which the test is judged to be of higher contrast in 50% of the trials is taken as the match.

Stimulus matching gives information on the relative subjective appearance of different stimuli. It is a relative measure since judgements are made with respect to another stimulus. Matching technique is useful in determining how stimuli change in appearance in relation to each other as their contrast is changed, but not in determining the sensation magnitude of a stimulus at various contrast levels.

Magnitude estimation, however, gives information on how the observers' judgements of the intensity of their sensations change as stimulus intensity or contrast changes. The task of the observer is to give numerical estimations of the sensation magnitudes produced by stimuli presented at various contrast levels. The observer may be shown a standard stimulus which is given a certain numerical value by the experimenter, and he then rates the other stimuli relative to the value of the standard. Alternatively, he may be allowed to use any values that subjectively correspond to the sensations produced by the stimuli. All stimuli are presented several times in a random order. The mean of the individual ratings is taken as the sensation magnitude estimate. Magnitude estimates plotted as a function of stimulus intensity or contrast show how sensation magnitude increases with the physical strength of the stimulus (see Figure 2.1). Magnitude estimates plotted as a function of, for example, stimulus area, are comparable to the results obtained by stimulus matching.

The magnitude estimation technique has been criticised of subjectivity, and sensitivity to experimental methodology. Stimulus familiarity may influence the observer's responses so that he gives responses not according to the sensations but his knowledge about the stimulus. Also, observer's responses may change on different occasions, and with practice (Gottesman, Rubin & Legge, 1981). The range of stimulus contrasts shown during the experiment affects magnitude estimation results (Cannon, 1984). For these reasons, magnitude estimation has not been used in the experiments of this thesis.

2.4 Psychophysics in research on contrast vision: basic concepts

Contrast can be defined as the extent to which different regions in an image or another stimulus differ in luminance. Contrast perception is studied in order to find out how the human visual system processes information about spatial luminance changes in a stimulus. A major part of the information about the visual environment is conveyed by luminance differences. The techniques described above are widely used in studies on human contrast perception.

The basic stimuli used in contrast vision research are sinusoidal i.e. sine-wave gratings. In a sine-wave grating the luminance modulates sinusoidally about a mean luminance from a maximum to a minimum. A sine-wave grating looks like a set of black and white stripes with blurred edges. A black and a white stripe together form a cycle. Spatial frequency of a grating is defined as the number of cycles within a degree of visual angle. Spatial frequency is thus expressed in cycles per degree (c/deg). Whether a sinusoidal grating is called a sine or cosine grating depends on its phase. In this thesis the stimuli were cosine gratings since their phase in the centre of the stimulus was 0 deg. For a sine grating the phase is 90 deg.

There are two main reasons for using sinusoidal gratings as stimuli. First, according to the Fourier theory any image can be decomposed into a set of sine-wave gratings with certain spatial frequencies, orientations and phases. Or conversely, any image can be constructed by adding together appropriate sine-wave gratings. The sine-wave grating components of an image are called the spectrum of the image. Secondly, when the modulation transfer function of a linear system for sinusoidal gratings of various spatial frequencies is known, it is possible to calculate the amplitudes of the sine-wave components of any image with a known spectrum after it has been filtered through the system. An example of a linear system is the eye's optics.

Contrast of a sinusoidal grating is normally expressed as Michelson contrast which is defined as $L_{max} - L_{min} / L_{max} + L_{min}$, where L_{max} is the maximum and L_{min} the minimum luminance. However, other contrast measures exist also, and one of the topics in this thesis was to investigate the applicability of different contrast measures when describing the responses of the visual system.

3. GENERAL METHODS

3.1 Apparatus

The experiments were performed with the apparatus described below. The only exception was chromatic contrast matching, the apparatus and methods for which are described in Section 4.4.2 of this thesis.

The stimuli were generated under computer control on a 16" high-resolution RGB monitor (Eizo Flexscan 9080i with a fast phosphor B22) driven at 60 Hz by a graphics board (Orchid's ProDesigner VGA Plus). Two computers were used to drive the graphics board: ALR Business Veisa PC-486 was used in most experiments, and Dell PC-586 in experiments described in Sections 4.3 (subject RL) and 5.4.

The monitor could show 1280 x 800 pixels but the graphics board was used in a mode that generated 640 x 480 pixels. The pixel size was 0.415 mm x 0.415 mm on the screen. The display was used in a white mode. The CIE 1931 (x, y) chromaticity coordinates of the display were measured with a Minolta Chroma Meter LS-110, and they were found to be (0.31, 0.34). The average photopic luminance of the display was measured with a Minolta Luminance Meter LS-110. It was set to 50 cd/m^2.

The VGA graphics board has a 6-bit digital-to-analogue converter (DAC) for each colour channel and a 8-bit look-up-table (LUT). It can thus simultaneously show 256 colours (8 bits) chosen from a palette of 262,144 colours (6+6+6=18 bits) but only 64 (6 bits) monochrome (blue, green or red) intensity levels. Six bits is not sufficient for measuring human contrast perception since the lowest contrast 64 grey levels in a linear system can produce is (32-31)/(32+31)=0.016. The lowest contrast threshold for a human observer is more than ten times lower than this. Consequently, the apparatus had to be modified to produce more grey levels. A monochrome signal of 1024 intensity levels (10 bits) was obtained by using a video summation device and by then adding a periodic dither to the signal.

The blue, green and red outputs of the VGA board were first combined by using a video summation device built according to Pelli and Zhang (1991). In order to obtain small steps in luminance, the green and blue outputs were attenuated by a factor of 1/13 and 1/166, respectively. The red output thus mediated the largest luminance changes. For the red and green colour channels only the four most significant bits were used in order to

minimise the inaccuracies in voltages corresponding to less significant bits. This procedure gave a palette of 14 (4+4+6) bits from which an 8-bit signal could be chosen.

Two additional bits were obtained by adding a periodic dither signal of very small contrast before intensity quantization. The size of the period was 2x2 pixels, and the amplitude of the dither signal was one quantization interval. The dither signal was d(0,0)=0, d(0,1)=0.75, d(1,0)=0.5 and d(1,1)=0.25. The dither signal produced a four-fold increase in the number of grey levels. The dithering algorithm is:

$$g_q(x,y) = \text{int}\,[g(x,y)+d(x,y)] \tag{3.1}$$

where int[·] denotes rounding to the nearest integer, $g_q(x,y)$ is the quantized signal with dither, g(x,y) is the continuous luminance signal and d(x,y) is the dither signal. The lowest spatial frequency component of the dither was 12 c/cm which is 1.6 octaves higher than the highest spatial frequency used, 4 c/cm. This guaranteed that dithering produced no masking effects. Dither contrast was determined by the smallest step in the luminance signal so that it decreased with stimulus contrast thus remaining always much lower than the stimulus contrast.

The luminance response of the display in white mode was measured as a function of the 6-bit red index value (0-63) with the Minolta Luminance Meter LS-110. The relationship with the luminance (L) in cd/m^2 and the index value (I) is described by the following expression:

$$L(I)=0.01176\ I^{2.271} \tag{3.2}$$

where L is the luminance in cd/m^2 and I is the index value. The luminance response of the display was linearised by using the inverse function of the non-linear luminance response when computing the stimulus images.

The function $L(I)=0.01176\ I^{2.271}$ describes the luminance response of the screen when sampled with 64 index values ranging from the minimum to the maximum luminance. However, the 14-bit system consists of a total of 16,384 (2^{14}) luminance steps within the same luminance range, i.e. each of the 64 steps comprised 256 additional luminance steps. When the luminance response function is converted to correspond to the total number of luminance steps, it gets the form $L(I_e)=0.01176\ (I_e/256)^{2.271}$, where I_e is the extended index value. In order to estimate the number of grey levels in a stimulus, the index values corresponding to the minimum and maximum luminances in the stimulus have to be calculated by means of the inverse of the converted luminance response function.

The lowest Michelson contrast measured in the experiments of this thesis was 0.0015, and the mean luminance of the screen was 50 cd/m^2. The minimum luminance of a grating with 0.0015 contrast was 49.925, and the maximum luminance was 50.075. According to the extended luminance response function the index values were 10125 and 10139 for minimum and maximum luminance, respectively. The video summation device (Pelli & Zhang, 1991) produced thus 14 grey levels. The dither produced a four-fold increase in grey levels so that the total number of grey levels was 56.

In contrast discrimination experiments the lowest pedestal contrast used was 0.0015625. The minimum luminance was thus 49.922, and the maximum luminance was 50.078. According to the extended luminance response function the index values were 10125 and 10139 for minimum and maximum luminance, respectively. The video summation device and the dither produced thus 14x4=56 grey levels. The smallest increment that could have been used with the pedestal was as small as 0.0001 (corresponding to contrast sensitivity of 10 000) which corresponds to a step of one index value from 10124 to 10139. The smallest increment measured, 0.006, was considerably higher than this. Thus, in all stimuli used there were enough contrast levels to produce a sine wave grating, and in contrast discrimination experiments there was always a contrast difference between the test and standard stimulus.

The effect of spatial frequency on contrast was measured using the Minolta Luminance Meter LS-110 with a close-up lens No. 110 having a spot diameter of 0.4 mm on the screen. Michelson contrasts of the simple cosine gratings at and above 0.1% were checked with the luminance meter. Contrast was found to be independent of orientation and spatial frequency up to 2 c/cm. The highest spatial frequency used in the experiments was 2 c/cm with one exception. In the experiments of Section 4.3. gratings at 16 c/deg were obtained by using spatial frequency of 4 c/cm for which contrast was attenuated by a factor of 0.7. Consequently contrasts measured at 4 c/cm were corrected by multiplying them by 0.7.

3.2 Stimulus generation

The stimuli were generated by means of software developed by Dr. Risto Näsänen. The software was written in BASIC and translated by a Microsoft professional BASIC 7.0 compiler. The software utilised the graphics subroutine library of Professional HALO 2.0 developed by Media Cybernetics. The stimuli were drawn on the screen with coordinates (x,y) varying between (0, 0) and (639, 479). The horizontal and vertical dimensions of the equiluminous surround were 26.9 and 20.2 cm. In contrast increment threshold

measurements the computer screen was limited to 20 cm in diameter by a black cardboard mask.

Generated stimuli were stored on the hard disk of the computer. Before starting an experiment the stimulus files needed were copied to the part of 17 MB main memory that was used as a fast RAM-disk. The stimuli were transferred to the VGA frame buffer upon request. The stimulus was rapidly switched on and off by changing the colour look-up table during the vertical retrace period.

3.3 Procedure

The experiments were performed in a dark room, the only light source being the computer display. The observer's head was stabilised using a chin rest. Viewing was binocular with natural pupils unless stated otherwise. The stimuli were always fixated directly but otherwise the movement of gaze was unrestricted.

3.3.1 Contrast detection and increment thresholds

Contrast detection and increment thresholds were determined by a two-alternative temporal forced-choice staircase algorithm.

Each trial consisted of two 500 msec exposures separated by about 600 msec. Both exposures contained a grating stimulus and were accompanied by sound signals. One exposure contained the increment and pedestal, and the other contained the pedestal only. In the case of detection threshold measurement, only one exposure contained a non-zero contrast, and in the other exposure the contrast was zero. Between the two exposures and during inter-trial intervals the observer saw only the equiluminous field. The first contrast increment shown for each pair of stimuli was clearly above threshold to reduce uncertainty of the stimulus. The observer indicated which exposure contained the grating of higher contrast by pressing one of two keys on a computer keyboard. A correct choice was followed by a sound signal, and a wrong choice by another sound signal to provide feedback about the correctness of the response. A new trial began 250 msec after the observer's response. Contrast was changed in 0.1 $\log_{10}$ unit steps.

Estimation of threshold contrast took place in two consecutive staircases. An example of a possible string of responses in a complete run of threshold estimation is shown in Figure 3.1.

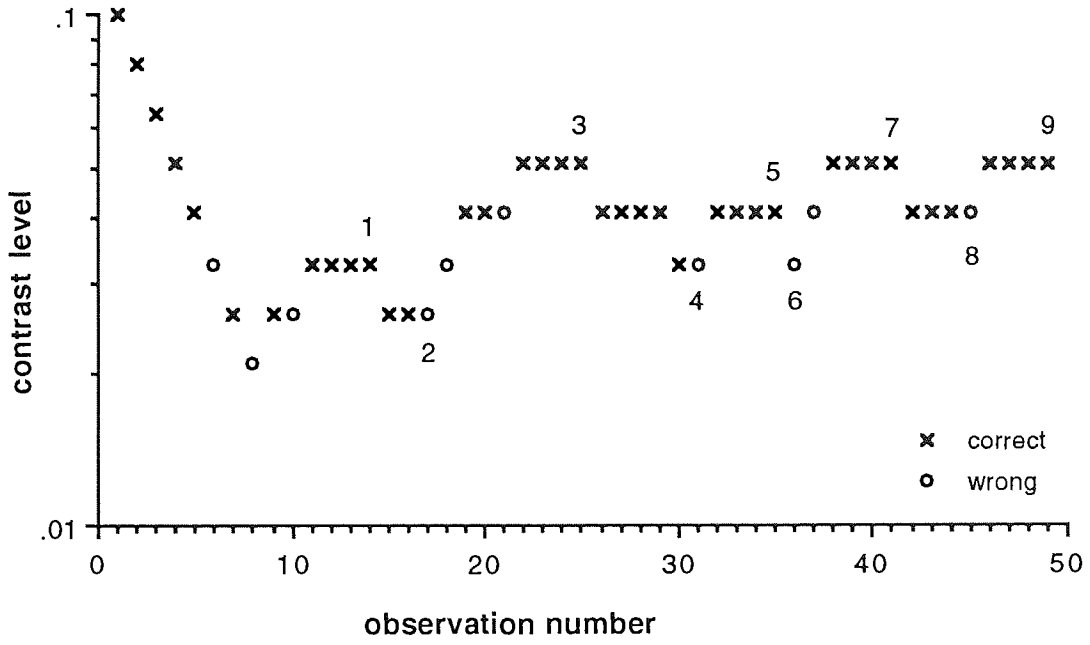

Figure 3.1 A possible string of responses in a complete run of threshold estimation.

The first staircase with one-correct-then-down/two-wrong-then-up rule established a random subthreshold starting point for the final threshold estimation, independent of the initial contrast selected. Contrast was decreased after each correct response. The first wrong choice had no effect, and contrast continued to decrease until the second wrong choice occurred. This caused the contrast to increase by a step and initiated the second staircase.

The second staircase with four-correct-then-down/one-wrong-then-up rule started from the contrast last shown. It was below threshold by an amount dependent on the hit rate of the observer's guesses. Now every wrong choice increased contrast, and four consecutive correct choices led to a contrast decrement. A smaller number of correct choices had no effect. This staircase continued until nine reversals of the direction of contrast change had occurred. Hence, estimation always terminated after a string of correct responses.

The threshold contrast required for the probability of 0.84 correct was estimated from the last 8 reversal contrasts according to the up-and-down transformed response or UDTR rule (Wetherill & Levitt, 1965). The UDTR rule is a modification of an up-and-down rule where one correct response is required for a contrast decrease, and one incorrect response is required for a contrast increase. This one-correct-then-down/one-wrong-then-up rule

results in an estimate of 50% probability of correct responses. The simple up-and-down rule cannot be used in a two-alternative forced-choice method, however, because 50% correct corresponds to pure guessing.

When using the UDTR rule, the number of correct responses required for a reversal of contrast can be varied, and thus it is also possible to vary the probability of correct responses. If the probability of a correct response at any level is x, then the probability of n consecutive correct responses is $x^n=0.5$. Conversely, if n consecutive correct responses are required, the probability of a correct response is $x=0.5^{1/n}$. The four-correct-then-down/one-wrong-then-up rule used in the experiments of this thesis thus resulted in the probability of $0.5^{1/4} = 0.84$ correct responses. (For the only exception see Section 4.4.2.3.2).

A threshold estimate was rejected if the standard deviation of the reversal contrasts was more than half of their mean. At least three acceptable threshold estimates were obtained for each stimulus condition. Geometric mean of the estimates was taken as the threshold.

3.3.2 Contrast matching

The method of adjustment was used in contrast matching experiments. The following nomenclature will be used throughout this thesis: "test" refers to the stimulus with changing contrast and "standard" to the stimulus with constant contrast. The test and standard gratings were presented either simultaneously with unlimited viewing time or sequentially in 500 msec exposures with standard always shown first. The test grating was adjusted to apparently match the standard grating in contrast. Test grating contrast was changed in 0.025 $\log_{10}$ unit steps, and standard grating contrast remained constant during each measurement. The initial contrast of the test grating was always higher than that of the standard. A sound signal accompanied stimulus exposures. The subject did not receive any feedback about the correctness of matches during the experiment.

Test grating contrast was reduced by pressing one of two keys on the computer keyboard until test and standard grating seemed to have equal contrast. Then the subject pressed the other key which recorded the contrast match, and caused the contrast of the test grating to decrease abruptly by 7-13 steps chosen randomly so that it seemed to have lower contrast than the standard. The subject now continued to press the other key until the gratings seemed to have equal contrast again. Then the subject changed the key pressed, matching contrast was recorded, and the test was increased in contrast by 7-13 steps so that it seemed to have a higher contrast than the standard. This procedure continued until 8

matches were recorded. The geometric mean of the 8 matches gave an estimate of the matching contrast. Two estimates were obtained for each stimulus condition, and their geometric mean was taken as the matching contrast.

The contrast range of the test grating bracketed the matching contrast. A suitable range for each matching condition was chosen on the basis of pilot experiments. All test gratings were matched to each contrast level of the standard grating.

3.4. Contrast measures

Three contrast measures were used to describe the results presented in this thesis: Michelson contrast, contrast energy and root-mean-square contrast.

Michelson contrast is defined as:

$$c_M = \frac{L_{max} - L_{min}}{L_{max} + L_{min}} \tag{3.3}$$

where L_{max} is the maximum and L_{min} the minimum luminance. Michelson contrast is a very simple contrast measure since it takes only the most extreme luminances in the stimulus into account.

Contrast energy is calculated as:

$$E=\sum\sum c^2(x,y)p^2 \tag{3.4}$$

where c(x,y) is the local contrast and p^2 is the area of a pixel in solid degrees. Local contrast is calculated as $c(x,y)=[L(x,y)-L_0]/L_0$, where L(x,y) is the luminance of a pixel at location (x,y) and L_0 is the luminance averaged across pixels. Contrast energy is calculated by adding the squared local contrasts together and multiplying the result by pixel area. Contrast energy thus takes both the luminance variation and stimulus area into account.

Root-mean-square (r.m.s.) contrast is calculated as:

$$c = \sqrt{\frac{E}{A}} \tag{3.5}$$

where E is the contrast energy and A is the stimulus area in deg^2. R.m.s. contrast is the standard deviation of luminances in the stimulus normalised by the average luminance. For a simple cosine grating r.m.s. contrast is approximately equal to Michelson contrast divided by $\sqrt{2}$ (see Appendix I for further details).

3.5 Statistical analysis of the experimental data

3.5.1 Explained variance

When a model or a descriptive function was applied to the experimental results, the accuracy of predictions was described by explained variance, R^2, which was calculated as:

$$R^2 = 1 - \frac{\sum(\log m - \log p)^2}{\sum(\log m - z)^2} \tag{3.6}$$

where m is the measured value, p is the predicted value and $z = \frac{\sum \log m}{n}$ where n is the number of measurements. The numerator in the equation is the variance of the experimental data from the predicted data, and the denominator is the total variance of the experimental data. Logarithms of measured and predicted contrast were used because the results were plotted on a logarithmic scale.

3.5.2 Standard error

Variability of the experimental data was described by the standard error of the mean. First, the standard deviation, S, was calculated according to:

$$S = \sqrt{\frac{\sum(x_i - \bar{x})^2}{n}} \tag{3.7}$$

where x_i is a measured value, $\bar{x}$ is the arithmetical mean of the measured values and n is the number of measurements. Then, the standard error, SE, was calculated by dividing the standard deviation by the square root of the number of measurements:

$$SE = \frac{S}{\sqrt{n}} \tag{3.8}$$

The standard error was calculated for each data point, and then it was expressed as a percentage of the mean. The arithmetic mean of the individual standard errors in percent was taken as the average relative standard error of the mean, $\overline{SE}$, of the data:

$$\overline{SE} = \frac{\sum \frac{SE}{\bar{x}}}{m} \times 100\% \qquad (3.9)$$

where m is the number of data points (or $\bar{x}$:s). Thus, the $\overline{SE}$:s given in this thesis give the average standard error of the mean in percent.

For contrast matching results presented in Section 4.2 a slightly different procedure was used to determine the standard error since one estimate of matching contrast included 8 adjustments, and a mean of two estimates was taken as the matching contrast. The computer calculated the standard deviation according to Equation (3.7) for each of the two estimates. To calculate the standard deviation for both estimates together, the following equation was used:

$$S_{12} = \sqrt{\frac{S_1^2 + S_2^2}{2}} \qquad (3.10)$$

First, the individual standard deviations, S_1 and S_2. were squared which gave the variance for each estimate. The arithmetical mean of the variances was then calculated. Its square root gave the standard deviation, S_{12}, for the two estimates including 16 adjustments. Standard error was then calculated for the matching contrast using Equation (3.8). Equation (3.9) is exactly correct only when the means of the two estimates are equal. But since the means differed very little, Equation (3.9) gave quite accurate approximations. The average standard error of the mean ($\overline{SE}$) was then calculated as described above.

4. CONTRAST MATCHING

4.1 Modelling of contrast perception

4.1.1 Factors affecting contrast perception

In research on contrast vision, detection thresholds have been extensively studied. The results are normally expressed as contrast sensitivity which is simply the reciprocal of contrast at detection threshold. Contrast sensitivity measurements give information on the limitations of the visual system. The main factors affecting the foveal contrast sensitivity for stationary cosine gratings are spatial frequency, grating area, exposure time, luminance level and the amount of external spatial noise in the stimulus. The importance of these factors for human contrast vision will be explained in more detail in subsequent sections of this thesis.

In everyday life most visual tasks are clearly suprathreshold, i.e. the contrast of stimuli is high. Suprathreshold contrast perception can be studied for example by using contrast matching technique which indicates when the contrasts of two stimuli are subjectively equal. In contrast matching, it is often found that at low contrast levels detection thresholds seem to affect perceived contrast, but at high contrast levels perceived contrast is equal for stimuli with equal physical contrast. The phenomenon that perceived contrasts of different stimuli are equal when their physical contrasts are equal is often called contrast constancy (e.g. Georgeson & Sullivan, 1975).

4.1.2 Earlier models for suprathreshold contrast perception

Kulikowski (1976) has proposed that contrast matching results could be described by simply subtracting the detection threshold from the physical contrast of the stimulus. Kulikowski's rule can be written as: $T - T_d = S - S_d$, where T is contrast of the test grating, T_d is detection threshold of the test grating, S is contrast of the standard grating, and S_d is detection threshold of the standard grating. Matching contrast T can thus be described by subtracting the detection threshold of the standard from its physical contrast and by adding the contrast threshold of the test, i.e. $T = S - S_d + T_d$. Contrast matching results obtained at different spatial frequencies can be described rather well with Kulikowski's rule except at low spatial frequencies (see Georgeson, 1991b, Figure 9.2).

More elaborate versions of Kulikowski's rule have also been developed. For example, it has been proposed that contrast magnitude estimation results can be fitted with a function of the form: $C_p=a(C-T)^b$, where C_p is perceived contrast, C is the physical contrast of the stimulus, T is the detection threshold of the stimulus, and a and b are constants derived from a linear regression on a plot of log C_p versus log (C-T), where a is the intercept and b is the slope (e.g. Cannon, 1985). The slope b is close to 1. Sometimes it has been found to be 1 (Cannon, 1979), and sometimes it has been found to vary between about 0.5 and 1.2 (Gottesman, Rubin & Legge, 1981). Investigators using the threshold-corrected (C-T) power function have concentrated on determining which stimulus parameters or procedural differences cause the exponent b to change. For example, the effect of spatial frequency has been studied by many investigators with very different results. Franzén and Berkley (1975) found that the exponent increases with spatial frequency, but Cannon (1979) found that it is independent of spatial frequency, meanwhile Biondini and de Mattiello (1985), and Quinn (1985) found that it increases at low and high spatial frequencies.

Georgeson and Sullivan (1975) have suggested that spatial frequency dependent contrast attenuation occurring at detection threshold gradually disappears with increasing contrast because of adjustment of gain in channels processing contrast information. They hypothesised that above threshold, the signal becomes more reliable so that it is possible for a channel to adjust its gain in inverse proportion to the amount of attenuation caused by early optical and neural filtering. The idea of contrast processing with spatial frequency selective channels or filters, each of which has its own gain or transducer function, has been applied to many models on contrast perception (Swanson, Georgeson & Wilson, 1988).

Most models attempting to explain the contrast response of the human visual system include a set of linear spatial frequency specific filters, each of which is followed by a nonlinear contrast transducer function, and after these filtering stages there is summation across filter outputs according to Quick's (1974) summation formula. Quick's formula gives the contrast response of the system, R, by summing the responses of individual filters, R_i, according to $R = [\Sigma(R_i)^\alpha]^{1/\alpha}$. The exponent α describes the extent of summation between the filters. When $\alpha=1$, summation is complete, and the extent of summation decreases with increasing value of α.

Swanson, Wilson and Giese (1984) have introduced a model which can be applied to contrast detection thresholds, contrast increment thresholds and contrast matching results. The model is based on the assumption that in each location in the visual space there are four psychophysical mechanisms. Each mechanism is composed of a medium bandwidth

linear spatial filter and a nonlinear contrast transfer function. The spatial filters peak at different spatial frequencies and are followed by different contrast transfer functions. Noise is added to each mechanism's output after which the contrast response of the system is computed from the mechanism outputs using Quick's summation formula. Suprathreshold contrast matching results are explained in terms of the convergence of contrast transfer functions for different mechanisms at high contrast levels. Thus, at low contrast levels the responses of different mechanisms to their peak frequencies are different. But as contrast is increased, the transfer functions of the mechanisms converge so that the responses become equal at high contrast levels.

Swanson et al. (1984) applied their model to contrast matching results obtained at various spatial frequencies and stimulus areas. The model was tested with gratings of various spatial frequencies at two suprathreshold standard contrast levels (at Michelson contrasts of 0.1 and 0.4) but not in the vicinity of the detection threshold. It produced good fits across spatial frequencies for two subjects. However, at low spatial frequencies it failed to exhibit contrast constancy, and the descriptions clearly deviated from the data for one subject. When applied to contrast matching results obtained with various areas, the model gave a good fit at the suprathreshold standard contrast tested (Michelson contrast of 0.1). The model includes spatial response summation to account for the increase of contrast sensitivity with increasing stimulus size at threshold. At suprathreshold contrasts response summation was simply omitted to simulate the behaviour of the matching contrast which became independent of stimulus size at high contrasts.

Cannon and Fullencamp (1988, 1991a) have developed a model for contrast magnitude estimation which can also be applied to contrast matching. Their model has more spatial frequency and orientation selective filters than that of Swanson et al. (1984). Also, their contrast transducers are more elaborate. They are threshold-corrected power functions which allow contrast perception to be simulated at all contrast levels from detection threshold to the maximum contrast. After the linear and nonlinear filtering operations, response summation across spatial frequency at each spatial location is accomplished using Quick's summation formula. The largest of the summed responses is then taken as the contrast response of the system.

Cannon and Fullencamp used the model to simulate the perceived contrast of grating stimuli of various areas at a wide range of contrasts. The fits to contrast magnitude estimation results were good at the two spatial frequencies tested, 4 and 16 c/deg. The model was also applied to magnitude estimation results obtained using compound gratings composed of two orthogonal gratings at 4 c/deg. At high contrast levels, the

experimentally measured perceived contrast of small compound gratings was lower than the prediction of the model.

Georgeson and coworkers (Georgeson 1991a,1991b; Georgeson & Shackleton 1994) have developed a model for contrast perception which is based on similar ideas as the two models described above, with linear spatial frequency and orientation specific filters, a threshold-corrected power-function response to contrast within each filter, and response summation across filter outputs according to Quick's summation formula. In the model Georgeson uses an elaborate version of Kulikowski's rule to describe the contrast response, R, of the visual system:

$$R=[g(C-T)]^m \qquad \text{(i)}$$

where g is contrast gain, C is the physical contrast of the stimulus, T is the contrast threshold of the stimulus and m is the exponent of the power function relating stimulus contrast to the filter response. Suprathreshold behaviour of the model is achieved by normalising the response by dividing it by the response to contrast C_{norm} which is about 1. The normalised response is:

$$R'=[(C-T)/C_{norm}-T)]^m \qquad \text{(ii)}$$

Contrast responses to two stimuli can be calculated according to this equation. When the responses are equal, the perceived contrasts of the stimuli are equal.

Georgeson tested the model with contrast matching results obtained using simple and compound cosine gratings of various spatial frequencies. The compound gratings were composed of two gratings with equal spatial frequency but different orientation. The model predictions were quite accurate. However, Georgeson's model does not include detection threshold predictions. Experimental threshold data at various spatial frequencies were only fitted with a third-order polynomial. Also, the model has not been tested with different stimulus areas.

Brady and Field (1995) have recently introduced a contrast matching model based on a fixed array of scale-invariant spatial-frequency-selective matched filters. Their model differs from the previous ones because they do not assume different contrast transducer functions for different mechanisms (i.e. matched filters) or summation across mechanism outputs. Instead, they propose that the maximum sensitivity is equal for all mechanisms, and that the mechanism bandwidth increases in proportion to spatial frequency. The model predicts that above detection threshold, perceived contrast is directly proportional to the root-mean-square contrast of the stimulus. In agreement with the model, they found that contrast matches obtained with Gabor stimuli and bandpass noise patterns centred at 0.5-32 c/deg become physically correct almost immediately above detection threshold. These results, however, are in disagreement with other studies which have demonstrated a

gradual increase in matching contrast as the contrast of the standard stimulus is increased above detection threshold. The model does not predict detection thresholds, and it has not been tested with grating stimuli of various areas.

4.1.3 Restoration model of human contrast perception

A new model describing contrast perception in the human visual system is introduced here. It is presented in schematic form in Figure 4.1. The model comprises (1) low-pass filtering by the ocular optics, (2) high-pass filtering by the neural visual pathways, (3) addition of internal neural noise, (4) a local matched filter whose response is (5) restored to compensate for the effects of low-level filtering and limited spatial integration before (6) response comparison.

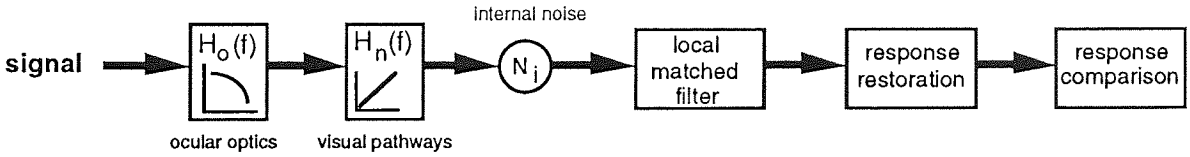

Figure 4.1 Restoration model of human contrast perception.

The contrast response function of the visual system can be interpreted to be a product of two factors: the response of a local matched filter and a restoring transfer function. A contrast detection threshold model based on local matched filters has been developed by Rovamo and coworkers (e.g. Rovamo, Luntinen & Näsänen, 1993; Rovamo, Mustonen & Näsänen, 1994ab&1995), and it is integrated into the new contrast restoration model.

The restoring transfer function is qualitatively similar to the restoration techniques used in digital image processing. Image restoration refers to removal or minimisation of known degradations in an image (e.g. Gonzales & Woods, 1992). The simplest restoration technique is inverse filtering where an output image is multiplied by the inverse of the imaging system's transfer function in Fourier space. A similar idea is applied in the present model where the restoring function is based on knowledge of the optical and neural modulation transfer functions, and the spatial integration function of the visual system so that distortions produced by them can be restored, and the original image recovered.

In order to be able to perform contrast restoration, the visual system has to have access to information on the effects of early visual processing. It seems that the visual system can learn the effects of the optical and neural modulation transfer functions and the spatial integration function. Evidence for this learning process has been presented by Stephens and Banks (1985) who studied the development of contrast constancy in infants. Their stimuli were gratings of various spatial frequencies. They found that for infants of 6 weeks of age, matching contrasts were directly proportional to the detection threshold at all contrast levels. However, for infants of 12 weeks of age, contrast matches were proportional to the detection threshold at low contrasts, but physically correct at high contrasts. Thus, contrast constancy for gratings of various spatial frequencies develops between 6 and 12 weeks of age. The learning mechanism is not known but it may involve comparison of perceived contrast at various viewing distances as described below.

The optical modulation transfer function attenuates contrast at high spatial frequencies. However, if an image containing high spatial frequencies is brought closer, it passes the ocular optics unattenuated since spatial frequencies are now lower. Thus, at a closer range perceived contrast is directly proportional to the physical image contrast. The observer knows that the physical contrast of the image does not change when it is moved further away. Consequently, any changes in the apparent contrast with increasing viewing distance are due to the attenuation by the ocular optics. By using this information, the visual system can deduce the form of the optical modulation transfer function.

The neural modulation transfer function attenuates contrast at low spatial frequencies. Thus, an image containing unattenuated mid-frequencies at a certain viewing distance will be attenuated when viewed at a closer range. Since the observer knows that the physical contrast of the image does not change with viewing distance, it can be deduced that a change in perceived contrast a closer viewing distance is due to the attenuation by the neural modulation transfer function.

The properties of the spatial integration function are such that small stimuli have higher thresholds and lower perceived contrast than large stimuli. Thus, repetitive patterns at a low contrast look more attenuated when only a small part is visible than when a large area is seen. However, the observer knows that the physical contrast of the image does not change with the area shown so that it can be deduced that a decrease in the apparent contrast with decreasing area is due to the attenuation by the spatial integration function.

Contrast restoration is effective only at high contrast levels where the signal-to-noise ratio is high because at low contrasts correction of the modulation transfer functions does not increase the signal strength sufficiently to improve the signal-to-noise ratio.

When an observer is shown a stimulus, the visual signal thus produced is filtered through the various stages in the visual system as described below. Here it should be kept in mind that when contrast matching is performed, two signals are presented and consequently two matched filters are created, one for each signal. Thus, each signal goes through the stages described below but the effect of modulation transfer functions, and the matched filter are different for each.

The first factor in the contrast response function is the response of a local matched filter to a grating that has been filtered by the visual transfer functions. The matched filter response R_d is given by:

$$R_d = H_o^2(f)\, H_n^2(f)\, E\, \eta(z) \tag{4.1a}$$

which is equal to:

$$R_d = H_o^2(f)\, H_n^2(f)\, c^2\, A\, \eta(z) \tag{4.1b}$$

where $H_o(f)$ and $H_n(f)$ are respectively the optical and neural modulation transfer functions of the human visual system, f is spatial frequency in c/deg, E is contrast energy which is equal to c^2A, c is root-mean-square contrast, A is grating area in deg^2, and $\eta(z)$ is detection efficiency as a function of square cycles $z=Af^2$. When the signal has a narrow spatial frequency bandwidth, the effects of the optical and neural modulation transfer functions can be approximated by multiplying the signal by the value of each transfer function at the spatial frequency of the signal. In Equation (4.1) the values of the transfer functions are squared because the matched filter response is proportional to the internal contrast squared, and the internal contrast is attenuated by the transfer functions.

The optical modulation transfer function is:

$$H_o(f) = \frac{1}{1+(f/f_c)^n} \tag{4.2}$$

where f_c is the critical spatial frequency at which $H_o(f) = 0.5$, and n is a constant which indicates the slope of decrease of the optical modulation transfer function in double logarithmic coordinates beyond the critical spatial frequency (Rovamo, Mustonen & Näsänen, 1994b).

The neural modulation transfer function is simply:

$$H_n(f) = f \tag{4.3}$$

This means that the neural modulation transfer function increases in direct proportion to spatial frequency (Rovamo, Luntinen & Näsänen,1993; Rovamo, Mustonen & Näsänen, 1995).

Spatial integration of contrast information occurs at the local matched filter which is a copy of the signal weighted by an aperture function. Its spatial integration properties can be described by an efficiency function. Detection efficiency, $\eta(z)$, decreases with the number of square cycles. That is, spatial integration of contrast information becomes less effective as the number of details increases. Therefore, $\eta(z)$ may also be called the spatial integration function. It can be modelled by the following equation:

$$\eta(z) = \frac{\eta_{max}}{1 + z/z_c} \tag{4.4}$$

where η_{max} is the maximum efficiency, z is the number of square cycles in the stimulus ($z=Af^2$), and z_c is the critical number of square cycles (Rovamo, Luntinen & Näsänen, 1993; Rovamo, Ukkonen, Thompson & Näsänen, 1994). When $z=z_c$, $\eta(z)=\eta_{max}/2$ which means that at the critical number of square cycles efficiency has fallen to half from its maximum. The critical number of square cycles which marks the saturation of spatial integration is calculated according to:

$$z_c = \frac{z_0 f^2}{f_0^2 + f^2} \tag{4.5}$$

where z_0 is the maximum of the critical number of square cycles in the integration function, and f_0 is the critical spatial frequency in the integration function. The critical number of square cycles is constant at z_0 when $f>>f_0$. At f_0 the critical number of square cycles is half of the maximum, i.e. $z_c=z_0/2$. At low spatial frequencies, i.e. when $f<<f_0$, z_c decreases in proportion to f^2 so that the critical area is constant. Thus, spatial integration saturates at a constant number of square cycles ($=z_0$) above f_0, and at a constant area below it.

The other factor in the contrast response, a restoring transfer function $H_r(f)$ attempts to correct the response R_d so that the product $R_dH_r(f)$ would be directly proportional to the physical contrast. The restoring transfer function is given by:

$$H_r(f) = \frac{c^{\kappa-1}}{\gamma H_o^2(f) H_n^2(f) c^{\kappa} A\eta(z) + N_{tot}'(f)} \tag{4.6}$$

where $N_{tot}'(f)$ is the total spectral density of noise in the human brain, and γ and κ are constants which determine at which contrast level restoration starts to influence perceived contrast, and how quickly perceived contrast becomes independent of factors affecting the detection threshold. The total spectral density of noise in the human brain is calculated by:

$$N_{tot}'(f) = H_o^2(f)\, H_n^2(f)\, N_e(f) + H_n^2(f)\, N_q + N_i \tag{4.7}$$

where $N_e(f)$, N_q and N_i are external spatial noise, quantal noise and internal noise, respectively. Quantal and internal noises are assumed to be white and are therefore independent of spatial frequency. Before signal interpretation in the brain, the external noise is filtered both by the ocular optics, $H_o(f)$, and the neural pathway, $H_n(f)$. This is because external noise is added to the pixels of the image so that it is a part of the image which is filtered by both transfer functions (Rovamo, Luntinen & Näsänen, 1995). Quantal noise is filtered by the neural visual pathway, but it is unaffected by the ocular optics because individual light quanta cannot be blurred by the point spread function of the ocular optics (Rovamo, Mustonen & Näsänen, 1994ab). Or in other words, even though the optical blur redistributes the light quanta so that contrast is attenuated more at high than at low spatial frequencies, the blur does not introduce correlations among neighbouring points, and thus it does not attenuate the high spatial frequencies in quantal noise (Graham & Hood, 1992). The neural pathways filter both external and quantal noise because at the event of quantal absorption both are transformed into neural noise which cannot bypass the neural pathways.

The purpose of the restoration function is to correct the degradations produced by the early stages of signal processing. The restoration function does not change the signal-to-noise ratio of the output of the local matched filter because it has exactly the same effect on both the signal and noise.

Contrast perception can be modelled by combining the response of the local matched filter, R_d, with the restoring transfer function, $H_r(f)$, to produce the visual response, R(c), to the stimulus:

$$R(c) = R_d H_r(f) \tag{4.8a}$$

which is equal to:

$$R(c) = \frac{H_o^2(f) H_n^2(f) c^{\kappa+1} A\eta(z)}{\gamma H_o^2(f) H_n^2(f) c^{\kappa} A\eta(z) + N_{tot}'(f)} \tag{4.8b}$$

Equation (4.8b) is thus obtained by multiplying Equation (4.1b) by Equation (4.6). It will be used to describe contrast matching results presented in the experiments of this chapter.

At low contrasts or, more precisely, at small signal-to-noise ratios the effect of the correction by the restoring transfer function on the local matched filter output is negligible. This is because in Equation (4.8b), the noise term $N_{tot}'(f)$ in the denominator is much larger than the term $\gamma H_o^2(f)H_n^2(f)c^{\kappa}A\eta(z)$. Therefore, Equation (4.8b) can be reduced to:

$$R(c_{low}) = \frac{H_o^2(f)H_n^2(f)c^{\kappa+1}A\eta(z)}{N_{tot}'(f)} = c^{\kappa-1}\frac{E'\eta(z)}{N_{tot}'(f)} \qquad (4.9a)$$

where $E'=H_o^2(f)H_n^2(f)c^2A$ is equal to the contrast energy in the brain, i.e. the external signal energy filtered by the optical and neural transfer functions.

Stimulus contrast can be expressed as multiples p of the detection threshold, i.e. $c=pc_d$. When this is substituted in Equation (4.9a), we get:

$$R(c_{low}) = \frac{H_o^2(f)H_n^2(f)\,(pc_d)^{\kappa+1}A\eta(z)}{N_{tot}'(f)} = p^{\kappa+1}c_d^{\kappa-1}\frac{E_d'\eta(z)}{N_{tot}'(f)} \qquad (4.9b)$$

At detection threshold, the signal-to-noise ratio for an ideal detector, i.e. a global matched filter in white noise N, is equal to the detectability index defined as $d' = \sqrt{E_i/N}$ (Tanner & Birdsall, 1958), where E_i is the energy threshold of the ideal observer. Efficiency can be defined as the ratio of the energy threshold of the ideal observer to that of the human, that is $\eta=E_i/E_d$ (Tanner & Birdsall, 1958). Consequently, $E_i=E_d\eta$. From this it follows that the signal-to-noise ratio at threshold for a human observer is $d' = \sqrt{E_d\,\eta/N}$. Thus, Equation (4.9b) can be written as:

$$R(c_{low}) = p^{\kappa+1}c_d^{\kappa-1}d'^2 \qquad (4.9c)$$

where d' represents the detection threshold. When $\kappa\approx1$, Equation (4.9c) reduces to:

$$R(c_{low}) = p^2d'^2 \qquad (4.9d)$$

Equation (4.9d) means that, at low contrast levels, the contrast response is proportional to the squared signal-to-noise ratio at threshold, d'^2. In contrast matching this implies that when the standard stimulus is set for example at twice its threshold, the test stimulus is adjusted at twice its own threshold.

At detection threshold the multiple of threshold p is 1. Consequently, Equation (4.9d) reduces to $R(c_{low})=d'^2$. In order to calculate contrast detection threshold predictions, Equation (4.9a) was written as:

$$d'^2 = \frac{H_o^2(f)H_n^2(f)c_d^2 A\eta(z)}{N_{tot}'(f)} \tag{4.10a}$$

Equation (4.10a) is derived from the previously developed contrast detection threshold model (e.g. Rovamo, Luntinen & Näsänen, 1993; Rovamo, Mustonen & Näsänen, 1994ab&1995). The numerator is the local matched filter response R_d which is perturbed by noise as shown by the denominator. Detection threshold contrast predictions were calculated by solving c_d in Equation (4.10a):

$$c_d = \sqrt{\frac{d'^2 N_{tot}'(f)}{H_o^2(f)H_n^2(f)A\eta(z)}} \tag{4.10b}$$

The value of the detectability index d' was 1.4 because the two-alternative forced-choice algorithm used in these experiments gives threshold estimates at the probability level of 0.84 correct responses (Elliott, 1964).

At high contrast levels, signal restoration is nearly perfect leading to veridical contrast perception. This is because in Equation (4.8b), the term $\gamma H_o^2(f)H_n^2(f)c^\kappa A\eta(z)$ is much greater than $N_{tot}'(f)$ in the denominator. Consequently, Equation (4.8b) may be written as:

$$R(c_{high}) = \frac{H_o^2(f)H_n^2(f)c^{\kappa+1}A\eta(z)}{\gamma H_o^2(f)H_n^2(f)c^\kappa A\eta(z)} = \frac{c}{\gamma} \tag{4.11}$$

This means that at high contrasts, the contrast response increases in direct proportion to the physical contrast of the stimulus.

In summary, Equation (4.8) predicts that as physical contrast is increased, perceived contrast gradually becomes independent of various factors affecting detection thresholds, until it is directly proportional to physical contrast. Matching contrast descriptions were computed using Equation (4.8b). First, the contrast response to the standard stimulus, $R_s(c_s)$, was calculated. Then the matching contrast, c_t, was solved by finding the contrast which produced an equal response to the test stimulus, $R_t(c_t) = R_s(c_s)$. The contrast restoration model will be tested in the following sections and evaluated in the end of this chapter.

4.2.1 Introduction

The aim of this investigation was to study whether the perceived contrasts of various two-dimensional compound gratings are equal when their root-mean-square (r.m.s.) contrasts are equal. This is an important question since the contrast restoration model introduced in Section 4.1. is based on r.m.s. contrast. A matched filter, which is the detector in the model, produces a response which is proportional to contrast energy, and r.m.s. contrast squared and multiplied by stimulus area yields contrast energy.

The contrast restoration model is based on ideas presented in various studies on human detection efficiency in which human performance is compared with that of an ideal detector. In these studies contrast energy is an essential measure because the energy threshold of an ideal detector for a signal known exactly is defined as $E_i=d'^2N$ (Tanner & Birdsall, 1958) [for further details see Appendix II]. The optimal performance is achieved when the incoming signal, which is embedded in noise, is cross-correlated with a copy of the signal (e.g. Burgess, 1985). An example of a detector which performs cross-correlation is a matched filter which is ideal in white noise (Hauske, Wolf & Lupp, 1976).

In addition, many investigators have found that the contrast of complex stimuli can be better described by using r.m.s. than Michelson contrast (e.g. Stromeyer & Julesz, 1972; Peli, 1990; Kukkonen, Rovamo, Tiippana & Näsänen, 1993). Michelson contrast is based only on the maximum and minimum luminances in the stimulus. R.m.s. contrast is defined as the standard deviation of luminances in the stimulus normalised by the average luminance. Thus, it takes into account the whole luminance distribution in the stimulus. This is important for example when the stimuli are aperiodic, or when the proportion of peak luminances in the stimulus is small. Also, it has been found that in contrast adaptation the visual system takes into account the luminance distribution in the stimulus and not only the peak luminances (Moulden, Kingdom & Gatley, 1990).

If the visual system uses r.m.s. contrast rather than Michelson contrast, matches at high contrast levels should be physically correct when results are expressed in terms of r.m.s contrast. For a simple cosine grating r.m.s. contrast is approximately equal to Michelson contrast divided by $\sqrt{2}$ (see Appendix I for further details). Since Michelson and r.m.s contrast of a cosine grating always differ by a constant factor, more complex stimuli had to be devised for which Michelson and r.m.s contrast would differ by different amounts. The stimuli chosen for this study were two-dimensional compound gratings which

consisted of 2, 3 or 4 orientation components, and whose Michelson and r.m.s contrasts differed by various amounts ranging from 1 to 2.

Most previous contrast matching experiments have been done with simple cosine gratings, but there are some studies where more complex stimuli have been used.

One-dimensional grating stimuli consisting of two spatial-frequency components of the same orientation have been used to investigate how the apparent contrast of a compound grating depends on the contrast of the components. Quick, Hamerly and Reichert (1976) adjusted the contrast of a two-component grating to match the contrast of a simple cosine grating. The two-component stimuli were composed of 4 and 12 or 20 c/deg vertical gratings of various contrasts added in cosine (peaks-add) or sine (peaks-subtract) phase. They used the Quick summation formula (Quick, 1974) to describe the results, and found that the results were best fitted when the exponent α was equal to 2. The Quick summation formula is based on the idea that the visual system consists of various frequency and orientation selective channels, and it gives the contrast response of the system, R, by summing the responses of individual channels, R_i, according to $R = [\Sigma(R_i)^{\alpha}]^{1/\alpha}$. The exponent α describes the extent of summation between the channels. When $\alpha=1$, summation is complete, and the extent of summation decreases with increasing value of α. Thus, Quick et al. (1976) found some summation between the components.

In a very similar study, in which stimuli consisted of 5 and 15 c/deg gratings, Arend and Lange (1980) found, however, that the match is determined by the grating component of higher contrast without any contribution from the weaker component.

Some experiments have also been done using two-dimensional complex stimuli. Mayhew and Frisby (1978) studied the perceived contrasts of band-pass filtered random textures by showing subjects stimuli of various contrasts and asking them to choose the best match for a comparison stimulus of standard contrast. They concluded that the perceived contrasts of random textures tended to be equal when the Quick summation formula with $\alpha=2$ gave the same value for the textures.

Cannon and Fullencamp (1988, 1991a) have studied contrast perception of Gabor patches composed of two orthogonal sine-wave gratings using contrast magnitude estimation. They explained their results with a multiple channel model based on response pooling from individual filters according the Quick summation formula with exponent $\alpha=2.5$. Their model predicted that at high Michelson contrast levels contrast magnitude estimates are equal for both simple and compound gratings.

Georgeson and Shackleton (1994) performed contrast matching experiments with simple and compound cosine gratings at various spatial frequencies. The compound gratings were composed of two orthogonal components. They found that the compound gratings had a lower perceived contrast than simple cosine gratings regardless of spatial frequency. They applied the Quick summation formula to the contrast responses calculated according to their model, and assumed the exponent α to be 2.

R.m.s. contrast is related to the Quick formula so that when the formula with $\alpha=2$ is applied to the Fourier amplitude spectrum of a stimulus, it gives a value directly proportional to r.m.s. contrast. Some previous studies thus imply that contrast matching is based on r.m.s. rather than Michelson contrast.

4.2.2 Methods

In the experiments the contrasts of various compound test gratings were adjusted to match a series of standard contrasts of a simple cosine grating. Both the test and the standard grating were presented simultaneously on the display screen with unlimited viewing time. The test grating was on the right and the standard on the left, separated by 7 cm from centre to centre. Contrast matching functions were measured using the method of adjustment as described in Section 3.3.2. Detection thresholds for the stimuli were measured using a two-alternative forced choice method as described in Section 3.3.1.

The grating fields were circular in shape. The gratings consisted of 8 cycles, and their diameter was 5.4 cm on the screen. Spatial frequencies of 0.5, 2 and 4 c/deg were obtained by viewing the gratings at the distance of 19.3, 77 and 154 cm, respectively.

The standard stimulus was a vertical cosine grating, and it had six r.m.s. contrast levels: 0.018, 0.035, 0.071, 0.14 and 0.28. The test stimuli were compound gratings, each of which was a sum of cosine gratings of equal contrast, spatial frequency and phase but different orientation. The number of components ranged from one to four. The orientation difference between components was 180°/n where n is the number of components.

Contrast of the stimuli was expressed using two measures: Michelson and root-mean-square contrast. Michelson contrast was calculated as $(L_{max} - L_{min})/(L_{max} + L_{min})$, where L_{max} is the maximum luminance and L_{min} is the minimum luminance in the grating. R.m.s. contrast was calculated as $c=\sqrt{E/A}$ where E is the contrast energy and A is the stimulus area in deg^2. The computer calculated contrast energy according to Equation

(3.8) in Section 3.5. The energy was then divided by the stimulus area, and square root was taken to give r.m.s. contrast.

Two experienced subjects, HK and KT, served as observers. HK was an uncorrected hyperope (oa.+0.5 DS) and KT was a corrected myope (od.-6.5 DS/ os.-4.5 DS). The binocular Snellen acuity was 1.5 for both subjects. HK performed matching at spatial frequency of 2 c/deg and KT at 0.5 and 4 c/deg. The average relative standard error of mean ($\overline{SE}$) for contrast matches was small for both subjects, 2.6 % and 1.6 % for HK and KT, respectively.

4.2.3 Results

The stimuli used in the experiments were compound gratings shown in Figure 4.2. Each compound grating was a sum of cosine gratings of equal contrast, spatial frequency and phase but different orientation. All components were in cosine phase at the centre of rotation. One of the components was always vertical. The orientation difference between components was 90°, 60° and 45° for 2-, 3- and 4-component gratings, respectively. All stimuli have the same Michelson contrast in Figure 4.2.

Figure 4.2(A) shows the 1-component grating which is a simple cosine grating. Figure 4.2(B) shows the 2-component grating which consists of two orthogonal components. Its r.m.s. contrast is 70 % of the r.m.s. contrast of the 1-component grating. The 3-component grating is shown in Figure 4.2(C). It consists of three cosine gratings which had an orientation difference of 60° between them. The r.m.s. contrast in Figure 4.2(C) is the same as in Figure 4.2(A). In the 4-component grating, shown in Figure 4.2(D), the orientation difference between components was 45°. The r.m.s. contrast in Figure 4.2(D) is 50 % of the r.m.s. contrast in Figure 4.2(A). The 4-component grating is not completely periodic unlike the other gratings. If more components are added, that is if there are 5 or more components, the grating loses its periodicity and contrast energy is concentrated in the centre of the stimulus. Therefore gratings with more than four components were not used in the present study where the perceived global contrast of the stimuli was matched.

Contrast signal histograms of the stimuli are shown in Figure 4.3. Contrast signal was calculated as $c(x,y) = [L(x,y)-L_0]/L_0$ where $L(x,y)$ is the luminance of a pixel and L_0 is the luminance averaged across pixels. As Figure 4.3 shows, luminance distributions $L(x,y)$ of the stimuli differ greatly from each other. In the 1-component grating shown in Figure 4.3(A) there are many pixels at the extreme luminances, but their proportion

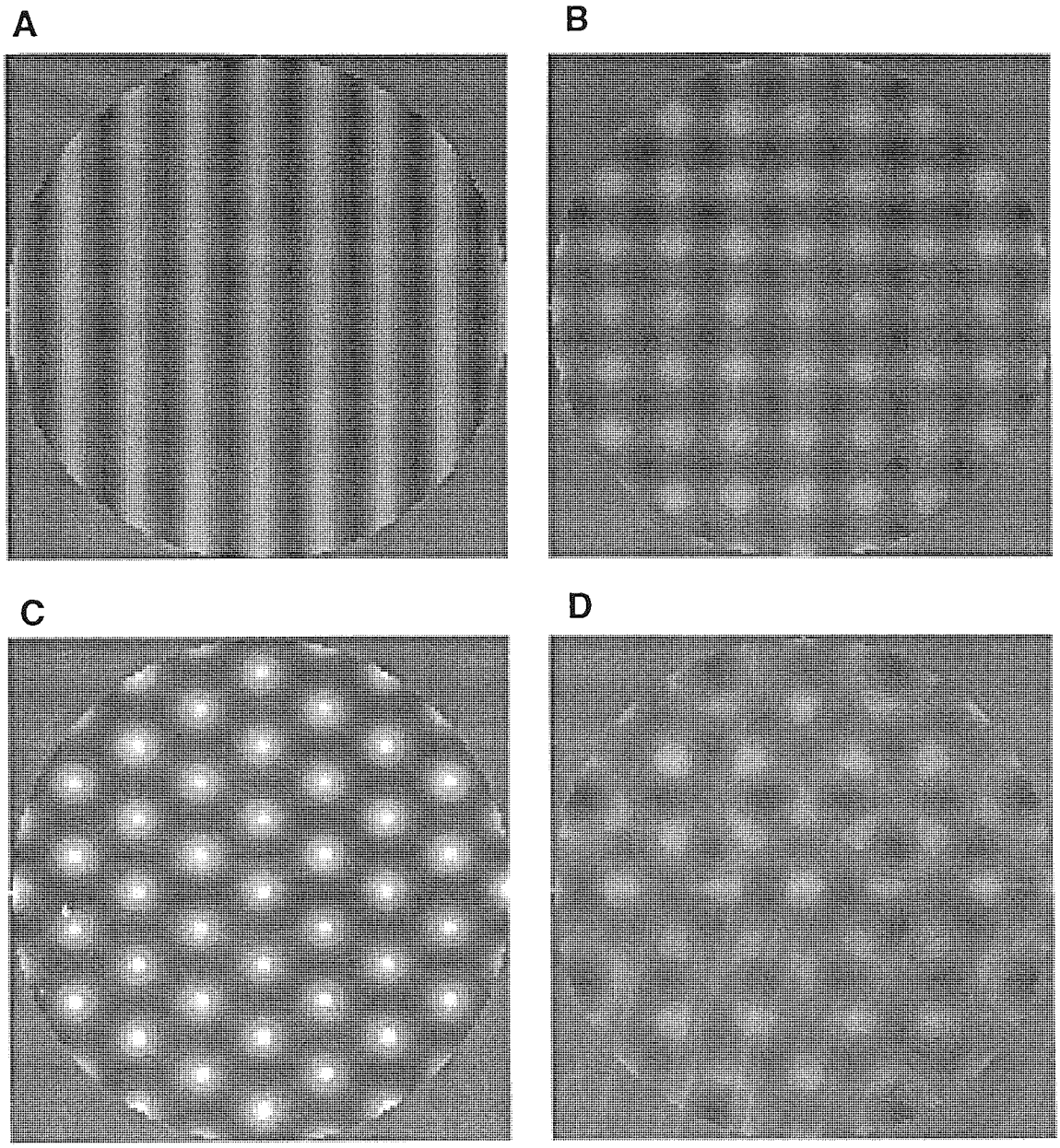

Figure 4.2 Compound gratings with 1, 2, 3 and 4 orientation components.

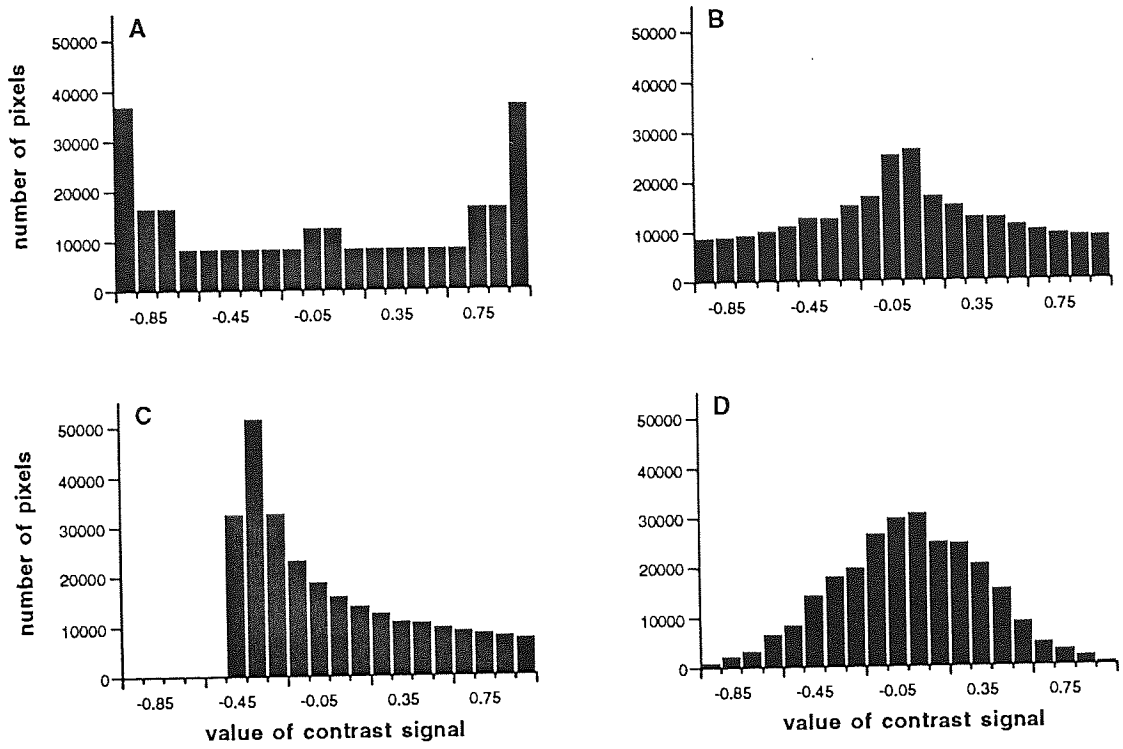

Figure 4.3 Contrast signal histograms of compound gratings with 1, 2, 3 and 4 orientation components.

decreases with increasing number of components as shown in Figure 4.3(B) for 2 components, in Figure 4.3(C) for 3 components, and in Figure 4.3(D) for 4 components. Note also that the luminance distribution for the 3-component grating Figure 4.3(C) is skewed whereas all the other distributions are symmetrical. Consequently, Michelson contrast is equal to the sum of the component contrasts in the 1-, 2- and 4-component gratings but lower in the 3-component grating. This is due to the fact that even though the luminance maxima of the orientation components are superimposed at various locations, the minima are never superimposed in the 3-component grating. Therefore, the minimum luminance in the 3-component grating is closer to the average luminance than the maximum luminance is.

In Figure 4.4 the Michelson contrasts of the test gratings, i.e. the matching contrasts, are plotted as a function of the Michelson contrast of the standard. For 1- and 3-component gratings matching in terms of Michelson contrast was correct because the matching contrast was nearly equal to the contrast of the standard, shown by the straight line,

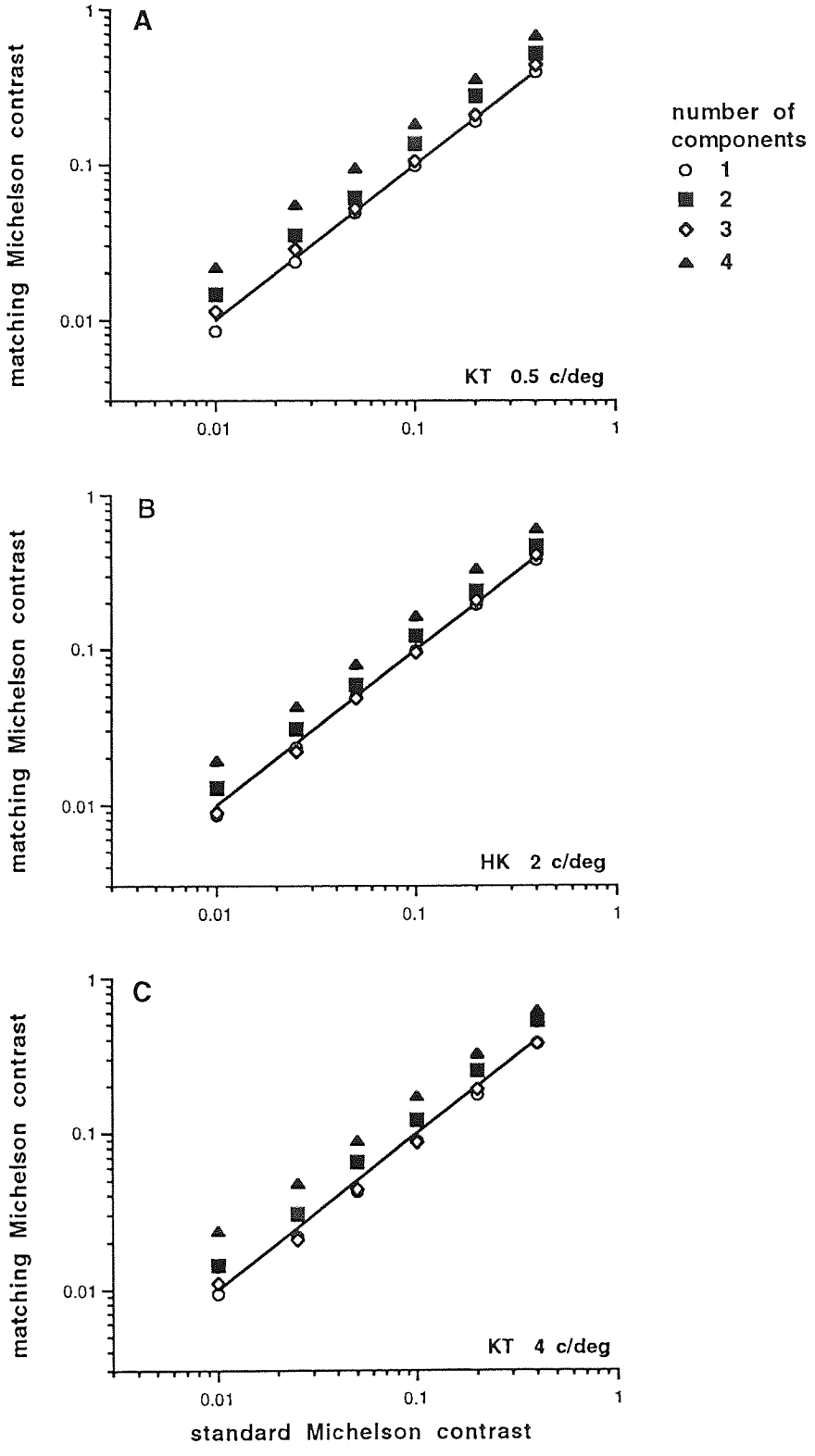

Figure 4.4 Matching Michelson contrast of compound gratings plotted as a function of Michelson contrast of the standard.

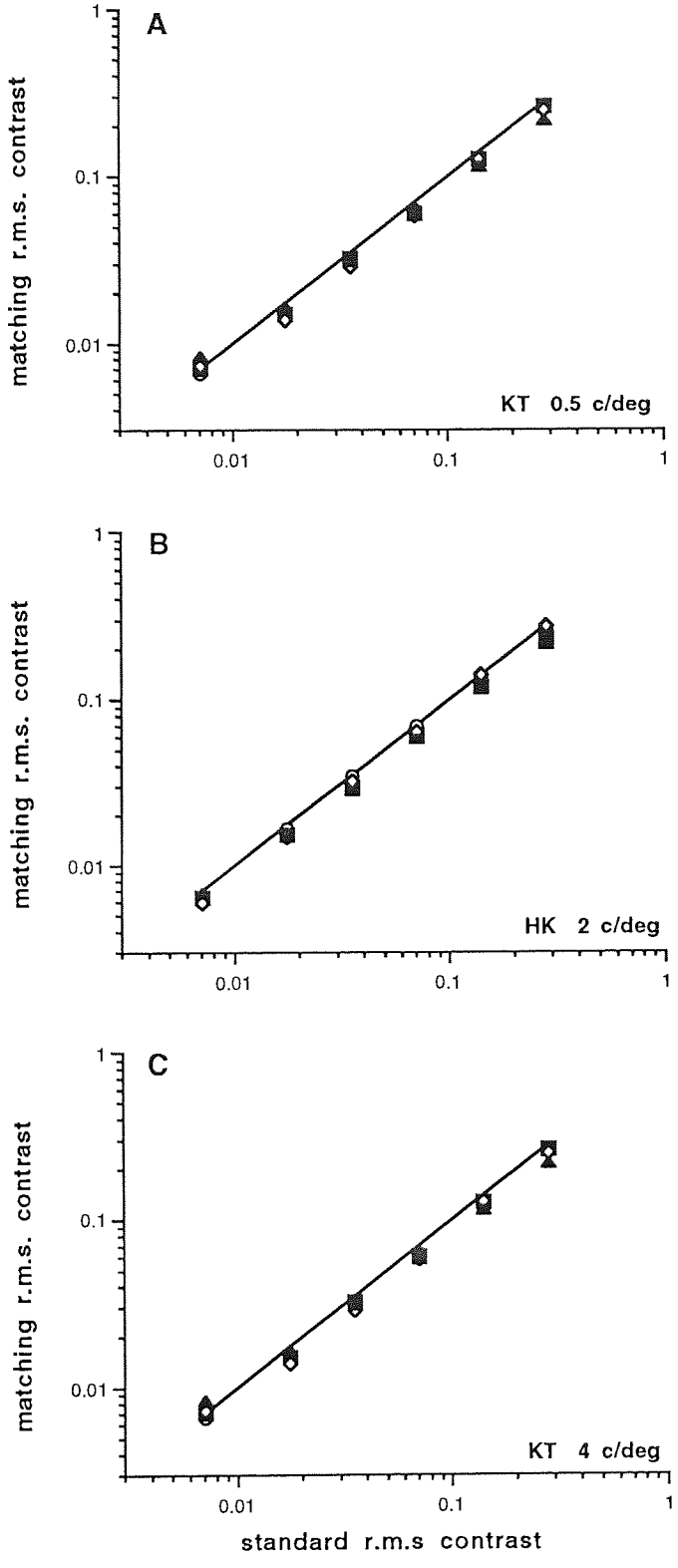

Figure 4.5 Matching r.m.s. contrast of compound gratings plotted as a function of r.m.s. contrast of the standard.

irrespective of spatial frequency and standard contrast level. However, for 2- and 4-component gratings matching was incorrect because the matching contrast was greater than the contrast of the standard for all spatial frequencies and standard contrasts studied. The difference between matching and standard contrast was always greater for 4- than 2-component gratings. The difference was practically independent of the level of standard contrast and spatial frequency. This is shown by the fact that the upward shifts were similar at all standard contrasts and spatial frequencies. Scrutiny of Figs 4A-C revealed that when the perceived contrasts were matched, the Michelson contrasts of the 2- and 4-component gratings were respectively 1.39 and 1.96 times higher than the Michelson contrasts of the 1- and 3-component gratings.

In Figure 4.5 the contrasts are expressed in terms of r.m.s. contrast. Now, irrespective of the number of components, the matching contrast was very close to the contrast of the standard for all spatial frequencies and standard contrasts. Thus, contrast matching in terms of r.m.s. contrast was always correct.

4.2.4 Discussion

The experiments described above show that when contrast was expressed in terms of Michelson contrast, matching contrast was equal to standard contrast for 1- and 3-component gratings but higher than standard contrast for 2- and 4-component gratings. When contrast was expressed in terms of r.m.s. contrast, matching contrast was found to be very close to standard contrast for all compound gratings irrespective of the number of orientation components.

The reason why contrast matching between 1- and 3-component gratings was correct both in terms of Michelson and r.m.s. contrast is that when the r.m.s. contrasts of 1- and 3-component gratings are the same, so are their Michelson contrasts. However, when the r.m.s. contrast of 2- and 4-component gratings is equal to that of 1- and 3-component gratings, then the Michelson contrasts of 2- and 4-component gratings are respectively 1.4 and 2 times higher than the Michelson contrast of both 1- and 3-component gratings. This explains why the matching Michelson contrast was higher than the standard contrast for 2- and 4-component gratings. The average ratios between the matching Michelson contrasts of the 2- and 4-component gratings and the matching Michelson contrast of the 1- and 3-component gratings was 1.39 and 1.96, respectively. This is in close agreement with the expected values.

The finding that the perceived contrast of a 2-component grating is lower than that of a simple grating when both gratings have equal Michelson contrast, is supported by a similar finding by Georgeson and Shackleton (1994). However, instead of expressing the results in terms of r.m.s. contrast, they explained the difference in the perceived contrast in terms of a model using the Quick summation formula with exponent $\alpha=2$.

The findings of this study are in agreement with Quick et al. (1976) who matched compound gratings composed of two spatial-frequency components of the same orientation. According to their results, perceived contrast seems to be directly proportional to the r.m.s. contrast of the stimuli. The results presented here are also in accordance with Mayhew and Frisby (1978) who studied the perceived contrasts of band-pass filtered random textures and found that the apparent contrasts are equal when the r.m.s. contrasts of the stimuli are equal. Both Quick et al. (1976) and Mayhew and Frisby (1978) explained their results with a multiple channel model based on a response pooling from individual filters according to the Quick summation formula with exponent $\alpha=2$. In addition, both admitted that their results are also consistent with a single-channel model in which perceived contrast is directly related to r.m.s. contrast. However, neither provided a description of a single-channel model that would explain their results.

Furthermore, the findings of this study are consistent with the results of Brady and Field (1995) who found that contrasts of Gabor stimuli and bandpass noise patterns of various scales were perceptually matched when their r.m.s. contrasts were equal.

A study on the adapting power of various random-dot images by Moulden et al. (1990) also gives support to the results of this study. Moulden et al. (1990) found that the standard deviation of luminances in an adapting stimulus determines the amount by which the apparent contrast of a standard stimulus is reduced. Standard deviation of luminances in an image is equal to the root mean square of the luminances of the image elements. When normalised (divided) by the mean luminance, it becomes independent of mean luminance and equal to r.m.s. contrast.

The results of this study support the hypothesis that in the human suprathreshold vision perceived contrasts of various grating stimuli are equal when their physical r.m.s. contrasts are equal. This is in agreement with the predictions of the new contrast restoration model. In order to perform a more rigorous test, the model was applied to the results of Figure 4.5.

First, the model parameter values yielding the best fit to the detection threshold data were found. There are six model parameters which determine the detection thresholds. They

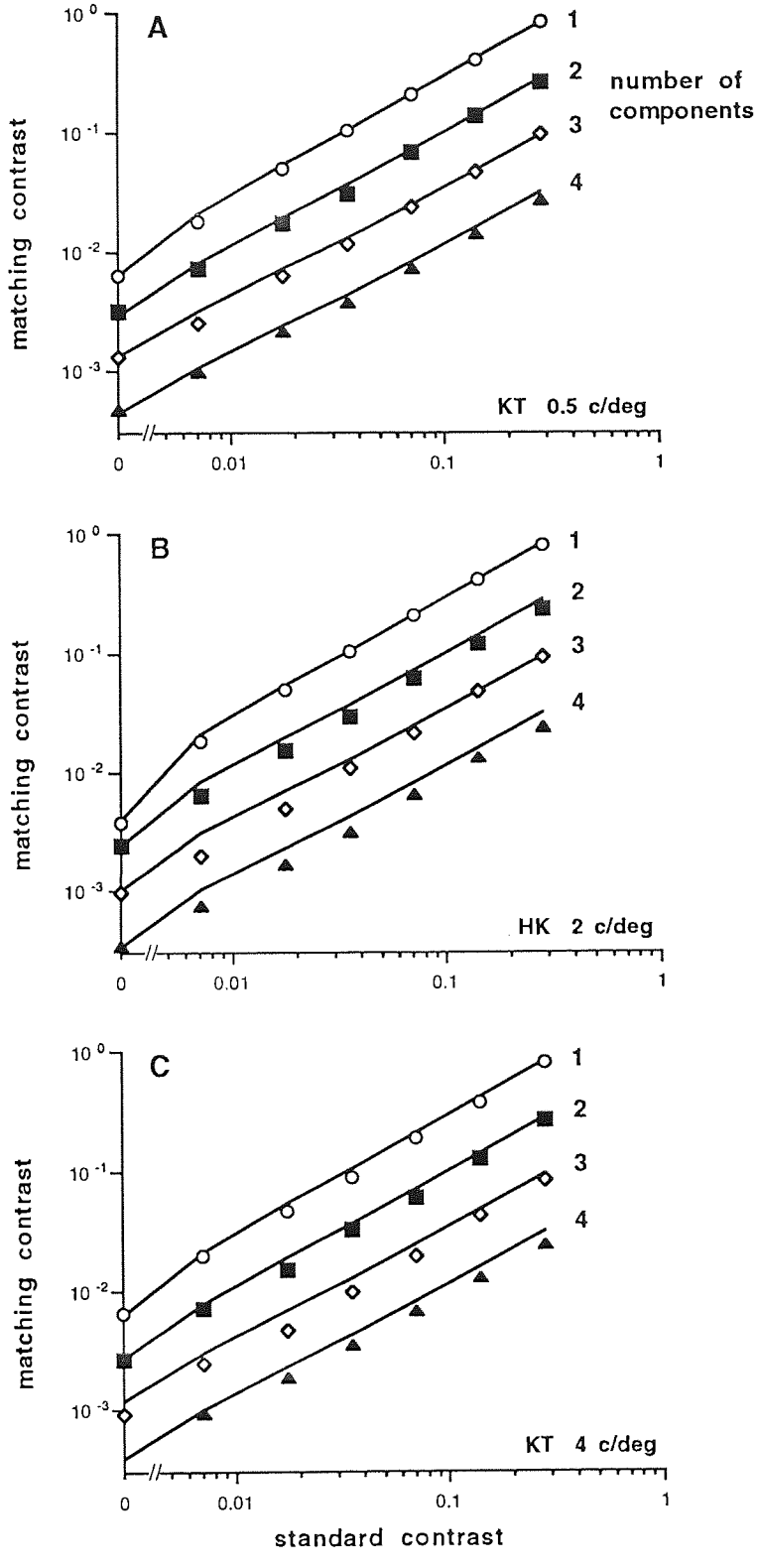

Figure 4.6 Descriptions of the contrast restoration model for contrast matching of compound gratings (data and curves have been displaced vertically for clarity).

are: (1) f_c, the critical spatial frequency of the optical transfer function, and (2) n, the exponent in the optical transfer function [see Equation (4.2) in Section 4.1.3]; (3) N_i, the spectral density of internal noise [see Equation (4.7)]; (4) z_0, a constant indicating the maximum of the critical number of square cycles in the integration function, and (5) f_0, the critical spatial frequency in the integration function [see Equation (4.5)]; and (6) η_{max}, the maximum efficiency [see Equation (4.4)]. The procedure for parameter fitting is described in detail in Section 4.3.3. In order to find the best parameter values, contrast detection thresholds had to be measured at various spatial frequencies and grating areas which was done in the experiments presented in Section 4.3.3, and the parameters were adjusted until the best fit for the threshold data was found.

The parameter values, determined in Section 4.3.3 and shown in Table 4.1, were applied directly to the detection threshold results for the one-component gratings of this study. Only the spectral density of internal noise (N_i) had to be altered slightly to compensate for small differences in sensitivity in the present experiment and the experiments of Section 4.3.3. Here N_i was 9×10^{-6} for HK and 17×10^{-6} for KT. With these parameters, detection threshold descriptions were calculated for simple cosine gratings.

The detection thresholds for the compound gratings used in these experiments depend on the number of orientation components. The thresholds increased with increasing number of components up to 3, and remained approximately constant from 3 to 4 components, in agreement with Rovamo, Ukkonen, Thompson and Näsänen (1994). The increase in thresholds with an increasing number of orientation components is due to a decrease in spatial integration (Rovamo, Ukkonen & al., 1994). In the model this is reflected by a decrease in the value of the parameter z_0 which determines the maximum of the critical number of square cycles in the integration function. A decrease in z_0 means that the extent of spatial integration has decreased. When the number of components increased from 1 to 2, z_0 decreased from 60 to 10 for subject HK, and from 60 to 25 for subject KT. For the 3- and 4-component gratings z_0 was found to be 6 and 12 for HK and KT, respectively. Detection threshold descriptions for compound gratings were calculated using the above mentioned values for z_0, the other parameters remaining the same as for simple cosine gratings.

Next, the restoration function parameters γ and κ [see Equation (4.8b) in Section 4.1.3] were applied to the results of Figure 4.5, and the model descriptions for matches at various contrast levels were calculated. The values determined in Section 4.3.3 were γ=0.001 and κ=1.

Detection thresholds, data from Figure 4.5, and model descriptions are plotted in Figure 4.6. The points on the ordinate are the detection thresholds. The solid lines show the threshold descriptions at zero standard contrast, and matching contrast descriptions at higher standard contrasts. The data and curves have been displaced vertically for clarity by a factor of 3, 1, 0.33 and 0.11 for 1-, 2-, 3- and 4-component gratings, respectively. The explained variance was 0.995 in (A), 0.982 in (B) and 0.984 in (C). The model could accurately describe results of contrast matching with compound gratings.

To conclude, the results of this study support the use of r.m.s. contrast when describing both threshold and suprathreshold phenomena, in agreement with the previously published contrast detection model and the new contrast restoration model.

4.3 Contrast matching of cosine gratings of various spatial frequencies and areas

4.3.1 Introduction

The effect of spatial frequency on contrast perception has been studied both at threshold and at suprathreshold contrast levels. For gratings of a constant area, contrast detection thresholds reach a minimum at about 4 c/deg, and they increase at lower or higher spatial frequencies (e.g. Campbell & Robson, 1968). The contrast sensitivity function is thus band-pass with the peak at about 4 c/deg.

The increase in thresholds at low and high spatial frequencies is due to the neural and optical transfer functions, respectively. The optical transfer function of the human eye passes low spatial frequencies unattenuated. High spatial frequencies, above about 5 c/deg, are attenuated the more the higher the frequency (e.g. Banks, Geisler & Bennett, 1987). The cut-off frequency, i.e. the resolution limit, is reached at about 30 c/deg (e.g. Michaels, 1985).

The neural transfer function is directly proportional to spatial frequency which means that attenuation increases as spatial frequency decreases (Rovamo, Mustonen & Näsänen, 1995). This is due to the neural lateral inhibition which attenuates the contrast of slow luminance gradients (Ratliff & Hartline, 1959). Abrupt luminance borders are attenuated less, and the attenuation becomes stronger the more gradual the change in intensity.

Dependence of perceived contrast on spatial frequency has been studied for example by Watanabe, Mori, Nagata and Hiwatashi (1968) and by Georgeson and Sullivan (1975). When cosine gratings of various spatial frequencies are matched to a grating whose frequency is close to the peak of the contrast sensitivity function, the matching curves resemble the detection threshold curve at low contrast levels. When the standard and test grating are of the same spatial frequency, the physical match is correct. But the further away the test frequency is from that of the standard, the more contrast is needed for a match. As the standard contrast increases, the increase in matching contrast becomes slower at low and high spatial frequencies than at medium frequencies, so that matching curves start to flatten gradually. When the standard contrast exceeds a certain level, perceived contrast is equal for all gratings of equal physical contrast regardless of spatial frequency.

Stimulus area is another important factor in contrast perception. Contrast detection thresholds decrease with increasing grating area up to a saturation point (Hoekstra, van der Goot, van den Brink & Bilsen, 1974; Howell & Hess, 1978; Virsu & Rovamo, 1979). This is due to a process called spatial integration. The visual system is capable of processing information from a limited area only. Within this area, spatial integration is complete which means that all energy is collected from the stimulus, so that the contrast energy threshold remains constant as stimulus area is increased. And since energy is equal to the product of grating area and r.m.s. contrast squared, contrast thresholds decrease with increasing area. Thus, when area is doubled, contrast thresholds decrease by a factor of $\sqrt{2}$ which produces a slope of -0.5 in double logarithmic coordinates when contrast thresholds are plotted as a function of area. When the grating area exceeds the limit of spatial integration, collection of contrast energy becomes incomplete, and energy thresholds start to increase in direct proportion to increasing area. Consequently, contrast thresholds remain constant and independent of area with large gratings.

The transition point between the decreasing and constant parts of the contrast threshold curve occurs with a smaller area as spatial frequency is increased (Howell & Hess, 1978). If contrast thresholds are measured for gratings whose area decreases in proportion to spatial frequency squared, the transition occurs at the same number of square cycles at all spatial frequencies (Virsu & Rovamo, 1979). The number of square cycles is calculated as $z=Af^2$, where z is the number of square cycles, A is grating area and f is spatial frequency. Relative grating area is independent of viewing distance, so that gratings with a constant number of square cycles are magnified or minified versions of one another. The fact that spatial integration ceases at a constant number of cycles rather than at a constant area implies that the detector employed by the visual system is limited by the number of details in the stimulus rather than its physical spatial extent.

Dependence of suprathreshold contrast perception on grating area has been investigated by Takahashi and Ejima (1984). They matched the contrast of a square-shaped cosine grating whose area was 36 deg^2 to the contrast of standard gratings of the same spatial frequency but different areas. The standard grating area could be varied by increasing the number of cycles from 1 up to 22. Three spatial frequencies were used: 1.5, 3 and 6 c/deg. The results show that at low contrast levels the test grating contrast increases with increasing standard grating area up to about 14 cycles, after which it remains constant. Matching curves thus resemble the contrast sensitivity curve at low contrast levels. When the Michelson contrast of the standard is higher than about 0.1, matching curves become flat so that apparent contrast is independent of area.

In the experiments presented here perceived contrast of gratings of various spatial frequencies and grating areas was studied at a wide range of contrast levels. The contrast restoration model presented in Section 4.1 was applied to the experimental results.

4.3.2 Methods

Contrast was always expressed in terms of r.m.s. contrast. Because all stimuli were simple cosine gratings, r.m.s. contrast could be calculated as $c=c_M \times 0.707$ where c_M is Michelson contrast. The maximum error introduced by using this equation was about 4% for the smallest grating size used, and less for larger gratings. For further details see Appendix I.

In Experiment I spatial frequency was the parameter. Cosine gratings of various spatial frequencies were adjusted in contrast to apparently match a grating of a constant spatial frequency and contrast. The standard and test grating were presented sequentially in 500 msec exposures, standard always first. In order to avoid any adaptation effects, standard was oriented horizontally and test vertically.

Gratings were circular in shape and their diameter was 16 cm. Spatial frequency on the screen ranged from 0.125 to 4 c/cm in one octave steps. At the viewing distance of 229 cm the test spatial frequencies were thus 0.5, 1, 2, 4, 8 and 16 c/deg. The standard spatial frequency was 4 c/deg. The standard had seven r.m.s. contrast levels: 0.0042, 0.0085, 0.017, 0.035, 0.071, 0.28 and 0.57. Grating area was 12.57 deg^2.

The highest spatial frequency used, 4 c/cm, was outside the unattenuated range of the screen (see Section 3.1). Contrast was attenuated by -0.155 log units, i.e. by a factor of 0.7 at 4 c/cm which corresponds to 16 c/deg. Thus, all matching contrasts obtained at 16 c/deg were corrected by multiplying them by 0.7. A control experiment was performed to ensure that the correction factor was correct. Matches at 16 c/deg were repeated by subject KT at all standard contrast levels at a viewing distance of 916 cm. The spatial frequency on the screen was thus 1 c/cm which was clearly within the unattenuated range. Matching contrasts obtained at 1 c/cm were nearly equal to the corrected matching contrasts obtained at 4 c/cm. This indicates that the correction factor was accurate, and that results obtained at 16 c/deg with 4 c/cm gratings were correct.

In Experiment II grating area was the parameter. Cosine gratings of various areas were adjusted in contrast to apparently match a grating of a constant area and contrast. The test and the standard grating were visible simultaneously on the screen with unlimited viewing

time. The test grating was on the left and standard on the right, separated by 8 cm from centre to centre. In order to avoid any adaptation effects, standard was oriented vertically and test horizontally.

The gratings were rectangular in shape. Spatial frequency was 2 c/cm on the screen. Matching was performed at two viewing distances, 28.6 and 115 cm which correspond to spatial frequencies of 1 and 4 c/deg. Four test grating sizes were used, with side lengths of 1, 2, 4 and 8 cm. Test grating areas were thus 4, 16, 64 and 256 deg^2 at 1 c/deg, and 0.25, 1, 4 and 16 deg^2 at 4 c/deg. The standard grating area was 64 and 4 deg^2 for 1 and 4 c/deg, respectively. The standard had seven r.m.s. contrast levels: 0.0071, 0.014, 0.027, 0.053, 0.106, 0.21 and 0.42.

Detection thresholds were measured for all gratings used in experiments I and II using a two-alternative forced choice method as described in Section 3.3.1.

Three experienced observers performed the experiments. HK, an uncorrected hyperope (oa.+0.5 DS), and KT, a corrected myope (od.-6.5 DS/os.-4.5 DS) performed the experiments at various spatial frequencies. KT and RL, who was a corrected myope (od. -2.25 DS/os. -2.0 DS -0.25 DC), performed the experiments at various grating areas. The binocular Snellen acuity was at least 1.5 for all subjects.

4.3.3 Results

In Experiment I, detection thresholds for different spatial frequencies were measured first, and a spatial frequency at the peak of the contrast sensitivity function, 4 c/deg, was chosen as the standard. Then gratings of various spatial frequencies were matched to the standard at various contrast levels.

In Figure 4.7 contrast matching results are plotted as a function of spatial frequency. The subject was HK in 4.7(A), and KT in 4.7(B). The lowest curve in the figures (filled diamonds) is the detection threshold curve. When matching was done at low contrast levels, the further the test grating spatial frequency was from the standard spatial frequency, the more contrast was needed in the test. Matching curves thus resembled the threshold curve in shape at the lowest standard contrasts. With increasing standard contrast, however, perceived contrast of extreme spatial frequencies approached that of the standard so that matching curves became flatter. At the highest contrast levels the test grating was adjusted to have the same physical contrast as the standard grating regardless of spatial frequency.

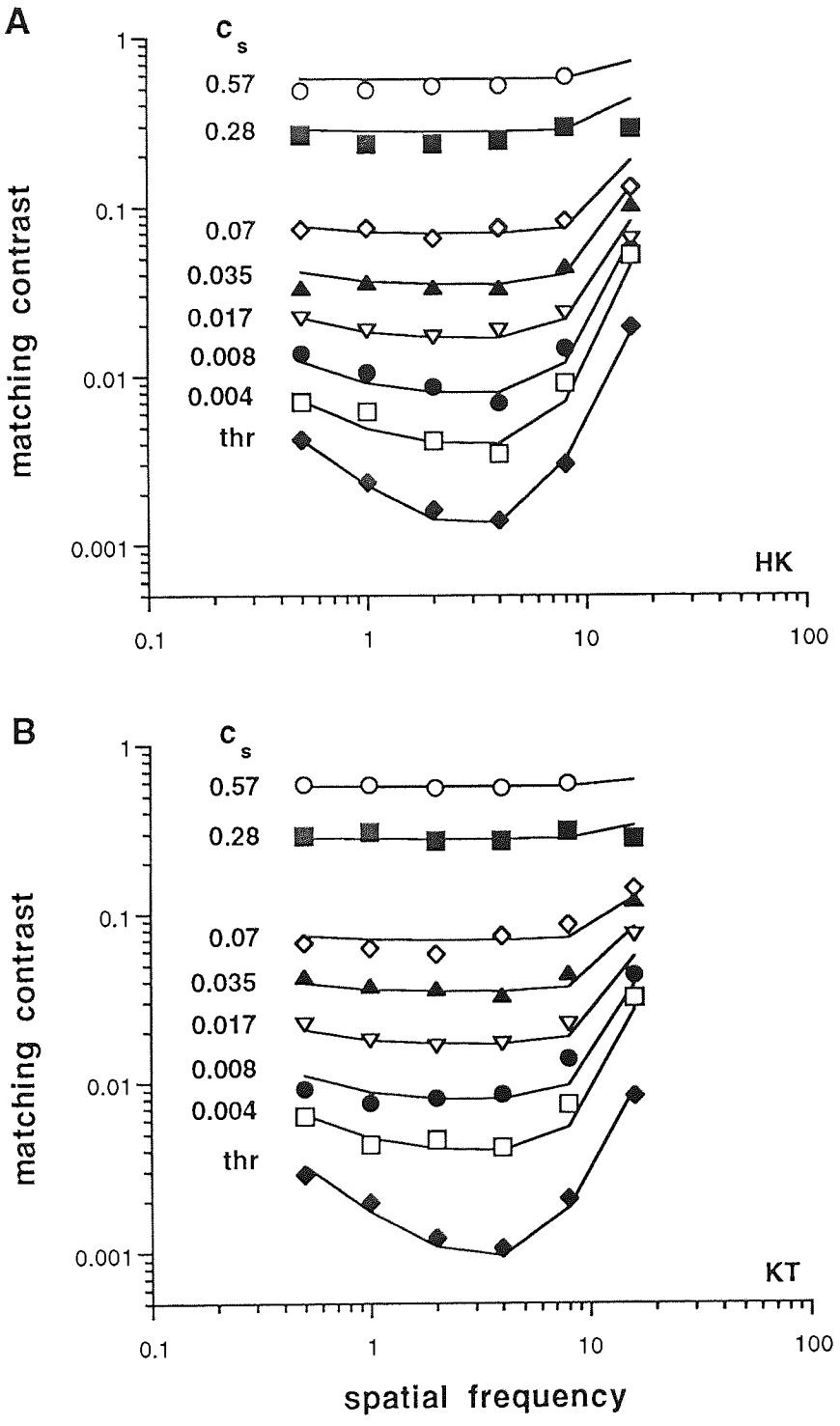

Figure 4.7 Matching contrast plotted as a function of spatial frequency with standard contrast as parameter.

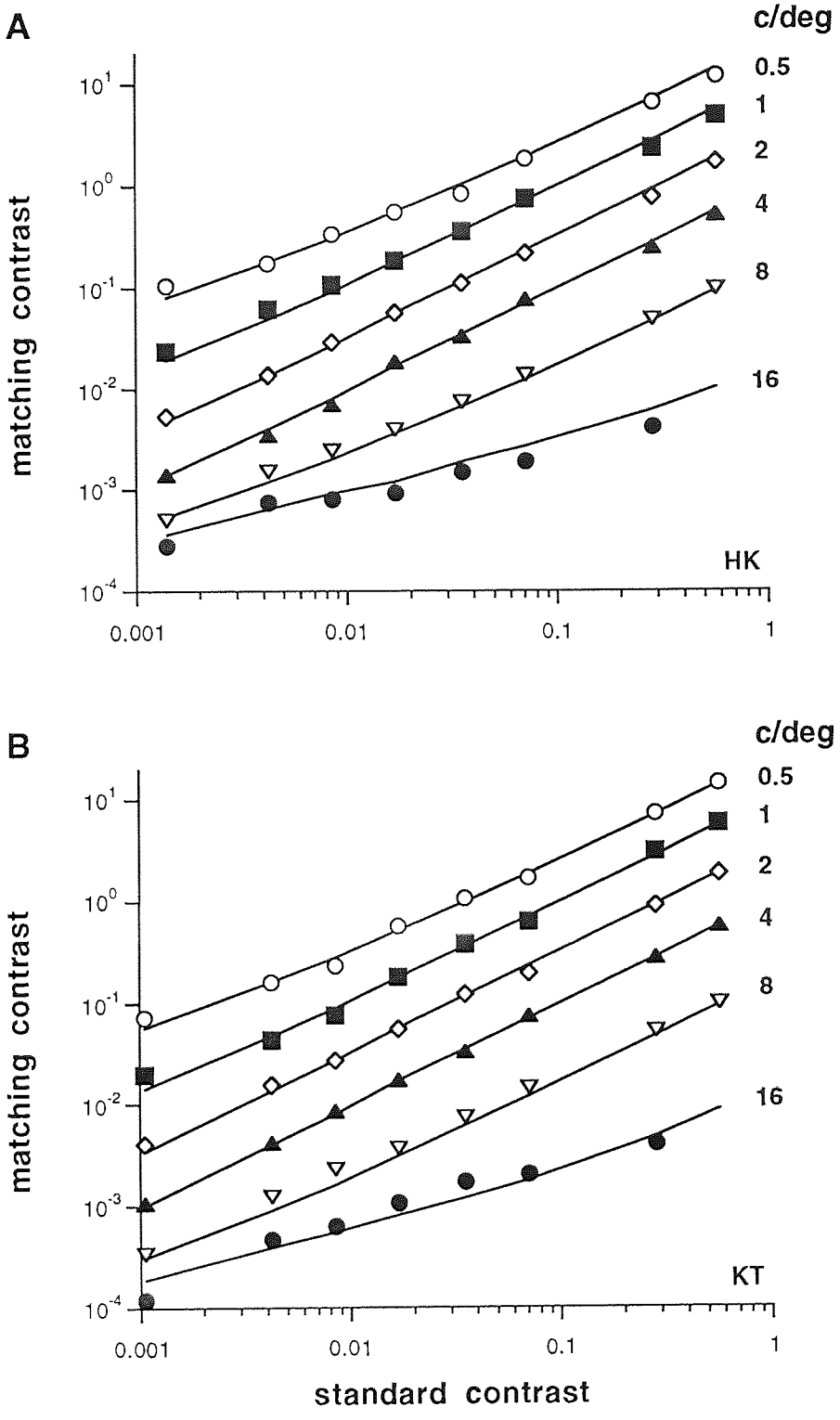

Figure 4.8 Matching contrast plotted as a function of standard contrast with spatial frequency as parameter (curves have been displaced vertically for clarity).

The results shown in Figure 4.7 are replotted in Figure 4.8 as a function of standard contrast. The data and the smooth curves for different spatial frequencies have been displaced vertically for clarity. They have been multiplied by a factor of 25, 10, 3.3, 1, 0.17 and 0.014 at a spatial frequency of 0.5, 1, 2, 4, 8 and 16 c/deg, respectively.

Detection thresholds are plotted as the leftmost points in Figure 4.8 at the value of the abscissa equal to the detection threshold of the standard (c=0.0014 for HK in A, and c=0.001 for KT in B). When the standard was matched to itself (4 c/deg shown as filled triangles), matching contrast increased linearly with standard contrast. For other spatial frequencies matching contrast increased initially more slowly, i.e. the slope of increase was less than one at low contrast levels. At high contrast levels, matching contrast increased linearly for all spatial frequencies except for 16 c/deg.

The contrast restoration model introduced in Section 4.1 was applied to the results. First, the parameter values were found which produced the most accurate descriptions to the detection threshold data. The model parameters which determine the threshold behaviour are the critical spatial frequency of the optical transfer function (f_c), the exponent in the optical transfer function (n), the spectral density of internal noise (N_i), the maximum of the critical number of square cycles in the integration function (z_0), the critical spatial frequency in the integration function (f_0), and the maximum efficiency (η_{max}). Then, the constants in the restoration function (γ and κ) were determined by calculating model descriptions to contrast matching data at various values of γ and κ. The parameter values which produced the visually best fits were found for each subject by iteration, and they are shown in Table 4.1.

Parameter	HK	KT
f_c	6	7
n	3	3
N_i	$10x10^{-6}$	$6x10^{-6}$
z_0	60	60
f_0	0.5	0.5
η_{max}	0.4	0.4
γ	0.001	0.001
κ	$1+0.0014f^2$	$1+0.0014f^2$

Table 4.1 Model parameters for HK and KT in spatial frequency matching.

Iteration was done so that the initial value of each parameter was based on previous findings, and the values were adjusted manually until the model descriptions corresponded to the experimental data as accurately as possible.

Two parameters, the maximum efficiency (η_{max}) and the critical spatial frequency in the integration function (f_0), were taken directly from previous studies since they could not be determined on the basis of the present data. This is because detection thresholds had not been measured in external spatial noise or at very low spatial frequencies in this study. The maximum efficiency determines the best possible human performance when compared to an ideal observer. It was set at 0.4 based on the value 0.375 found by Rovamo, Luntinen and Näsänen (1995). The critical spatial frequency in the integration function determines how spatial integration depends on spatial frequency. At spatial frequencies below f_0, the critical area of spatial integration remains constant, but at spatial frequencies above f_0 it decreases in inverse proportion to spatial frequency squared. The f_0 was set at 0.5 c/deg based on the value 0.465 c/deg found by Rovamo, Mustonen and Näsänen (1994a).

The critical spatial frequency of the optical transfer function (f_c) and the exponent in the optical transfer function (n) determine the shape of the contrast threshold curve at high spatial frequencies. At f_c, the optical transfer function has decreased to 0.5 of the maximum. The higher the f_c, the later the optical modulation transfer function starts to attenuate high spatial frequencies. The higher the n, the steeper the high-frequency attenuation is. The critical spatial frequency was found to be 6 and 7 c/deg for HK and KT, respectively. The exponent n was equal to 3 for both subjects. This is in agreement with Rovamo, Luntinen and Näsänen (1993) who found f_c equal to 7.2 c/deg and n equal to 3.

The maximum of the critical number of square cycles in the integration function (z_0) determines the upper limit of spatial integration. The higher the z_0, the more extensive the spatial integration is. When contrast thresholds are measured at various spatial frequencies with a grating of a constant area, an increase in z_0 results in a decrease of threshold at high spatial frequencies. Thus, in addition to f_c and n, z_0 was used to determine the shape of the contrast threshold curve. The value of z_0 was found to be 60 square cycles. This is in agreement with Rovamo, Mustonen and Näsänen (1994a) who found z_0 equal to 69.2 square cycles.

The spectral density of internal noise (N_i) determines the absolute sensitivity of the subject. An increase in the internal noise increases all detection thresholds by an equal amount. The N_i was chosen so that the experimental data and the model descriptions

coincided in the vertical direction in Figure 4.7. The N_i was expressed as an equivalent spectral density of spatial noise (deg^2). The spectral density of internal noise was found to be $10x10^{-6}$ for HK and $6x10^{-6}$ for KT.

When the parameters determining the threshold descriptions were set, contrast matching descriptions were calculated for various values of γ and κ, and the best values for the constants were found. The effect of changing the values of parameters γ and κ on matching contrast predictions of the model is demonstrated in Appendix III.

The constant γ determines the contrast level at which restoration starts to influence perceived contrast. A suitable value of γ was found to be 0.001. The value of γ was kept constant at 0.001 in all conditions when descriptions were calculated for luminance modulated stimuli.

The constant κ is the exponent of the restoration function. It affects the speed of restoration. In other words, it determines how quickly matching curves flatten with increasing standard contrast. The larger the κ is, the higher the contrast level at which matches become physically correct, i.e. the slower is the flattening of the curves. When $\kappa=1$, the contrast response near threshold is proportional to the square of the signal-to-noise ratio of the local matched filter.

Exponent κ was found to depend on spatial frequency. The model descriptions for spatial frequencies at and below 4 c/deg were very accurate when κ was equal to 1. However, at 8 and 16 c/deg contrast restoration occurred too rapidly with $\kappa=1$. That is, flattening of matching curves was too rapid especially at low contrast levels. Consequently, larger values of κ were required above 8 c/deg. It was found that the most accurate descriptions were obtained when κ increased as a power function of spatial frequency according to:

$$\kappa=1+0.0014f^2 \qquad (4.12)$$

Thus, κ was 1 up to about 5 c/deg and increased thereafter. It was 1.1 at 8 c/deg and 1.4 at 16 c/deg.

The smooth curves in Figures 4.7 and 4.8 are the descriptions of the model. The experimental results were accurately described by the model. The explained variance was 0.993 and 0.994 in Figures 4.7(A) and (B), respectively, and 0.991 and 0.992 in Figures 4.8(A) and (B), respectively. Explained variance was calculated for the undisplaced data in Figure 4.8.

In Figure 4.7 contrast detection thresholds are plotted as the lowermost data points (filled diamonds) together with the threshold descriptions of the model (R_d). In Figure 4.8 detection thresholds are plotted as the leftmost data points together with the restored contrast response predictions of the model ($R_dH_r(f)$) when the standard was set at its detection threshold (c=0.0014 for HK in A and c=0.0011 for KT in B). Both predictions are in close agreement with the detection threshold data, as was expected because when the standard is at its threshold, the matching contrast should be equal to the threshold of the test stimulus. Predictions for contrast matches are the same in both figures.

In Experiment II, contrast matching was performed with gratings of different areas. In Figure 4.9 matching contrast is plotted as a function of grating area at various levels of standard contrast. The subject was RL in 4.9(A), and KT in 4.9(B). The lowest data points (filled diamonds) show the detection thresholds. First they decreased with a slope of -0.5 in double logarithmic coordinates, and then they started to saturate at the largest grating areas. The transition occurred similarly for both spatial frequencies because the number of square cycles increased equally at 1 and 4 c/deg.

At low contrast levels, matching contrast was higher than standard contrast when the test grating was smaller than the standard. This means that perceived contrast of the test was lower than that of the standard. But when the test was of the same size or larger than the standard, its perceived contrast was equal to that of the standard. At high standard contrast levels, the test was adjusted to have equal physical contrast to that of the standard regardless of the test grating area.

The results shown in Figure 4.9 are replotted in Figure 4.10 as a function of standard contrast. The data and the smooth curves for different areas have been displaced vertically for clarity relative to the largest grating. They have been multiplied by a factor of 8, 4 and 2 for 4, 16 and 64 deg^2 gratings in (A), and for 0.25, 1 and 4 deg^2 gratings in (B), respectively. At low contrast levels matching contrast increased more slowly for the smallest gratings, but at high contrast levels matching contrast increased linearly with standard contrast for all grating areas.

Next, the contrast restoration model was applied to the results. The best values for the parameters determining the detection threshold were found for each subject. They are shown in Table 4.2. For KT the values determined in Experiment I were used except for the spectral density of internal noise which had to be adjusted because the detection thresholds were slightly different in the two experiments. This was probably due to the inherent random variation in an observer's performance. For RL it was not necessary to individually determine the parameters f_c and n since he performed the experiment at 1

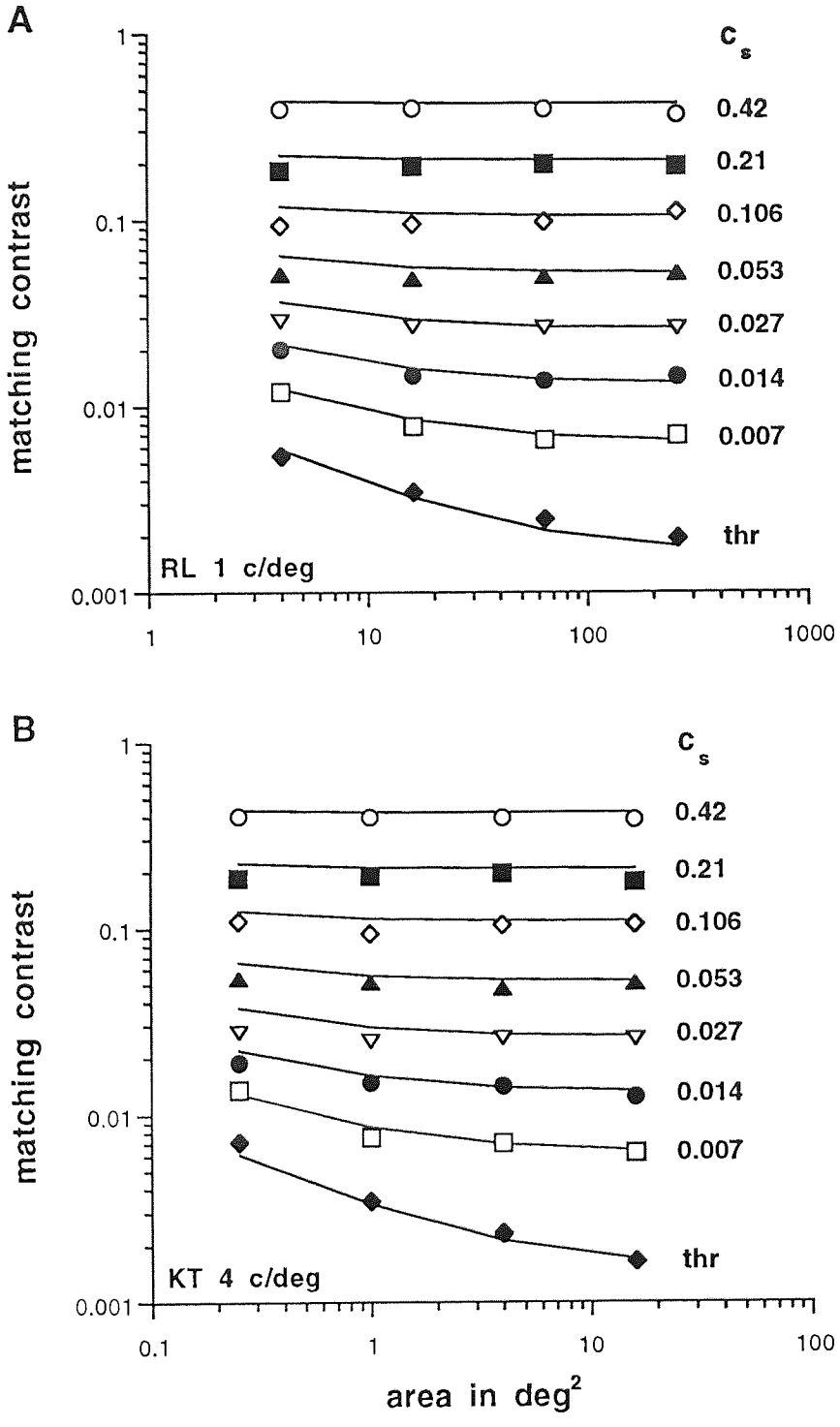

Figure 4.9 Matching contrast plotted as a function of grating area with standard contrast as parameter.

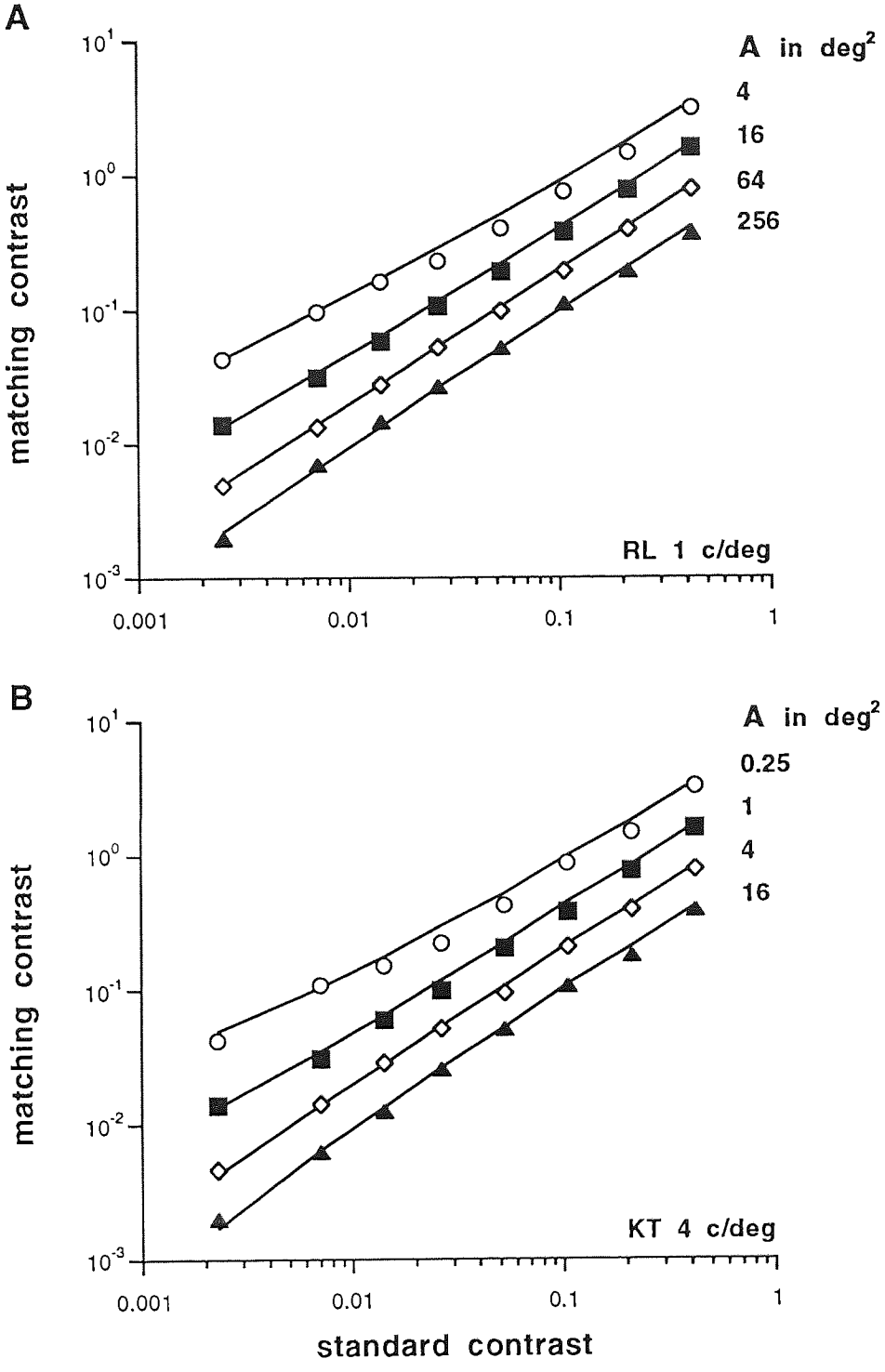

Figure 4.10 Matching contrast plotted as a function of standard contrast with grating area as parameter (curves displaced vertically for clarity).

Parameter	KT	RL
f_c	7	7
n	3	3
N_i	$20x10^{-6}$	$25x10^{-6}$
z_0	60	60
f_0	0.5	0.5
η_{max}	0.4	0.4
γ	0.001	0.001
κ	1	1

Table 4.2 Model parameters for KT and RL in area matching.

c/deg, and these parameters have almost no effect on such a low spatial frequency. The parameters z_0, f_0 and η_{max} were kept constant at values determined in Experiment I. Consequently, the same parameters were used for RL as for KT except for the spectral density of internal noise which was $25x10^{-6}$ for RL and $20x10^{-6}$ for KT.

The values of contrast restoration parameters γ and κ were kept constant at 0.001 and 1, respectively, as determined in Experiment I.

The smooth curves in Figures 4.9 and 4.10 show the model descriptions. In Figure 4.9 detection thresholds are plotted as the lowest data points (filled diamonds) together with the threshold descriptions of the model (R_d). In Figure 4.10 detection thresholds are plotted as the leftmost data points together with the restored contrast response predictions ($R_dH_r(f)$) when the standard was at its detection threshold (c=0.0025 for RL in A and c=0.0023 for KT in B). Both predictions are in close agreement with the detection threshold data. Contrast matching predictions are the same in both figures.

The explained variance was 0.995 and 0.994 in Figure 4.9(A) and (B), respectively, and 0.995 and 0.991 for the undisplaced data in Figure 4.10(A) and (B), respectively. The model descriptions were thus very accurate. Only the data for the smallest gratings shown by the uppermost curves in Figure 4.10(A) and (B) deviated slightly from the predictions at intermediate standard contrasts because the measured matching contrast of test gratings became equal to the physical contrast of the standard at a lower contrast level than what the model predicted. This may be related to the fact that the Fourier spectrum of a stimulus

becomes broader with decreasing stimulus area. The model does not take this phenomenon into account since it is designed for the use of narrow-band stimuli.

4.3.4 Discussion

Contrast matching results of Experiment I are in agreement with the findings of Watanabe et al. (1968) and Georgeson and Sullivan (1975). When gratings of various spatial frequencies are matched to a standard grating of a fixed spatial frequency, the matching curves resemble the detection threshold curve at low contrast levels, but at high contrast levels matching curves are flat indicating that perceived contrast is equal for gratings of equal physical contrast regardless of spatial frequency.

Contrast matching results of Experiment II are in agreement with Takahashi and Ejima (1984). In these studies it was found that at low contrast levels matches are influenced by the detection thresholds of gratings of various areas so that matching curves resemble contrast sensitivity (Takahashi & Ejima, 1984) or threshold (Experiment II) curves at low contrasts but at high contrast levels matches are independent of area. Takahashi and Ejima (1984) used a test grating of a constant size and standard gratings of various sizes, meanwhile in Experiment II there were test gratings of various sizes and a standard grating of a constant size. Consequently, Takahashi and Ejima (1984) found that less contrast was needed in the test grating of a constant size for a match when the standard grating was small than when it was large. In Experiment II it was found that more contrast was needed in the test grating for a match when it was small than when it was large relative to the standard grating of a constant size. Both results thus show that at low contrast levels perceived contrast is lower for a small grating than for a large grating of equal physical contrast.

On the other hand, Cannon and Fullencamp (1991b & 1993) have found an opposite effect at low contrast levels. According to their contrast matching results, apparent contrast is often higher for small than for large gratings. They found pronounced differences between observers, and concluded that individual differences determine whether the contrast of large gratings is enhanced or suppressed. Their results differ from those of Ejima and Takahashi (1985) who performed similar experiments, and found consistent contrast enhancement for large gratings at low contrasts. There is a procedural difference between these two studies which may account for the discrepancy in the results. Cannon and Fullencamp (1991b & 1993) presented the two stimuli to be compared sequentially in the same spatial location, meanwhile Ejima and Takahashi (1985) presented the stimuli simultaneously side by side. The mode of presentation may have large effects on

perceived contrast. In the pilot experiments of the present study both modes of presentation were used, and it was found that perceived contrast was higher for large gratings with a simultaneous presentation mode, but with a successive presentation mode apparent contrast was higher for small gratings. This phenomenon may be due to temporal interactions and/or local adaptation and will require further study.

When matching contrast was plotted as a function of standard contrast (see Figures 4.8 and 4.10), it could be seen that the increase in matching contrast was slower at low standard contrasts for gratings with high detection thresholds than for gratings with low thresholds. Matching contrast thus increased more slowly for high and low spatial frequencies and small gratings than for mid-frequencies and large gratings. Consequently, the physically correct contrast matches occurred at a higher standard contrast for gratings with high thresholds. This phenomenon is most easily seen at high spatial frequencies (8 and 16 c/deg) in Figure 4.8.

The above finding is in apparent conflict with a conclusion often made in studies on contrast magnitude estimation which states that the perceived contrast of a stimulus with a high threshold increases more steeply than the perceived contrast for a stimulus with a low threshold (e.g. Cannon, 1985). The conclusion is derived from plots of magnitude estimate versus stimulus contrast, where magnitude estimate is directly proportional to the magnitude of perceived contrast. A hypothetical example of a typical graph is shown in Figure 4.11(A), where the increase in perceived contrast with physical contrast is shown for gratings at 4 and 16 c/deg. The curve for the high-threshold stimulus (16 c/deg) rises initially more steeply than the curve for the low-threshold stimulus (4 c/deg), but at high stimulus contrasts the curves merge. The initial steep rise at 16 c/deg means that a certain change in the physical contrast of the stimulus produces a larger change in the perceived contrast (i.e. the magnitude estimate) for the high-threshold stimulus (16 c/deg) than for the low-threshold stimulus (4 c/deg). Or conversely, a certain change in the perceived contrast is produced by a smaller change of contrast for the high-threshold stimulus than for the low-threshold stimulus.

The results of contrast magnitude estimation are of course related to the results of contrast matching. A hypothetical result of contrast matching is shown in Figure 4.11(B) where matching contrast is plotted as a function of spatial frequency at various standard contrasts (c1-c4). The general trend is that matching curves become flatter as standard contrast is increased. Each matching curve measured at a constant standard contrast shows the physical stimulus contrasts which produce a constant perceived contrast. At low contrast levels when standard contrast is increased, for example from c1 to c2, the increase in the physical matching contrast is smaller for a high-threshold stimulus (e.g. 16 c/deg) than for

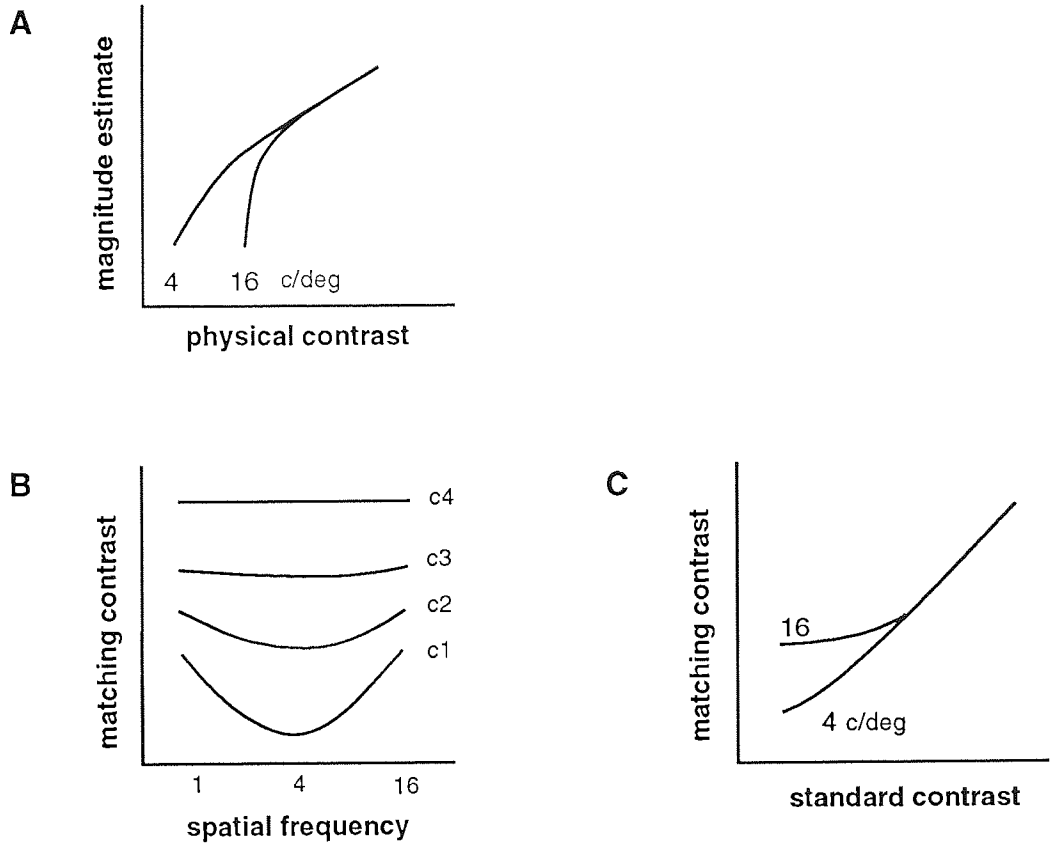

Figure 4.11 Comparison of magnitude estimation and contrast matching.

a low-threshold stimulus (e.g. 4 c/deg) even if the increase in perceived contrast is equal for both gratings. This is consistent with the results of magnitude estimation which show that a certain change in the magnitude estimate (e.g. a change corresponding to a change of standard contrast from c1 to c2) is produced by a smaller change of contrast at 16 c/deg than at 4 c/deg.

Matching contrast can also be plotted as a function of standard contrast, and when gratings of various spatial frequencies are matched to a standard of a fixed spatial frequency, the results are as shown in the hypothetical example of Figure 4.11(C). If compared to the magnitude estimation curves in Figure 4.11(A), the curves for 4 and 16 c/deg have been practically inverted in Figure 4.11(C). If these figures are compared superficially, the results shown in Figures 4.11(A) and (C) may seem opposite. A scrutiny of the figures reveals, however, that the difference is only due to an interchange of axes. That is, the magnitude estimate, i.e. perceived contrast in (A) corresponds to the standard contrast in (C), and the physical stimulus contrast in (A) corresponds to the matching contrast in (C). From both Figures 4.11(A) and (C) it can be deduced that at low contrast levels a certain

change in the standard (or perceived) contrast produces a smaller change in the matching (or physical) contrast for 16 than for 4 c/deg [cf. Figure 4.11(B)].

The above argument applies also to contrast magnitude estimation and matching results obtained with gratings of various areas. Thus, at low contrasts a certain change in the standard (or perceived) contrast produces a smaller change in the matching (or physical) contrast for a small grating (high-threshold stimulus) than for a large grating (low-threshold stimulus). But at high contrasts perceived contrast increases equally for small and large gratings.

The general finding in the contrast matching experiments presented here is that the detection thresholds of gratings of various spatial frequencies and areas influence contrast matches at low contrast levels, but at high contrast levels perceived contrast becomes independent of spatial frequency and stimulus area, and contrast matches are physically correct. This phenomenon can be accounted for by assuming that the visual system performs contrast restoration. That is, the visual system attempts to compensate for the degradations caused by early signal processing so that perceived contrast would be directly proportional to the physical contrast of the stimulus. However, restoration is effective only at high contrast levels. The contrast restoration model introduced in Section 4.1 exhibits this behaviour, and it described the contrast matching results very accurately.

4.4 Contrast matching of achromatic luminance and chromatic isoluminant gratings of various spatial frequencies

4.4.1 Introduction

Isoluminant chromatic stimuli are used to study the visual system's responses to exclusively chromatic stimulation with no luminance information. Isoluminant chromatic cosine gratings are composed of two sinusoidal luminance gratings modulated in counterphase. The wavelength of each grating is different but the luminance contrast is equal in both gratings. Chromaticity thus varies across the grating but luminance remains constant. The contrast of a chromatic grating is usually taken as the luminance contrast of one of its components. This is an arbitrary measure because the maximum contrast of the chromatic grating does not depend on the extreme colour coordinates chosen for the stimulus. However, it has been shown to describe contrast rather well, especially when the results are normalised relative to the detection threshold (Switkes, Bradley & DeValois, 1988; Mullen, 1991; Mullen & Losada, 1994).

When chromatic stimuli are used, the chromatic aberrations of the ocular optics cause problems because they introduce wavelength-dependent blur and consequently a reduction in contrast at blurred wavelengths. Transverse chromatic aberration refers to a difference of magnification for different wavelengths. It is negligible in foveal vision for small stimuli, for example for gratings extending less than 5 degrees from fixation (Thibos, Bradley, Still, Zhang & Howarth, 1990). Longitudinal chromatic aberration refers to a difference of focus for different wavelengths. The difference of focus can be quite large. For example, across wavelengths from 400 to 700 nm it amounts to 2 dioptres (for a review see Charman, 1991; Thibos, Ye, Zhang & Bradley, 1992). Longitudinal chromatic aberration can also introduce luminance artefacts into isoluminant stimuli especially at high spatial frequencies because the accommodation system of the eye can bring one colour into focus so that the other colour becomes blurred which reduces its contrast (Cavanagh, 1991). Transverse chromatic aberration can be corrected by adjusting the stimulus size at different wavelengths, and longitudinal chromatic aberration by focusing each wavelength on the retina with lenses of appropriate powers (Mullen, 1985).

An observer's performance with isoluminant chromatic stimuli is often compared with his performance with luminance modulated stimuli in order to investigate the differences between luminance and colour processing. For example, the contrast threshold curve measured as a function of spatial frequency is different for luminance and chromatic cosine gratings.

Contrast detection thresholds for luminance modulated gratings are lowest at spatial frequencies of about 4 c/deg, and they increase at higher or lower frequencies (Campbell & Robson, 1968). The contrast sensitivity function is thus band-pass in shape. The low-frequency increase in thresholds is due to lateral inhibition which attenuates spatially slow luminance gradients, i.e. low spatial frequencies (Ratliff & Hartline, 1959). The high-frequency increase in thresholds is caused by the optical transfer function which attenuates high spatial frequencies (e.g. Banks, Geisler & Bennett, 1987).

Dependence of chromatic contrast thresholds on spatial frequency has been thoroughly investigated by Mullen (1985). She measured thresholds for red-green and yellow-blue isoluminant cosine gratings whose spatial frequencies ranged from 0.09 to 7 c/deg. Chromatic contrast thresholds remain constant at low spatial frequencies, and start to increase when spatial frequency is increased above about 0.8 c/deg. Chromatic contrast sensitivity functions are thus low-pass in shape. The low-pass shape of colour contrast sensitivity functions is normally attributed to the absence of lateral inhibition for chromatic stimuli (e.g. Cavanagh, 1991).

According to Mullen (1985), thresholds are lower for red-green than yellow-blue gratings up to about 5 c/deg after which they are equal for both. Chromatic contrast thresholds are lower than luminance thresholds up to 0.5 c/deg, above which thresholds become higher for chromatic than luminance gratings.

The high spatial frequency cut-off is much lower for chromatic than for luminance gratings even when the ocular chromatic aberrations are corrected. According to Mullen and Kingdom (1991) the high-frequency cut-off occurs at about 12 c/deg for both red-green and yellow-blue isoluminant gratings, and at about 36 c/deg for luminance modulated gratings. Possible reasons for the lower chromatic resolution are differences in the cone sampling density and in the neural modulation transfer function. The sampling density is higher for luminance modulated than for chromatic stimuli since for chromatic stimuli an opponent signal has to be involved with input from at least two receptors which leads to a lower resolution (Mullen & Kingdom, 1991). The neural modulation transfer function is high-pass for luminance modulated stimuli (Rovamo, Mustonen & Näsänen, 1995), and it has been postulated to be less dependent on spatial frequency for chromatic stimuli, or in other words, lateral inhibition is assumed to be absent or weak for chromatic stimuli (e.g. Cavanagh, 1991). Support for this assumption will be given later in this chapter. Because of this difference in the neural modulation transfer function, chromatic stimuli lack the relative amplification at high spatial frequencies which increases the resolution limit for luminance modulated stimuli. Also, it should be taken into account that the large

differences in chromatic and luminance resolution and sensitivity may at least partly be due to the measure of chromatic contrast used to describe the results (Mullen & Kingdom, 1991).

Contrast matching of achromatic luminance gratings of various spatial frequencies yields matching curves which resemble the detection threshold curve at low contrasts but which are flat at high contrasts (e.g. Georgeson & Sullivan, 1975). Isoluminant chromatic gratings have not been previously used in contrast matching experiments.

However, the matching technique has been used to study the relationship between chromaticity, light intensity and perceived brightness (Guth, 1967; Boynton & Kaiser, 1968). In heterochromatic brightness matching two uniform fields of light with different chromaticities are juxtapositioned, and one of them is adjusted in radiance until the fields seem equal in brightness. The aim of these experiments is to determine the radiances of lights of various wavelengths which produce an equal sensation of brightness. In order to determine a function relating radiance to perceived brightness, it must be assumed that the function is additive. That is, when two fields equated in perceived brightness are superimposed, their luminances should add linearly (Abney's law), i.e. the superimposed fields should look equal in brightness to one of the fields doubled in radiance. However, this is not always true in brightness matching, especially when complementary lights are used. For example, if a red and a green field are both adjusted to match a white field in brightness, and then superimposed, the mixture should appear equal in brightness to the white field doubled in radiance. Instead, the mixture seems less bright than the white field doubled (Boynton, 1979). Thus, brightness matches have not been successful with chromatic stimuli because of the additivity failure. Also, the great variance in adjustments makes the measurements unreliable (Boynton & Kaiser, 1968).

This study was designed to investigate two questions. First, can contrast matching technique be reliably used to investigate the perceived contrast of isoluminant chromatic gratings? And second, are contrast matching functions similar for isoluminant chromatic as for achromatic luminance gratings of various spatial frequencies? Furthermore, the contrast restoration model was applied to the results of this experiment.

4.4.2 Methods

4.4.2.1 Apparatus

Stimuli were produced by a Venus Visual Stimulator (Neuroscientific Ltd.) and presented on the face of a Princeton 14" RGB monitor. Presentation and stimulus generation were controlled by a 386-PC using application software written and compiled in Microsoft C. The stimuli consisted of black-and-white and coloured gratings, modulated either along a red-green (constant S-cone) axis or along yellow-blue (tritanopic confusion) axis. The extent of colour modulation was limited by the phosphors of the monitor. At the maximum available modulation, the red-green stimulus varied between CIE 1931 chromaticity coordinates of (0.451, 0.269) and (0.237, 0.379) whilst the equivalent coordinates for the yellow-blue stimulus were (0.417, 0.503) and (0.233, 0.126). The point of intersection of the red-green and yellow-blue axes was at the white point of (0.33, 0.33) in chromaticity coordinates. Black-and-white gratings were luminance modulated at the white point.

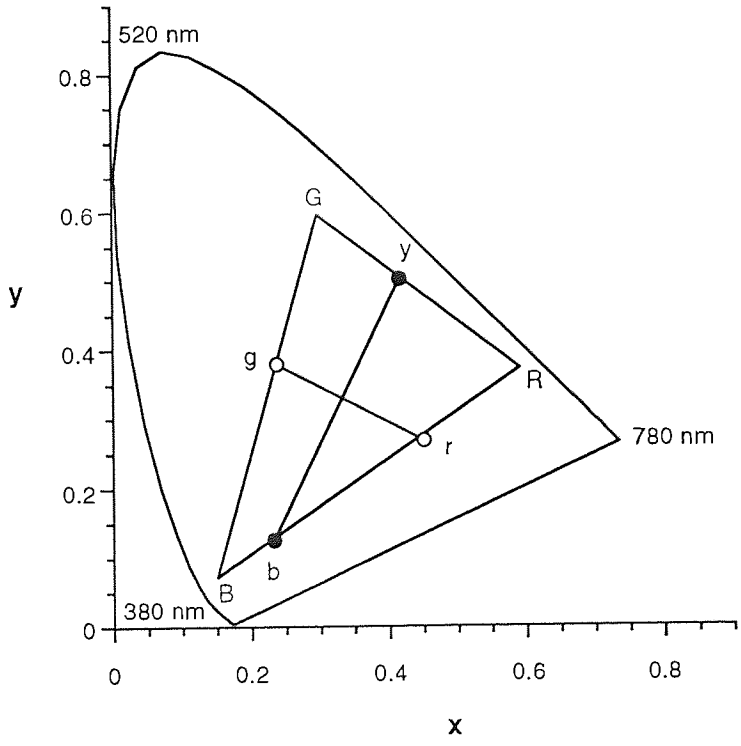

Figure 4.12 CIE chromaticity coordinates for the colour matching stimuli.

A CIE chromaticity diagram showing the axes of chromatic modulation is depicted in Figure 4.12. The colours realisable with the monitor phosphors are encompassed within the triangle RGB. The red-green (r-g) modulation axis is shown by a line connecting the open circles. The yellow-blue (y-b) modulation axis is shown by a line connecting the filled circles.

Stimuli were presented on a square-shaped background the extent of which was 18 cm x 18 cm and the mean luminance was 9.0 cd/m^2. Outside this background the screen was black. The background colour for the chromatic gratings was chosen to be the mean colour of the two components. When two different grating types were shown simultaneously, the screen was divided into two halves, and the background of each half-screen was the mean colour of the grating presented. Mean luminance remained constant at 9.0 cd/m^2.

4.4.2.2 Stimuli

The stimuli were horizontal circular sinusoidal gratings with a diameter of 8 cm. At the viewing distance of 250 cm the grating area was 2.64 deg^2.

Chromatic gratings were created by adding two luminance modulated sine gratings of equal contrasts 180° off phase. Colour contrast of the stimuli was defined as the luminance contrast of one of the components. Luminance contrast was given as Michelson contrast by the computer, and transformed into r.m.s. contrast by multiplying the Michelson contrast by 0.707 (for further details see Appendix I).

In contrast matching experiments two stimuli were presented simultaneously on the screen. The stimulus on the left was the standard grating which had a constant contrast. The stimulus on the right was the test grating which was adjusted in contrast to apparently match the standard. Each of the three grating types, black-and-white (BW), red-green (RG) and yellow-blue (YB), was matched to a standard of the same type at various spatial frequencies.

Standard gratings were of a fixed spatial frequency at 2 c/deg. Each standard grating type had four contrast levels: 2, 4, 8 and 16 times its detection threshold.

Test gratings were presented at various spatial frequencies. For the BW and RG gratings the frequencies were 0.5, 1, 2, 4 and 8 c/deg. For the YB gratings only frequencies 0.5, 1, 2 and 4 c/deg were used. This was because at spatial frequencies higher than 4 c/deg

the longitudinal chromatic aberration of the eye's optics may have caused unwanted luminance artefacts in the YB grating (Cavanagh, 1991).

Contrast detection thresholds were measured for all gratings used in the experiments. In detection threshold measurements and in contrast matching the phase of both gratings varied randomly from one presentation to another.

4.4.2.3 Procedure

The experiments were performed monocularly with the dominant eye and with the optimal spectacle correction at the viewing distance used. The subjects, PM and KT, used the right eye and wore a spectacle correction of -2.25 DS and -6.75 DS, respectively. Both subjects had normal colour vision when tested with the Ishihara test for colour deficiency. Both subjects performed the experiments with black-and-white luminance modulated and red-green isoluminant gratings. Subject KT also performed further experiments using yellow-blue isoluminant gratings.

4.4.2.3.1 Determination of subjective isoluminance

Heterochromatic flicker photometry was used to determine the subjective isoluminant points for the chromatic gratings at all spatial frequencies used. This procedure was undertaken to ensure that luminance modulation artefacts within the stimuli were minimised. The following explanation will take the red-green colour grating as an example. The same procedure was used for the yellow-blue stimuli.

A horizontal sinusoidal red-green grating was presented on the screen which was divided into eight vertical strips of equal width. The photometrically measured luminance ratio between the red and green colours comprising the grating varied between strips, and ranged from 0.3 log units below photometric isoluminance in the extreme left-hand strip (i.e. a red-green ratio of 0.5) to 0.3 log units above photometric isoluminance in the extreme right-hand strip (a red-green ratio of 2). Mean luminance across the grating was maintained at 9.0 cd/m^2. Thus when the red-green ratio was 0.5, the mean luminance of red and green components were 3 and 6 cd/m^2, respectively. The red-green ratio in the intermediate strips was varied sequentially from left to right in 1.26 logarithmic steps. The whole stimulus was then made to counterphase at a temporal frequency of 16 Hz. At such a high temporal frequency, any residual luminance modulation within the stimulus produces a strong sensation of flicker, whereas flicker is minimum or absent at subjective isoluminance.

The observer was asked to report which of the eight strips of grating was flickering the least, and the red-green photometric ratio in this strip was taken to represent an estimate of the observers subjective isoluminant point. The procedure was then repeated but this time the range of luminance ratios was reduced to 0.15 log units on either side of the newly obtained estimate of isoluminance. The procedure was again repeated, each time reducing the logarithmic range of luminance ratios by half, until the observer could no longer distinguish between the amount of residual flicker in any of the strips. The luminance ratio at the centre of the screen was then taken as the observers final isoluminant point, and this luminance ratio was used in all subsequent experiments. The luminance ratios for the two subjects are shown in Table 4.3. The red-green and yellow-blue ratios decreased with spatial frequency, in agreement with Mullen (1985).

c/deg	r-g ratio for PM	r-g ratio for KT	y-b ratio for KT
0.5	0.95	0.95	1.14
1	1.00	0.95	1.11
2	1.00	0.90	1.02
4	0.82	0.79	0.91
8	0.91	0.78	-

Table 4.3 Red-green luminance ratios for PM, and red-green and yellow-blue luminance ratios for KT.

4.4.2.3.2 Contrast detection threshold measurement

Contrast detection thresholds for the gratings used in the matching experiments were determined using a split-screen forced-choice paradigm. A grating was presented either on the right or left side of the display screen, and the observer's task was to indicate on which side the grating had appeared. Contrast was ramped up in a linear fashion and remained at its maximum until the observer responded, after which it ramped down to zero, again in a linear manner. Initial presentations were always clearly suprathreshold. The initial step size was 0.15 log units, but this decreased to 0.075 log units after the first incorrect response which also caused the contrast to increase by one step. Three successive correct responses were then required before the contrast of the subsequent presentation was reduced, whereas a single incorrect response led to an increase in contrast. The sequence continued in staircase fashion until 5 reversals had occurred, after which the sequence terminated and threshold contrast required for the probability of 0.79 percent correct was

calculated as the arithmetic mean of the final 4 reversals (Wetherill and Levitt, 1965). The final data represent the geometrical mean of four threshold estimates.

Two threshold estimations were randomly interleaved. A sound signal accompanied stimulus exposures. There was no feedback about the correctness of responses.

The criterion level of 0.79 percent correct corresponds to a detectability index of 1.14 (Elliott, 1964). In the other experiment of this thesis d' was always 1.4. This difference was taken into account when calculating the predictions of the contrast restoration model.

4.4.2.3.3 Contrast matching paradigm

Contrast matching was performed using the method of adjustment. The standard grating was presented on the left and the test grating on the right side of the screen. In the beginning of the experimental session, contrast of the standard grating was set to a desired multiple of threshold. In one session all possible stimulus pairs were shown in a random order. That is, all three test grating types at all spatial frequencies were matched to the standard grating of the same type at a multiple of threshold.

For each stimulus pair, the initial contrast of the test grating was chosen randomly from an even distribution extending ±0.5 log units from the standard contrast. Contrast of the test was increased by pressing one in a set of three keys on the keyboard and reduced by pressing one in another set of three keys. The three keys changed the contrast in 0.06, 0.02 and 0.01 log unit steps. When the contrast of the test appeared equal to that of the standard, the subject pressed an 'end'-key, the matching contrast was recorded, and another stimulus pair was displayed to be matched. When all stimulus pairs had been shown once, the session ended, and the matching contrasts were displayed and printed.

Viewing time was unlimited. In most conditions matching could be done very quickly, however. Normally the stimuli remained on the screen for less than 500 msec before the test contrast level was changed. There was a pause of about 1500 msec before the next contrast level was displayed during which the screen remained at the mean colour and luminance level of the grating to be displayed. This reduced contrast adaptation caused by extended exposure to high-contrast stimuli.

Adaptation effects were minimised also by other means. The stimulus pairs were matched in a random order, and all possible stimulus pairs were matched only once in a session, so that the same stimulus pair was never shown twice straight after each other. This also prevented any effects of learning or memorising since it was impossible for the subjects to remember how they had adjusted the contrast last time the condition was shown.

Matching sessions were arranged so that the standard contrast was always set at 2 times threshold first, and then at higher multiples. Matching was done four times for each condition, and the final data represent the geometrical mean of the matching contrast estimates.

4.4.3 Results

4.4.3.1 Contrast matching of isochromatic black-and-white and isoluminant red-green and yellow-blue gratings

The results of contrast matching of black-and-white luminance gratings at spatial frequencies ranging from 0.5 to 8 c/deg are shown in Figure 4.13. The subject was KT in 4.13(A), and PM in 4.13(B). The results were very similar to those presented in Figure 4.7 in this chapter where contrast matching was done with similar stimuli. As Figure 4.13 shows, the detection threshold curve (filled diamonds) was band-pass in shape with the minimum at about 2-4 c/deg. When standard contrast was set at twice the detection threshold (open circles), matching curves resembled the threshold curve. Matching curves became gradually flatter as standard contrast was increased to 4 (filled squares), 8 (open diamonds) and 16 (filled circles) times above threshold. The reason why the matching curves did not become totally flat was that standard contrasts higher than 16 times threshold were not used. In Figure 4.7 the matching curves became flat when the standard was more than 50 times above threshold.

The contrast restoration model was applied to the results of Figure 4.13. The model parameter values that yielded the best fit to the data are shown in Table 4.4. The maximum of the critical number of square cycles in the integration function (z_0), the critical spatial frequency in the integration function (f_0) and the maximum efficiency (η_{max}) were kept constant at values chosen in Section 4.3.3.

The critical spatial frequency of the optical transfer function (f_c) was found to be slightly lower for KT here than in Section 4.3 (6 instead of 7 c/deg). For PM f_c was 5.5 c/deg. The exponent in the optical transfer function (n) was equal to 3 for both subjects, thus remaining at the same value for KT as in section 4.3.

The spectral density of internal noise (N_i) was determined so that the experimental data and the model descriptions coincided in the vertical direction in Figure 4.13. For subject PM the value of N_i was 46×10^{-6}. For subject KT, who performed both this and the previous experiments, the value of N_i here was found to be 92×10^{-6}. This value was

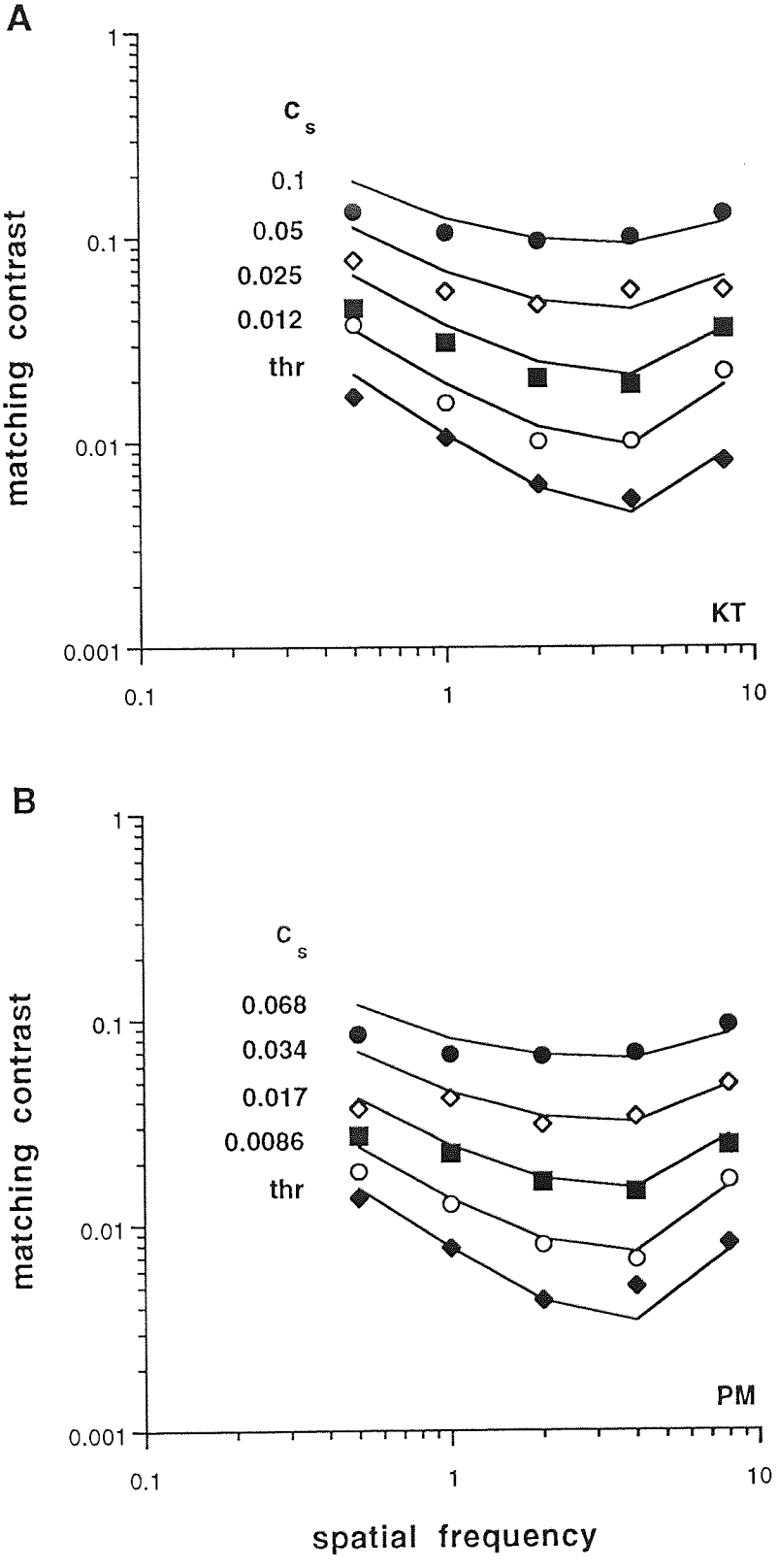

Figure 4.13 Contrast matching of achromatic luminance gratings.

considerably higher than the previous values which were $17x10^{-6}$ in Section 4.2, and $6x10^{-6}$ (Table 4.1) and $20x10^{-6}$ (Table 4.2) in Section 4.3.

A higher value for internal noise means that contrast sensitivity for KT was lower in this experiment than in the previous experiments. There are many possible reasons for the difference. First, these experiments were performed monocularly, not binocularly like the previous experiments. Monocular contrast sensitivity is lower than binocular approximately by a factor of 1.5 (Legge, 1984a). Second, the mean luminance of the screen in these experiments was 9 cd/m^2 instead of 50 cd/m^2, and contrast sensitivity decreases with decreasing luminance level (e.g. van Nes & Bouman, 1967). The lower screen luminance may have been partly compensated for by an increase in pupil size, however. Third, small differences in the calibration of the two apparatuses used in this and previous experiments may have caused differences in contrast sensitivity. And fourth, the day-to-day variability in the observer's performance, due to various factors such as the observer's alertness and motivation at the time of the experiment, may affect the performance quite considerably.

When the threshold descriptions had been obtained, contrast matching descriptions were calculated. The parameters γ and κ were set at the same values as in Section 4.3. The constant γ was equal to 0.001. The exponent κ depended on spatial frequency f according to $\kappa=1+0.0014f^2$.

Parameter	KT	PM
f_c	6	5.5
n	3	3
N_i	$92x10^{-6}$	$46x10^{-6}$
z_0	60	60
f_0	0.5	0.5
η_{max}	0.4	0.4
γ	0.001	0.001
κ	$1+0.0014f^2$	$1+0.0014f^2$

Table 4.4 Model parameters for KT and PM in luminance grating matching.

The smooth curves in Figure 4.13 are the descriptions of the model. The explained variance was 0.964 and 0.946 in Figures 4.13(A) and (B), respectively. The model predictions were thus generally quite accurate. However, at 0.5 c/deg the predictions deviated from the experimental data. They were higher than the data at almost all contrast levels. This may be due to the fact that in the 0.5 c/deg grating there was less than one square cycle since the grating was only 0.9 cycles wide. Since the Fourier spectrum becomes broader as the number of grating cycles decreases, the bandwidth for the grating was quite broad. Consequently, other spatial frequencies may have contributed to contrast perception at 0.5 c/deg, so that the detection thresholds and matching contrasts were lower than if the grating had been narrow-band. Consequently, the model predictions were too high because the model is designed for narrow-band stimuli only. In Experiment I in Section 4.3 there were 3 square cycles in the 0.5 c/deg grating so that the bandwidth was narrower and this problem did not occur.

Next, contrast matching was performed with isoluminant chromatic gratings. The task proved to be easy. Colour contrast seemed to be a concept which was instinctively understood. The variability in contrast matches was very similar for all grating types. For subject PM, the average relative standard error of the mean ($\overline{SE}$) for luminance matching was 6.6 %, and for red-green matching it was 9.8 %. For subject KT the $\overline{SE}$ was 5.6 % for luminance, 6.2 % for red-green and 4.4 % for yellow-blue matching. The standard errors were thus quite small, so that contrast matches were equally reliable.

In Figure 4.14 matching contrasts of red-green test gratings are plotted as a function of test spatial frequency at various contrast levels of the red-green standard. The subject was KT in 4.14(A), and PM in 4.14(B). Detection thresholds are plotted as the lowest data points (filled diamonds). Thresholds remained constant up to about 1 c/deg after which they started to increase. Contrast matching curves resembled the threshold curve at low levels of standard contrast, but at high contrast levels they became flat. Hence, contrast matching with red-green gratings exhibited a similar behaviour as matching with black-and-white gratings. However, the flattening of matching curves occurred at a lower contrast level, respective to the threshold, for the red-green than black-and-white gratings. The matching curves were rather flat already when standard contrast was 2 times above threshold (open circles), and they continued to flatten as standard contrast was increased to 4 (filled squares) and 8 (open diamonds) times above threshold. When standard contrast was 16 times above threshold (filled circles), matching curves were flat and independent of spatial frequency.

In Figure 4.15 matching contrasts of yellow-blue test gratings are plotted as a function of test spatial frequency at various contrast levels of the yellow-blue standard for subject KT.

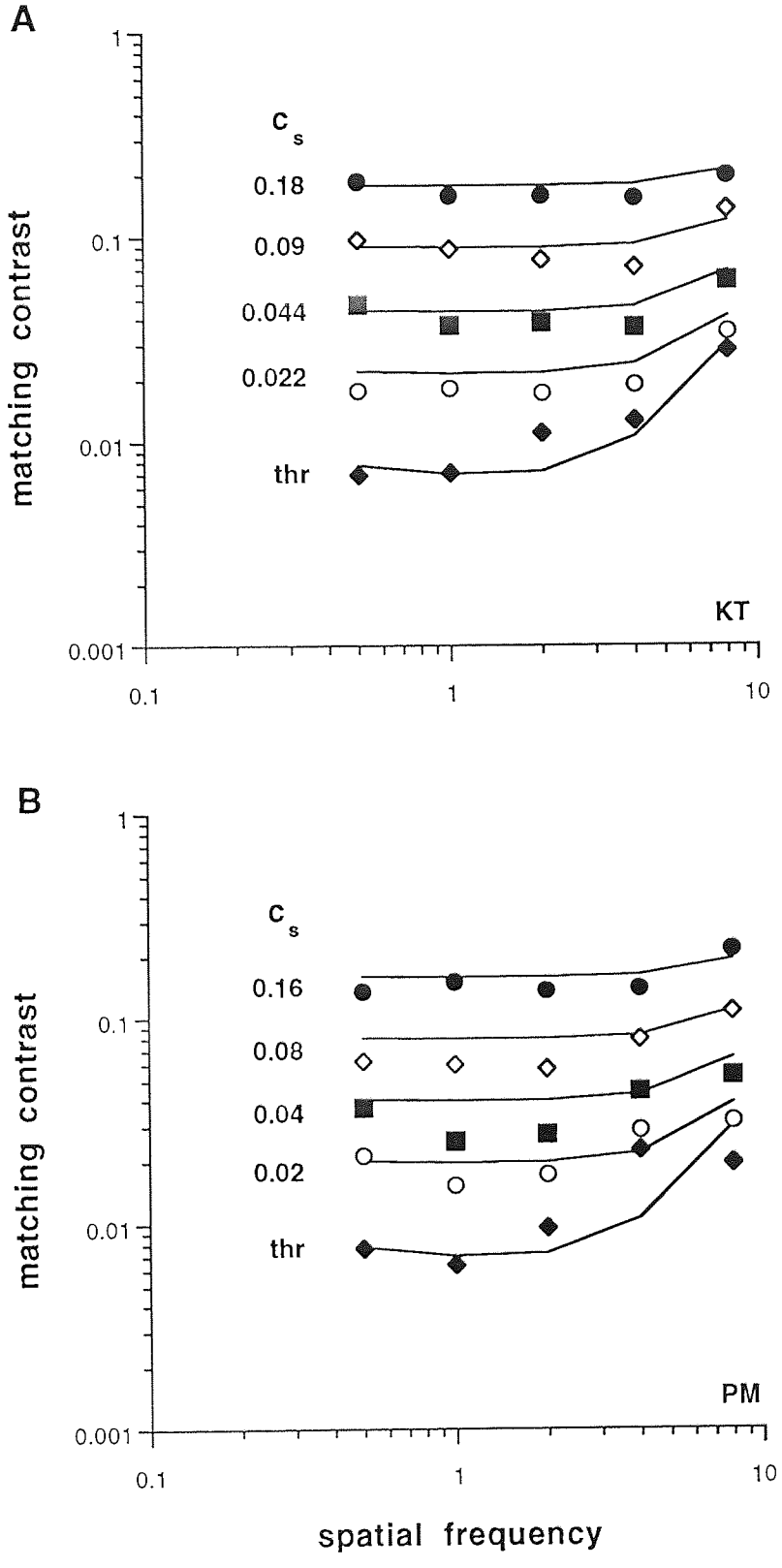

Figure 4.14 Contrast matching of isoluminant red-green gratings.

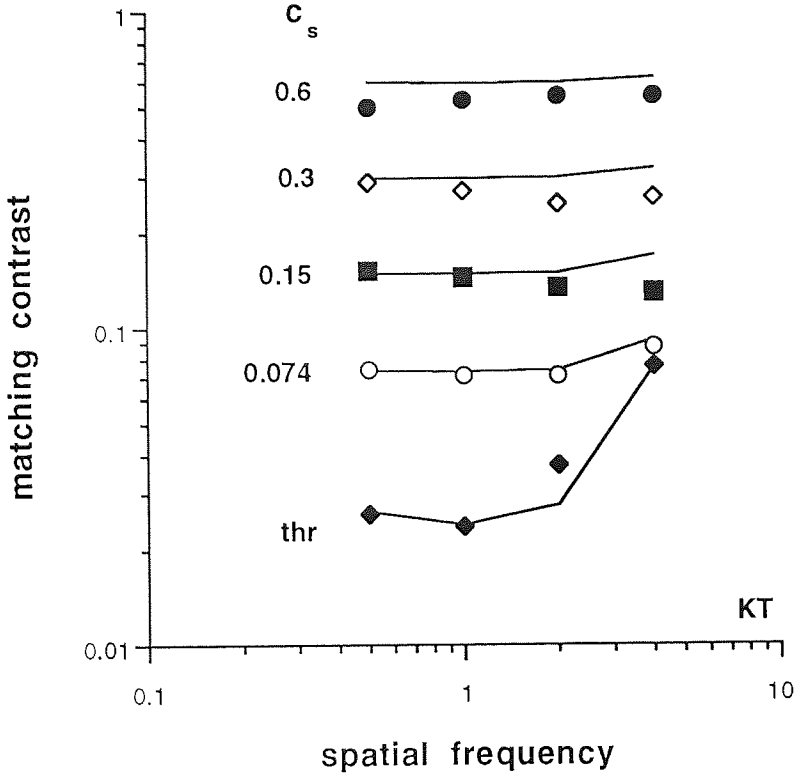

Figure 4.15 Contrast matching of isoluminant yellow-blue gratings.

Detection thresholds are plotted as filled diamonds. Thresholds were almost equal for 0.5 and 1 c/deg, but started to increase for 2 and 4 c/deg. Contrast matching results obtained with yellow-blue gratings were similar to the results obtained with red-green gratings but the flattening of contrast matching curves was even more rapid. When standard contrast was 2 times above threshold (open circles), the matching curve was quite flat already. Only at the highest spatial frequency did the threshold have an effect on the matching contrast. As standard contrast was increased to 4 (filled squares), 8 (open diamonds), and 16 (filled circles) times above threshold, the matching curves were practically flat.

The contrast restoration model was applied to the chromatic contrast matching results. First, however, the model had to be modified to account for the difference in the contrast threshold curves for luminance and chromatic gratings which are band-pass and low-pass in shape, respectively.

4.4.3.2 The neural modulation transfer function for luminance modulated and isoluminant chromatic gratings

Ganglion and lateral geniculate nucleus cell responses are different to luminance and colour stimuli, and this is reflected in their sensitivities to various spatial frequencies (e.g. DeValois & Jacobs, 1984; Boynton, 1979). The receptive field organisation of these cells is antagonistic for luminance variations and synergic for colour variations. The centre-surround antagonism, which can also be called lateral inhibition, produces low-frequency attenuation. The synergic action means that increases in stimulus size above the optimum have little or no effect on the cell response, so that there is practically no lateral inhibition and thus no low-frequency attenuation within the receptive field. This implies that the neural modulation transfer function is independent of spatial frequency for chromatic gratings.

According to the contrast restoration model, it should be possible to determine how the chromatic neural modulation transfer function depends on spatial frequency by comparing luminance and chromatic contrast detection thresholds measured at various spatial frequencies. The rationale behind this hypothesis is that, according to Equation (4.10b) in Section 4.1, in the absence of external spatial and quantal noises, contrast detection thresholds are determined by:

$$c = \sqrt{\frac{d'^2 N_i}{H_o^2(f) H_n^2(f) A\eta(z)}} \tag{4.13}$$

If chromatic aberrations of the ocular optics are corrected, the optical modulation transfer function is equal for luminance and colour gratings. Spatial integration has been found to be similar for luminance and chromatic gratings (Noorlander, Heuts & Koenderink, 1980; Mullen, 1991; Sekiguchi, Williams & Brainard, 1993). The detection efficiency is equal for luminance and chromatic stimuli (Gegenfurtner & Kiper, 1992). Thus, the only differences in the visual processing of luminance and chromatic gratings are in the neural modulation transfer function and the amount of internal neural noise. Consequently, contrast detection thresholds for luminance and chromatic gratings are determined by:

$$c_L = \sqrt{\frac{d'^2 N_{iL}}{H_o^2(f) H_{nL}^2(f) A\eta(z)}} \tag{4.14}$$

and

$$c_K = \sqrt{\frac{d'^2 N_{iK}}{H_o^2(f) H_{nK}^2(f) A\eta(z)}} \tag{4.15}$$

where c_L is the detection threshold, N_{iL} is the spectral density of internal noise and $H_{nL}(f)$ is the neural modulation transfer function for a luminance modulated grating, and c_K is the detection threshold, N_{iK} is the spectral density of internal noise and $H_{nK}(f)$ is the neural modulation transfer function for an isoluminant chromatic grating.

By combining Equations (4.14) and (4.15) we get the ratio of luminance and colour thresholds:

$$\frac{c_K}{c_L} = \frac{H_{nL}(f)\sqrt{N_{iK}}}{H_{nK}(f)\sqrt{N_{iL}}} \tag{4.16a}$$

Since internal noise is assumed to be white, its spectral density is constant across spatial frequency so that the ratio $\frac{\sqrt{N_{iK}}}{\sqrt{N_{iL}}}$ can be denoted by a constant b:

$$\frac{c_K}{c_L} = b\,\frac{H_{nL}(f)}{H_{nK}(f)} \tag{4.16b}$$

Equation (4.16b) means that the ratio of detection thresholds gives the ratio of the neural modulation transfer functions for luminance and colour multiplied by a constant. The square of constant b gives the ratio of the internal noise for the chromatic grating to the internal noise for the luminance grating.

It is known that $H_{nL}(f)=f$ (e.g. Rovamo, Mustonen & Näsänen, 1995). Here it is now assumed that $H_{nK}(f)=f^d$, where the exponent d describes the dependence of $H_{nK}(f)$ on spatial frequency. Thus, Equation (4.16b) can be written as:

$$\frac{c_K}{c_L} = b\frac{f}{f^d} = b\,f^{1-d} \tag{4.16c}$$

The constant b and the exponent d were determined with the aid of the contrast sensitivity data measured by Mullen (1985) as a function of spatial frequency for green luminance modulated and isoluminant red-green gratings. Mullen's data were used for this purpose because her luminance and chromatic contrast sensitivity functions were measured in conditions where both longitudinal and transverse chromatic aberration of the eye had been corrected so that the optical modulation transfer function was equal for luminance and

colour gratings. Since Mullen (1985) used gratings of equal sizes for both luminance and chromatic gratings, the effect of spatial integration was equal for both grating types.

Michelson contrast sensitivities measured by Mullen (1985) were first transformed into Michelson contrast detection thresholds by taking the inverse, and then into r.m.s contrast detection thresholds by multiplying Michelson contrasts by 0.707. This was done in order to facilitate comparison with the other figures of this thesis in which r.m.s. contrast thresholds are plotted.

When the ratio c_K/c_L was plotted as a function of spatial frequency as shown in Figure 4.16, the data fell on a straight line with a slope of 0.8 and intercept equal to 2.2. By solving Equation (4.14), it was found that b=2.2 and d=0.2. Thus, the neural modulation transfer function for chromatic gratings is proportional to $f^{0.2}$. If d had been equal to zero, $H_{nK}(f)$ would have been independent of spatial frequency. Instead, $H_{nK}(f)$ depends on spatial frequency but much more weakly than $H_{nL}(f)$.

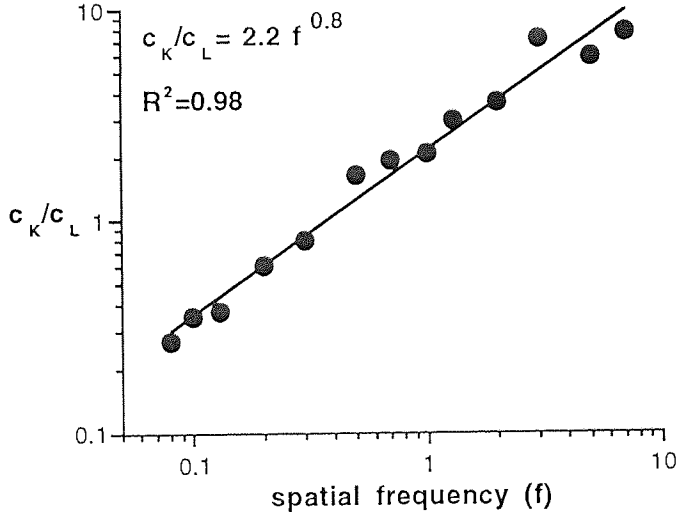

Figure 4.16 Ratio of chromatic to luminance detection thresholds (data from Mullen, 1985).

The hypothesis that a difference in the neural modulation transfer function only can account for the difference in the shape of the detection threshold curves for luminance and chromatic gratings was tested with the aid of the luminance and chromatic contrast threshold data from Mullen (1985). If the hypothesis is correct, it should be possible to

transform a luminance contrast threshold curve into a chromatic contrast threshold curve simply by multiplying the luminance contrast thresholds by the ratio of luminance to chromatic neural modulation transfer function. And conversely, it should be possible to transform a chromatic contrast threshold curve into a luminance contrast threshold curve by multiplying the chromatic thresholds by the ratio of chromatic to luminance neural modulation transfer function. In addition, the different spectral densities of internal noise have to be taken into account to superimpose the curves.

The original and transformed data from Mullen (1985) are shown in Figure 4.17. Figure 4.17(A) shows contrast detection thresholds for green luminance modulated gratings (open circles) and for red-green isoluminant gratings (filled squares) plotted as a function of spatial frequency. Figure 4.17(B) replots the detection thresholds for luminance gratings (open circles). The other set of data (filled circles) shows the transformed thresholds for the red-green chromatic gratings. The transformed data were obtained by first dividing the chromatic thresholds by $f^{0.8}$. This converted the low-pass chromatic curve into a band-pass curve which had the same shape and x-axis position as the luminance threshold curve but it was situated above the luminance curve. To superimpose the curves, the transformed curve was divided by a factor of 2.2 which was the mean difference in the vertical direction between the two curves. This operation takes into account the differences in internal noise. The luminance threshold curve and the transformed colour curve then collapsed together, as can be seen in Figure 4.17(B).

Figure 4.17(C) replots the detection thresholds for isoluminant red-green gratings (filled squares). The other set of data (open squares) shows the transformed thresholds for the luminance gratings. The transformed data were obtained by multiplying the luminance thresholds by $f^{0.8}$ and then by a factor of 2.2. The colour threshold curve and the transformed luminance curve were then quite accurately superimposed.

The same procedure was also applied to the yellow-blue data of Mullen (1985), and the results were very similar with b equal to 2.7 and d equal to 0.2 (results not shown). By changing the neural modulation transfer function only and taking into account the differences in internal noise, it was possible to transform a luminance threshold curve into yellow-blue threshold curve and vice versa.

In order to be able to change the neural transfer function in the contrast restoration model, Equation (4.3) was written as:

$$H_n(f) = f^d \qquad (4.16)$$

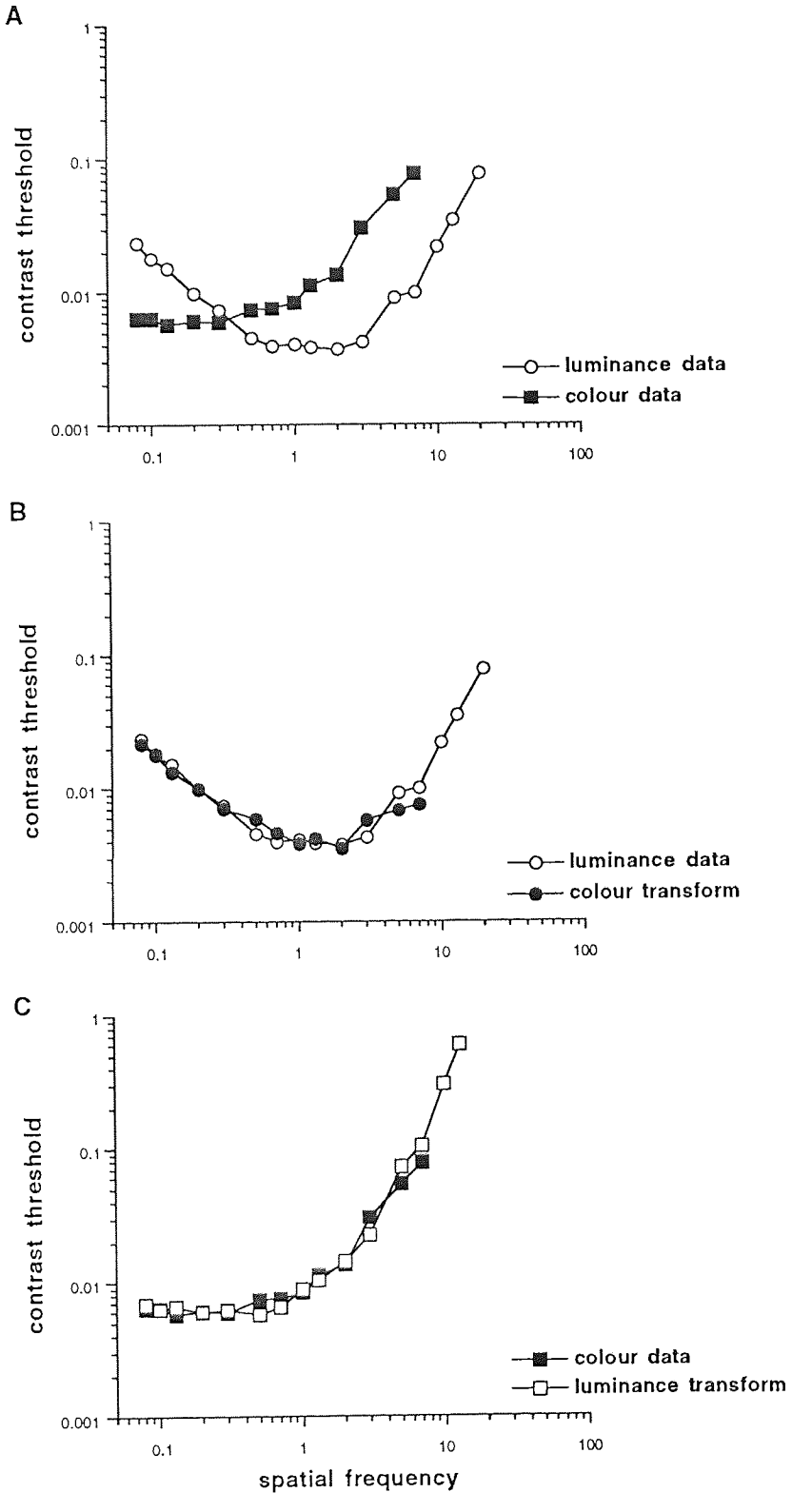

Figure 4.17 Transformations of luminance and colour detection threshold data of Mullen (1985).

For luminance gratings the exponent of the neural transfer function d was 1 so that the neural transfer function was directly proportional to spatial frequency. For colour gratings d was 0.2 so that the neural transfer function increased very slowly with spatial frequency. After this modification, the model could be applied to the colour contrast matching results.

4.4.3.3 Application of the contrast restoration model to the results of chromatic contrast matching

The contrast restoration model was applied to the results of chromatic contrast matching. First, the best values for the model parameters determining the detection thresholds were found. The exponent of the neural modulation transfer function was set at 0.2 as determined in Section 4.4.3.2. Next, the best values for the restoration parameters were determined. Fitting of the model parameters is first described for red-green gratings, and the values found are shown in Table 4.5.

Parameter	KT	PM
f_c	5	5
n	2	2
N_i	$35x10^{-6}$	$35x10^{-6}$
z_0	60	60
f_0	0.5	0.5
η_{max}	0.4	0.4
γ	0.01	0.01
κ	1	1

Table 4.5 Model parameters for KT and PM in red-green grating matching.

Spatial integration is similar for achromatic luminance and chromatic isoluminant gratings (Noorlander et al., 1980; Mullen, 1991; Sekiguchi et al., 1993). Detection efficiency is equal for luminance and chromatic stimuli (Gegenfurtner & Kiper, 1992). Consequently, the values for spatial integration parameters (z_0, f_0, η_{max}) were equal for all grating types.

For red-green gratings the critical spatial frequency of the optical transfer function (f_c) was 5 c/deg, and the exponent in the optical transfer function (n) was 2 for both subjects. The

f_c was thus almost equal to the f_c for luminance gratings which was 6 and 5.5 c/deg for KT and PM, respectively. The exponent n was lower for red-green (n=2) than for luminance gratings (n=3). Consequently, the attenuation by the optical modulation transfer function seemed to be less steep for red-green gratings. This may, however, be an artefact since contrast detection thresholds were not measured at high spatial frequencies so that the determination of n could not be done very accurately.

The spectral density of internal noise (N_i) was $35x10^{-6}$ for both subjects for red-green gratings. For subject PM the N_i was almost the same for red-green and luminance gratings ($N_{iL}=46x10^{-6}$). But for subject KT the spectral density of internal noise was lower for red-green than luminance gratings ($N_{iL}=92x10^{-6}$). This may appear strange especially because detection thresholds are lowest for luminance gratings at spatial frequencies above 1 c/deg as shown in Figure 4.18(A), where contrast detection threshold descriptions of the model are plotted as a function of spatial frequency for KT. However, the decrease in luminance thresholds above 1 c/deg is due to the enhancement by the neural modulation transfer function. If the neural modulation transfer function for luminance gratings is transformed from f to $f^{0.2}$, all threshold curves have identical modulation transfer functions, and any differences in the curves are due to differences in internal noise. In Figure 4.18(B) this has been done, i.e. the luminance threshold curve has been transformed by multiplying it by $f^{0.8}$, and it can be seen that now the transformed luminance threshold curve lies above the red-green threshold curve which means that the internal noise is larger for luminance than red-green gratings.

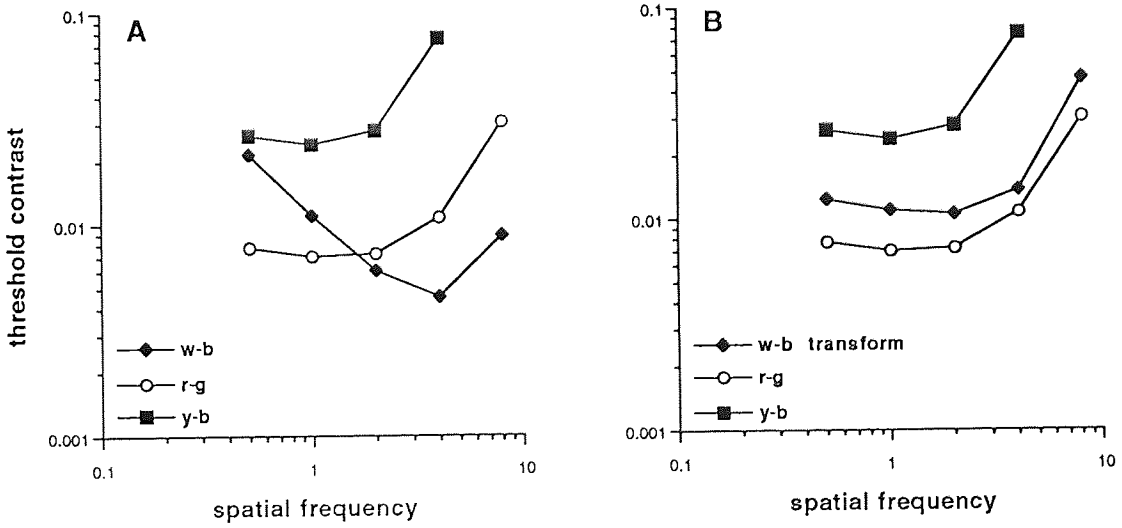

Figure 4.18 Contrast detection threshold descriptions for achromatic and chromatic gratings.

For contrast matching predictions, the restoration parameters γ and κ were initially given the same values as in black-and-white grating matching. However, the fits were poor because at high spatial frequencies matching contrast predictions were too high especially at high contrasts. Better fits were obtained when κ was independent of spatial frequency, and equal to 1. The constant γ was found to be 0.01. The fact that γ was ten times larger for red-green than luminance gratings implies that restoration starts to influence perceived contrast at a lower contrast level for red-green than luminance gratings.

The model descriptions are shown as smooth lines in Figure 4.14. The explained variance was 0.972 and 0.921 in Figure 4.14(A) and (B), respectively. The model descriptions were quite accurate.

Next, the model was applied to the results obtained by subject KT with yellow-blue gratings, and the parameter values found are shown in Table 4.6.

For yellow-blue gratings the critical spatial frequency of the optical modulation transfer function (f_c) was 3 c/deg. The exponent in the optical transfer function (n) was 3. The attenuation by the optical modulation transfer function started at a lower spatial frequency for yellow-blue gratings than for luminance or red-green gratings. The optical modulation transfer function was thus worse for yellow-blue than for black-and-white or red-green gratings. This is because of the longitudinal chromatic aberration. The difference of focus is quite large between yellow and blue so that both cannot be in focus simultaneously. Normally yellow is brought into focus which causes blue to be blurred.

Parameter	KT
f_c	3
n	3
N_i	42×10^{-5}
z_0	60
f_0	0.5
η_{max}	0.4
γ	0.1
κ	1

Table 4.6 Model parameters for KT in yellow-blue grating matching.

The spectral density of internal noise (N_i) was $42x10^{-5}$. It was considerably higher than N_i for luminance or red-green gratings. This is because sensitivity to yellow-blue gratings was lower at all spatial frequencies than sensitivity to other grating types.

The restoration parameters γ and κ were adjusted to give best fits for the contrast matching data. The exponent of the restoration function κ was equal to 1. The constant γ was found to be 0.1. It was hundred times larger than for luminance gratings and ten times larger than for red-green gratings. This means that restoration starts to influence perceived contrast at a lower contrast level for yellow-blue gratings than for luminance or red-green gratings.

The model descriptions are shown as the smooth curves in Figure 4.15. The model descriptions were quite accurate since the explained variance was 0.977.

4.4.4 Discussion

The chromatic contrast detection thresholds measured here for isoluminant red-green and yellow-blue gratings remained first constant up to about 1 c/deg and then increased with spatial frequency. The colour contrast sensitivity functions were thus low-pass in shape, in agreement with van der Horst and Bouman (1969) and Mullen (1985). Contrast thresholds were higher for luminance modulated than for red-green gratings up to 1 c/deg, above which this relationship was reversed. This is in rather close agreement with Mullen (1985) who found that the luminance and red-green threshold functions intersect at about 0.5 c/deg. Detection thresholds for yellow-blue gratings were higher than thresholds for black-and-white or red-green gratings at all spatial frequencies studied (0.5-4 c/deg), in agreement with Mullen (1985).

Mullen (1985) measured contrast detection thresholds with at least 4 cycles present at all spatial frequencies in attempt to avoid the reduction of sensitivity occurring when a grating has very few cycles (Howell & Hess, 1978). However, here it was found that chromatic contrast threshold functions were quite flat at low spatial frequencies even when there was only one cycle present in the grating (at 0.5 c/deg). Since spatial integration is similar for luminance and chromatic gratings (e.g. Sekiguchi et al., 1993), the fact that contrast thresholds decrease very slowly at low spatial frequencies for chromatic gratings is due to the neural modulation transfer function which attenuates low spatial frequencies much less for chromatic than for luminance gratings. Thus, there is very little low-frequency attenuation for chromatic gratings even with small areas.

In this study it was found that the spectral density of internal noise (N_i) was different for luminance modulated black-and-white, and isoluminant red-green and yellow-blue gratings. The N_i was higher for black-and-white than for red-green gratings, but highest for yellow-blue gratings. These differences may be genuine. On the other hand, it could also be assumed that the internal noise is constant while there is a multiplicative constant in the neural modulation transfer functions for luminance and colour which causes the differences in sensitivity. That is, instead of assuming that the constant b in Equation (4.16) is proportional to the ratio of internal noises, it could be presumed that it reflects the ratio of the neural modulation transfer functions so that the attenuation of the $H_n(f)$ would be stronger for black-and-white than red-green gratings, and strongest for yellow-blue gratings. Differences in the N_i (or the constant associated with the $H_n(f)$) may also be related to the definition of chromatic contrast, so that when it is defined as the luminance contrast of one of the grating components, the spectral density of internal noise is only apparently higher for example for yellow-blue gratings.

The results of this study show that contrast matching of isoluminant chromatic gratings produces reliable results. The variability in matches was small and almost equal for both luminance and chromatic gratings, and contrast matches yielded nearly identical results when repeated. Hence, contrast matching technique can be used to study the perceived contrast of isoluminant chromatic gratings.

Contrast matching functions measured as a function of spatial frequency were found to behave similarly for isoluminant chromatic as for achromatic luminance gratings. That is, at low contrast levels the matching curves resembled the contrast detection threshold curve but at high contrast levels they became flat so that perceived contrast was equal for all gratings of equal physical contrast regardless of spatial frequency.

When standard contrast was expressed as multiples of detection threshold, flattening of matching curves was slowest for black-and-white gratings since matching curves were not totally flat even at the highest standard contrast level of 16 times above threshold. Matching curves for red-green gratings were flat when the standard was 16 times above threshold so that flattening was faster than for black-and-white gratings. For yellow-blue gratings, matching curves were considerably flatter than the threshold curve already when the standard was 2 times above threshold, and at 4 times above threshold the curves were practically flat. The rapid flattening of matching curves was accompanied by an increase in the restoration parameter γ from 0.001 for black-and-white to 0.01 for red-green, and to 0.1 for yellow-blue gratings. This suggests that restoration starts to influence perceived contrast at a lower contrast level for yellow-blue than for red-green, but at the highest level for black-and-white gratings.

However, when the results were inspected in terms of physical contrast, flattening of contrast matching curves was very similar for all grating types. Matching curves became flat at a standard contrast of about 0.15-0.2. The explanation for this finding may be that it actually is the physical contrast that determines when restoration starts to be effective. Or perhaps it is that the flattening of matching curves only seems to occur at a certain physical contrast because of the contrast measure used.

According to the model, contrast responses are smaller to chromatic than to black-and-white gratings since the restoration parameter γ is larger for chromatic than black-and-white gratings. Also, responses are smaller to yellow-blue than to red-green gratings since γ is larger for yellow-blue. Contrast responses decrease as γ increases because the denominator in Equation (4.8b) increases. Since γ is larger chromatic gratings, flattening of matching curves starts earlier relative to threshold. At high contrasts the response is proportional to c/γ. Thus, the maximum response to the highest contrast is greatest for black-and-white, smaller for red-green, and smallest for yellow-blue gratings. If contrast matching was performed between different grating types (e.g. red-green matched to black-and-white), matches would be expected not to be physically correct at any contrast level. The question of the definition of chromatic contrast arises again here. Perhaps γ would be equal for all grating types if contrast was expressed in other terms. This is an important issue since in order to be able to account for contrast matches between different grating types, the problem of whether contrast responses are genuinely different for different grating types should be solved. Further investigations will be needed to answer these questions.

In conclusion, in the experiments of this study it was found that the detection thresholds of achromatic luminance modulated and isoluminant chromatic gratings of various spatial frequencies influence contrast matches at low contrast levels, but at high contrast levels matches become physically correct and independent of spatial frequency. The contrast restoration model introduced in Section 4.1 described luminance and chromatic contrast matching results accurately.

4.5 *General discussion on contrast matching*

In the experiments of this chapter, contrast detection thresholds and contrast matching functions were measured for simple luminance modulated cosine gratings of various areas and spatial frequencies, complex gratings with 2, 3 or 4 orientation components, and isoluminant chromatic gratings of various spatial frequencies. Contrast detection thresholds increased with decreasing area, and with increasing number of orientation components. Detection thresholds plotted as a function of spatial frequency formed a band-pass function for luminance modulated gratings, and a low-pass function for isoluminant chromatic gratings. Contrast matches were affected by detection thresholds at low contrasts levels, so that more contrast was needed for a match when the test stimulus had a high detection threshold. At high contrast levels, contrast matches became physically correct and thus independent of detection threshold.

The new contrast restoration model introduced in the beginning of this chapter was applied to the results of contrast matching. The model combines a previously published detection threshold model developed by Rovamo, Näsänen and coworkers (e.g. Rovamo, Luntinen & Näsänen, 1993; Rovamo, Mustonen & Näsänen, 1994ab&1995), with a restoring transfer function which is qualitatively similar to restoration techniques used in digital image processing. According to the model, detection thresholds are determined by six parameters: critical spatial frequency of the optical transfer function, exponent in the optical transfer function, spectral density of internal noise, maximum of the critical number of square cycles in the integration function, critical spatial frequency in the integration function, and maximum efficiency. In addition, contrast matches are affected by the restoration parameters, γ and κ, which determine the contrast level at which restoration starts to take effect, and the speed of restoration.

The parameter values determined in Sections 5.2, 5.3 and 5.4 were fairly similar for similar stimuli in different experiments. Similar stimuli refer to a stimuli within one of the three main stimulus types: simple cosine gratings, compound gratings or chromatic gratings. The parameter which varied the most was the spectral density of internal noise. The largest differences found were not genuine, however, since they were caused by the use of two different apparatuses and by different experimental conditions (compare Sections 4.2 and 4.4 with Section 4.5). When the same apparatus was used and the experimental conditions were similar, the estimates of internal noise varied maximally by a factor of 3.3 for one subject (KT), and by a factor of 4.2 between subjects. The variation in an individual observer's internal noise reflects the variability of his or her day-to-day performance. The variation between observers reflects inter-subject differences in contrast

sensitivity which may be rather large, so that a difference of 4.2 in internal noise is not surprising. In addition, it should be taken into account that sensitivity differences between subjects may be also be due to differences in detection efficiency as discussed below.

Some detection threshold parameters could not be determined on the basis of the available data. For example, the critical spatial frequency in the integration function could not be calculated since detection thresholds were not measured below 0.5 c/deg. In these cases, values found in previous studies were used. Nevertheless, the model descriptions were accurate which suggests that the values used were close to the correct values.

Another parameter which could not be exactly determined was the maximum efficiency. This is because detection thresholds were not measured at various levels of external noise (for an explanation see Section 5.3 of this thesis.) The maximum efficiency was set at a previously found value, 0.4, and detection threshold descriptions were made to coincide with the data by adjusting the spectral density of internal noise. This may have produced slightly inaccurate estimates of internal noise since if a subject's real maximum efficiency were for example lower than 0.4, the estimate of the internal noise spectral density with η_{max}=0.4 would be too high. However, in the experiment of this chapter the main aim was to obtain accurate detection threshold descriptions, meanwhile the exact ratio of maximum efficiency to internal noise was not of interest.

Some threshold parameters were strongly affected by the stimulus type. The most important findings were that the maximum of the critical number of square cycles in the integration function decreased with the number of components for complex gratings, and that the optical modulation transfer function and the spectral density of internal noise were different for luminance modulated and chromatic gratings. The implications of these findings have been discussed in Sections 4.2 and 4.4, respectively. It was also shown that the neural modulation transfer function is considerably less dependent on spatial frequency for chromatic than for luminance modulated gratings.

The restoration parameter κ depended on spatial frequency for luminance gratings. It was 1 at low spatial frequencies but above about 5 c/deg it started to increase very slowly. For chromatic stimuli κ was kept constant at 1. However, for chromatic gratings only one spatial frequency above 5 c/deg was used so that determination of κ at high spatial frequencies could not be done very reliably. Thus, it may be that if thresholds were measured at several high spatial frequencies, the dependence of κ on spatial frequency would turn out to be similar for luminance and chromatic gratings.

The restoration parameter γ was always constant at 0.001 for all luminance modulated stimuli. Constancy of γ is important since it permits the contrast responses for different stimuli to become equal at high contrast levels. However, for chromatic stimuli γ was higher. It was 0.01 for red-green and 0.1 for yellow-blue gratings. In the framework of the model this means that contrast responses were greatest for luminance modulated stimuli, smaller for red-green and smallest for yellow-blue stimuli at all contrast levels. Further research would be required to find out whether different values of γ can be found in other stimulus conditions, and whether contrast matches are ever physically correct in cross-matching conditions, that is, when stimuli with different values of γ are matched.

On the basis of the results of this chapter, it is concluded that the contrast restoration model could accurately describe contrast detection threshold and contrast matching data obtained using grating stimuli with various numbers of orientation components, spatial frequencies, areas and chromaticities.

5. CONTRAST DISCRIMINATION

5.1 Modelling of contrast discrimination

5.1.1 Contrast increment thresholds

Contrast increment threshold is defined as the smallest detectable contrast difference between two stimuli which are identical in other respects. In contrast increment threshold measurements, the subject is shown two stimuli one of which is of a constant contrast (c_p) and the other has an increment added to the constant contrast ($c_p+\Delta c$). The increment is adjusted until the smallest value permitting the two stimuli to be discriminated is found. The constant contrast present in both stimuli is called the pedestal contrast. Measurements are normally done at many different pedestal contrast levels. Contrast detection threshold is obtained when the pedestal contrast is zero.

Contrast discrimination functions, i.e. contrast increment thresholds plotted as a function of pedestal contrast, normally exhibit a 'dipper shape' (e.g. Nachmias & Sansbury, 1974; Legge & Kersten, 1987). As pedestal contrast is increased slightly above zero, there is a considerable decrease in the increment threshold from the detection threshold. This decrease below the detection threshold produces a 'dip'. When pedestal contrast is further increased, thresholds start to increase following a power function which can be written as $\Delta c=kc_p^n$, where Δc is contrast increment, c_p is pedestal contrast, k is a proportionality constant and n is the exponent of the power function. Exponent n gives the slope of the best-fitting straight line in double logarithmic coordinates (e.g. Legge, 1981). Estimates of exponent n have varied between 0.5 (Pelli, 1985) and 0.9 (Legge & Kersten, 1987), the most common value being about 0.6 (e.g. Legge, 1981).

Many factors which have a large effect on detection thresholds influence increment thresholds very little at high pedestal contrasts. For example, when measured as a function of spatial frequency or retinal eccentricity, detection thresholds differ greatly but increment thresholds are almost equal at high contrast levels (Bradley & Ohzawa, 1986).

The overall shape of the contrast discrimination function is very similar in various conditions. In many cases, different contrast discrimination curves can be superimposed by normalising both increment thresholds and pedestal contrasts by the detection threshold. For example, Legge (1979) has used this normalisation technique for gratings

differing in spatial frequency, and Legge and Kersten (1987) for gratings presented at various eccentricities in the visual field.

5.1.2 Earlier models for contrast discrimination

There have been many attempts to explain the shape of the contrast discrimination function. The most influential model was introduced by Legge and Foley in 1980. To account for the initial decrease and the subsequent increase in increment thresholds they proposed a nonlinear contrast transducer function. The transducer function has an accelerating nonlinearity at low contrasts and a compressive but nonsaturating nonlinearity at high contrasts. The accelerating nonlinearity produces the dip in the function, and the compressive nonlinearity produces the steadily rising part. This idea was first proposed by Nachmias and Sansbury (1974), and it has been applied to several models describing contrast discrimination and also other suprathreshold phenomena such as contrast matching or magnitude estimation (e.g. Wilson, 1980; Foley & Legge , 1981; Swanson, Wilson & Giese, 1984; Cannon & Fullencamp, 1991a).

The fundamental assumptions in nonlinear transducer models are that contrast increment thresholds are determined by a constant response difference, and that the internal noise is constant and additive. A constant response difference means that two contrasts can be discriminated if the responses to them differ at least by a constant factor, ΔR. The models normally include the following stages: linear filtering, a nonlinear transducer function, addition of constant noise, and a decision.

First, the signal is filtered by linear spatial frequency and orientation sensitive filters. Then it goes through a nonlinear contrast transducer. In the accelerating region of the transducer, constant increments at the output are associated with decreasing increments at the input. Consequently, contrast increment thresholds decrease at low contrast levels. In the compressive region, constant increments at transducer output are associated with increasing increments at its input, so that increment thresholds increase at high contrast levels. The slope of the transducer determines the slope of the discrimination function. If the slope in the accelerating region is 1.4, the slope of the discrimination function is approximately -0.4 (=1-1.4) which means that the function is decreasing. If the slope in the compressive region is 0.4, the slope in the increasing part of the discrimination function is 0.6 (=1-0.4), and the function is increasing.

Next, Gaussian noise with constant variance is added to the transducer output to account for variability in subject's responses. The decision process is generally based on the

assumption that many outputs from different detectors are monitored. The detector with the greatest output difference to the two stimuli (c_p and $c_p+\Delta c$) is chosen. The interval in which the detector's output is greater is chosen as the signal with an increment.

Nonlinear contrast transducer models have not been very extensively tested on experimental data, however. Legge and Foley's (1980) model was designed to account for contrast masking. Contrast discrimination is only a special case of masking where the spatial frequency and orientation of the test and the mask are equal. Thus, Legge and Foley tested the model with only two sets of discrimination data obtained with two grating areas. The model predictions were accurate for the smaller but not for the larger grating.

Swanson et al. (1984) tested their model at four spatial frequencies ranging from 0.4 to 11 c/deg. However, their data showed only the increasing part of the discrimination functions so that the position and depth of the dips could not be verified. Wilson (1980) tested his model with a difference of Gaussians pattern but the experimental data shown was rather sparse. Foley and Legge (1981) measured psychometric functions at three near-threshold pedestal contrasts and used their model to describe the shapes of the psychometric functions. Cannon and Fullencamp (1991a) applied their contrast transducer model on the results of contrast magnitude estimation only.

A critical test for the nonlinear transducer models is to measure contrast increment thresholds in external spatial noise. These models predict that in the presence of external spatial noise the dipper-shape of the contrast discrimination function should disappear. This is because the transducer amplifies or attenuates both signal and noise equally. Consequently, if the external noise is so strong relative to the internal noise that it determines the thresholds, increments thresholds should remain constant with increasing pedestal contrast because the signal-to-noise ratio is assumed to be constant at threshold. Contrary to this prediction, Pelli (1985) has shown that the dipper-shape of the contrast discrimination function remains unchanged in external noise.

Pelli (1985) has assumed a different approach in his uncertainty model. According to his model, a signal is detected by a set of different detectors. The observer monitors the output of all detectors with which the signal is cross-correlated. At detection threshold, the signal is judged to be present if the output of at least one detector exceeds a criterion level. The observer is uncertain because he monitors all detectors. Facilitation in contrast discrimination can be explained by a reduction in uncertainty when the pedestal is suprathreshold. The pedestal will ensure that the maximum response will always arise from the signal-specific detector so that other detectors can be ignored. Thus, uncertainty does not reduce performance in contrast discrimination at suprathreshold contrasts. The

model predicts that increment thresholds remain constant and lower than the detection threshold at high contrast levels which is contrary to the experimental findings. The uncertainty model can describe contrast detection and near-threshold discrimination but the power law cannot be explained by it. Pelli assumes that at suprathreshold contrasts there is noise which is dependent on the pedestal contrast. Introduction of signal-dependent noise would then account for the power law at high contrast levels.

Legge (1984b) has introduced a binocular energy-detector model for describing binocular contrast summation for example in contrast discrimination. According to the model, constant-variance input noise is added to each monocular signal which is then passed through a linear filter. The output of each filter is squared so that it becomes proportional to the r.m.s. contrast squared. The squaring operation produces an accelerating nonlinearity which explains the dip in the contrast discrimination function. The squared outputs are integrated over the stimulus area so that the resulting signal is proportional contrast energy. Next, the monocular signals are added to form the binocular signal. Contrast discrimination at high contrast levels is modelled by a compressive transformation followed by addition of constant-variance central noise. Model predictions for the experimental data were not shown.

Many authors have pointed out that the power law behaviour of contrast increment thresholds at high pedestal contrasts can be explained equivalently either by a nonlinear contrast transducer followed by constant-variance noise, or by a linear contrast response followed by signal dependent noise (e.g. Legge, 1984b; Pelli, 1985; Ahumada & Watson, 1985; Legge et al., 1987). There is neurophysiological evidence for the existence of signal dependent noise. Tolhurst, Movshon and Thompson (1981) and Tolhurst, Movshon and Dean (1983) have found that, in the primary visual cortex of the cat and macaque monkey, the variance of a neuron's firing rate is directly proportional to its mean firing rate. Despite this support from neurophysiology, there are no models for contrast discrimination based on signal dependent noise.

5.1.3 Difference-signal discriminator model for contrast discrimination

A new model for human contrast discrimination is introduced here. The model has been developed on the basis of a contrast detection model (e.g. Rovamo, Mustonen & Näsänen, 1994ab; see also Section 4.1) and a model for human pattern discrimination (Näsänen, Kukkonen & Rovamo, 1995ab). In the pattern discrimination model, the main idea is to calculate the response differences of two local matched filters tuned to the two stimuli being discriminated. The pattern discrimination model can describe how orientation

discrimination thresholds depend on grating area at various contrast levels, and how contrast increment thresholds depend on grating area at a constant suprathreshold contrast of 0.3. Here these models are combined and extended to contrast discrimination tasks at a wide range of contrasts from detection threshold to suprathreshold levels.

According to the new contrast discrimination model, decisions made by the human brain are based on the responses of local matched filters, and the accuracy of decisions is limited by noise. There is both pre- and post-filter noise in the visual system. In other words, there is noise preceding the matched filter and noise occurring after it. Pre-filter noise includes external spatial noise, quantal noise and internal neural noise, and it produces variability in the matched filter response. Post-filter noise is signal dependent since on the basis of neurophysiology it is reasonable to assume that response variability increases with response magnitude (Tolhurst et al., 1981 & 1983).

The ideal discriminator for two signals of equal energy contains two matched filters, one for each signal, and the decision variable is the difference of the matched filter outputs (Goodyear, 1971). On this basis, it is assumed that the decision made by the human brain is based on comparison between the response differences of the two matched filters to the two stimuli to be discriminated, and the accuracy of the decision is limited both by pre- and post-filter noise.

The model is presented in schematic form in Figure 5.1. The two signals to be discriminated, which may be embedded in external spatial noise, first undergo (1) low-pass filtering by the ocular optics, then (2) quantal noise is added at the event of quantal

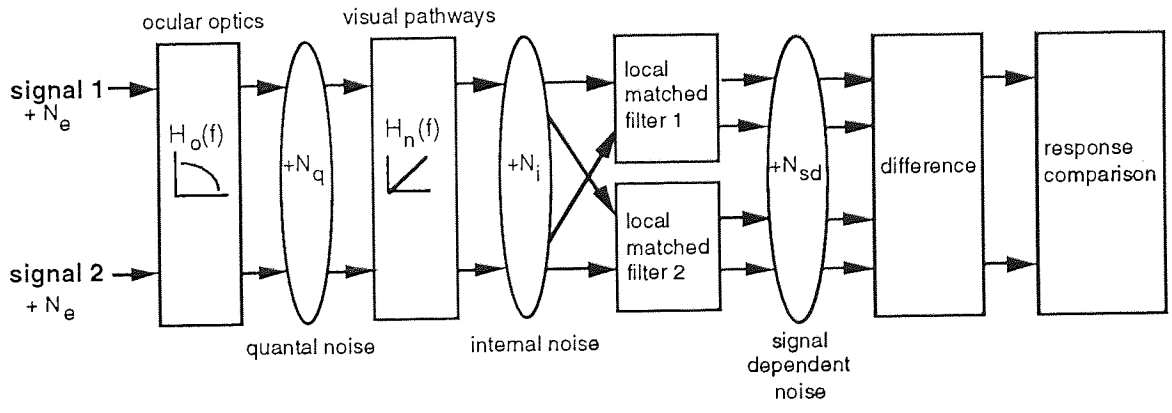

Figure 5.1 Difference-signal discriminator model for human contrast discrimination.

absorption in the photoreceptors. Next, the signals are (3) high-pass filtered by the neural visual pathways, and (4) constant variance internal neural noise is added. Then the signals are correlated with (5) two local matched filters tuned to each stimulus to be discriminated. (6) Signal dependent noise is added to the matched filter responses before (7) response differences of the two matched filters to each stimulus are calculated. The decision is based on (8) comparison of response differences. The response difference of the two matched filters is equal to the difference in the signals, and therefore the model is called the difference-signal discriminator model.

In a contrast discrimination task, two stimuli differing only in contrast are exposed in a random order. In the experiments of this thesis the stimuli were always cosine gratings. One of the gratings, g_1, had a constant pedestal contrast c_p. The other grating, g_2, had an increment Δc added to the pedestal contrast, so that the total contrast of the grating g_2 was $c=c_p+\Delta c$. The gratings were thus:

$$g_1=L_0[1+c_{Mp}\cos(2\pi fx)] \tag{5.1a}$$

$$g_2=L_0[1+(c_{Mp}+\Delta c_M)\cos(2\pi fx)] \tag{5.1b}$$

where subscript M refers to Michelson contrast, and L_0 is the mean luminance of the grating.

In the visual system the luminance signal of each grating is transformed into a contrast signal. In the following, signal processing and the responses to the signals are described separately from the response variability introduced at various stages of signal processing.

The two luminance signals are first low-pass filtered by the optical modulation transfer function of the ocular optics, $H_o(f)$. It is described by $H_o(f)=[1+(f/f_c)^n]^{-1}$ where f_c is the critical spatial frequency at which $H_o(f)=0.5$ and n is a constant which indicates the slope of decrease of the optical transfer function beyond the critical spatial frequency.

After quantal absorption in the photoreceptors the luminance distributions are normalised by the mean luminance L_0. Then the signals are high-pass filtered by the modulation transfer function of the neural visual pathways, $H_n(f)$, which is directly proportional to spatial frequency so that at f=0 it is zero. Consequently, the neural modulation transfer function removes the normalised mean luminance. Contrast signals are thus obtained from the luminance signals.

Next, subtractive contrast adaptation affects the pedestal contrast which is always present in both signals (Georgeson, 1985). A constant proportion of the pedestal contrast is subtracted from the signals. Thus, after adaptation the effective pedestal contrast is c_p-d $c_p = c_p(1\text{-}d) = b\ c_p$. That is, due to adaptation pedestal contrast is attenuated by a factor of b.

After these preprocessing stages the signals are the following:

$$s_1(x,y) = H_0(f)\ H_n(f)\ b\ c_{Mp} \cos(2\pi fx) \tag{5.2a}$$

$$s_2(x,y) = H_0(f)\ H_n(f)\ (b\ c_{Mp}+\Delta c_M) \cos(2\pi fx) \tag{5.2b}$$

Signal detection is mediated by the sampled mean response of a local matched filter. Each signal creates a local matched filter tuned to its root-mean-square contrast. The tuning of the matched filters is continuously updated because the contrast of one of the signals changes. This may be realised in a manner similar to for example Kohonen's self-organizing-map neural network (Kohonen, 1990).

The signals are discriminated by comparing the differences of the sampled mean responses of the two matched filters $m_i(x,y)$ to each signal. The sampled mean response, r, of the matched filter $m_i(x,y)$ (i=1,2) to the signal $s_j(x,y)$ (j=1,2) is:

$$r_{ij} = \eta \iint m_i(x,y)\ s_j(x,y)\ dx\ dy \tag{5.3a}$$

This means that the signal is cross correlated with the matched filter. The sampling efficiency of the matched filter is calculated by $\eta=\eta_{max}(1+z/z_c)^{-1}$ where η_{max} is the maximum efficiency, z is the number of square cycles in the stimulus ($z=Af^2$), and z_c is the critical number of square cycles which marks the saturation of spatial integration in signal detection. The critical number of square cycles is calculated according to $z_c=z_0f^2/(f_0^2+f^2)$ where z_0 is the maximum of the critical number of square cycles in the integration function, and f_0 is the critical spatial frequency in the integration function.

Since a matched filter is equal to a copy of the signal, Equation (5.3a) can be written as:

$$r_{ij} = \eta \iint s_i(x,y)\ s_j(x,y)\ dx\ dy \tag{5.3b}$$

The responses of the two matched filters $m_1(x,y)$ and $m_2(x,y)$ tuned to signals $s_1(x,y)$ and $s_2(x,y)$ are calculated using this equation. The first subscript (i) refers to the matched filter and the second (j) to the signal.

The sampled mean response of the matched filter $m_1(x,y)$ to the signal $s_1(x,y)$ is calculated by inserting Equation (5.2a) into Equation (5.3b):

$$\begin{aligned} r_{11} &= \eta \iint s_1(x,y)\, s_1(x,y)\, dx\, dy \\ &= \eta\, H_o^2(f)\, H_n^2(f)\, b^2\, c_{Mp}^2\, A/2 \\ &= \eta\, H_o^2(f)\, H_n^2(f)\, (b\, c_p)^2\, A \\ &= \eta E_p' \end{aligned} \tag{5.4}$$

where the root-mean-square contrast of the signal is $c_p=c_{Mp}/\sqrt{2}$ (see Appendix I for further details), A is stimulus area and E_p' denotes the contrast energy of signal $s_1(x,y)$, calculated as $E_p=(b\, c_p)^2 A$, which has been filtered by the optical and neural modulation transfer functions.

Similarly, the sampled mean response of the matched filter $m_2(x,y)$ to the signal $s_2(x,y)$ is calculated as:

$$\begin{aligned} r_{22} &= \eta \iint s_2(x,y)\, s_2(x,y)\, dx\, dy \\ &= \eta\, H_o^2(f)\, H_n^2(f)\, (b\, c_p+\Delta c)^2\, A \\ &= \eta E' \end{aligned} \tag{5.5}$$

where E' denotes the contrast energy of signal $s_2(x,y)$, calculated as $E=(b\, c_p+\Delta c)^2 A$, which has been filtered by the optical and neural modulation transfer functions.

The sampled mean responses of the matched filter $m_1(x,y)$ to the signal $s_2(x,y)$, and of the matched filter $m_2(x,y)$ to the signal $s_1(x,y)$ are equal:

$$\begin{aligned} r_{12} = r_{21} &= \eta \iint s_1(x,y)\, s_2(x,y)\, dx\, dy \\ &= \eta\, H_o^2(f)\, H_n^2(f)\, b\, c_p\, (b\, c_p+\Delta c)\, A \\ &= \eta\, (E_p'E')^{0.5} \end{aligned} \tag{5.6}$$

The greatest sampled mean response is that of the matched filter $m_2(x,y)$ tuned to contrast $c_p+\Delta c$ and cross-correlated with signal $s_2(x,y)$ with contrast $c_p+\Delta c$. The smallest sampled mean response is that of the matched filter $m_1(x,y)$ tuned to contrast c_p and cross-correlated with signal $s_1(x,y)$ with contrast c_p. The mean responses of the matched filter $m_1(x,y)$ to signal $s_2(x,y)$ and of the matched filter $m_2(x,y)$ to signal $s_1(x,y)$ are equal to the geometric mean of the responses r_{11} and r_{22}. Thus, it is always true that $r_{22} > r_{12} = r_{21} > r_{11}$.

The response differences, R_h (h=1,2), are then calculated as:

$$R_1 = r_{11} - r_{21} \text{ and}$$
$$R_2 = r_{22} - r_{12} \tag{5.7a}$$

or as their complementary i.e. negative values:

$$-R_1 = r_{21} - r_{11} \text{ and}$$
$$-R_2 = r_{12} - r_{22} \tag{5.7b}$$

where R_1 and R_2 refer to the responses of the visual system to signals $s_1(x,y)$ and $s_2(x,y)$, respectively. Equation (5.7a) means that if the response difference R_1 for signal $s_1(x,y)$ is calculated as the response of matched filter $m_1(x,y)$ minus the response of matched filter $m_2(x,y)$, then the response difference R_2 for signal $s_2(x,y)$ is calculated as the response of matched filter $m_2(x,y)$ minus the response of matched filter $m_1(x,y)$. Or conversely, Equation (5.7b) means that if the response difference $-R_1$ for signal $s_1(x,y)$ is calculated as the response of matched filter $m_2(x,y)$ minus the response of matched filter $m_1(x,y)$, then the response difference R_2 for signal $s_2(x,y)$ is calculated as the response of matched filter $m_1(x,y)$ minus the response of matched filter $m_2(x,y)$. Hence, if R_1 is negative, then R_2 is positive and vice versa. This optimises the visual performance by maximising the absolute value of the discrimination variable.

The decision in a discrimination task is based on the discrimination variable which is calculated by subtracting the response differences to the two signals:

$$R_2 - R_1 = \eta E' - \eta E_p' = \eta H_o^2(f) H_n^2(f) (E - E_p) \tag{5.8a}$$

The discrimination variable could also be calculated as $R_1 - R_2$ or by using the negative response differences. In all cases the absolute value of the discrimination variable remains unchanged.

Equation (5.8) explains why there is a dip in contrast discrimination functions. This becomes more evident if the equation is rewritten in terms of contrast:

$$\begin{aligned} R_2 - R_1 &= \eta H_o^2(f) H_n^2(f) [(b c_p + \Delta c)^2 A - (b c_p)^2 A] \\ &= \eta H_o^2(f) H_n^2(f) (\Delta c^2 + 2b c_p \Delta c) A \end{aligned} \tag{5.8b}$$

The signal-to-noise ratio is constant at threshold (e.g. Rovamo, Kukkonen, Tiippana & Näsänen, 1993) which means that the ratio of discrimination variable to its variance is constant [see Equation (5.12) below]. Equation (5.8b) shows that if Δc remained constant or increased, the value of the discrimination variable would increase with increasing

pedestal contrast. Thus, in order to keep the signal-to-noise ratio constant, contrast increment thresholds must decrease as pedestal contrast is increased above a certain level, provided that the noise level is constant. However, the noise in the visual system is composed of signal independent pre-detector noise and signal dependent post-detector noise, the latter of which becomes significant at high contrast levels.

The pre-detector noise causes variance in each response difference R_h (h=1,2). The variance is calculated as:

$$\begin{aligned}\sigma_{preRh}^2 &= \eta \iint [M_2(u,v) - M_1(u,v)]^2 N_{tot}'(u,v)\, du\, dv \\ &= \eta\, N_{tot}' \iint [M_2(u,v) - M_1(u,v)]^2\, du\, dv \\ &= \eta\, N_{tot}' \iint [m_2(x,y) - m_1(x,y)]^2\, dx\, dy \\ &= \eta\, N_{tot}'\, H_o^2(f)\, H_n^2(f)\, \Delta c^2\, A \end{aligned} \qquad (5.9)$$

where $N_{tot}'(u,v)$ is the variance (spectral density) of the pre-detector noise in the Fourier space and M(u,v) is the Fourier transform of the matched filter. Thus, according to Equation (5.9) the variance of each response difference caused by the pre-detector noise is calculated by integrating the power spectrum of noise $N_{tot}'(u,v)$ weighted by the power spectrum of the difference of the detectors, $M_2(u,v) - M_1(u,v)$, across the Fourier space. The contrast energy of the difference of the matched filters (or signals) is the same irrespective of whether it is calculated in Fourier space or in the visual field. The pre-detector noise can be considered white since the quantal and internal noises are independent of spatial frequency, and in the experiments of this thesis so is the external noise within the spatial frequency range of the stimuli used. The spectral density of pre-detector noise in the human brain is calculated by $N_{tot}' = H_o^2(f)\, H_n^2(f)\, N_e + H_n^2(f)\, N_q + N_i$, where N_e, N_q and N_i are external spatial noise, quantal noise and internal noise, respectively. (For further details on quantal noise see Appendix IV.) The variance due to the pre-detector noise is equal for both signals.

Post-filter noise is signal dependent since according to the model the response variability increases with response magnitude. To calculate the variance of each response difference R_h due to the signal dependent post-detector noise it is assumed that $\sigma_{post}^2 = k\, r_{ij}^m$. Thus, on the basis of Equations (5.4)-(5.6) the variance due to the post-detector noise for signal $s_1(x,y)$ is:

$$\begin{aligned}\sigma_{postR1}^2 &= \sigma_{post}\, r_{11}^2 + \sigma_{post}\, r_{21}^2 \\ &= k\, r_{11}^m + k\, r_{21}^m \\ &= k\, \eta^m [E_p'^m + (E_p'E')^{0.5m}] \end{aligned} \qquad (5.10a)$$

and for signal $s_2(x,y)$ it is:

$$\begin{aligned}\sigma_{postR2}^2 &= \sigma_{post}\, r_{22}^2 + \sigma_{post}\, r_{12}^2 \\ &= k\, r_{22}^m + k\, r_{12}^m \\ &= k\, \eta^m\, [E'^m + (E_p'E')^{0.5m}]\end{aligned} \tag{5.10b}$$

The average variance of R_1 and R_2 is calculated as:

$$\begin{aligned}(\sigma_{R1}^2 + \sigma_{R2}^2)/2 &= (\sigma_{postR1}^2 + \sigma_{preR1}^2 + \sigma_{postR2}^2 + \sigma_{preR2}^2)/2 \\ &= \{k\,\eta^m[E_p'^m + (E_p'E')^{0.5m}] + \eta\, N_{tot}'\, H_o^2(f)\, H_n^2(f)\, \Delta c^2\, A + \\ &\quad k\,\eta^m[E'^m + (E_p'E')^{0.5m}] + \eta\, N_{tot}'\, H_o^2(f)\, H_n^2(f)\, \Delta c^2\, A\}/2 \\ &= \{k[\eta H_o^2(f) H_n^2(f)]^m (E_p^{0.5m} + E^{0.5m})^2 + 2\eta\, N_{tot}'\, H_o^2(f) H_n^2(f) \Delta c^2 A\}/2\end{aligned} \tag{5.11}$$

where σ_{R1}^2 is the variance of the matched filter responses to signal $s_1(x,y)$ due to pre- and post-filter noises, and σ_{R2}^2 is the variance of the matched filter responses to signal $s_2(x,y)$ due to pre- and post-filter noises.

According to the model, contrast increment thresholds are determined by the signal-to-noise ratio of the discrimination variable. This is equivalent to calculating the ratio of the response, i.e. the value of the discrimination variable, to the standard deviation of the response. And equivalently, signal-to-noise ratio squared is equal to the square of the discrimination variable divided by the average variance of the responses:

$$d'^2 = \frac{(R_2 - R_1)^2}{\left(\sigma_{R1}^2 + \sigma_{R2}^2\right)/2} \tag{5.12}$$

Squaring of the signal-to-noise ratio and the discrimination variable is not necessary here if square root is taken of the variance term. However, the value of d' is always positive. Hence, it is more convenient to use the squared values since squaring ensures that the discrimination variable is also always positive.

By inserting Equations (5.8a) and (5.11) into Equation (5.12) the squared signal-to-noise ratio becomes:

$$d'^2 = \frac{H_o^2(f)\, H_n^2(f) \eta\, (E - E_p)^2}{N_{tot}'\, \Delta c^2\, A + \frac{k}{2}\left[H_o^2(f)\, H_n^2(f)\, \eta\right]^{m-1}\left(E^{0.5m} + E_p^{0.5m}\right)^2} \tag{5.13}$$

Equation (5.13) was used to calculate model descriptions for contrast increment thresholds. The two-alternative forced-choice algorithm used in the experiments gives threshold estimates at the probability level of 0.84 correct responses (Elliott, 1964). Thus, the value of the detectability index d' was 1.4, and the signal-to-noise ratio squared was equal to 2.

The contrast increment threshold Δc was solved numerically using an iterative method. A random value was set for the Δc, and d'^2 was solved. If the result was greater than 2, the value of Δc was halved and the calculation repeated. If this value of Δc gave a result of less than 2, the mean of the two previous values of Δc was taken as the next guess. This procedure was repeated until a value of Δc was found which gave d'^2 equal to 2 within ± 0.001.

The model predicts that contrast increment thresholds first remain constant and then start to decrease as pedestal contrast increases when the pre-detector noise is the dominant source of noise. But when the post-detector noise becomes the dominant source of noise, contrast increment thresholds start to increase as a power function of pedestal contrast.

5.2 *Dependence of contrast increment thresholds on grating area*

5.2.1 Introduction

It is well known how contrast detection thresholds depend on grating area. As grating area is increased, detection thresholds decrease up to a saturation point after which they become independent of area (Hoekstra & al., 1974; Howell & Hess, 1978; Virsu & Rovamo, 1979; Rovamo, Luntinen & Näsänen, 1993). When plotted as a function of area in double logarithmic coordinates, detection thresholds first decrease with a slope of -0.5, but then they become constant. The transition between the decreasing and constant parts of the contrast threshold curve occurs at a constant number of square cycles ($z=Af^2$) at spatial frequencies above about 0.5 c/deg (e.g. Rovamo, Mustonen & Näsänen, 1994a). This means that spatial integration saturates at a smaller area as spatial frequency is increased. Also, it means that saturation occurs at a constant number of details in the stimulus.

The effect of grating area on contrast increment thresholds has not been extensively studied. Legge and Foley (1980) measured increment thresholds with two grating widths and found that at suprathreshold pedestal contrasts increment thresholds were similar for both gratings even though they differed markedly at and near detection threshold. They explained this finding in terms of their model for contrast masking. According to the model, decisions are normally based on the responses of many detectors. This is called response pooling, and it causes increment thresholds to decrease as stimulus area is increased. To model the independence of increment thresholds of stimulus area at high pedestal contrasts, they simply eliminated the response pooling so that at high contrasts the decisions were based on the response of one detector. Swanson et al. (1984) used the same solution in their model, i.e. at low contrasts they had response pooling which was omitted at suprathreshold contrasts. However, neither of these studies attempted to give an explanation for the transition between the extensive spatial integration at detection threshold and lack of integration at high contrasts.

Cannon and Fullencamp (1991) modified Legge and Foley's contrast transducer function to model the dependence of contrast magnitude estimates on grating area. In their model spatial integration decreases smoothly as contrast level is increased. They did not apply their model to contrast discrimination, however.

The purpose of this study was to investigate thoroughly the dependence of contrast increment thresholds on grating area by measuring contrast discrimination functions for

ten grating areas at spatial frequencies of 0.5 and 4 c/deg at a large range of pedestal contrasts, and to apply the new difference-signal discriminator model to the results.

5.2.2 Methods

The stimuli were square-shaped, vertical cosine gratings. Five side lengths were used: 1, 2, 4, 8 and 16 cm. Spatial frequency was 1 c/cm on the screen. The experiments were performed at 0.5 c/deg for which the viewing distance was 28.6 cm, and at 4 c/deg for which the viewing distance was 229 cm. The grating areas were 4, 16, 64, 256 and 1024 deg^2 at 0.5 c/deg, and 0.0625, 0.25, 1, 4 and 16 deg^2 at 4 c/deg. When expressed as the number of square cycles, the areas were equal for both spatial frequencies. The number of square cycles is defined as grating area in solid degrees multiplied by the spatial frequency squared (Virsu & Rovamo, 1979). The number of square cycles was 1, 4, 16, 64 and 256 for 1x1, 2x2, 4x4, 8x8 and 16x16 cm gratings, respectively.

Contrast increment thresholds were measured at pedestal contrasts ranging from 0.0011 to 0.57 in 0.3 log unit steps. Contrast increment thresholds were calculated as $\Delta c = c - c_p$, where c is the total contrast of the grating with both pedestal and increment and c_p is the pedestal contrast. Detection thresholds ($c_p=0$) were also measured. Contrast was always expressed as r.m.s. contrast.

All data points shown are based on geometric means of at least three threshold estimates. In order to cover a slight flashing effect from the borders of the screen sometimes visible at high contrasts, a black cardboard mask was placed in front of the computer screen to create a square opening with a side length of 20 cm.

The subjects, OL and KT, were both fully corrected myopes with visual acuities of 1.7 and 1.5, respectively. OL's correction was oa.-1.25 DS, and KT's od.-6.5 DS/ os.-4.5 DS. The average relative standard errors of mean ($\overline{SE}$) for contrast increment thresholds were 15% for OL and 13% for KT.

5.2.3 Results

Contrast increment thresholds were measured for five relative grating sizes at two spatial frequencies with a large range of pedestal contrasts. In Figure 5.2 contrast increment thresholds (Δc) are plotted as a function of pedestal contrast. Spatial frequency is 0.5 c/deg for subject OL in (A) and 4 c/deg for subject KT in (B). Grating area is 1 (open

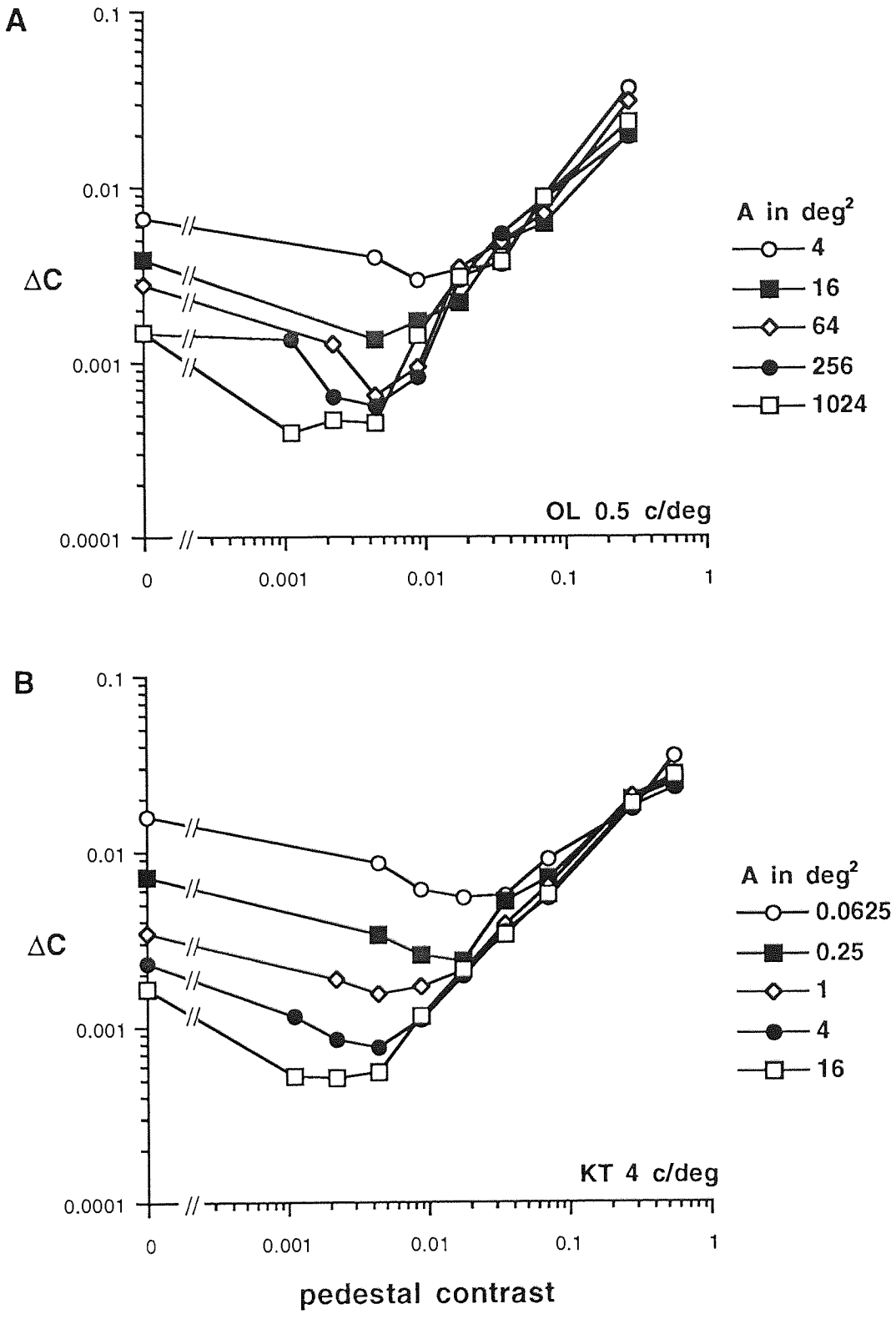

Figure 5.2 Contrast increment thresholds measured with various grating areas.

circles), 4 (filled squares), 16 (open diamonds), 64 (filled circles) and 256 (open squares) square cycles in both (A) and (B). The points on the abscissae are contrast detection thresholds.

Contrast discrimination functions measured with different grating areas had a similar overall shape. As pedestal contrast was increased from zero, increment thresholds first decreased to a minimum thus producing a dip but then they started to increase, and fell on a straight line on double logarithmic coordinates. The depth of the dip and the slope of the increase were quite similar for all grating areas. At low pedestal contrasts, discrimination curves for different grating areas were vertically displaced so that increment thresholds were lower for larger gratings. At high pedestal contrasts, however, increment thresholds became almost equal for different grating areas. The position of the dip depended on grating area so that the dip occurred at a lower pedestal contrast as grating area was increased.

In order to investigate spatial integration in contrast discrimination, increment thresholds were plotted as a function of grating area in Figure 5.3, where (A) shows the data for OL and (B) for KT. The uppermost spatial integration curves are for detection thresholds, and below them are the integration curves for increment thresholds measured at various pedestal contrasts. The data have been displaced vertically for clarity since the curves for different pedestal contrasts overlapped when they were in their original positions. In Figure 5.7(A), the curves at 0 (open circles), 0.0044 (filled squares), 0.0088 (open diamonds), 0.018 (filled triangles), 0.035 (open triangles), 0.071 (filled circles), and 0.28 (open squares) have been divided respectively by a factor of 1, 1, 4, 20, 80, 320 and 1800. In Figure 5.7(B), the curves at 0 (open circles), 0.0044 (filled squares), 0.0088 (open diamonds), 0.018 (filled triangles), 0.035 (open triangles), 0.071 (filled circles), 0.28 (open squares), and 0.57 (filled diamonds) have been divided respectively by a factor of 2, 2, 6, 24, 100, 300, 2000 and 8000.

As grating area was increased, contrast detection thresholds first decreased with a slope of -0.5 but then the decrease slowed down or saturated. The straight line segments in the upper left-hand corner of each figure show a slope of -0.5. By comparing Figures 5.3(A) and (B), it can be seen that spatial integration has saturated for OL in (A) since the detection thresholds for the two largest gratings were equal. However, for KT in (B) detection thresholds decreased at all areas which means that spatial integration has not saturated. With the two largest gratings decrease has just started to slow down since slope has become less steep.

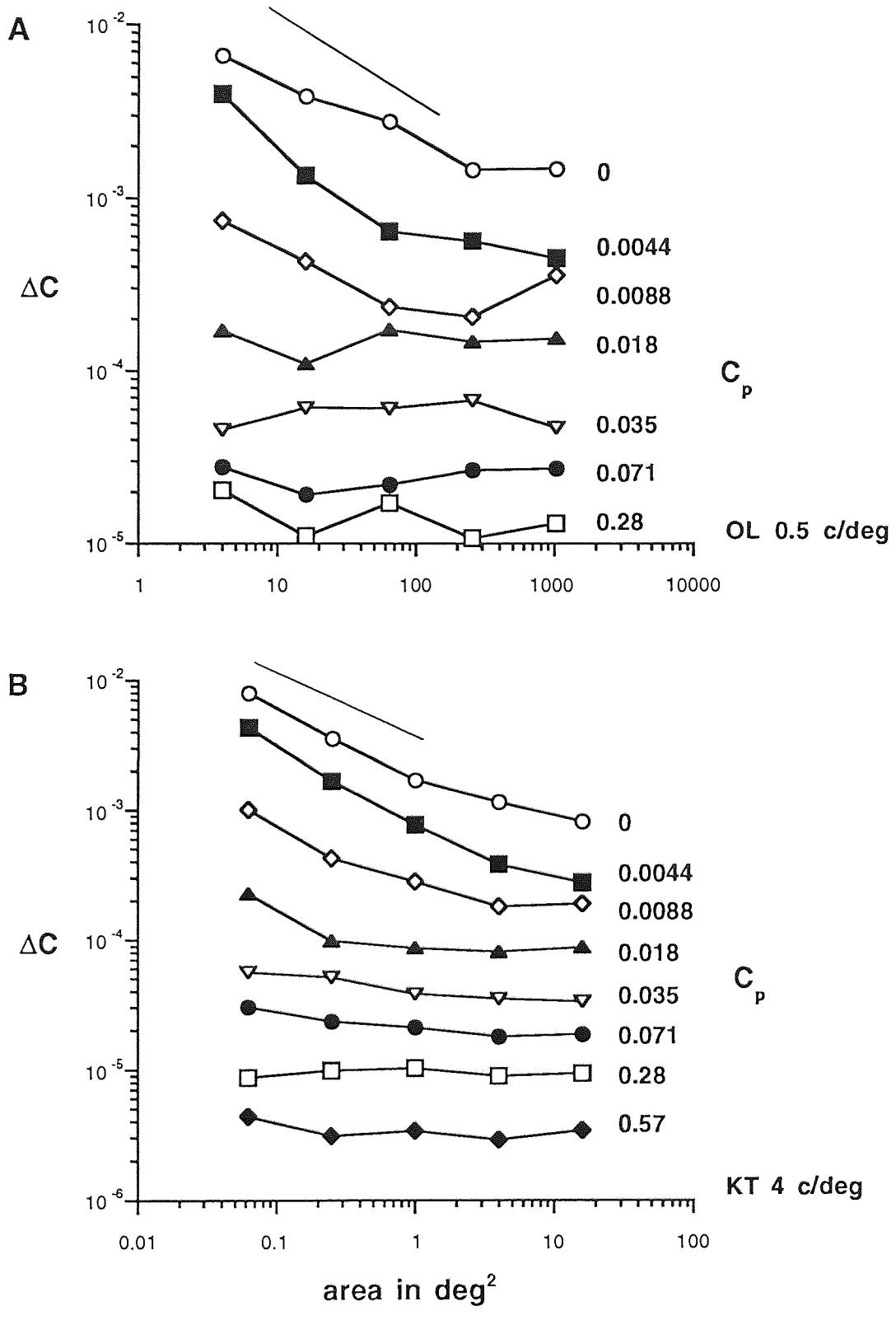

Figure 5.3 Contrast icrement thresholds plotted as a function of grating area (curves have been displaced).

Spatial integration was quite different for increment thresholds than for detection thresholds. At the lowest pedestal contrast, increment thresholds tended to increase at a slightly faster rate with area than detection thresholds, as can be seen by comparing the filled squares with the open circles in Figure 5.3. As pedestal contrast was increased, spatial integration saturated progressively at smaller areas so that at the highest pedestals, integration functions were practically flat.

Next, the contrast discrimination model introduced in Section 5.1 was applied to the experimental results. First, contrast detection threshold predictions were obtained as described in Section 4.3 where the contrast restoration model was applied to contrast matching results. The contrast detection model is of course a common feature in both contrast discrimination and contrast restoration models. Consequently, the model parameters which determine the detection thresholds are the critical spatial frequency of the optical transfer function (f_c), the exponent in the optical transfer function (n), the spectral density of internal noise (N_i), the maximum of the critical number of square cycles in the integration function (z_0), the critical spatial frequency in the integration function (f_0), and the maximum efficiency (η_{max}).

The parameters f_0, f_c and n have already been determined for subject KT in Section 4.3 where their values were found to be 0.5, 7 and 3, respectively. These parameters could not be determined individually for OL since his detection thresholds were not measured at various spatial frequencies. Thus, the same values were used for both OL and KT.

The maximum efficiency was taken as 0.4 for OL based on a previous study where detection thresholds were measured as a function of external spatial noise (Rovamo, Luntinen and Näsänen, 1995). For KT the maximum efficiency was determined on the basis of detection threshold results obtained in the experiments presented in Section 5.3 of this thesis where contrast increment thresholds were measured at various levels of external spatial noise. The η_{max} was found to be 0.33 for KT.

The maximum of the critical number of square cycles in the integration function (z_0) was determined by plotting detection thresholds as a function of grating area, and by finding the value of z_0 which produced the best visual fit to the spatial integration function. The z_0 was found to be 60 for OL and 90 for KT. In Section 4.3 the value of z_0 was set at 60 for KT. However, when it was chosen, more emphasis was imposed on the detection threshold function measured at various spatial frequencies than at various areas, so that the estimate may have been slightly inaccurate.

The spectral density of internal noise (N_i) was chosen so that the experimental detection threshold curves and the spatial integration curves predicted by the model coincided. The spectral density of internal noise was $8x10^{-6}$ for OL and $22x10^{-6}$ for KT.

Once the detection thresholds parameter values were set, the model parameters determining the strength of the post-detector noise, k and m, were determined on the basis of the contrast increment threshold results. The values which produced the visually best fits in shape were found by calculating model predictions to contrast discrimination data at various values of k and m. The effect of changing the values of parameters k and m on contrast increment threshold predictions of the model is demonstrated in Appendix V.

The parameter k determines how strong the signal dependent post-detector noise is relative to the pre-detector noise. Thus, the larger the k, the stronger the post-detector noise, and the earlier it starts to affect contrast increment thresholds. The k also affects the depth of the dip in the discrimination function. The dip becomes shallower as k increases.

The parameter m determines how fast signal dependent noise increases with signal strength. If m were 1, signal dependent noise would increase in proportion to signal contrast and increment thresholds would be constant. When m is larger than 1, signal dependent noise increases with increasing signal strength so that at high contrast levels it becomes greater than the pre-detector noise (which includes N_e, N_q and N_i). Thus, at high contrasts signal dependent noise determines the increment thresholds which start to increase. Parameter m determines the slope of the increasing part of the contrast discrimination function. The slope s is equal to s=m-1. For example when m=1.8, the slope is 0.8.

The parameters k and m were found to be respectively 0.02 and 1.85 for OL, and 0.01 and 1.8 for KT. These values mean that the dip in the contrast discrimination functions was slightly shallower and the slope of the increasing parts of the functions was steeper for OL than KT. The slope of the increasing part of the functions was 0.85 for OL and 0.8 for KT.

Finally, the adaptation parameter b was determined. Since b was not included in the computer program which was used to solve Equation (5.13) presented in Section 5.1, the value for b was found by transferring the predicted contrast discrimination curves along the pedestal contrast axis until they were superimposed on the experimental data. Without adaptation the correct shape of contrast discrimination curves could be determined by adjusting k and m but the predicted curves always laid to the left of the experimental data, i.e. the dip and the increasing slope occurred at too low pedestal contrasts. The

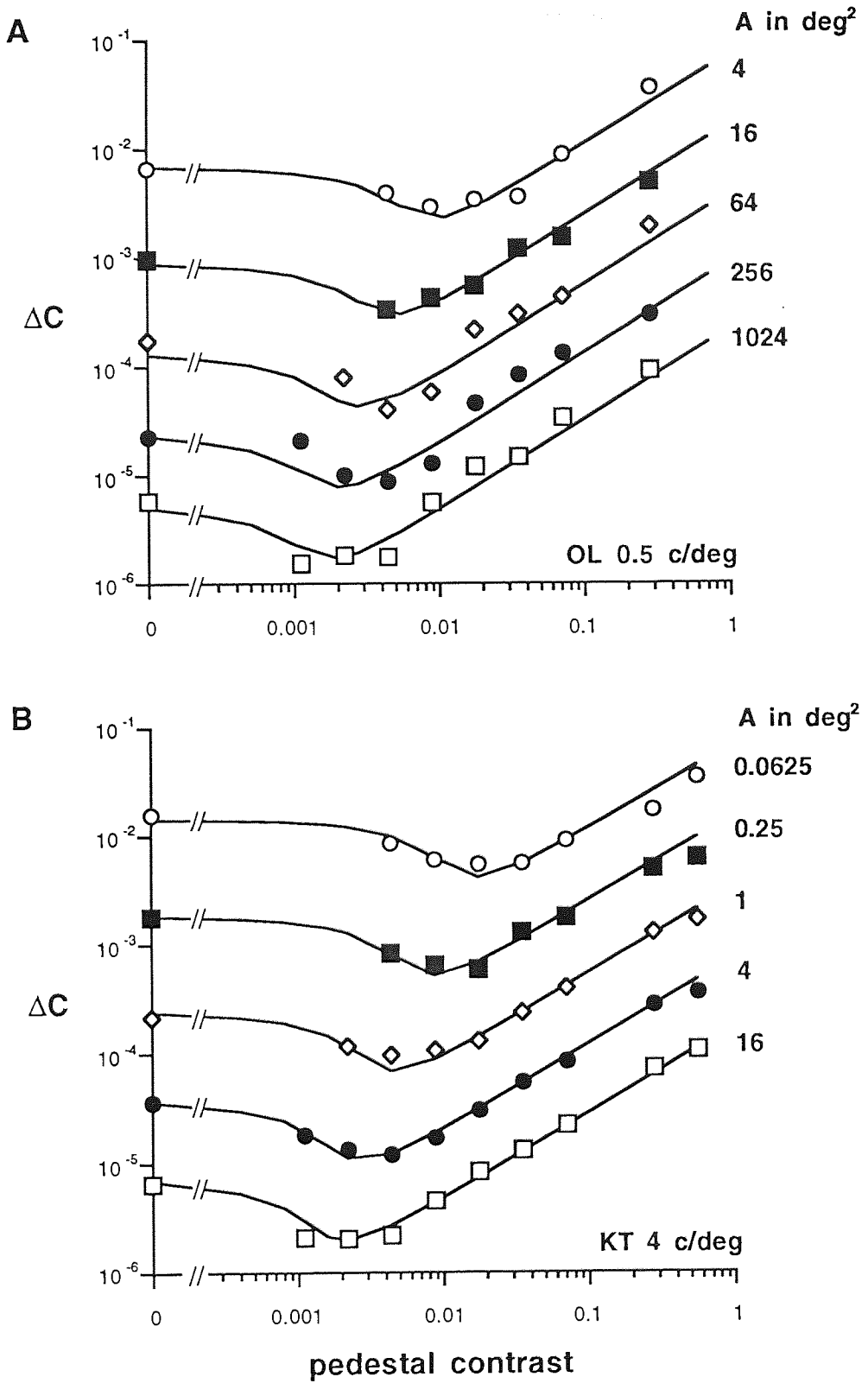

Figure 5.4 Contrast increment threshold data and model predictions with various grating areas (curves have been displaced vertically for clarity).

Parameter	OL	KT
f_c	7	7
n	3	3
N_i	$8x10^{-6}$	$22x10^{-6}$
z_0	60	90
f_0	0.5	0.5
η_{max}	0.4	0.33
k	0.02	0.01
m	1.85	1.8
b	0.4	0.5

Table 5.1 Model parameters for OL and KT in contrast discrimination with various areas.

predictions and data were superimposed when the pedestal contrast was assumed to be reduced by a factor of 2.5 and 2 for subjects OL and KT, respectively. In other words, the adaptation parameter b was 0.4 for OL and 0.5 for KT.

The parameter values which produced the visually best fits to the contrast increment threshold data are collected in Table 5.1. The contrast discrimination functions calculated using these values are plotted in Figure 5.4 together with the experimental data replotted from Figure 5.2. The data and predictions for different areas have been displaced vertically relative to the smallest grating in order to show the individual discrimination curves more clearly. They have been divided by a factor of 1, 4, 16, 64 and 256 for the respective numbers of square cycles.

The model predictions were very accurate. The explained variance for the undisplaced data was 0.944 for OL and 0.976 for KT.

5.2.4 Discussion

Contrast discrimination functions were measured with various grating areas in this study. When pedestal contrast was low, contrast increment thresholds depended strongly on grating area. That is, at low pedestal contrasts, increment thresholds decreased as area increased. At high pedestal contrasts grating area had a smaller effect so that increment thresholds were almost equal for gratings of different areas.

As grating area increased, or in other words, as the detection threshold decreased, the contrast discrimination function retained its shape but moved downwards and to the left. That is, when the detection threshold decreased, increment thresholds also decreased, and the dip in the discrimination function occurred at a lower pedestal contrast. The dip reached its minimum when the pedestal contrast was approximately at detection threshold or slightly above it. This is in agreement with Legge (1979), Bradley and Ohzawa (1986), and Legge and Kersten (1987) who found that the dip is at its deepest when the pedestal is at its detection threshold.

The slope of the increasing parts of contrast discrimination functions was found to be 0.8 for subject KT and 0.85 for subject OL. Previously, estimates of the slope have varied between 0.5 (Pelli, 1985) and 0.9 (Legge & Kersten, 1987). Legge (1979) has pointed out that the steepness of the slope depends on whether it is determined for the entire increasing part of the function starting from the bottom of the dip, or whether only increment thresholds exceeding the detection threshold are taken into account. In the former case the slope is steeper. Not all studies have indicated which range was used but where it has been stated, the slope is about 0.6-0.7 when only increment thresholds above detection threshold are considered (Legge, 1979; Legge, 1981; Legge, 1984b; Swanson & Wilson, 1985). But when estimated from the dip onwards, the slope is about 0.8-0.9 (Kulikowski, 1976; Legge, 1979). Slopes of about 0.8-0.9 have been also been reported in some studies where the method of determination was not clearly stated (Wilson, 1980; Bradley & Ohzawa, 1986; Legge & Kersten, 1987). The slopes found in this study were determined for the entire increasing part of the function, and thus they were in agreement with previous findings.

The results of this study show that spatial integration in contrast discrimination decreases as pedestal contrast increases. At detection threshold, spatial integration is quite extensive. As grating area was increased, detection thresholds decreased up to about 60-90 square cycles after which spatial integration saturated and detection thresholds became independent of area. As pedestal contrast was increased, spatial integration functions for increment thresholds became gradually flatter.

It has been proposed that spatial integration is absent at high contrasts (Legge & Foley, 1980). This would mean that discrimination functions measured with various grating areas should fall together at high pedestal contrasts. According to the new difference-signal discriminator model for contrast discrimination, however, spatial integration only becomes less extensive at high contrast levels. This can be seen in Figure 5.5(A) where the predictions of the model for different grating areas are plotted as a function of pedestal contrast. The predictions are replotted from Figure 5.4(B) but now they are in their

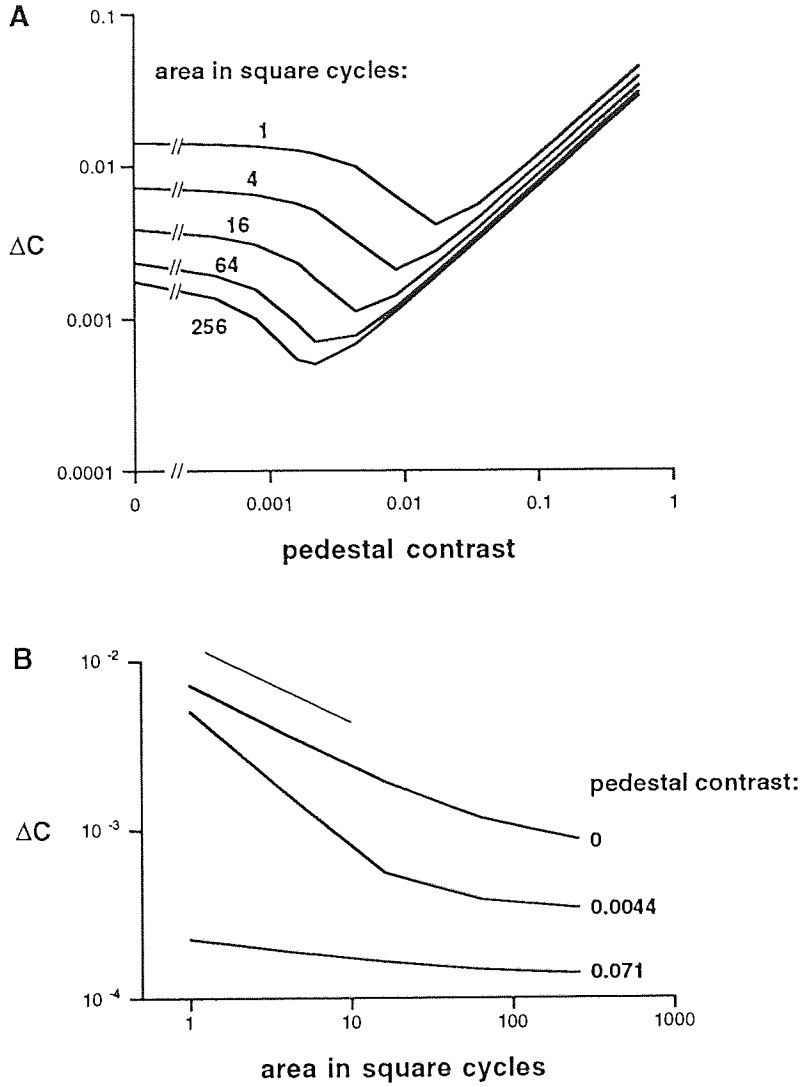

Figure 5.5 Model predictions for contrast increment thresholds with various grating areas.

original positions along the ordinate. Detection thresholds differ clearly for different areas, and so do increment thresholds at low pedestal contrasts. At high pedestals where all functions are increasing, increment thresholds are very similar but still slightly higher for smaller stimuli. The model thus predicts that spatial integration diminishes with increasing pedestal contrast but that it does not totally disappear. However, spatial integration is very limited at high contrast levels. This can be seen in Figure 5.5(B) where three vertical sections of Figure 5.5(A) are plotted to show spatial integration curves at three contrast levels. The curves have been displaced vertically for clarity by dividing

them by a factor of 2, 2 and 40 from top to bottom. The uppermost curve in Figure 5.5(B) shows contrast detection threshold predictions plotted as a function of grating area in square cycles. They decrease with a slope of -0.5 (as shown by the short, straight line above the curve), but at the largest areas the decrease starts to saturate. The lowermost curve shows an example of a curve at a pedestal contrast of 0.071 where spatial integration is at its minimum. The curve is fairly flat implying that spatial integration is weak.

To pursue further the theoretical issue of whether there is no spatial integration or whether integration is very limited at high contrast levels, the experimental data was scrutinised. It was not immediately obvious whether the data supported the no-integration or the diminished-integration hypothesis since the increasing parts of the contrast discrimination functions were very close together, and consequently even small measurement errors caused the curves to mingle. However, in Figure 5.2 there was a tendency for the discrimination curve for the smallest grating to lay slightly above the other curves, and for the curve for the largest grating to lay below others. Also, if there were no spatial integration at high contrast levels contrary to the model predictions, the fits in Figure 5.4 would be expected to deviate systematically from the data with either small or large grating areas. Instead, the model predictions were very accurate at all areas and pedestal contrast levels. These facts give support to the diminished-integration hypothesis.

In Figure 5.5(B), it should also be noted that spatial integration is more rapid at low to medium pedestal contrasts than at detection threshold. That is, when plotted as a function of grating area, increment thresholds decrease with a slope steeper than -0.5. This is shown by the middle curve in Figure 5.5(B) which plots increment threshold predictions at a pedestal contrast of 0.0044. The rapid decrease in increment thresholds occurs because contrast disrimination functions are displaced as grating area is increased so that the dips occur at lower pedestal contrast the larger the grating [see Figure 5.5(A)]. Therefore, at a medium pedestal, an increment threshold for a small grating has decreased very little from the detection threshold, meanwhile for a large grating it is close to its minimum, and thus increment thresholds plotted as a function of grating area decrease with a slope steeper than -0.5 at medium pedestal contrasts.

Spatial integration functions in contrast discrimination differ from those found in contrast detection because of the shape and position of contrast discrimination functions. According to the difference-signal discriminator model, the shape of the discrimination function is determined by the discrimination variable and signal dependent noise. The dip is due to the fact the discrimination variable is calculated on the basis of the response differences of the matched filters. From this it follows that the value of the discrimination variable increases with increasing pedestal contrast, and consequenctly increment

thresholds decrease. The subsequent increase in increment thresholds is due to signal dependent noise. At high contrast levels, signal dependent noise becomes the main factor determining increment thresholds, so that the effect of spatial integration is reduced.

The reason why signal dependent noise reduces spatial integration at high contrast levels is the following. A local matched filter integrates contrast energy across space within a limited window. At low contrast levels where additive pre-filter noise is the dominant noise source, the signal-to-noise ratio increases with stimulus area, and spatial integration is thus extensive. At high contrast levels where signal dependent noise is the dominant noise source, increase in the signal-to-noise ratio with area decelerates because an increase in area produces not only a larger contrast response, but also greater signal dependent noise. Therefore, spatial integration is reduced at high contrasts.

According to the difference-signal discriminator model, the effect of contrast adaptation on pedestal contrast is quite large. Pedestal contrast was reduced to 0.4 and 0.5 of the unadapted value for subjects OL and KT, respectively. It is reasonable to assume that considerable contrast adaptation took place during the experiments since the pedestal contrast was always present in all stimulus exposures, and in each increment threshold measurement many exposures were shown in succession with only a short pause in between.

Previously Georgeson (1985) and Snowden and Hammett (1992) among others have studied the effect of adaptation on perceived contrast. Georgeson (1985) used contrast matching technique to study adapted and unadapted perceived contrast and found that after adaptation the perceived contrast of a grating is reduced by about a third, that is, to 0.67 of the unadapted value. Snowden and Hammett (1992) have presented a similar result in which adaptation to a grating reduces its perceived contrast to about 0.7 of the unadapted value. The adaptation effects found in this and previous studies cannot be directly compared, however, since the effect found in this study is due to instant, spontaneous adaptation which cannot be avoided but in previous studies the effect is due to deliberately induced adaptation.

A possible advantage of contrast adaptation is that it increases the operating range of contrast-encoding neurons by preventing response saturation at high contrasts (Sclar, Lennie & DePriest, 1989). A similar effect can be observed in contrast discrimination since according to the present model, without adaptation contrast discrimination functions would be situated at lower pedestal contrasts so that increment thresholds would start to increase already at rather low contrast levels. Without adaptation contrast discrimination would then be poor at high contrast levels. If the detection threshold for a stimulus were

high, contrast discrimination would not be possible at the highest pedestals. This is because at the highest pedestal contrasts, the maximum contrast increment obtainable would be too small to be discriminated.

In this study, the difference-signal discriminator model for contrast discrimination was successfully applied to describe contrast increment thresholds measured at various grating areas at a large range of contrast levels. The model will be tested further in the next two sections of this thesis.

5.3 Dependence of contrast increment thresholds on the spectral density of external spatial noise

5.3.1 Introduction

External visual noise refers to random luminance variations which mask a stimulus, and thus reduce its visibility. The luminance variations can occur in space or time, or both. Accordingly, the noise is called spatial, temporal or spatiotemporal noise. In the experiments of this chapter only two-dimensional spatial noise was used. Two-dimensional noise consists of dots or pixels which vary randomly in luminance.

The masking effect of visual noise is expressed in terms of spectral density across the spatial frequency spectrum (e.g. Pelli, 1981). Spectral density gives the variance of the contrast signal of the noise at each spatial frequency. The contrast signal is obtained by first calculating the luminance deviation of each noise sample or pixel from the mean luminance and then dividing the deviation by the mean luminance. Spectral density is also affected by the noise pixel size so that it increases as noise pixel size increases. Noise is called white if its spectral density is constant at all spatial frequencies. White noise has thus an equal effect at all spatial frequencies.

External visual noise has been a used in studies applying ideas derived from the signal detection theory because the presence of external noise enables comparison between the performance of an ideal detector and that of a human (Kersten, 1984). An ideal detector represents the best possible performance in a task. Ideal detector's performance is limited only by external noise in the stimulus. Human performance is compared to the ideal to calculate human efficiency (Burgess, 1990). Efficiency, η, is defined as the ratio of the energy threshold of the ideal detector to the energy threshold of a human observer (Tanner & Birdsall, 1958). For further details see Appendix II.

When measured as a function of spectral density of external spatial noise, contrast detection thresholds for cosine gratings are first constant but then they start to increase in proportion to the square root of the noise spectral density (Pelli, 1981). This is because when the external noise is weak, the internal neural noise dominates and determines the detection thresholds which remain at the same level as when measured without external noise. But when the spectral density of external noise is increased so that its effect becomes larger than the effect of internal noise, detection thresholds start to increase with increasing noise level.

When contrast detection thresholds are plotted as a function of noise spectral density, the transition point between the constant and increasing parts of the threshold function is independent of grating area (Nagaraja, 1964; Rovamo, Luntinen & Näsänen, 1995). This means that spatial integration is similar with and without external spatial noise. The position of the transition point depends on spatial frequency, however. The transition point occurs at higher noise levels for low and high spatial frequencies than for mid-frequencies (Rovamo, Luntinen & Näsänen, 1995). The dependence of the transition point on spatial frequency is due to the filtering of the external noise by the optical and neural modulation transfer functions at high and low spatial frequencies, respectively.

Contrast increment thresholds have been measured as a function of spectral density of external spatial noise by Burgess, Wagner, Jennings and Barlow (1981), and Legge, Kersten and Burgess (1987). They have studied the efficiency of human contrast discrimination. Burgess et al. (1981) found that efficiency is higher in contrast discrimination than detection. They showed very little data and did not specify their stimuli very accurately so that it is difficult to make any other conclusions from their study.

Legge et al. (1987) measured contrast increment thresholds as a function of spectral density of external noise. They used 2 c/deg cosine gratings embedded in two-dimensional spatiotemporal noise. Four noise spectral densities including zero were used. The results were expressed in terms of threshold signal energy which was calculated by first subtracting the contrast signal of the pedestal from that of the increment-and-pedestal, and then by squaring the result and integrating it across space. The threshold signal energies were plotted as a function of noise spectral density. Contrast discrimination functions were not plotted perhaps because increment thresholds were measured at only three pedestal contrasts. Legge et al. (1987) concluded that the shape of the contrast discrimination function is due to an initial decrease and a subsequent increase in an observer's equivalent noise, and not due to changes in efficiency. Observer's equivalent noise is equal to the internal noise backprojected into the visual field and expressed in terms of external noise spectral density.

Pelli (1985) has studied the effect of external noise on contrast discrimination functions. He measured discrimination functions for a 4 c/deg cosine grating at three spatiotemporal noise levels including zero. The discrimination function measured without external noise was dipper-shaped. When external noise was added, the function retained its shape but shifted upwards and to the right so that increment thresholds increased at low pedestal contrasts. At high pedestals increment thresholds were almost equal with and without noise.

In this study contrast discrimination functions were measured at various noise spectral densities. Measurements were done with three grating areas at two spatial frequencies. The difference-signal discriminator model for contrast discrimination was then tested with the extensive experimental data obtained with and without external spatial noise.

5.3.2 Methods

The stimuli were square-shaped, vertical cosine gratings. Gratings with side lengths of 1, 4, 8, and 16 cm were used. Spatial frequency was 1 c/cm on the screen. The experiments were performed at two spatial frequencies: 1 c/deg at a viewing distance of 57.3 cm, and 4 c/deg at a viewing distance of 229 cm. At 1 c/deg the grating areas used were 16, 64 and 256 deg^2 and equal in square cycles. At 4 c/deg the grating areas used were 0.0625, 1 and 16 deg^2 which are equal to 1, 16 and 256 square cycles. Henceforth grating area will be expressed in square cycles.

Contrast increment thresholds were measured at pedestal contrasts ranging from 0.0044 to 0.071 in 0.3 log unit steps at various levels of external spatial noise. Contrast detection thresholds were also measured in all conditions. Contrast was always expressed as r.m.s. contrast.

Two-dimensional external spatial noise was created by adding to each noise pixel a random number drawn independently from a Gaussian distribution with zero mean and truncation at ±2.5 standard deviation units. The magnitude of noise was varied by changing the standard deviation of the Gaussian distribution which is equivalent to changing the root-mean-square contrast of the noise. Neighbouring noise pixel luminances were uncorrelated. The noise pixel comprised 3x3 image pixels so that the noise pixel side length was 3x0.0415=0.1245 cm. Spatial frequency of the noise was 8 c/cm. Since the spatial frequency of the stimuli was 1 c/cm, there were 8 noise pixels per grating cycle which is clearly above the critical value of 4. This confirms that the noise could be considered white (Kukkonen, Rovamo & Näsänen, 1995).

When external noise was used, many different noise samples were created because with just one sample it may have been possible to distinguish the stimuli on the basis of noise structure only. With small stimuli it is easier to distinguish different noise samples so that more samples were created for small than large stimuli. For test gratings (increment+ pedestal+noise) 11 different samples were created for each contrast level when grating area was 1 or 16 square cycles, and 5 different samples when grating area was 64 or 256 square cycles. One of the samples was chosen randomly for each exposure. For

comparison gratings (pedestal+noise) 35 samples were created when grating area was 1 or 16 square cycles, and 20 samples when grating area was 64 or 256 square cycles. The same comparison set was used at all grating contrast levels. One of the samples was chosen randomly for each exposure. The same set of test and comparison stimuli was used for three threshold measurements only. If further measurements were needed, a new set of stimuli was created.

The noise field size was equal to the stimulus field size, and the background was of uniform luminance at 50 c/m^2. A black cardboard mask was placed in front of the computer screen to create a square opening with a side length of 20 cm. At least three threshold estimates were obtained for all stimuli, and the data points shown in the figures are based on the geometric means of the estimates.

The spectral density of the two-dimensional spatial noise was calculated according to:

$$N_e = c_n^2 \, p_n \tag{5.14}$$

where c_n is the root-mean-square contrast of the noise and p_n is the noise pixel area in deg^2 (Legge & al., 1987; Kukkonen, Rovamo & Näsänen, 1995). The noise contrasts (c_n) used were 0, 0.019, 0.0375, 0.075, 0.15 and 0.3. The noise pixel area was 0.016 deg^2 at 1 c/deg and 0.00097 deg^2 at 4 c/deg.

Subject HR performed the experiments at 1 c/deg with grating areas of 16, 64, and 256 square cycles at four noise spectral densities. The noise contrasts were 0, 0.0375, 0.15 and 0.3, corresponding to noise spectral densities of 0, 2.18×10^{-5}, 3.49×10^{-4}, and 1.39×10^{-3}.

Subject KT performed the experiments at 4 c/deg with grating areas of 1, 16 and 256 square cycles at six noise spectral densities. The noise contrasts were 0, 0.019, 0.0375, 0.075, 0.15 and 0.3, corresponding to noise spectral densities of 0, 3.41×10^{-7}, 1.36×10^{-6}, 5.45×10^{-6}, 2.18×10^{-5}, and 8.73×10^{-5}.

HR was a corrected hyperope (od.+0.75 DS/os.+1.00 DS), and KT was a corrected myope (od.-6.5 DS/ os.-4.5 DS). The binocular Snellen acuity was at least 1.5 for both subjects.

5.3.3 Results

Figures 5.6 and 5.7 show contrast discrimination functions at various noise spectral densities and grating areas at two spatial frequencies. The experimental data are less regular than data shown in Section 5.2 because external noise causes increased variability in detection and increment threshold measurements.

Figure 5.6 shows contrast increment thresholds plotted as a function of pedestal contrast for HR at 1 c/deg. Grating area was 16, 64 and 256 square cycles in (A), (B) and (C), respectively. Noise spectral density was 0 (filled circles), 2.18×10^{-5} (open diamonds), 3.49×10^{-4} (filled squares), and 1.39×10^{-3} (open circles).

Figure 5.7 shows contrast increment thresholds plotted as a function of pedestal contrast for KT at 4 c/deg. Grating area was 1, 16 and 256 square cycles in (A), (B) and (C), respectively. Noise spectral density was 0 (filled diamonds), 3.41×10^{-7} (open squares), 1.36×10^{-6} (filled circles), 5.45×10^{-6} (open diamonds), 2.18×10^{-5} (filled squares), and 8.73×10^{-5} (open circles). The data at $N_e=0$ have been replotted from Figure 5.2(B).

Figures 5.6 and 5.7 exhibit similar tendencies. Contrast detection thresholds increased with noise spectral density. In Figure 5.7 detection thresholds were very similar at the lowest noise levels, however, which means that the effect of external noise was small relative to the internal noise. Contrast increment thresholds also increased with increasing external noise. The increase was greater at low pedestal contrasts. At high pedestal contrasts increment thresholds became more similar and thus less dependent on external noise.

By comparing (A), (B) and (C) in Figures 5.6 and 5.7 it can be seen that discrimination functions measured at various levels of external noise were quite similar in shape for different areas. Also, in Figure 5.7 it is evident that as grating area was increased, detection and increment thresholds decreased, and the dip occurred at a lower pedestal contrast, in agreement with the results of Section 5.2. In Figure 5.6 the dip is often not very clearly delineated because increment thresholds were not measured at low enough pedestal contrasts to show the exact position of the dip. This applies also to the largest areas and lowest noise levels in Figure 5.7.

The dip in the contrast discrimination functions occurred at a higher pedestal contrast the higher the noise spectral density. The dip also became shallower as noise spectral density increased. It did not totally disappear, however, since increment thresholds were always lower than the detection threshold at a certain range of pedestal contrasts. There was only

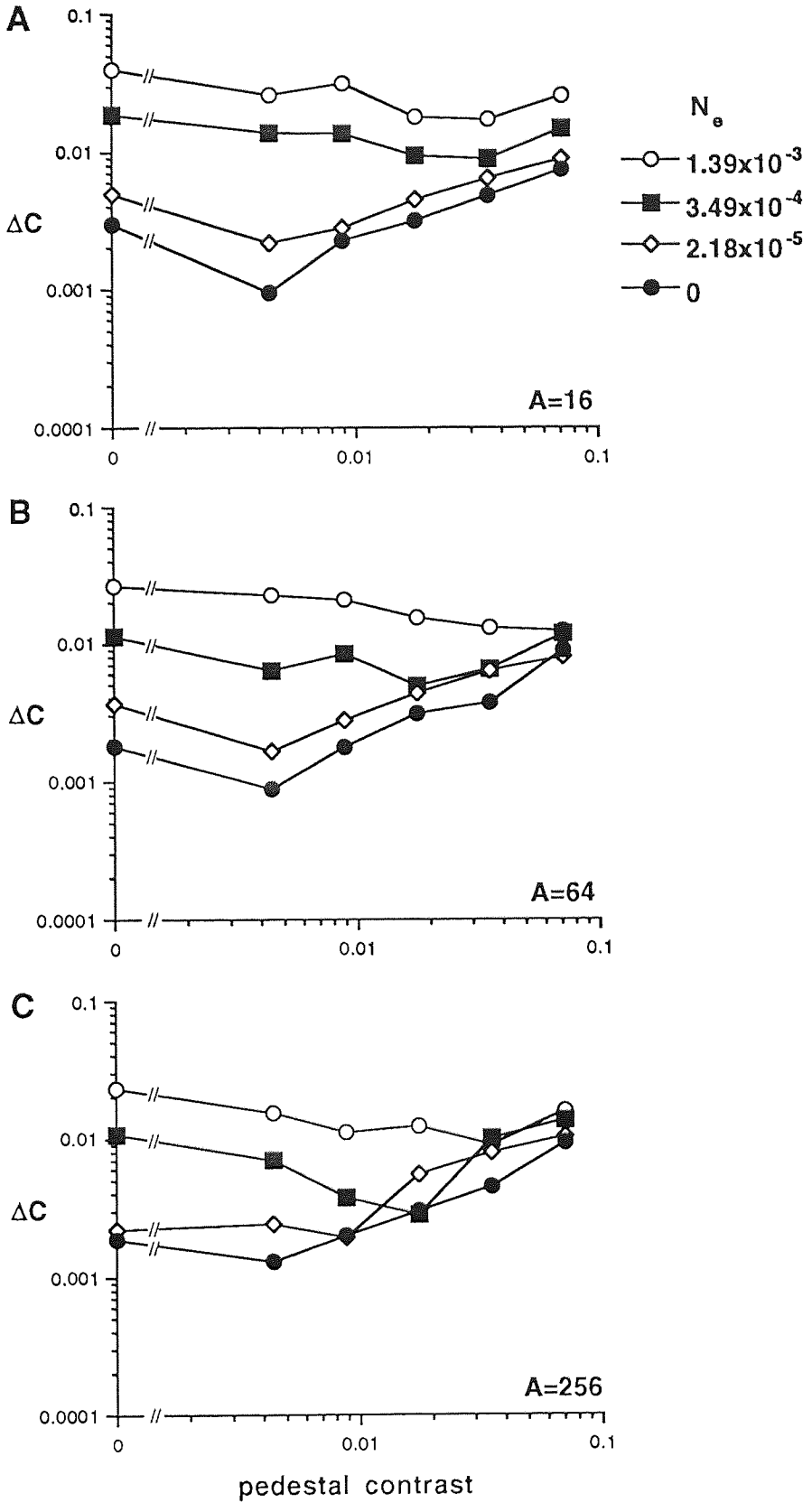

Figure 5.6 Contrast increment thresholds at various noise spectral densities at 1 c/deg.

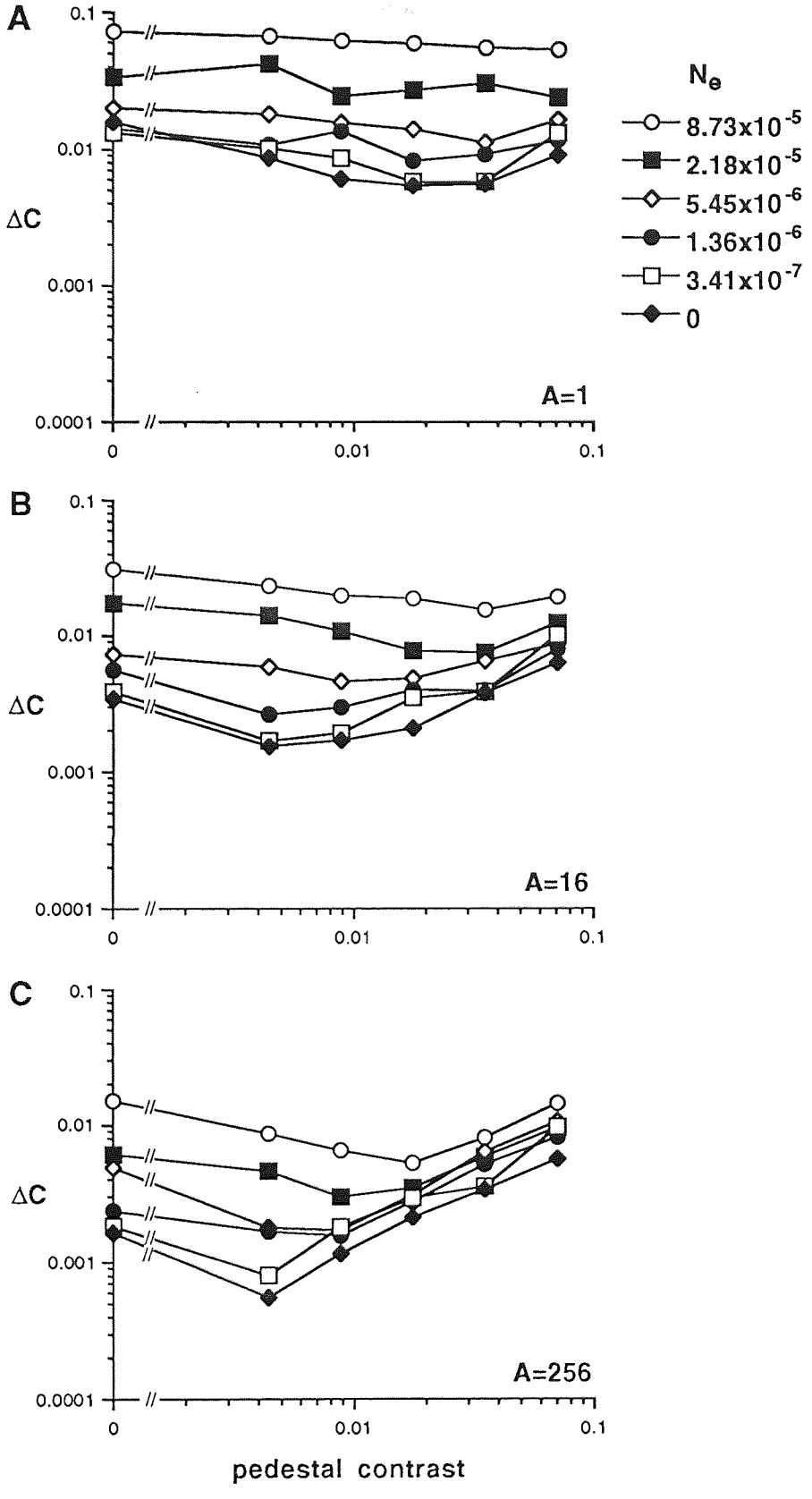

Figure 5.7 Contrast increment thresholds at various noise spectral densities at 4 c/deg.

one exception; the discrimination function was flat at the highest noise level in Figure 5.7(A). This is because increment thresholds were not measured at pedestal contrasts high enough to produce a dip in this condition. At sub-threshold pedestals, increment thresholds remain constant at the same level as the detection threshold, and this is why the above-mentioned discrimination function was flat.

The slope of the increasing parts of the functions was similar at all noise levels. Increment thresholds started to increase at a higher pedestal contrast the higher the noise spectral density. Contrast discrimination functions did not always exhibit an increase especially at high levels of external noise, as can be seen for example in the data plotted with open circles in Figure 5.6(B). An increase in increment thresholds was absent when the detection threshold was so high that the highest pedestal contrast used in the experiments was at or near detection threshold. An increase in increment thresholds would be expected at higher pedestal contrasts.

However, increment thresholds could not be measured at pedestal contrasts higher than 0.071 since when the noise contrast was 0.3, the maximum and minimum luminances in the noise corresponded to a contrast of 0.75 since the Gaussian distribution was truncated at ±2.5 standard deviation units. The maximum contrast available for the stimulus was then 0.25. When pedestal contrast was 0.071, the largest increment available was 0.179, and the highest increment threshold measured was 0.054. If the pedestal contrast had been set at 0.14, the maximum increment would have been 0.11 which would not have been large enough for a reliable increment threshold measurement.

Next, contrast increment thresholds were plotted as a function of noise spectral density. All data behaved similarly when plotted in this way. Therefore only two examples are shown in Figure 5.8 where data from HR at 64 square cycles are plotted in (A) and from KT at 16 square cycles in (B). The leftmost points show increment thresholds measured without external noise. The uppermost curves show detection thresholds (open circles), and pedestal contrast increases towards the bottom of each figure. The pedestal contrasts were 0.0044 (filled squares), 0.0088 (open diamonds), 0.018 (filled circles), 0.035 (open squares), and 0.071 (filled diamonds).

The data have been displaced vertically because the curves for different pedestal contrasts crossed and overlapped considerably when they were in their original positions. The curves at 0, 0.0044, 0.0088, 0.018, 0.035 and 0.071 have been multiplied respectively by a factor of 3, 2, 0.5, 0.17, 0.056 and 0.016 in Figure 5.8(A), and by a factor of 3, 1, 0.33, 0.11, 0.037 and 0.0062 in Figure 5.8(B).

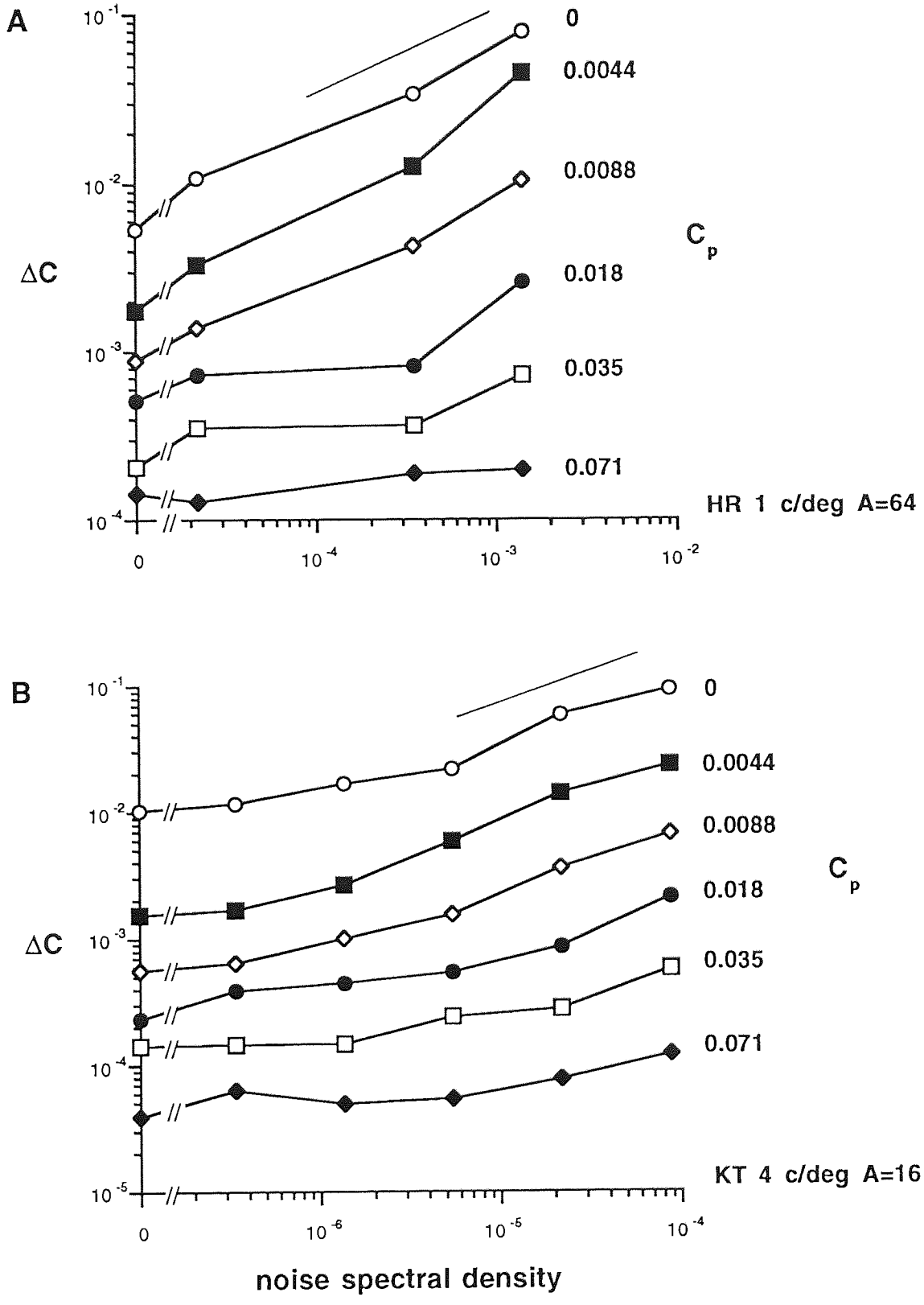

Figure 5.8 Contrast increment thresholds plotted as a function of noise spectral density (displaced vertically).

As noise spectral density was increased, contrast detection thresholds first remained constant and then started to increase with a slope of 0.5, in agreement with previous findings (e.g. Pelli, 1981). The short, straight lines on top of each figure show a slope of 0.5. Constancy of detection thresholds can only be seen in Figure 5.8(B) since in experiments of Figure 5.8(A) detection thresholds were not measured at noise spectral densities low enough to show the constant part of the functions.

As pedestal contrast was increased, the slope of increase seemed to remain approximately at 0.5 but the transition point between the constant and increasing parts of the curves tended to displace to higher noise spectral densities. This suggests that the effect of external noise grew smaller as pedestal contrast was increased. There is a tendency for the increment thresholds to increase at a slightly faster rate at low pedestal contrasts than at detection threshold, and for the transition point to occur at a slightly lower level of external noise (see the filled squares).

Next, the model of contrast discrimination was applied to the increment threshold results. Contrast detection threshold parameters were determined first. The parameters f_0, f_c and n were set at the previously determined values 0.5, 7 and 3 for both subjects.

Initial estimates of the spectral density of internal noise (N_i), the maximum efficiency (η_{max}), and the maximum of the critical number of square cycles in the integration function (z_0) were determined for both subjects on the basis of the detection threshold model (e.g. Rovamo, Luntinen & Näsänen, 1993&1995).

An estimate of the spectral density of internal noise was obtained by first calculating the critical spectral density of external noise, N_c. The external noise used in these experiments was spatial whereas quantal noise is spatiotemporal. However, internal noise can be described in terms of static external noise since both spatial and spatiotemporal noise have a qualitatively similar effect on detection thresholds (cf. e.g. Nagaraja, 1964; Rovamo, Luntinen & Näsänen, 1995). When detection thresholds are measured as a function of external noise, the critical spectral density marks the transition between the constant and increasing parts of the functions. Contrast energy threshold has doubled from the minimum at N_c. From this it follows that, when filtered through the optical and neural modulation transfer functions, N_c is equal to N_i (Rovamo, Luntinen & Näsänen, 1995):

$$N_i = H_o^2(f)\, H_n^2(f)\, N_c \qquad (5.15)$$

The critical spectral density of spatial noise was determined on the basis of contrast detection thresholds measured at various levels of external noise by a method described in

Appendix VI. The N_c was found to be $8x10^{-6}$ for HR, and $1.6x10^{-6}$ for KT. Equation (5.15) was then solved, and the estimated N_i:s were $8x10^{-6}$ for HR and $18x10^{-6}$ for KT.

Then, the maximum efficiency and the maximum of the critical number of square cycles in the integration function were estimated. First, efficiencies for each measured detection threshold were calculated by: $\eta=d'^2(N_e+N_c)\ E_d^{-1}$, where E_d is contrast energy at detection threshold. This equation is equal to Equation (4) in Appendix II. The dependence of efficiency on grating area was then modelled by: $\eta=\eta_{max}(1+z/z_c)^{-1}$ as explained in Sections 4.1 and 5.1. Estimates of η_{max} and z_c were obtained by solving Equation (5.17) using the method described in Appendix VI. For HR the estimated values were $\eta_{max}=0.16$ and $z_c=65$ ($R^2=0.847$). For KT they were $\eta_{max}=0.47$ and $z_c=39$ ($R^2=0.767$). The estimate for z_0 was then calculated by $z_0=z_c(f_0^2+f^2)/f^2$. It was 81 for HR and 40 for KT. These estimates were not very reliable, though, since the explained variances were rather poor.

Next, the estimated parameter values were applied and model predictions for detection thresholds were calculated. The values were then adjusted to produce best fits to the data. The visually best fits were obtained with the parameter values shown in Table 5.2. The maximum of the critical number of square cycles in the integration function (z_0) was 45 for HR, and 90 for KT which is the same value as in Section 5.2.

It was necessary to determine the η_{max} accurately since if it was set at a wrong value, detection threshold predictions at various noise levels did not coincide with the data. For example, if η_{max} was too high, the predictions and data could be made to coincide at $N_e=0$

Parameter	HR	KT
f_c	7	7
n	3	3
N_i	$8x10^{-6}$	$22x10^{-6}$
z_0	45	90
f_0	0.5	0.5
η_{max}	0.17	0.33
m	1.8	1.8
b	0.5	0.5

Table 5.2 Model parameters for HR and KT in contrast discrimination at various levels of external noise.

by increasing the spectral density of internal noise, but at higher external noise spectral densities model predictions were too low. This is because when the external noise was the dominant source of noise, the detection thresholds were determined by $d'^2 = \eta E/(N_e + N_c) \approx \eta E/N_e$, where d'^2=2, and E is the contrast energy threshold. Thus if η was increased, the predicted energy threshold E decreased and vice versa. The maximum efficiency which produced the most accurate detection threshold predictions at different levels of external noise was found to be 0.17 for HR and 0.33 for KT.

The spectral density of internal noise (N_i) was adjusted so that the experimentally measured and predicted detection thresholds coincided. The spectral density of internal noise was 8×10^{-6} for HR. For KT it was 22×10^{-6} which is the same value as in Section 5.2.

With these parameters the model could describe contrast detection thresholds at various external noise spectral densities very accurately.

N_e	k
0	0.010
2.18×10^{-5}	0.025
3.49×10^{-4}	0.040
1.39×10^{-3}	0.045

Table 5.3 Dependence of k on the spectral density of external noise for HR.

N_e	k
0	0.010
3.41×10^{-7}	0.015
1.36×10^{-6}	0.020
5.45×10^{-6}	0.033
2.18×10^{-5}	0.040
8.73×10^{-5}	0.045

Table 5.4 Dependence of k on the spectral density of external noise for KT.

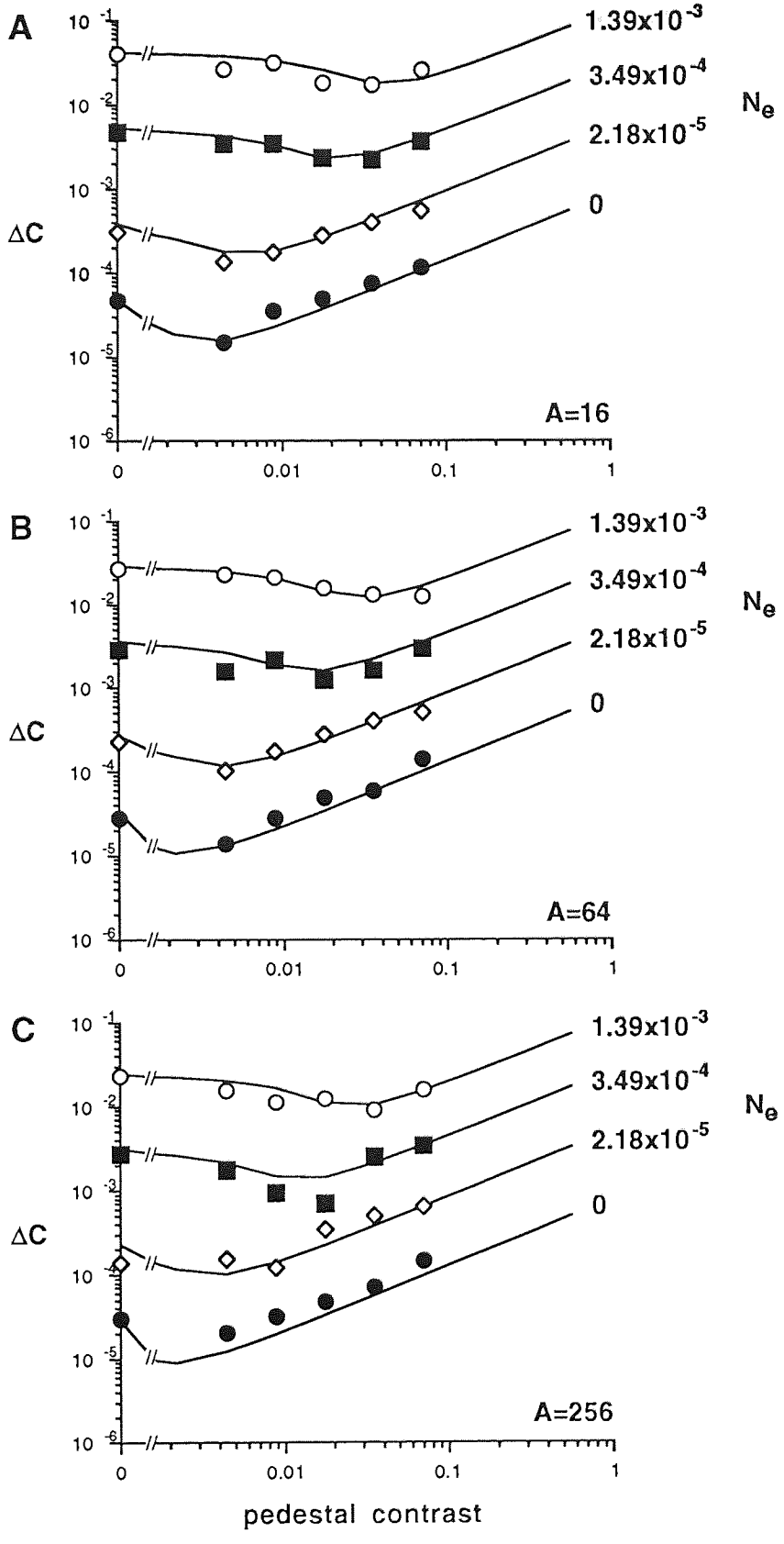

Figure 5.9 Contrast increment threshold data and model predictions at various noise spectral densities at 1 c/deg (curves have been displaced vertically for clarity).

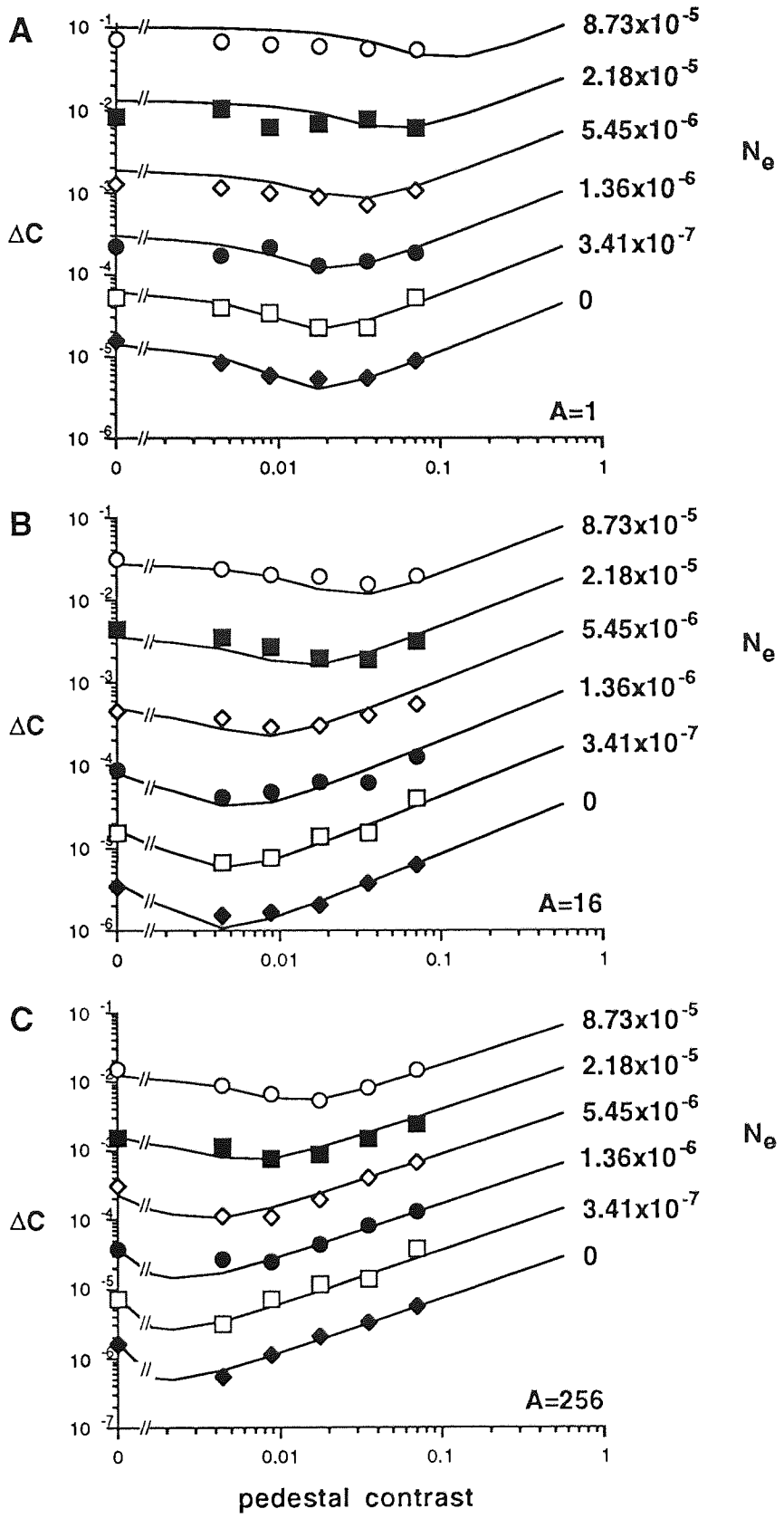

Figure 5.10 Contrast increment threshold data and model predictions at various noise spectral densities at 4 c/deg (displaced vertically).

The model parameters determining the strength of the post-detector noise, k and m, were then adjusted so that the shape of the predicted contrast discrimination functions was as similar as possible to that of the measured discrimination functions. The parameter m was found to be 1.8 for both subjects. Thus, the slope of the increasing part of the functions was 0.8. This is the same slope as was found for KT in Section 5.2.

The parameter k depended on the spectral density of external noise since the dip in the contrast discrimination functions became shallower as the noise level was increased and since the increasing parts of the contrast discrimination functions did not converge at high contrasts. The most appropriate value for k was found by adjusting it so that the dip in the predicted contrast discrimination function was of the same depth as in the experimentally measured functions at each noise level. The values of k are shown in Table 5.3 for HR and in Table 5.4 for KT.

The adaptation parameter b was found to be equal to 0.5 for both subjects. All parameter values used to calculate the model predictions are shown in Tables 5.2, 5.3, and 5.4.

The model predictions are plotted in Figures 5.9 and 5.10 together with the experimental data replotted from Figures 5.6 and 5.7, respectively. The data and predictions have been displaced vertically so that the individual contrast discrimination curves can be seen more clearly. In Figure 5.9 the data and predictions have been divided by 1, 4, 16 and 64 for noise spectral densities of 0, 2.18×10^{-5}, 3.49×10^{-4} and 1.39×10^{-3}, respectively. In Figure 5.10 the data and predictions have been divided by 1, 4, 16, 64, 256 and 1024 for noise spectral densities of 0, 3.41×10^{-7}, 1.36×10^{-6}, 5.45×10^{-6}, 2.18×10^{-5} and 8.73×10^{-5}, respectively.

As Figures 5.9 and 5.10 show, the model predictions were quite accurate. The explained variance for the undisplaced data was 0.956, 0.936 and 0.838 in Figure 5.9(A), (B) and (C) respectively, and 0.893, 0.928 and 0.950 in Figure 5.10(A), (B) and (C) respectively.

5.3.4 Discussion

Contrast increment thresholds were measured at various levels of external spatial noise with different grating areas at spatial frequencies of 1 and 4 c/deg. Increment thresholds increased with noise spectral density but the increase was smaller at high pedestal contrasts. This means that the effect of external noise reduced at high pedestal contrasts. Pelli (1985) has found that at pedestal contrasts above about 0.1 increment thresholds are independent of external noise. In this study pedestal contrasts higher than 0.1 could not

be used, and consequently it could not be experimentally verified whether increment thresholds become independent of noise level at higher pedestal contrasts. However, the data obtained in this study exhibit a trend which implies that increment thresholds measured at various levels of external noise do not totally converge even at the highest pedestal contrasts.

The finding that the effect of external noise is reduced at high pedestal contrasts can be explained by assuming that the intrinsic noise in the visual system increases with signal contrast so that it becomes the dominant source of noise at high contrast levels. This assumption is supported also by another finding. When increment thresholds were plotted as a function of noise spectral density, the transition between the constant and increasing parts of the curves occurred at a higher noise spectral density the higher the pedestal contrast. This implies that the effect of intrinsic noise grew larger as pedestal contrast was increased since the critical noise spectral density increased.

Legge et al. (1987) have found that in contrast discrimination the observer's equivalent noise, i.e. the critical noise first decreases and then increases as pedestal contrast is increased. The results presented in this chapter are in agreement with Legge et al. (1987) since at high contrasts there was an increase in the critical noise as pedestal contrast was increased. Also, an initial decrease was observed here in Figure 5.8(B) at the lowest pedestal contrasts since increment thresholds seemed to start to increase at a lower noise spectral density than detection thresholds.

According to the contrast discrimination model, the apparent increase in intrinsic noise is due to an increase in signal dependent noise. The variance of matched filter responses increases with response magnitude and consequently with signal strength. At high contrasts signal dependent noise becomes greater than the pre-filter noise, i.e. external, quantal and internal noises which are all additive and independent of signal strength. Hence, at high contrast levels signal dependent noise becomes the main factor determining increment thresholds which then become less dependent on pre-filter noise.

The results of this study showed that in the presence of external noise the dip in the contrast discrimination functions was displaced towards higher pedestal contrasts. The reason for this is that external noise increased detection thresholds, and as detection threshold increases, increment thresholds increase and the dip occurs at a higher pedestal contrast. Pelli (1985) has found that the dip in contrast discrimination functions measured in external noise occurs when the pedestal is approximately at its detection threshold. This is in agreement with the present results.

The shape of contrast discrimination functions changed slightly with increasing level of external spatial noise. The slope of increase was independent of external noise but the dip in the functions decreased as noise spectral density was increased. The dip did not disappear, though, which confirms Pelli's (1985) similar finding.

In order to describe the decrease in the depth of the dip, and the finding that discrimination functions did not converge at high pedestal contrast in the presence of external noise, the parameter k in the contrast discrimination model was increased with external noise level. Had the k been kept constant, the depth of the dip would have been constant, and increment threshold predictions would have been equal for all levels of external noise at high pedestal contrasts.

The increase of k with external noise suggests that post-filter noise includes a component which depends on the spectral density of external spatial noise. Thus, it seems that post-filter noise is not only signal dependent but it also depends on external noise. Since a noise-dependent-noise component is not included in the post-filter noise in the model, its existence is reflected in the dependence of the parameter k on the spectral density of external noise.

Burgess and Colborne (1988) have found that internal noise increases with external noise in contrast detection and discrimination. They proposed that internal noise includes two components: one is constant, and the other is proportional to the spectral density of external noise. The second component is thus noise dependent noise. Their findings are in agreement with the present findings if signal dependent noise is also taken into account. Then the constant noise component would correspond to the pre-filter noise, and the increasing component would correspond to the noise and signal dependent post-filter noises.

An example of the model predictions for contrast increment thresholds at various spectral densities of external noise is shown in Figure 5.11(A) where predictions are plotted as a function of pedestal contrast. The predictions are replotted from Figure 5.10(B) but now they are in their original positions. Contrast discrimination functions measured at different levels of noise do not overlap. External noise increases increment thresholds most at low pedestal contrasts. At high pedestals, the discrimination functions are increasing and very close together but they remain parallel.

In Figure 5.11(B) three vertical sections of Figure 5.11(A) have been plotted as a function of noise spectral density. The curves have been displaced vertically for clarity by multiplying them by a factor of 4, 3 and 0.2 from top to bottom. Figure 5.11(B) shows

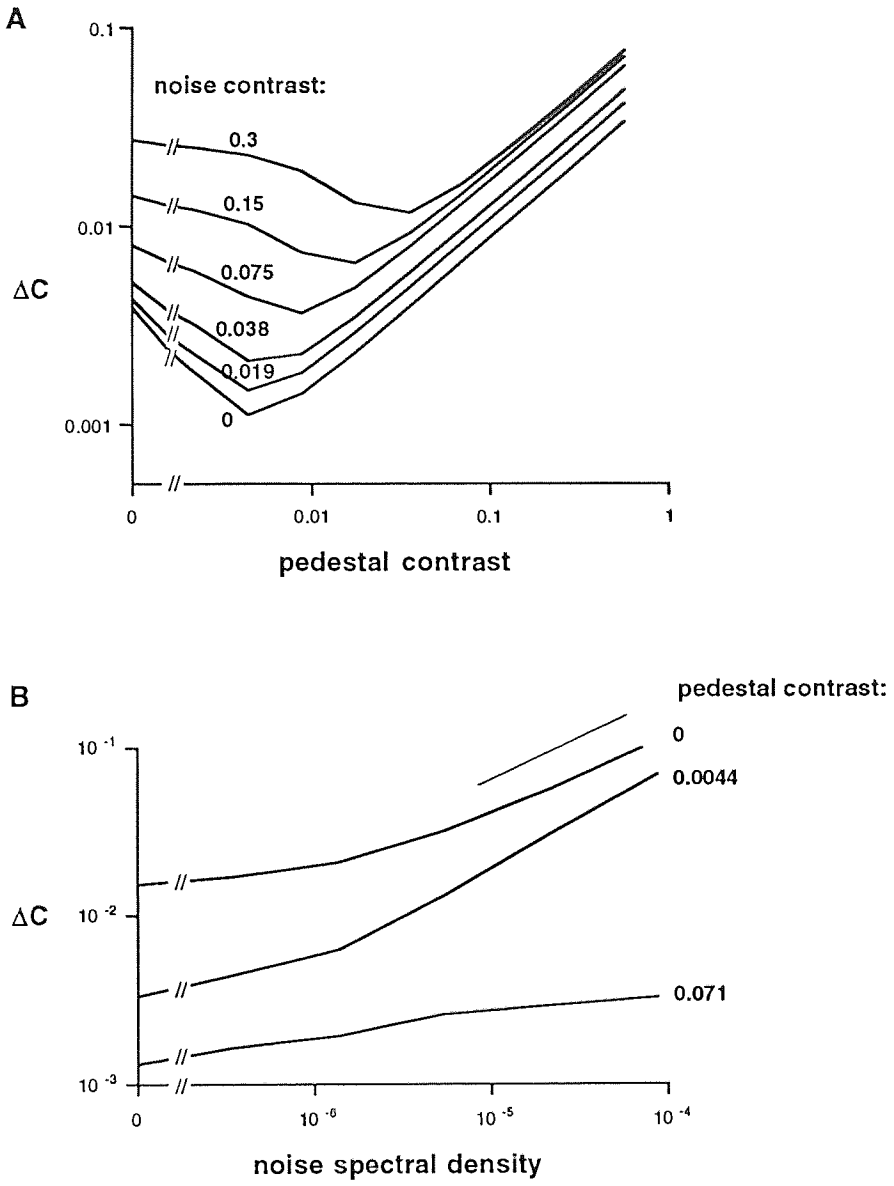

Figure 5.11 Model predictions for contrast increment thresholds at various levels of external noise.

that contrast detection and increment thresholds increase with noise spectral density after external noise exceedes a certain level. The uppermost curve shows contrast detection threshold predictions. They are first constant, but as noise spectral density increases, they start to increase with a slope of 0.5, which is demonstrated by the short line segmant above the curve. The middle curve shows that at a medium pedestal contrast, increment thresholds increase at a faster rate than detection thresholds with external noise, so that the

slope of increase is greater than 0.5. The lowermost curve shows an example of a curve at a pedestal contrast of 0.071 where all contrast discrimination functions are increasing, and where the effect of external noise is smallest. The fact that the curve is not flat indicates that increment thresholds are not totally independent of external noise.

The reason why contrast increment thresholds behave differently from detection thresholds when plotted as a function of external noise is that contrast discrimination functions shift upwards, and that the dip is displaced towards higher pedestals with increasing noise level. Therefore, at a medium pedestal, an increment threshold measured at a low noise level is close to its minimum, while when measured at a high noise level, it has decreased only little from the detection threshold. Consequently, increment thresholds plotted as a function of external noise level increase with a slope greater than 0.5 at medium pedestal contrasts. Then at high pedestal contrasts, discrimination functions are increasing and close together so that when increment thresholds are plotted as a function of noise spectral density, the slope of increase is shallower than 0.5.

Finally, it can be concluded that the dependence of contrast increment thresholds on the spectral density of external spatial noise could be described accurately by the difference-signal discriminator model for contrast discrimination.

5.4 *Dependence of contrast increment thresholds on retinal illuminance*

5.4.1 Introduction

Contrast detection thresholds have been measured as a function of retinal illuminance for cosine gratings of various areas and spatial frequencies (van Nes & Bouman, 1967; Mustonen, Rovamo & Näsänen, 1993). Detection thresholds obey DeVries-Rose law at low and Weber's law at high retinal illuminances (DeVries, 1943; Rose, 1948). That is, at low luminance levels detection thresholds decrease in proportion to the square root of the retinal illuminance, and at high luminance levels detection thresholds are independent of the retinal illuminance. The transition point between the decreasing and constant parts of the detection threshold curve is independent of area but depends on the spatial frequency of the grating. It is directly proportional to spatial frequency squared (van Nes, Koenderink, Nas & Bouman, 1967).

A decrease in retinal illuminance results in an increase of quantal noise. The spectral density of quantal noise (N_q) is inversely proportional to the retinal illuminance (I). That is: $N_q=k/I$, where k is a constant (Pelli, 1990; Rovamo, Mustonen & Näsänen, 1994a). The effect of quantal noise on contrast detection thresholds is thus similar to the effect of external spatial noise since detection thresholds are constant at low levels of spatial or quantal noise but at high noise levels they increase in proportion to the square root of the spectral density of spatial or quantal noise.

Dependence of contrast increment thresholds on retinal illuminance has been studied only at a very narrow range of parameters. Kulikowski (1976) has measured contrast increment thresholds for a 5 c/deg grating of a constant area at three luminance levels: 0.1, 1 and 10 cd/m^2. His results show that at low pedestal contrasts increment thresholds increase with decreasing luminance but at high pedestal contrasts they are very similar at all light levels.

Bradley and Ohzawa (1986) measured contrast increment thresholds for a 4 c/deg grating of a constant area at retinal illuminances of 2 and 1250 trolands (td). Contrast discrimination functions were dipper-shaped at both retinal illuminances. At low pedestal contrasts detection thresholds and increment thresholds were higher at 2 than at 1250 td. The dip in the discrimination function occurred at a higher pedestal contrast at 2 than at 1250 td. At high pedestal contrasts increment thresholds were almost equal at both retinal illuminances.

In the experiments presented in this section the dependence of contrast increment thresholds on retinal illuminance was systematically studied. Contrast discrimination functions were measured for gratings of various sizes at spatial frequencies of 2 and 8 c/deg at up to five retinal illuminances. The aim of these investigations was to study the dependence of contrast discrimination functions on luminance level, and the dependence of increment thresholds plotted as a function of retinal illuminance on pedestal contrast. The contrast discrimination model was also applied to the experimental results. According to the model, external spatial and quantal noises should have a similar effect on both detection and increment thresholds so that one may expect similar results here as in the previous Section 5.3 where increment thresholds were measured in external spatial noise.

5.4.2 Methods

The stimuli were square-shaped, vertical cosine gratings. Five grating sizes were used with side lengths of 1, 2, 4, 8, and 16 cm. Spatial frequency was 1 c/cm on the screen. The number of square cycles ($z=Af^2$) in the gratings was thus 1, 4, 16, 64 and 256, respectively. The experiments were performed at two spatial frequencies: 2 c/deg at a viewing distance of 115 cm, and 8 c/deg at a viewing distance was 458 cm.

At 2 c/deg the experiments were performed by subject SU with a 16 square cycle (=4 deg^2) grating, and by subject TK with a 256 square cycle (=64 deg^2) grating at four retinal illuminances: 2513, 157, 9.8, and 0.6 td (=photopic trolands). At 8 c/deg the experiments were performed by subject KT with grating areas of 1, 4, 16, 64 and 256 square cycles (i.e. 0.0156, 0.0625, 0.25, 1 and 4 deg^2) at five retinal illuminances: 2513, 628, 157, 39 and 9.8 td. The subjects viewed the screen monocularly with the dominant eye. They wore a full spectacle correction which was od.-6.50 DS for KT, od.-4.0 DS for SU, and os.-7.25 DS/-0.75 x 165 for TK. The Snellen acuity was at least 1.2 for all subjects.

The pupil of the dominant eye was dilated to 8 mm with two drops of 10% Phenylephrine (Metaoxedrine) Hydrochloride. This was preceded by installation of one drop of 0.4% Benoxinate (Oxybuprocaine) Hydrochloride to increase drug absorption. Both drugs were obtained from single use disposable units (Smith & Nephew Pharmaceuticals Ltd, Romford, England). Metaoxedrine leaves accommodation unaffected. The other eye was covered by a black eye pad.

The average retinal illuminance produced by the display at 50 cd/m^2 mean luminance through a pupil with 8 mm diameter was 2513 td (=photopic trolands). Lower levels of retinal illuminance were obtained by placing a desired number of neutral density filters

(Lee Filters Ltd., Hampshire, U.K.) of 0.6 logarithmic units (No 210 ND) on the screen. A black cardboard mask was placed in front of the computer screen to create a square opening with a side length of 20 cm. The filters were inserted in the mask and fixed by black opaque tape that prevented leakage of light from between the filters and screen. After each luminance reduction of 0.6 logarithmic units, the subject adapted to the new screen luminance for 5 minutes.

Contrast increment thresholds were measured at pedestal contrasts ranging from 0.0011 to 0.28 in 0.3 log unit steps. Contrast detection thresholds were also measured. Contrast was always expressed as r.m.s. contrast All data shown are based on geometric means of at least three threshold estimates.

5.4.3 Results

Contrast increment thresholds measured with different grating areas at various levels of retinal illuminance are shown in Figures 5.12 and 5.13 where they are plotted as a function of pedestal contrast. Quantal noise increases the variability of threshold measurements so that contrast discrimination functions are somewhat more irregular than those shown in Section 5.2.

Figure 5.12 shows the results at 2 c/deg. In (A) the subject was SU and grating area was 16 square cycles. In (B) the subject was TK and grating area was 256 square cycles. In both (A) and (B) retinal illuminances were 2513 (filled circles), 157 (open diamonds), 9.8 (filled squares), and 0.6 trolands (open circles).

Figure 5.13 shows the results for KT at 8 c/deg. Grating area was 1, 4, 16, 64 and 256 square cycles in (A), (B), (C), (D) and (E), respectively. Retinal illuminances were 2513 (open squares), 628 (filled circles), 157 (open diamonds), 39 (filled squares), and 9.8 trolands (open circles).

As retinal illuminance was decreased, contrast detection thresholds in Figures 5.12 and 5.13 increased. Between the two highest light levels the increase was often small, however. Contrast increment thresholds also increased with decreasing retinal illuminance but the increase was greater at low pedestal contrasts and decreased towards high pedestal contrasts.

The shape of the contrast discrimination functions measured at various light levels was rather similar for different areas as can be seen by comparing (A), (B), (C), (D) and (E) in

Figure 5.13. The functions shifted downwards on the ordinate, and the dip displaced towards lower pedestals as area was increased. These results give further support to the results of Section 5.2.

As retinal illuminance was decreased, the dip in the contrast discrimination functions was displaced towards higher pedestal contrasts, and it also tended to become shallower.

The slope of the increasing parts of the functions was similar at all light levels. As retinal illuminance was decreased, the increase in increment thresholds started at higher pedestal contrasts. The increase was not always visible in the discrimination functions especially at low light levels, as can be seen for example in the data plotted with open circles in Figure 5.13(A). Discrimination functions did not exhibit an increase when the highest pedestal contrast used in the experiments was at or near detection threshold. An increase in increment thresholds would occur if increment thresholds could be measured at higher pedestal contrasts. That was not possible, however, since at pedestal contrasts higher than 0.28, the maximum increment available would have been too low to permit threshold measurement at the lowest light levels.

Contrast increment thresholds were then plotted as a function of retinal illuminance. Only two sets of results are shown in Figure 5.14 since all data behaved rather similarly when plotted in this way. Data from TK at 256 square cycles are plotted in (A) and from KT at 16 square cycles in (B). The uppermost curves show detection thresholds (open circles). Pedestal contrast increases towards the bottom of each figure.

The data have been displaced vertically to avoid overlapping of the curves. In Figure 5.14(A) the curves at 0, 0.0088, 0.018, 0.035, 0.071, 014 and 0.28 have been multiplied respectively by a factor of 16, 8, 1, 0.25, 0.03, 0.004 and 0.001. In Figure 5.14(B) the curves at 0, 0.018, 0.035, 0.071, 014 and 0.28 have been multiplied respectively by a factor of 4, 2, 1, 0.25, 0.06 and 0.016.

Contrast detection thresholds decreased with increasing retinal illuminance with a slope of -0.5 which indicates that DeVries-Rose law was valid. The short, straight lines on top of each figure show a slope of -0.5. The curves in Figure 5.14 do not show the constancy of detection thresholds at high light levels. However, the decrease in thresholds decelerated at the highest retinal illuminances implying that if measured at a higher light level, the decrease would have saturated.

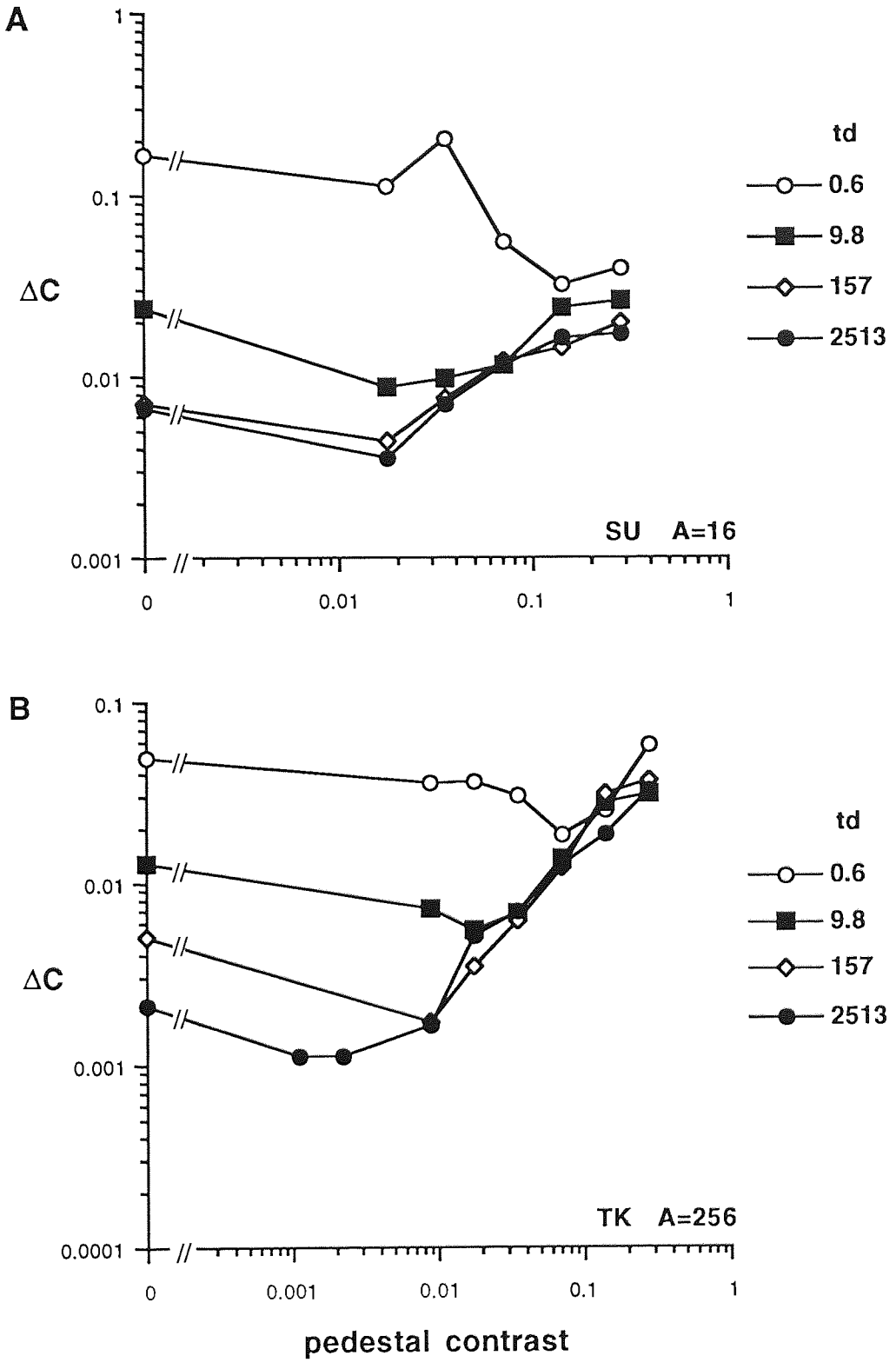

Figure 5.12 Contrast increment thresholds at various retinal illuminances at 2 c/deg.

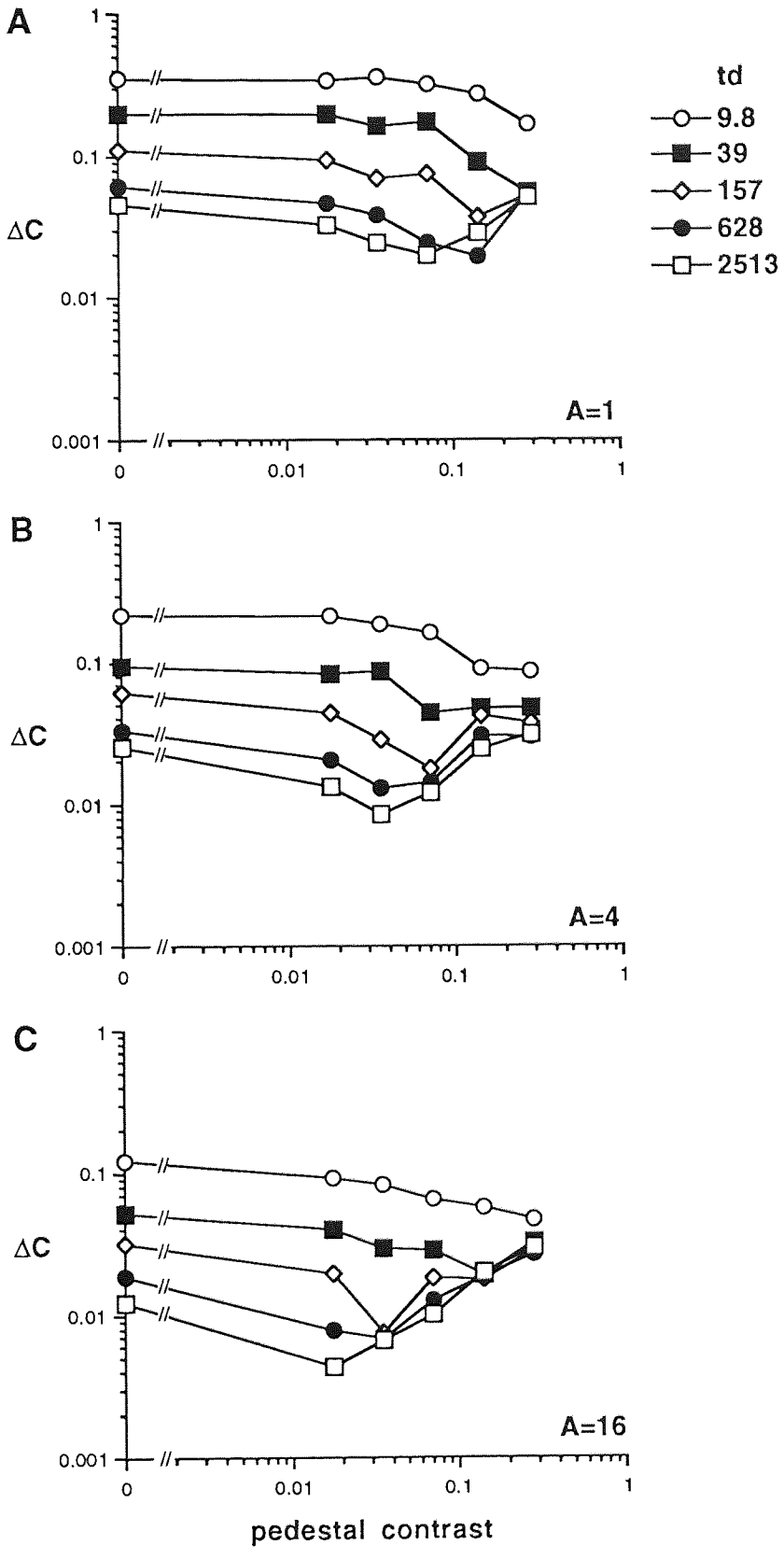

Figure 5.13 (Continues on the next page).

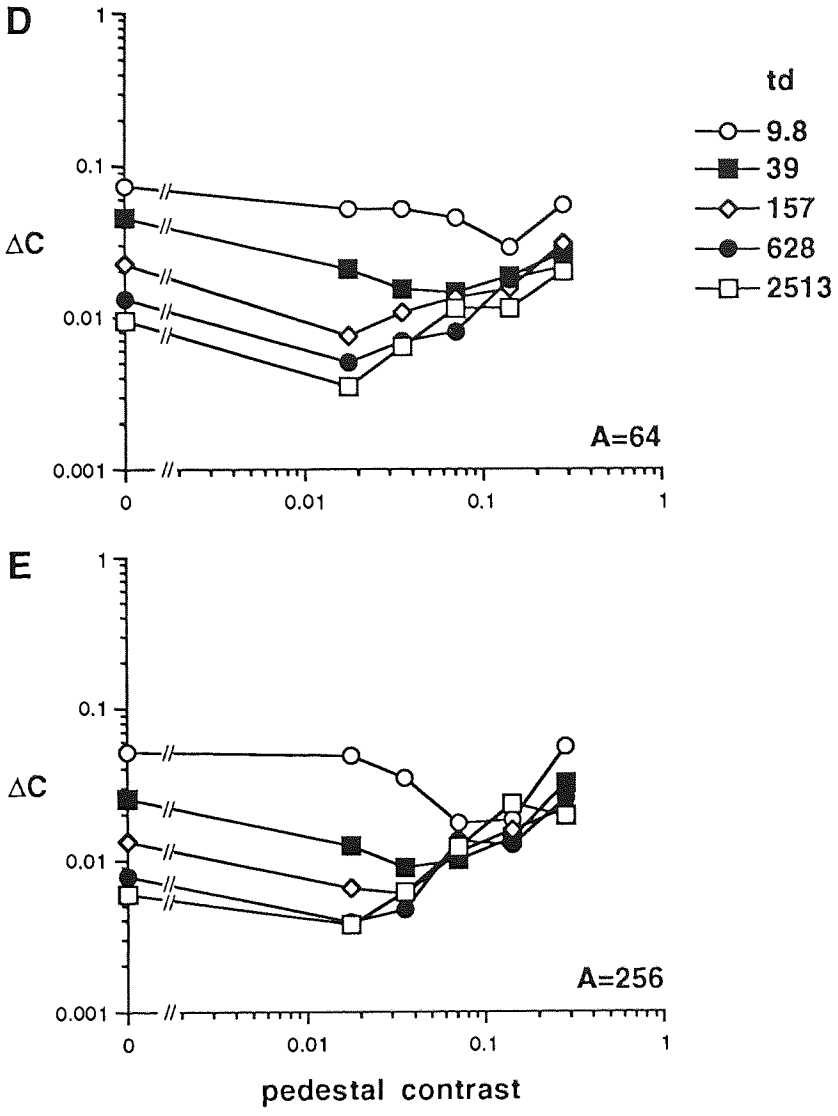

Figure 5.13 Contrast increment thresholds at various retinal illuminances at 8 c/deg.

Contrast increment thresholds plotted as a function of retinal illuminance behaved in a broadly similar manner as detection thresholds but there were also significant differences. As retinal illuminance was increased, increment thresholds decreased. The decrease, however, did not always obey DeVries-Rose law. In some conditions thresholds decreased at a faster rate than predicted by DeVries-Rose law, i.e. the slope of decrease was steeper than -0.5. This can be seen for example at pedestal contrast of 0.035 (open diamonds) in Figure 5.14(B). At high light levels thresholds were nearly independent of luminance thus obeying Weber's law. The transition point between the decreasing and constant parts of the curves depended on pedestal contrast. As pedestal contrast was

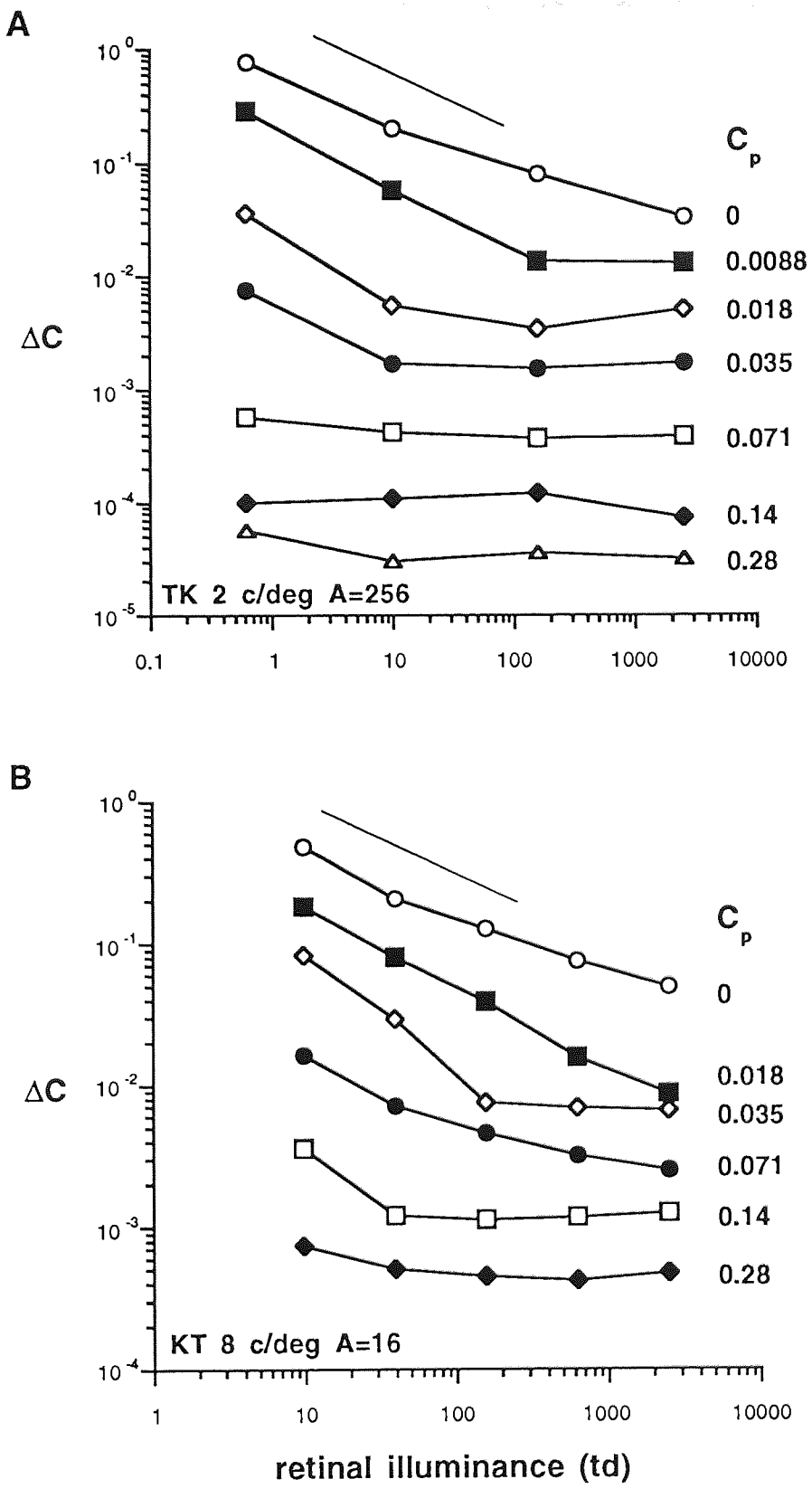

Figure 5.14 Contrast increment thresholds plotted as a function of retinal illuminance (displaced vertically).

increased, the transition point transferred to lower retinal illuminances. This implies that the effect of quantal noise grew smaller as pedestal contrast was increased.

Next, the experimental increment thresholds were described by the contrast discrimination model. The model was first applied to detection threshold data. Model parameters which determine the detection threshold behaviour are the critical spatial frequency of the optical transfer function (f_c), the exponent in the optical transfer function (n), the spectral density of internal noise (N_i), the critical spatial frequency in the integration function (f_0), the maximum of the critical number of square cycles in the integration function (z_0), and the maximum efficiency (η_{max}). Quantal noise was taken to be negligible at the highest luminance level. Detection threshold parameters were then determined to fit the data obtained at the retinal illuminance of 2513 td.

For KT the parameter values determined previously in this chapter (see Sections 5.2 and 5.3) were applied and model predictions for the present data at 8 c/deg were calculated. As expected, all parameters remained at the previously determined values except for the spectral density of internal noise. Thus, model predictions were accurate when f_c, n, f_0, z_0 and η_{max} were set at 7, 3, 0.5, 90 and 0.33, respectively. The spectral density of internal noise was higher at 55×10^{-6} than in the previous sections by a factor of 2.5 because here the experiments were performed monocularly. Monocular detection thresholds are higher than binocular approximately by a factor of 1.5 (Legge, 1984a). In the model an increase by a factor of 1.5 in thresholds is reflected as an increase in internal noise by a factor of $(1.5)^2=2.25$ which is very close to the increase found.

For SU and TK the parameters f_0, f_c and n had a negligible effect since at a medium spatial frequency of 2 c/deg they influence threshold predictions very little. Thus, they were set at the previously used values 0.5, 7 and 3. In order to be able to determine the spatial integration parameter z_0, detection thresholds were measured at three grating areas (1, 16 and 256 square cycles) for both subjects, and z_0 was adjusted until the predicted spatial integration curves had the same shape as the data. The z_0 was 40 for SU and 90 for TK. The maximum efficiency was set at 0.3 for both subjects. The spectral density of internal noise was adjusted until the model predictions coincided with the data. The N_i was 55×10^{-6} for SU and 35×10^{-6} for TK.

The effect of quantal noise on detection and increment thresholds can be described by the model. However, the spectral density of quantal noise cannot be calculated since it is given by $N_q=k/I$ where the value of constant k is unknown (e.g. Pelli, 1990). Therefore, it was necessary to express the spectral density of quantal noise as an equivalent spectral density of external spatial noise (N_{qe}). Quantal noise is of course spatiotemporal in nature

but its equivalent spectral density was expressed in terms of static external spatial noise, N_e. This did not have any effect on the correctness of the predictions, however, since static external spatial noise has a similar effect on detection thresholds as quantal noise.

Detection threshold predictions at low light levels were determined by finding the spectral density of external noise which increased detection thresholds by the same amount as quantal noise at the lowest retinal illuminance. The equivalent spectral density of external spatial noise at higher levels of retinal illuminance were then calculated simply by halving the maximum N_{qe} as retinal illuminance was doubled. At the highest retinal illuminance the N_{qe} was set to zero since the calculated values were at least 24 times smaller than the spectral density of internal noise (c.f. Tables 5.5 and 5.6) so that quantal noise did not have any effect on model predictions. The retinal illuminances and corresponding equivalent external noise spectral densities are shown in Table 5.5.

td	N_{qe} for KT	N_{qe} for SU & TK
2513	$1.25\times10^{-6}\approx0$	$1.44\times10^{-6}\approx0$
628	5×10^{-6}	-
157	2×10^{-5}	2.3×10^{-5}
39	8×10^{-5}	-
9.82	3.2×10^{-4}	3.75×10^{-4}
0.6	-	6×10^{-3}

Table 5.5 Equivalent spectral densities of external spatial noise corresponding to quantal noise for KT, SU and TK.

Detection threshold predictions at various retinal illuminances were then calculated using the parameter values listed above and shown in Table 5.6.

The model parameters determining the strength of the post-detector noise, k and m, were then adjusted so that increment threshold predictions were as close to the experimental results as possible. The parameter m was found to be 1.8 for all subjects. Thus, the slope of the increasing part of the functions was 0.8.

The parameter k depended on retinal illuminance because the dip in the contrast discrimination functions became slightly shallower as retinal illuminance decreased and

because the increasing parts of the discrimination functions did not converge at high contrasts. The most appropriate value was found by adjusting k so that the dip in the predicted contrast discrimination function was of the same depth as in the experimentally measured functions at each noise level. The values of k are shown in Table 5.7.

The adaptation parameter b remained equal to 0.5 for KT as in the previous sections. For SU b was found to be 0.4. For TK the effect of adaptation was smallest since b was equal to 0.67. After all parameter values had been determined, model predictions were calculated. The parameter values used are collected in Tables 5.6 and 5.7.

Parameter	KT	SU	TK
f_c	7	7	7
n	3	3	3
N_i	$55x10^{-6}$	$55x10^{-6}$	$35x10^{-6}$
z_0	90	40	90
f_0	0.5	0.5	0.5
η_{max}	0.33	0.3	0.3
m	1.8	1.8	1.8
b	0.5	0.4	0.67

Table 5.6 Model parameters for KT, SU and TK in contrast discrimination at various levels of retinal illuminance.

td	k for KT	k for SU	k for TK
2513	0.010	0.015	0.020
628	0.015	-	-
157	0.023	0.023	0.030
39	0.035	-	-
9.8	0.043	0.040	0.040
0.6	-	0.045	0.045

Table 5.7 Dependence of k on retinal illuminance for KT, SU and TK.

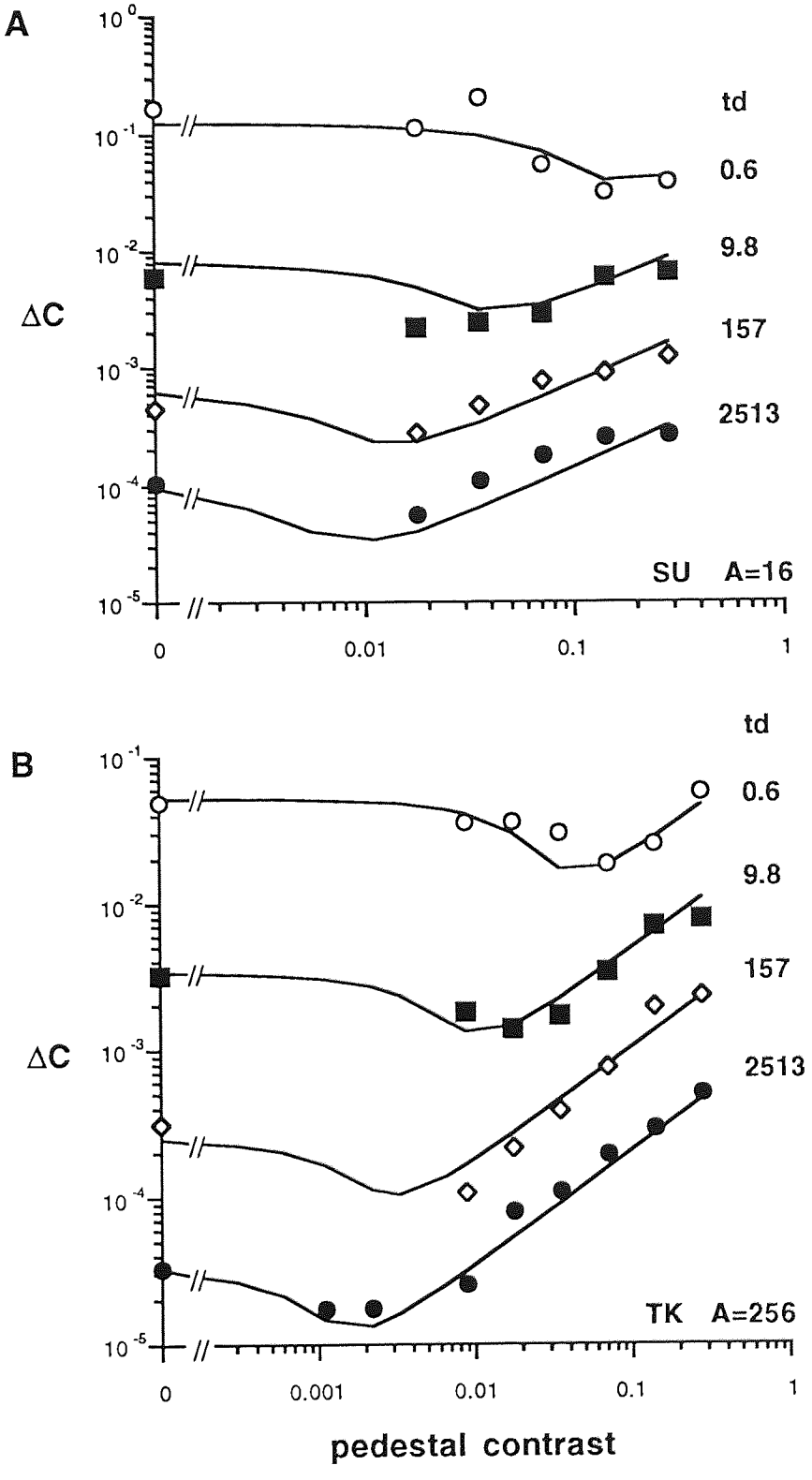

Figure 5.15 Contrast increment threshold data and model predictions at various retinal illuminances at 2 c/deg (curves have been displaced vertically for clarity).

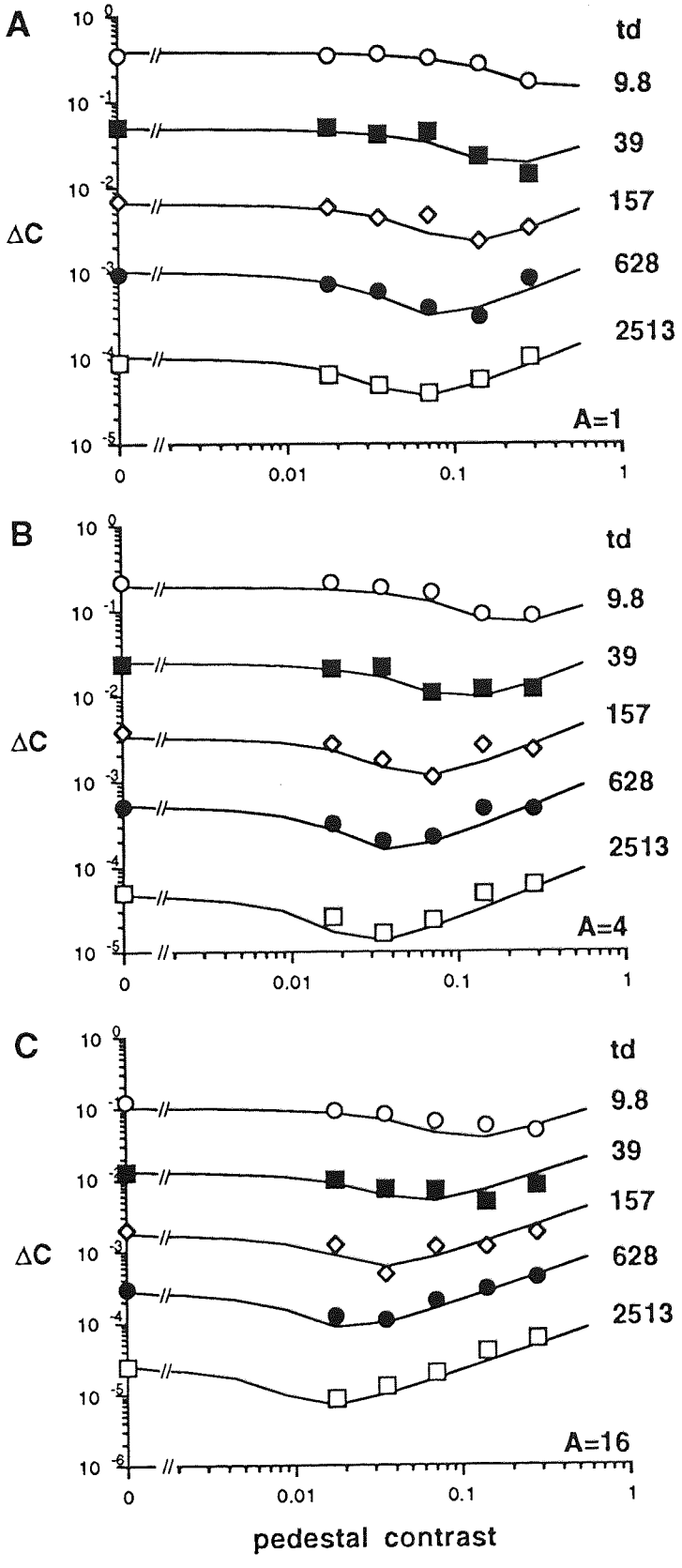

Figure 5.16 (Continues on the next page).

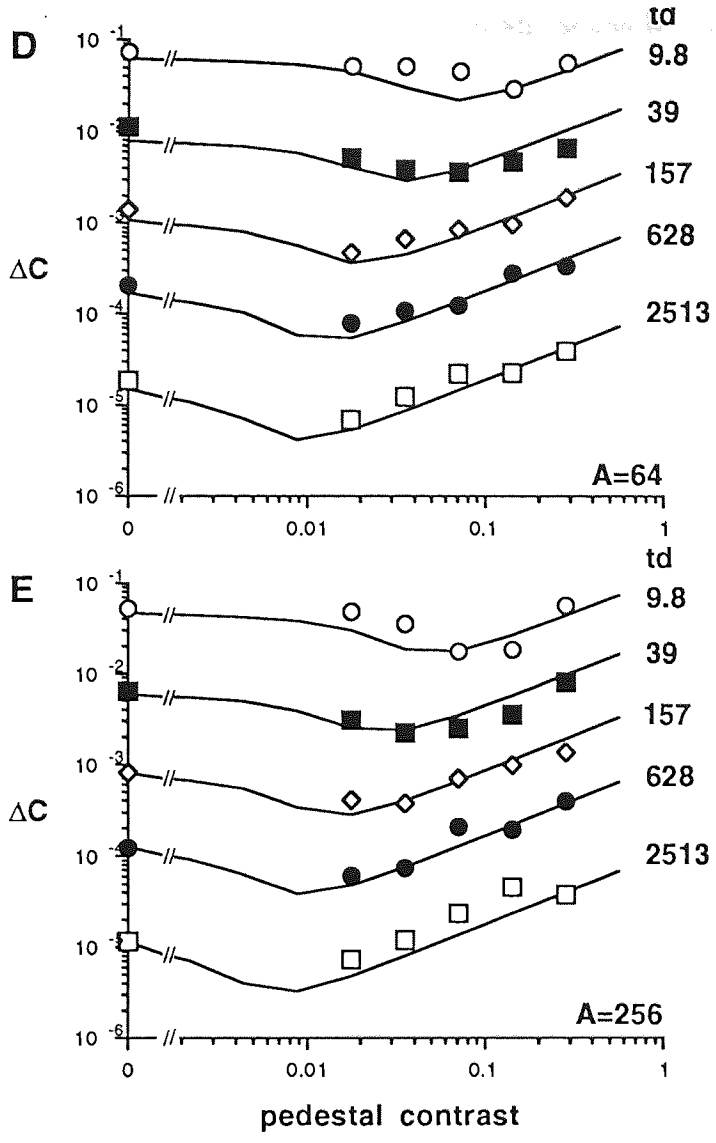

Figure 5.16 Contrast increment threshold data and model predictions at various retinal illuminances at 8 c/deg (displaced vertically).

Figures 5.15 and 5.16 show the model predictions and the experimental data replotted from Figures 5.12 and 5.13, respectively. The data and predictions have been displaced vertically so that each contrast discrimination curve is more clearly visible. In Figure 5.15 the data and predictions have been divided by 1, 4, 16 and 64 for retinal illuminances 0.6, 9.8, 157 and 2513, respectively. In Figure 5.16 the data and predictions have been divided by 1, 4, 16, 64 and 512 for retinal illuminances 9.8, 39, 157, 628 and 2513, respectively.

The model predictions were quite accurate, as can be seen in Figures 5.15 and 5.16. The explained variance for the undisplaced data was 0.889 and 0.960 in Figure 5.15(A) and (B) respectively, and 0.943, 0.938, 0.911, 0.851 and 0.814 in Figure 5.16(A), (B), (C), (D) and (E) respectively.

5.4.4 Discussion

Contrast increment thresholds were measured at various retinal illuminances for gratings of 2 and 8 c/deg with different areas. A reduction in retinal illuminance results in an increase in quantal noise. It was found that the effect of quantal noise on increment thresholds was similar to the effect of external spatial noise which was studied in Section 5.3.

When measured at different luminance levels, contrast discrimination functions were always dipper-shaped but they were displaced both vertically and horizontally. As retinal illuminance was decreased, increment thresholds increased and the dip in the discrimination functions was displaced towards higher pedestal contrasts. The dip occurred when the pedestal was approximately at its detection threshold, in agreement with Bradley and Ohzawa (1986). The depth of the dip decreased slightly as retinal illuminance was decreased. The slope of the increasing part of the discrimination functions was independent of retinal illuminance.

The increase in increment thresholds with decreasing retinal illuminance was larger at low than at high pedestal contrasts which suggests that the effect of quantal noise reduced with contrast level. This can be explained by an increase in signal dependent noise with stimulus contrast as proposed by the difference-signal discriminator model for contrast discrimination. At high contrasts, the effect of signal dependent noise becomes greater than that of quantal noise so that increment thresholds become less dependent on quantal noise. The effect of quantal noise did not totally disappear, however, since even at the highest pedestal contrasts increment thresholds were almost always slightly higher at lower retinal illuminances.

The decrease in the depth of the dip with decreasing retinal illuminance, and the fact that increment thresholds did not become independent of luminance level at high contrasts were described in the model by increasing the value of parameter k as retinal illuminance was decreased. If the value of k had been constant, the depth of the dip would have been constant, and increment threshold predictions would have been equal at all light levels at high pedestal contrasts.

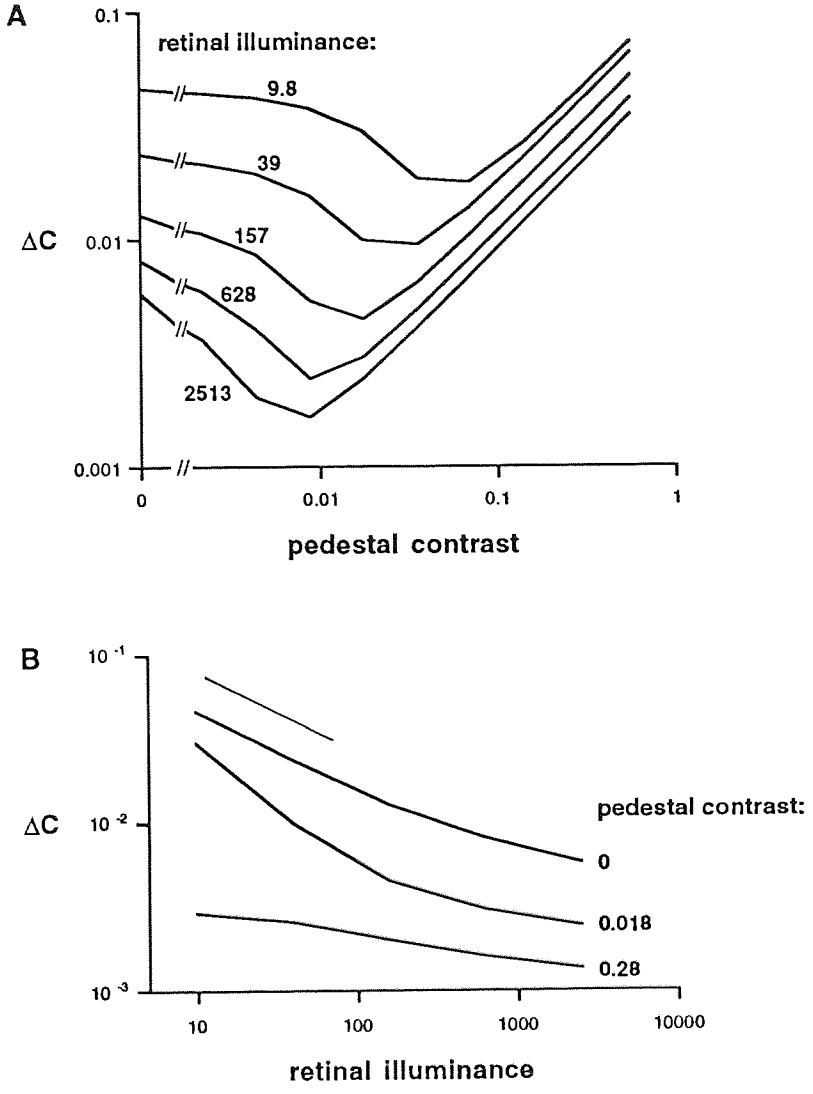

Figure 5.17 Model predictions for contrast increment thresholds at various retinal illuminances.

The increase in the value of parameter k with decreasing retinal illuminance implies that post-filter noise includes a component which depends on the spectral density of quantal noise. Since in the previous Section 5.3 it was found that post-filter noise is also influenced by external spatial noise, it can be assumed that post-filter noise increases both with signal strength and with the level of pre-filter noise. A pre-filter-noise dependent component is not included in the post-filter noise in the model so that its existence is reflected in the dependence of the parameter k on the spectral density of quantal and external noises. This topic will be discussed in detail in the next Section 5.5.

An example of contrast discrimination functions predicted by the model at various retinal illuminances is shown in Figure 5.17(A). The predictions are replotted from Figure 5.16(E) but now they are in their original positions. Contrast discrimination functions measured at different retinal illuminances are displaced horizontally and vertically, and they do not overlap. Increment thresholds increase with decreasing retinal illuminance, and the increase is largest at low pedestal contrasts. At high pedestal contrasts, discrimination functions increase in parallel.

When increment thresholds were plotted as a function of retinal illuminance, as shown in Figure 5.17(B), they first decreased and then became constant. In contrast detection, the transition point between the decreasing and constant parts of the functions marks the critical retinal illuminance which is inversely proportional to internal noise (Rovamo, Mustonen & Näsänen, 1994a). The transition between the decreasing and constant parts of the curves tended to occur at a lower retinal illuminance the higher the pedestal contrast. This decrease in the critical retinal illuminance implies that the effect of intrinsic noise in the visual system grew larger as pedestal contrast was increased. According to the model, the increase in intrinsic noise is due to an increase in signal dependent noise.

Detection thresholds plotted as a function of retinal illuminance obeyed DeVries-Rose law, as shown by the uppermost curve in Figure 5.17(B). At medium pedestal contrasts, increment thresholds decreased more rapidly than predicted by DeVries-Rose law, as shown by the middle curve in Figure 5.17(B) where pedestal contrast is 0.018. This is because an increment threshold measured at a low luminance level has decreased very little from the detection threshold, while an increment threshold measured at a higher luminance level is close to its minimum [cf. Figure 5.17(A)]. At high pedestal contrasts where discrimination functions were increasing and close together, the slope of decrease when increment thresholds were plotted as a function of retinal illuminance was shallower than predicted by DeVries-Rose law, as shown by the lowermost curve in Figure 5.17(B) where pedestal contrast is 0.28.

It is concluded that the difference-signal discriminator model for contrast discrimination could accurately describe the dependence of contrast increment thresholds on retinal illuminance.

5.5 *General discussion on contrast discrimination*

In the experiments of this chapter, contrast increment thresholds were measured for cosine gratings of various areas and spatial frequencies at different levels of external spatial noise, and at various retinal illuminances. Contrast discrimination functions were dipper-shaped. That is, as pedestal contrast was increased, increment thresholds first decreased but then increased as a power function of pedestal contrast. As the spectral density of spatial or quantal noise was increased, contrast increment thresholds increased and the dip in the discrimination functions displaced to higher pedestal contrasts and became shallower. An increase in grating area decreased increment thresholds and caused the dip to move towards lower pedestal contrasts without affecting its depth. The increasing parts of the functions had a constant slope and they were parallel.

A new difference-signal discriminator model introduced in the beginning of this chapter was used to describe the experimental results. According to the model, decisions in discrimination tasks are based on the response differences of local matched filters, and the accuracy of decisions is limited by noise. Pre-filter noise includes external spatial, quantal and internal noises which precede the matched filters, and it is unaffected by the signal. Post-filter noise occurs after the matched filters, and it is signal dependent since it increases with signal strength.

According to the model, the initial decrease in contrast increment thresholds is due to the fact that the discrimination variable, which determines the magnitude of the contrast response in the visual system, is calculated on the basis of the response differences of the matched filters. The response differences are subtracted so that the value of the discrimination variable increases with increasing pedestal contrast. Therefore, increment thresholds decrease as pedestal contrast increases as long as noise level is constant. The subsequent increase in increment thresholds is due to signal dependent noise which becomes the dominant factor determining increment thresholds at high contrast levels.

The position of the dip in contrast discrimination functions depended on the contrast detection threshold. In this and several previous studies (e.g. Pelli, 1985) it has been found that increment thresholds reach their minimum when the pedestal is approximately at its detection threshold. Bradley and Ohzawa (1986) have found that when the pedestal contrast is subthreshold, the total contrast of a grating at increment threshold is equal to the detection threshold, that is $\Delta c+c_p=c_d$. This indicates that the pedestal starts to facilitate contrast discrimination when its contrast approaches detection threshold. The difference-signal discriminator model predicts that detection threshold influences the position of the

dip. This is because when pedestal contrast is low, its effect on the discrimination variable is negligible [see Equation 5.8b in Section 5.1, p. 106]. But when the pedestal contrast approaches the detection threshold, it starts to increase the value of the discrimination variable so that increment thresholds start to decrease.

The model predicts that if signal dependent post-filter noise is independent of pre-filter noise, contrast increment thresholds become independent of spatial and quantal noises at high contrast levels. However, the experimental data showed that increment thresholds were slightly elevated at high levels of spatial or quantal noise even at the high pedestal contrasts. Also, the dip in the discrimination functions was shallower at high noise levels. These findings were postulated to be due to noise dependent noise which increases with pre-filter noise. In the model an increase in noise dependent noise was reflected as an increase in the parameter k. This implies that post-filter noise includes a component which depends on the spectral density of pre-filter noise.

To investigate how parameter k increased with pre-filter noise, the spectral density of pre-filter noise (N_{tot}') was calculated for each subject and the values of k determined in Sections 5.2, 5.3 and 5.4 were plotted as a function of N_{tot}'. Pre-filter noise includes external spatial (N_e), quantal (N_q) and internal (N_i) noises. The spectral density of pre-filter noise was calculated using Equation (4.7) in Section 4.1. The spectral density of quantal noise was calculated by a method described in Appendix VII. When k was plotted against N_{tot}', it could be seen that as N_{tot}' was increased, k increased first rapidly but then the increase saturated. However, the values of k for each subject did not form a single curve.

When k was plotted as a function of N_{tot}'/N_i, as shown in Figure 5.18, the values of k for all subjects collapsed together. The data in Figure 5.18 could be well described by a function of the form:

$$k = \frac{0.045}{1 + 2.8N_i/N_{tot}'} \tag{5.15}$$

where 0.045 is the maximum value of k and 2.8 is the value of N_{tot}'/N_i at which the value of k has been halved from the maximum. The explained variance in Figure 5.18 was 0.889. Equation (5.15) means that the noise dependent component in signal dependent noise increased in proportion to the ratio of the total spectral density of pre-filter noise to the spectral density of internal noise. At high levels of external spatial or quantal noise the increase in noise dependent noise saturated. In other words, when internal noise was the dominant pre-filter noise source so that $N_{tot}' \approx N_i$, noise dependent noise was constant,

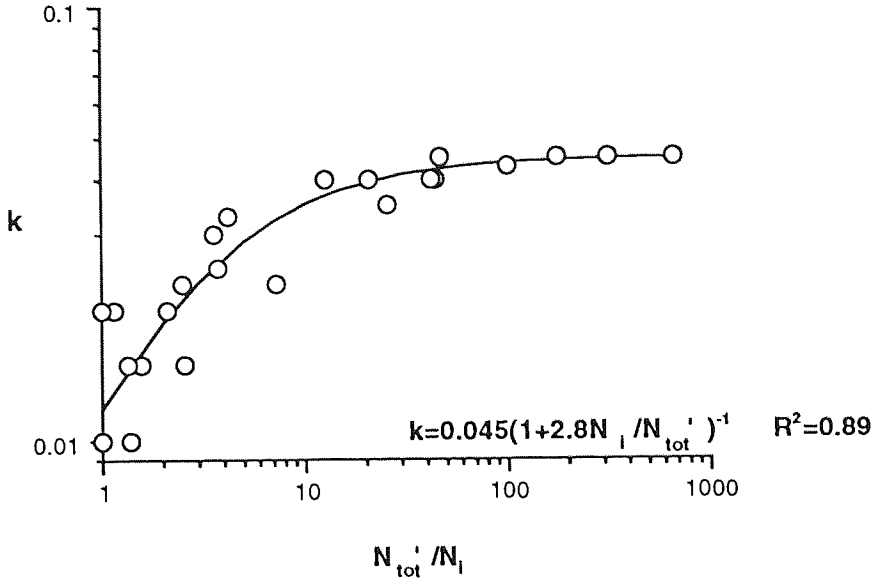

5.18 Model parameter k plotted as a function of the ratio of pre-filter to internal noise spectral density.

and the value of k was about 0.01. But when external spatial or quantal noise was dominant, the value of k was about 0.045.

The parameter k has a small effect on detection threshold predictions when it becomes large enough. Since the value of k did not remain constant when pre-filter noise increased, its influence on detection threshold predictions was tested at the range of values used in the fits. When k is zero, the contrast discrimination model reduces to the previously presented contrast detection model. When k is small, its effect on detection thresholds is negligible. For example, when k was 0.01, detection threshold predictions were equal to predictions obtained when k was zero. When k increased from 0.01 to the maximum of 0.045, detection threshold predictions increased by less than 10 percent. Thus, it may be concluded that the range of values of k used had a negligible effect on detection threshold predictions.

It has been previously found that contrast discrimination curves can be superimposed if both increment thresholds and pedestal contrasts are normalised by the detection threshold (Legge, 1979; Bradley & Ohzawa, 1986; Legge & Kersten, 1987). On the other hand, in several studies it has been stated that increment thresholds become independent of various

factors affecting detection thresholds at high pedestal contrasts (Legge & Foley, 1980; Pelli, 1985; Bradley & Ohzawa, 1986). Since the slope of increase in discrimination functions is less than 1, these two findings are contradictory. If contrast discrimination functions merge at high pedestal contrasts, then the normalised increment thresholds will scatter at high contrasts being lower for stimuli with higher detection thresholds. This can be seen clearly in Pelli's (1985) Figure 11.(b) even though he does not point out this fact.

If it is assumed that one of the above findings is valid, it follows that either the normalisation technique does not work, or that increment thresholds do not become independent of factors affecting detection thresholds even at high contrast levels. The first assumption is supported by the finding that the dip in discrimination functions decreased with increasing external or quantal noise. Consequently, when increment thresholds were normalised, there was scatter around the dip. The second assumption, that factors which determine detection thresholds also affect increment thresholds at all contrast levels, is supported by the finding of this chapter that increment thresholds were almost always higher for stimuli with high detection thresholds. It should also be noted that the researchers who applied the normalisation technique successfully found that increment thresholds depended on spatial frequency (Legge, 1979) and retinal eccentricity (Legge & Kersten, 1987) even at the highest pedestal contrasts. As an exception, Bradley and Ohzawa (1986) stated both that increment thresholds were independent of spatial frequency at high pedestals, and that discrimination functions could be normalised. Their conclusions were based on just two spatial frequencies, however, so that the scarcity of their data may explain why they could make these conflicting statements. Also, the slopes of increase they found were about 0.9 which is very close to 1, so that even if their increment thresholds were almost equal for different spatial frequencies at high contrasts, the normalised plots did not scatter much. On the basis of these findings, it can be concluded that neither assumption is unequivocally supported but that there is more evidence for the second one.

Contrast detection thresholds plotted as a function of grating area or retinal illuminance first decreased with a slope of 0.5, and then became constant. Detection thresholds plotted as a function of the spectral density of external spatial noise were first constant and then started to increase with a slope of 0.5. A slope of 0.5 in double logarithmic coordinates can be called the square-root law. Thus, detection thresholds obeyed the square-root law. Contrast increment thresholds obeyed the square-root law also at low pedestal contrasts. However, at medium pedestal contrasts, the slopes of increase or decrease for increment thresholds were steeper than 0.5, and at high contrast levels they were shallower.

Deviations from the square-root law are due to the shape and position of discrimination functions. The dip in the contrast discrimination functions is displaced towards higher pedestals with decreasing grating area and retinal illuminance, or with increasing external noise. At a medium pedestal, an increment threshold measured at a large area, high luminance level or low noise level is therefore close to its minimum, while when measured at a small area, low luminance level or high noise level, it has decreased only little from the detection threshold. Consequently, increment thresholds increase or decrease more rapidly as a function of area, retinal illuminance and external noise than predicted by the square root law at medium pedestal contrasts. But at high pedestal contrasts, discrimination functions are increasing and close together so that increment thresholds increase or decrease more slowly than predicted by the square root law.

The data presented in this chapter show that the influence of various factors such as grating area, external spatial noise and retinal illuminance on contrast increment thresholds depends strongly on the contrast level at which thresholds are measured. Interactions between different factors are more complex in contrast discrimination than in simple detection. Nevertheless, the difference-signal discriminator model could describe contrast increment thresholds with a relatively narrow range of parameter values. The only exception was parameter k which depended on the spectral density of pre-filter noise and varied maximally by factor of 4.5. This variation was accepted because the model predictions could thus be considerably improved. Also, the variation in parameter k is probably not real but due to noise dependent noise which was not included in the present model. It can be concluded that the model could accurately describe extensive contrast discrimination data obtained in various conditions.

6. CONCLUSIONS

Human contrast perception was studied in various stimulus conditions at a large range of contrasts by measuring contrast detection and increment thresholds, and by performing contrast matching. Contrast detection thresholds indicate the smallest detectable contrast. Suprathtreshold contrast perception was investigated from two different points of view using the complementary techniques of contrast matching and discrimination.

In contrast matching, the effects of spatial frequency, grating area, image complexity and chromaticity on perceived contrast were studied. The general findings were that as contrast level was increased, first matches seemed to be affected by detection thresholds, but then they became physically correct. The first finding implies that the modulation transfer functions and the spatial integration process in the visual system interfere with perceived contrast at low contrast levels, so that perceived contrast is lower when attenuation by these factors is stronger. The second finding implies that at high signal-to-noise ratios the visual system is capable of compensating for the distortions introduced during the early stages of signal processing, perhaps in a manner similar to signal restoration techniques used in digital image processing.

In contrast discrimination, the effects of grating area, external spatial noise and retinal illuminance were studied. Contrast discrimination functions were dipper-shaped which means that increment thresholds first decreased and then increased falling on a straight line in double logarithmic axes as pedestal contrast was increased. The general findings were that as contrast level was increased, first increment thresholds seemed to be affected by detection thresholds, but then they became less dependent on them so that at high pedestal contrasts increment thresholds were rather similar for different stimuli. The first finding implies that contrast increment thresholds are determined by the same factors that determine detection thresholds when pedestal contrast is low. The second finding can be attributed to signal dependent noise which becomes the dominant noise source at high contrasts, and consequently the main factor determining increment thresholds.

The dipper-shape of the contrast discrimination functions can be explained by assuming that the visual system calculates a difference-signal for the stimuli to be discriminated, and that there is signal dependent noise in the visual system. Calculation of a difference-signal decreases increment thresholds since it produces a response which increases with increasing contrast level. Signal dependent noise then causes the increase in increment thresholds at high contrasts.

The results of the research reported here show that at high contrast levels, contrast matches become nearly independent of factors affecting detection thresholds but contrast increment thresholds always show some dependence on them. At first sight one might assume that matches and increment thresholds should behave similarly. However, it has to be borne in mind that the two tasks are different, in fact opposite, since in matching the aim is to achieve apparent equality of contrast but discrimination investigates differences in contrast. Therefore, superficial comparisons based on apparent similarities between the contrast matching and discrimination results should not be made.

Naturally contrast matching and discrimination are also linked. The connection between them is the response variability. Contrast increment thresholds increase at suprathreshold pedestal contrasts because of the signal dependent noise which increases response variability. Signal dependent noise is also present in contrast matching, and it increases the response variability and thus the variability of matches, but it does not influence the mean matching contrast. On the basis of this, it could be expected that standard error in contrast matching would increase as a power function of matching contrast with the exponent close to that found in contrast discrimination.

This hypothesis was tested by plotting standard errors as a function of matching contrast where they had been calculated for contrast matches with luminance modulated gratings (Sections 4.2 and 4.4). It was found that standard error indeed increased as a power function of matching contrast with a mean exponent of 0.85. This is very close to the exponent in contrast discrimination which was 0.8 for most subjects. The hypothesis was thus clearly supported. A related finding has been reported in contrast magnitude estimation by Baro, Lehmkuhle and Applegate (1988) who observed that the ratio of standard error of magnitude estimate to the mean magnitude estimate behaves in a similar manner as the ratio of increment threshold to pedestal contrast.

On the basis of the above, it would be interesting to see whether standard errors in contrast matching are generally larger in the presence of external or quantal noise. This would be expected since external and quantal noises increase response variance. Contrast matching was not studied in external noise or at various luminance levels in the experiments presented in this thesis so that the comparison cannot be made here.

The results of contrast matching and discrimination could be accurately described by two models based on the idea that the visual system can be considered as an image processor where the visual signal is filtered by the optical and neural modulation transfer functions, internal noise is added, and then the signal is correlated with a local matched filter whose spatial integration properties are limited by an aperture function.

Contrast matching results were described by introducing a restoring transfer function at the output of each matched filter tuned to each stimulus. The restoring transfer function multiplies the matched filter output by the inverse of the early visual transfer functions. At low contrast levels the effect of restoration is negligible. But at high contrast levels degradations caused by the optical and neural modulation transfer functions and the spatial integration function are corrected, and consequently contrast perception is veridical.

Contrast discrimination results were described by assuming that the two stimuli to be discriminated are correlated with two matched filters each of which is tuned to the contrast of one of them, and that there is signal dependent noise in the visual system. According to the model, the decision in a discrimination task is based on a difference signal which is calculated by subtracting the response difference of the matched filters to one stimulus from the response difference of the matched filters to the other stimulus. The model could accurately describe the effect of various factors on contrast increment thresholds.

The aim of future research will be to find a successful way to combine the two models. A joint model for contrast detection, discrimination and matching would be of significance since it would provide a coherent view of several aspects of human contrast perception.

PUBLICATIONS AND PRESENTATIONS

PUBLICATIONS

Papers

Kukkonen H., Rovamo J., Tiippana K. and Näsänen R. (1993). Michelson contrast, RMS contrast and energy of various spatial stimuli at threshold. Vision Research, 33, 1431-36.

Rovamo J., Kukkonen H., Tiippana K. and Näsänen R. (1993). Effects of luminance and exposure time on contrast sensitivity in spatial noise. Vision Research, 33, 1123-1129.

Tiippana K., Näsänen R. and Rovamo J. (1994). Contrast matching of compound gratings. Vision Research, 34, 1157-1163.

Manuscripts under preparation

Contrast restoration in human vision. Näsänen R. E., Tiippana K. M. and Rovamo J. M.

Contrast matching of achromatic luminance and chromatic isoluminant gratings. Tiippana K. M., Rovamo J. M., Mäkelä P. K. and Whitaker D. J.

Modelling of contrast discrimination. Rovamo J. M., Tiippana K. M. and Näsänen R. E.

Dependence of contrast increment thresholds on the spectral density of external spatial noise. Rovamo J. M., Tiippana K. M. and Näsänen R. E.

Dependence of contrast increment thresholds on retinal illuminance. Tiippana K. M., Rovamo J. M. and Näsänen R. E.

Kukkonen H., Rovamo J., Tiippana K. and Näsänen R. (1992). Contrast thresholds for gratings in spatial noise with various picture element areas and shapes. Supplement to Optics and Photonic News 3 and OSA Technical Digest Series 23.

Kukkonen H., Rovamo J., Tiippana K. and Näsänen R. (1992). The effect of retinal illuminance, exposure time and grating area on contrast sensitivity for gratings with and without spatial noise. Perception, Vol. 21 Supplement 2.

Näsänen R., Tiippana K. and Rovamo J. (1992). Perceived contrast of two-dimensional compound gratings. Perception, Vol. 21 Supplement 2.

Tiippana K. M. (1994). Psychophysical contrast increments thresholds measured in external spatial noise. Neural Bases of Visual Cognition Abstract Book, 55.

Tiippana K., Näsänen R. and Rovamo J. (1993). Dependence of contrast increment thresholds on grating area. Supplement to Optics and Photonic News 4 and OSA Technical Digest Series Vol. 16.

Tiippana K. M., Rovamo J. M. and Näsänen R. E. (1994). Contrast increment thresholds measured at various levels of external spatial noise. Perception, Vol. 23 Supplement, 3.

Tiippana K. M., Rovamo J. M. and Näsänen R. E. (1994). Dependence of contrast increment thresholds on luminance level. Investigative Ophthalmology and Visual Science Annual Meeting Abstract Issue, Vol 35, No.4, 1900.

Tiippana K. M., Rovamo J. M. and Näsänen R. E. (1995). A model for contrast restoration in human vision. Investigative Ophthalmology and Visual Science Annual Meeting Abstract Issue, Vol 36, No.4, 904.

Tiippana K., Rovamo J. and Whitaker D. (1993). Contrast matching of chromatic and luminance gratings at various spatial frequencies. Perception, Vol. 22 Supplement.

PRESENTATIONS

Oral presentations

Psychophysical contrast increments thresholds measured in external spatial noise.
European Science Foundation Autumn School, Spain, 28.9.1994

Contrast increment thresholds measured at various levels of external spatial noise.
17th European Conference on Visual Perception, the Netherlands, 7.9.1994

Dependence of contrast increment thresholds on luminance level.
Annual Meeting of the Association for Research in Vision and Ophthalmology, U.S., 5.5.1994

Dependence of contrast increment thresholds on light level.
Departmental seminar, University of Aston, U.K., 8.3.1994

Suprathreshold contrast perception.
SERC Image interpretation Initiative Summer School, U.K., 11.7.1993

Posters

Dependence of contrast increment thresholds on grating area.
Annual Meeting of the Optical Society of America, Canada, 3.-8.10.1993

Contrast matching of chromatic and luminance gratings at various spatial frequencies.
16th European Conference on Visual Perception, U.K., 25.-29.8.1993

Contrast detection and discrimination thresholds as a function of grating area.
2nd Meeting of the Society for Promotion of Visual Sciences, U.K., 5.-8.7.1993

Perceived contrast of two-dimensional compound gratings.
15th European Conference on Visual Perception, Italy, 30.8.-3.9.1992

REFERENCES

Ahumada A. Jr. and Watson A. B. (1985). Equivalent-noise model for contrast detection and discrimination. Journal of the Optical Society of America, 2, 1133-1139.

Arend L. E. and Lange R. V. (1980). Narrow-band spatial mechanisms in apparent contrast matching. Vision Research, 20, 143-147.

Banks M. S., Geisler W. S. and Bennett P. J. (1987). The physical limits of grating visibility. Vision Research, 27, 1915-1924.

Biondini A. R. and de Mattiello M. L. F. (1985). Suprathreshold contrast perception at different luminance levels. Vision Research, 25, 1-9.

Boynton R. M. (1979). Human color vision. Holt, Rinehart and Winston, U.S.A.

Boynton R. M & Kaiser P. K. (1968). Vision: the additivity law made to work for heterochromatic photometry with bipartite fields. Science, 161, 366-368.

Bradley A. and Ohzawa I. (1986). A comparison of contrast detection and discrimination. Vision Research, 26, 991-997.

Brady N. and Field D. J. (1995). What's constant in contrast constancy? The effects of scaling on the percieved contrast of bandpass patterns. Vision Research, 35, 739-756.

Burgess A. E. (1985). Visual signal detection. III. On Bayesian use of prior knowledge and cross correlation. Journal of the Optical Society of America, 2, 1498-1507.

Burgess A. E. (1990). High level visual decision efficiencies. In: Blakemore C. (Ed) Vision: Coding and Efficiency (pp. 431-440). Cambridge University Press.

Burgess A. E. and Colborne B. (1988). Visual signal detection. IV. Observer inconsistency. Journal of the Optical Society of America, 5, 617-627.

Burgess A. E. and Ghandeharian H. (1984). Visual signal detection. I. Ability to use phase information. Journal of the Optical Society of America, 1, 900-905.

Burgess A. E. and Ghandeharian H. (1984). Visual signal detection. II. Signal location identification. Journal of the Optical Society of America, 1, 906-910.

Burgess A. E., Wagner R. F., Jennings R. J. and Barlow H. B. (1981). Efficiency of human visual signal discrimination. Science, 214, 93-94.

Campbell F. W. and Robson J. G. (1968). Application of Fourier analysis to the visibility of gratings. Journal of Physiology, 197, 551-556.

Cannon M. W. Jr (1979). Contrast sensation: a linear function of stimulus contrast. Vision Research, 19, 1045-1052.

Cannon M. W. Jr (1984). A study of stimulus range effects in free modulus magnitude estimation of contrast. Vision Research, 24, 1049-1055.

Cannon M. W. Jr (1985). Perceived contrast in the fovea and periphery. Journal of the Optical Society of America, 2, 1760-1768.

Cannon M. W. Jr and Fullencamp S. C. (1988). Perceived contrast and stimulus size: experiment and simulation. Vision Research, 28, 695-709.

Cannon M. W. Jr and Fullencamp S. C. (1991a). A transducer model for contrast perception. Vision Research, 31, 983-998.

Cannon M. W. Jr and Fullencamp S. C. (1991b). Spatial interactions in apparent contrast: inhibitory effects among grating patterns of different spatial frequencies, spatial positions and orientations. Vision Research, 31, 1985-1998.

Cannon M. W. and Fullencamp S. C. (1993). Spatial interactions in apparent contrast: individual differences in enhancement and suppression effects. Vision Research, 33, 1685-1695.

Cavanagh P. (1991). Vision at equiluminance. In Kulikowski J. J., Walsh V. and Murray I. J. (Eds) Vision and Visual Dysfunction, Vol. 5, Limits of Vision (Chapter 18, pp. 234-250). The Macmillan Press, U.K.

Charman W. N. (1991). Limits on visual performance set by the eye's optics and the retinal cone mosaic. In Kulikowski J. J., Walsh V. and Murray I. J. (Eds) Vision and

Visual Dysfunction, Vol. 5, Limits of Vision (Chapter 7, pp. 81-96). The Macmillan Press, U.K.

DeValois R. L. and Jacobs G. H. (1984). Neural mechanisms of color vision. In I. Darian-Smith (Ed.) Handbook of Physiology, The Nervous System, Vol. III Sensory Processes (Chapter 10, pp. 425-455), American Physiological Society, Baltimore.

DeVries H. L. (1943). The quantum character of light and its bearing upon threshold of vision, the differential sensitivity and visual acuity of the eye. Physica X, 553-564.

Ejima Y. and Takahashi S. (1985). Apparent contrast of a sinusoidal grating in the simultaneous presence of peripheral gratings. Vision Research, 25, 1223-1232.

Elliott P. B. (1964). Forced choice tables (Appendix 1). In Swets J. A. (Ed) Signal Detection and Recognition by Human Observers (pp. 679-684). Wiley, New York.

Foley J. M. and Legge G. E. (1981). Contrast detection and near-threshold discrimination in human vision. Vision Research, 21, 1041-1053.

Franzén O. and Berkley M. (1975). Apparent contrast as a function of modulation depth and spatial frequency: a comparison between perceptual and electrophysiological measures. Vision Research, 15, 655-660.

Gegenfurtner K. R. and Kiper D. C. (1992). Contrast detection in luminance and chromatic noise. Journal of the Optical Society of America, 9, 1880-1888.

Georgeson M. A. (1985). The effect of spatial adaptation on perceived contrast. Spatial Vision, 1 No. 2, 103-112.

Georgeson M. A. (1991a). Contrast overconstancy. Journal of the Optical Society of America, 8, 579-586.

Georgeson M. A. (1991b). Over the limit: encoding contrast above threshold in human vision. In Kulikowski J. J., Walsh V. and Murray I. J. (Eds) Vision and Visual Dysfunction, Vol. 5, Limits of Vision (Chapter 9, pp. 106-119). The Macmillan Press. U.K.

Georgeson M. A. and Shackleton T. M. (1994). Perceived contrast of gratings and plaids: non-linear summation across oriented filters. Vision Research, 34, 1061-1075.

Georgeson M. A. and Sullivan G. D. (1975). Contrast constancy: deblurring in human vision by spatial frequency channels. Journal of Physiology, 252, 627-656.

Gonzalez R. C. and Woods R. E. (1992). Image restoration. In Digital image processing (Chapter 5, pp. 253-305). Addison-Wesley, Reading.

Goodyear C. C. (1971). Signals and information. Butterworths, London, pp. 240-244.

Gottesman J., Rubin G. S. and Legge G. E. (1981). A power law for perceived contrast in human vision. Vision Research, 21, 791-799.

Graham N. and Hood D. C. (1992). Quantal noise and decision rules in dynamic models of light adaptation. Vision Research, 32, 779-787.

Green D. M. and Swets J. A. (1966). Signal detection theory and psychophysics. Theory of ideal observers, 151-179. Wiley, New York.

Guth S. L. (1967). Nonadditivity and inhibition among chromatic luminances at threshold. Vision Research, 7, 319-328.

Hauske G., Wolf W. and Lupp U. (1976). Matched filters in human vision. Biological Cybernetcis, 22, 181-188.

Hoekstra J., van der Goot D. P. J., van den Brink G. and Bilsen F. A. (1974). The influence of the number of cycles upon the visual contrast threshold for spatial sine wave patterns. Vision Research, 14, 365-368.

van der Horst G. J. C. and Bouman M. A. (1969). Spatiotemporal chromaticity discrimination. Journal of the Optical Society of America, 59, 1482-1488.

Howell E. R. and Hess R. F. (1978). The functional area for summation to threshold for sinusoidal gratings. Vision Research, 18, 369-374.

Kersten D. (1984). Spatial summation in visual noise. Vision Research, 24, 1977-1990.

Kohonen T. (1990). The self-organizing map. Proceedings of the IEEE, 78, 1464-1480.

Kukkonen H., Rovamo J. and Näsänen R. (1995). Masking potency and whiteness of noise at various noise check sizes. Investigative Ophthalmology and Visual Sicence, 513-518.

Kukkonen H., Rovamo J., Tiippana K. and Näsänen R. (1993). Michelson contrast, RMS contrast and energy of various spatial stimuli at threshold. Vision Research, 33, 1431-1436.

Kulikowski J. J. (1976). Effective contrast constancy and linearity of contrast sensation. Vision Research, 16, 1419-1431.

Legge G. E. (1979). Spatial frequency masking in human vision: binocular interactions. Journal of the Optical Society of America, 69, 838-847.

Legge G. E. (1981). A power law for contrast discrimination. Vision Research, 21, 457-467.

Legge G. E. (1984a). Binocular contrast summation - I. Detection and discrimination. Vision Research, 24, 373-383.

Legge G. E. (1984b). Binocular contrast summation - II. Quadratic summaton. Vision Research, 24, 385-394.

Legge G. E. and Foley J. M. (1980). Contrast masking in human vision. Journal of the Optical Society of America, 70, 1458-1471.

Legge G. E. and Kersten D. (1987). Contrast discrimination in peripheral vision. Journal of the Optical Society of America, 4, 1594-1598.

Legge G. E., Kersten D. and Burgess A. E. (1987). Contrast discrimination in noise. Journal of the Optical Society of America, 4, 391-404.

Mäkelä P., Whitaker D. and Rovamo J. (1993). Modelling of orientation discirmination across the visual field. Vision Research, 33, 723-730.

Mayhew J. E. W. and Frisby J. P. (1978). Suprathreshold contrast perception and complex random textures. Vision Research, 18, 895-897.

Michaels D. D. (1985). Visual optics and refraction: a clinical approach. The C. V. Mosby Company, St. Louis.

Moulden B., Kingdom F. and Gatley L. F. (1990). The standard deviation of luminance as a metric for coontrast in random-dot images. Perception, 19, 79-101.

Mullen K. T. (1985). The contrast sensitivity of human colour vision to red-green and blue-yellow chromatic gratings. Journal of Physiology, 359, 381-400.

Mullen K. T. (1991). Colour vision as a post-receptoral specialization of the central visual field. Vision Research, 31, 119-130.

Mullen K. T. and Kingdom F. A. A. (1991). Colour contrast in form perception. In Gouras P. (Ed.) Vision and Visual Dysfunction, Vol. 6, The Perception of Colour (Chapter 12, pp. 198-217). The Macmillan Press, U.K.

Mullen K. T. and Losada M. A. (1994). Evidence for separate pathways for color and luminance detection mechanisms. Journal of the Optical Society of America, 11, 3136-3151.

Mustonen J., Rovamo J. and Näsänen R. (1993). The effects of grating area and spatial frequency on contrast sensitivity as a function of light level. Vision Research, 33, 2065-2072.

Nachmias J. and Sansbury R. V. (1974). Grating contrast: discrimination may be better than detection. Vision Research, 14, 1039-1042.

Nagaraja N. S. (1964). Effect of luminance noise on contrast thresholds. Journal of the Optical Society of America, 54, 950-955.

Näsänen R. E., Kukkonen H. T. and Rovamo J. M. (1995a). A window model for spatial integration in human pattern discrimination. Submitted to Investigative Ophthalmology & Visual Science.

Näsänen R., Kukkonen H. and Rovamo J. (1995b). Spatial integration in orientation discrimination at different contrast levels. In preparation.

van Nes F. L. and Bouman M. A. (1967). Spatial modulation transfer in the human eye. Journal of the Optical Society of America, 57, 401-406.

van Nes F. L., Koenderink J. J., Nas H. and Bouman M. A. (1967). Spatiotemporal modulation transfer in the human eye. Journal of the Optical Society of America, 57, 1082-1088.

Noorlander C., Heuts M. J. G. and Koenderink J. J. (1980). Influence of the target size on the detection threshold for luminance and chromaticity contrast. Journal of the Optical Society of America, 70, 1116-1121.

Peli E. (1990). Contrast in complex images. Journal of the Optical Society of America, A 7, 2032-2040.

Peli E. (1995). Suprathreshold contrast perception across differences in mean luminance: effects of stimulus size, dichoptic presentation, and length of adaptation. Journal of the Optical Society of America, A 12, 817-823.

Pelli D. G. (1981). Effects of visual noise. Doctoral dissertation. Cambridge University, U.K.

Pelli D. G. (1985). Uncertainty explains many aspects of visual contrast detection and discrimination. Journal of the Optical Society of America, A2, 1508-1532.

Pelli D. G. (1990). The quantum efficiency of vision. In: Blakemore C. (Ed) Vision: Coding and Efficiency (Chapter 1, pp. 3-20). Cambridge University Press, U.K.

Pelli D. G. and Zhang L. (1991). Accurate control of contrast on microcomputer displays. Vision Research, 31, 1337-1350.

Quick R. F. (1974). A vector-magnitude model of contrast detection. Kybernetik, 16, 65-67.

Quick R. F., Hamerly J. R. and Reichert T. A. (1976). The absence of a measurable "critical band" at low suprathreshold contrasts. Vision Research, 16, 351-355.

Quinn P. C. (1985). Suprathreshold contrast perception as a function of spatial frequency. Perception and Psychophysics, 38, 408-414.

Ratliff F. and Hartline H. K. (1959). The responses of limulus optic nerve fibers to patterns of illumination on the receptor mosaic. J. Gen. Physiol., 42, 1241-1255.

Rose A. (1948). The sensitivity performance of the human eye on an absolute scale. Journal of the Optical Society of America, 38, 196-208.

Rovamo J., Kukkonen H., Tiippana K. and Näsänen R.(1993). Effects of luminance and exposure time on contrast sensitivity in spatial noise. Vision Research, 33, 1123-1129.

Rovamo J., Luntinen O. and Näsänen R. (1993). Modelling the dependence of contrast sensitivity on grating area and spatial frequency. Vision Research, 33, 2773-2788.

Rovamo J., Luntinen O. and Näsänen R. (1995). Contrast sensitivity as a function of grating area and spectral density of external spatial noise. In preparation.

Rovamo J., Mustonen J. and Näsänen R. (1994a). Modelling contrast sensitivity as a function of retinal illuminance and grating area. Vision Research, 34, 1301-1314.

Rovamo J., Mustonen J. and Näsänen R. (1994b). Two simple psychophysical methods for determining the optical modulation function of the human eye. Vision Research, 34, 2493-2502.

Rovamo J., Mustonen J. and Näsänen R. (1995). Neural modulation transfer function of the human visual system at various eccentricities. Vision Research, 35, 767-774.

Rovamo J., Ukkonen O., Thompson C. and Näsänen R. (1994). Spatial integration of compound gratings with various numbers of orientation components. Investigative Ophthalmology & Visual Science, 35, 2611-2619.

Sclar G., Lennie P. and DePriest D. (1989). Contrast adaptation in striate cortex of macaque. Vision Research, 29, 747-755.

Sekiguchi N., Williams D. R. and Brainard D. H. (1993). Efficiency in detection of isoluminant and isochromatic interference filters. Journal of the Optical Society of America, 10, 2118-2133.

Snowden R. J. and Hammett S. T. (1992). Subtractive and divisive adaptation in the human visual system. Nature, 355, 248-250.

Stephens B. R. and Banks M. S. (1985). The development of contrast constancy. Journal of Experimental Child Psychology, 40, 528-547.

Stevens S. S. (1961). The psychophysics of sensory function. In W. A. Rosenblith (Ed.). Sensory communication (Chapter 1, pp. 1-33). The M. I. T. Press and John Wiley & Sons, New York.

Stromeyer C. F. III and Julesz B. (1972). Spatial-frequency masking in vision: critical bands and spread of masking. Journal of the Optical Society of America, 62, 1221-1232.

Swanson W. H., Georgeson M. A. and Wilson H. R. (1988). Comparison of contrast responses across spatial mechanisms. Vision Research, 28, 457-459.

Swanson W. H. and Wilson H. R. (1985). Eccentricity dependence of contrast matching and oblique masking. Vision Research, 25, 1285-1295.

Swanson W. H., Wilson H. R. and Giese S. C. (1984). Contrast matching data predicted from contrast increment thresholds. Vision Research, 24, 63-75.

Switkes E., Bradley A. and DeValois K. (1988). Contrast dependence and mechanisms of masking interactions among chromatic and luminance gratings. Journal of the Optical Society of America, 5, 1149-1162.

Takahashi S. and Ejima Y. (1984). Dependence of apparent contrast for a sinusoidal grating on stimulus size. Journal of the Optical Society of America, A1, 1197-1201.

Tanner W. P. and Birdsall T. G. (1958). Definitions of d' and η as psychophysical measures. Journal of the Optical Society of America, 30, 922-928.

Thibos L. N., Bradley A., Still D. L., Zhang X. and Howarth P. A. (1990). Theory and measurement of ocular chromatic aberration. Vision Research, 30, 33-49.

Thibos L. N., Ye M., Zhang X. and Bradley A. (1992). The chromatic eye: a new reduced-eye model of ocular chromatic aberration in humans. Applied Optics, 31, 3594-3600.

Tolhurst D. J., Movshon J. A. and Dean A. F. (1983). The statistical reliability of signals in single neurons in cat and monkey visual cortex. Vision Research, 23, 775-785.

Tolhurst D. J., Movshon J. A. and Thompson I. D. (1981). The dependence of response amplitude and variance of cat visual cortical neurones on stimulus contrast. Experimental Brain Research, 41, 414-419.

Virsu V. and Rovamo J. (1979). Visual resolution, contrast sensitivity, and the cortical magnification factor. Experimental Brain Research, 37, 475-494.

Watanabe A., Mori T., Nagata S. and Hiwatashi K. (1968). Spatial sine-wave responses of the human visual system. Vision Research, 8, 1245-1263.

Wetherill G. B. and Levitt H. (1965). Sequential estimation of points on a psychometric function. British Journal of Mathematical and Statistical Psychology, 18, 1-10.

Wilson H. R. (1980). A transducer function for threshold and suprathreshold human vision. Biological Cybernetics, 38, 171-178.

APPENDIX I

Michelson and root-mean-square contrast for a cosine grating

Root-mean-square (r.m.s.) contrast in one spatial dimension is defined as:

$$c = \sqrt{\frac{1}{n}\int_0^n c^2(x)\,dx} \tag{1}$$

where function c(x) is the contrast signal which is calculated by:

$$c(x) = \frac{L(x) - L_0}{L_0} \tag{2}$$

where function L(x) is the luminance signal and L_0 is the mean luminance. The luminance signal for a cosine grating has a form:

$$L(x)=L_0[1+c_M \cos(2\pi fx)]=L_0+L_0\, c_M \cos(2\pi fx) \tag{3}$$

where c_M is the Michelson contrast and f is the spatial frequency of the cosine grating. The contrast signal for a cosine grating is achieved by combining equations (2) and (3):

$$c(x) = \frac{L_0 + L_0\, c_M \cos(2\pi f x) - L_0}{L_0} = c_M \cos(2\pi f x) \tag{4}$$

The r.m.s. contrast for a cosine grating is then calculated as:

$$\begin{aligned} c &= \sqrt{\frac{1}{n}\int_0^n \left[c_M \cos(2\pi f x)\right]^2 dx} \\ c &= \sqrt{\frac{{c_M}^2}{n}\left|\frac{x}{2} + \frac{\sin(4\pi f x)}{8\pi f}\right|_0^n} \\ c &= \sqrt{\frac{{c_M}^2}{n}\left[\frac{n}{2} + \frac{\sin(4\pi f n)}{8\pi f}\right]} \\ c &= \sqrt{\frac{{c_M}^2}{2} + \frac{{c_M}^2 \sin(4\pi f n)}{8\pi f n}} \end{aligned} \tag{5}$$

The right-hand side term in Equation (5) becomes smaller with increasing n, i.e. with increasing extent of the grating. Thus the r.m.s. contrast of a cosine grating is approximately:

$$c = \sqrt{\frac{c_M^2}{2}} = \frac{c_M}{\sqrt{2}} = 0.707 c_M \qquad (6)$$

Equation (6) is exactly accurate when $\sin(4\pi fn)=0$. A sine function is zero when its value is a multiple p of π . That is, $\sin(4\pi fn)=0$, when $4\pi fn=p\pi$. From this follows that Equation (6) is accurate when $n=p/4f$, where p=0, 1, 2, 3...

APPENDIX II

Definition of efficiency (η) and detectability index (d')

The signal detection theory (see e.g. Green & Swets, 1966) has been applied to visual perception in studies where the performance of an ideal detector is compared to the human visual performance (e.g. Burgess & Ghandeharian, 1984ab; Burgess, 1985). An ideal detector represents the best possible performance in a task. The human performance is compared to the ideal to calculate human efficiency (Burgess, 1990). The concept of detection efficiency has been adopted to describe the fact that the human visual system is not capable of collecting all information in the stimulus (Legge, Kersten & Burgess, 1987). The visual system seems to sample the stimulus information, and efficiency tells how complete the sampling is.

The performance of an ideal detector is limited only by noise. Therefore, human and ideal performance can only be compared when thresholds are measured in a known magnitude of noise.

The definition of efficiency given here applies to a signal-known-exactly task where uncertainty about the stimulus is minimised. This definition is widely used, and it is appropriate here because in the experiments of this thesis the observer was always shown the stimulus at a suprathreshold level before a threshold measurement in order to minimise uncertainty.

Efficiency is defined as the ratio of the energy threshold of the ideal detector to the energy threshold of a human observer (Tanner & Birdsall, 1958):

$$\eta = \frac{E_i}{E_h} \qquad (1)$$

The energy threshold of the human observer, E_h, represents the stimulus energy needed for a human to achieve a certain level of performance in a task (e.g. 84% correct responses in a two-alternative forced-choice task). The energy threshold of the ideal observer, E_i, represents the stimulus energy needed for the ideal detector to achieve the same level of performance as the human observer under known noise conditions.

The level of performance can also described by the detectability index d' which for a signal-known-exactly task is:

$$d' = \sqrt{\frac{E_i}{N}} \tag{2}$$

where N is the spectral density of noise (Tanner & Birdsall, 1958). The detectability index gives the signal-to-noise ratio, i.e. the value of $\sqrt{E_i/N}$, necessary for the ideal observer to obtain the required level of performance. Thus, a certain value of detectability index corresponds a certain percent correct (Elliott, 1964). In an experiment where contrast detection or increments thresholds are measured, the percent correct and consequently the value of d' is kept constant, so that the signal-to-noise ratio is constant at threshold.

By combining Equations (1) and (2), the detectability index can also be defined as:

$$d' = \sqrt{\frac{E_h \eta}{N}} \tag{3}$$

On the basis of Equation (3), efficiency can be written as:

$$\eta = \frac{d'^2 N}{E_h} \tag{4}$$

Efficiency can be easily calculated using Equation (4) since the energy threshold of the ideal observer is given by the detectability index squared and multiplied by the spectral density of noise, and efficiency is then calculated by dividing the numerator, i.e. E_i, by the measured energy threshold of the human observer.

APPENDIX III

Predictions of the contrast restoration model at various values of parameters γ and κ.

Figure AIII.1 shows matching contrast predictions of the contrast restoration model plotted as a function of the contrast of the standard grating. The predictions have been calculated for a 16 c/deg grating matched to a 4 c/deg standard grating. The value of restoration parameters γ and κ were varied, and the values of parameters determining detection thresholds were kept constant at values shown in Table 4.1 subject KT (see page 59). The straight line segment shows the locus of physically correct matches.

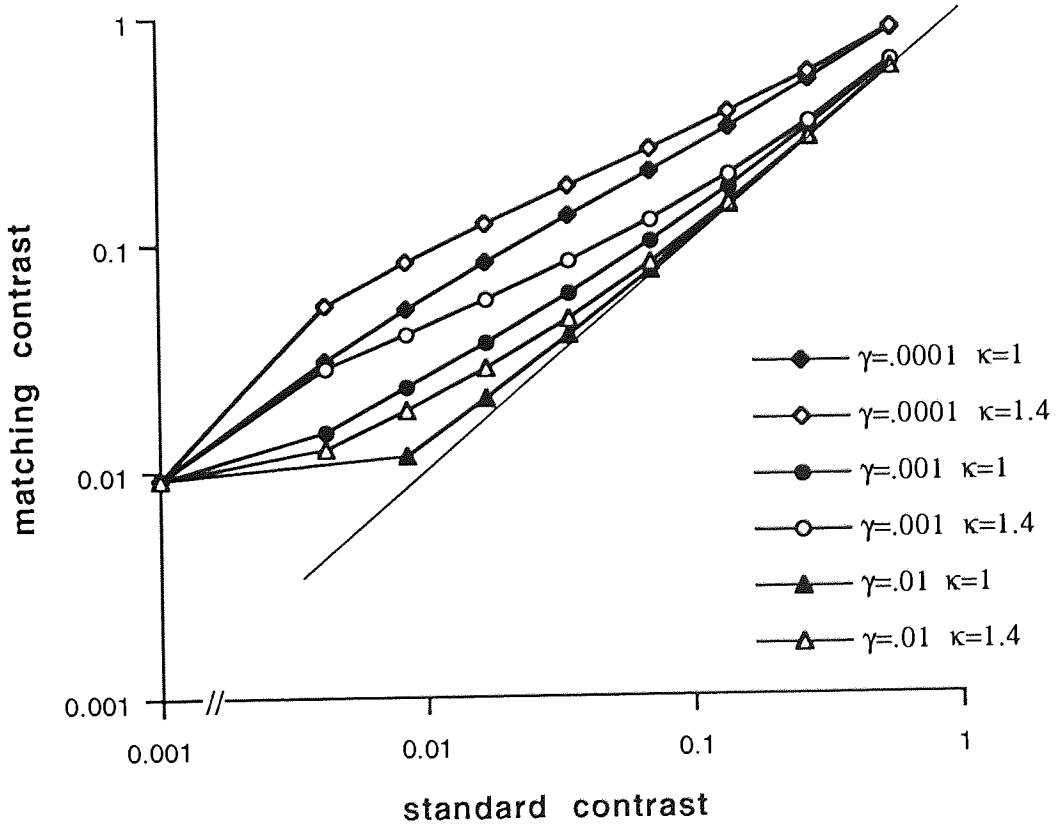

Figure AIII.1 Predictions of the contrast restoration model at various values of parameters γ and κ.

APPENDIX IV

Dependence of quantal noise on signal contrast.

Quantal noise is often regarded as being independent of the contrast of the visual stimulus. That is, the spectral density of quantal noise is normally taken to be constant at all contrast levels. However, this is not strictly true at high contrast levels. When the contrast of a stimulus is increased, its maximum (L_{max}) and minimum (L_{min}) luminances deviate progressively more from the mean luminance (L_0). When contrast is low, the deviations are small, and the spectral density of quantal noise is given by $N_{q0}=k/L_0$, where k is a constant. When contrast is high, the difference between L_{max} and L_{min} is large, and therefore quantal noise is weaker at L_{max} and stronger at L_{min} than at L_0. This can be demonstrated by calculating quantal noises at L_{max} and at L_{min} as $N_{q1}=k/L_{max}$, and $N_{q2}=k/L_{min}$, respectively.

Figure AIV.1 shows a graph of the relative quantal noises at the maximum and minimum luminance, N_{q1}' and N_{q2}', plotted as a function of Michelson contrast. The relative quantal noises are calculated as $N_{q1}'=N_{q1}/N_{q0}=L_0/L_{max}$ and $N_{q2}'=L_0/L_{min}$. Thus, the N_q' on the abscissa indicates the strength of quantal noises at maximum and minimum

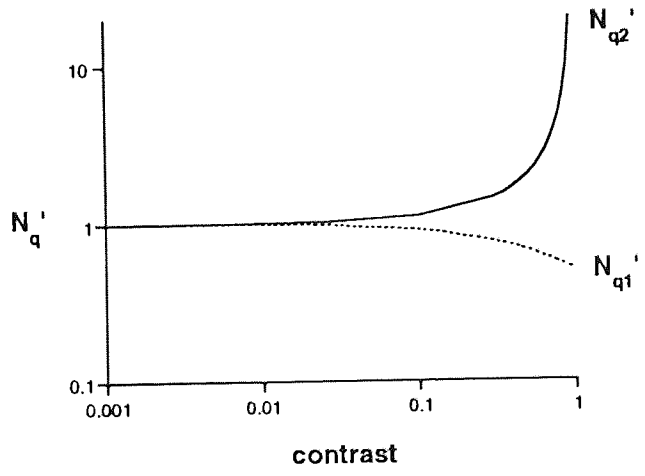

Figure AIV.1 Dependence of local quantal noise on stimulus contrast.

luminance relative to the quantal noise at mean luminance. At low contrasts, the relative quantal noises are equal and quantal noise is thus independent of stimulus contrast. But at high contrasts, the relative quantal noise at the luminance maximum, N_{q1}', starts to decrease and the relative quantal noise at the luminance minimum, N_{q2}', starts to increase. The N_{q1}' decreases maximally by a factor of 2. The N_{q2}' increases in an accelerating manner so that at a contrast of 0.99, it is 100 times larger than quantal noise at the mean luminance.

Even though quantal noise was signal dependent in some conditions in the experiments presented in Section 5.4 of this thesis, in practice the effect was negligible since the difference-signal discriminator model could predict contrast increment thresholds accurately even though it is based on the assumption that quantal noise is always additive.

APPENDIX V

Predictions of the contrast discrimination model at various values of parameters m and k.

Figure AV.1 shows contrast discrimination functions predicted by the difference-signal discriminator model. The predictions have been calculated for a 4 c/deg, 16 deg^2 grating. The values of parameters determining detection thresholds were kept constant at values shown in Table 5.1 subject KT (see page 118). The values of parameters m and k were varied.

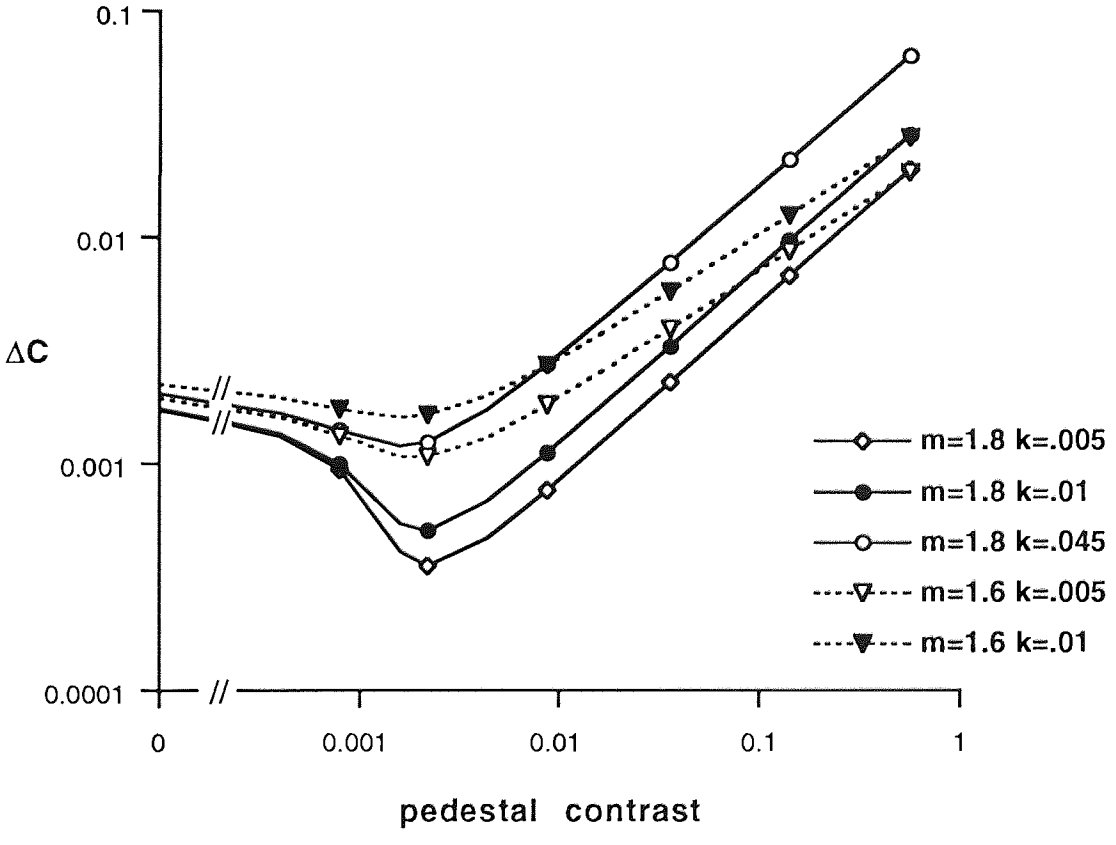

Figure AV.1 Predictions of the contrast discrimination model at various values of parameters m and k.

APPENDIX VI

Estimation of the critical spectral density of external noise (N_c), maximum efficiency (η_{max}), critical number of square cycles (z_c), and critical retinal illuminance (I_c) on the basis of the contrast detection model.

Estimation of the critical spectral density of external noise:

After filtering by the optical and neural modulation transfer functions of the visual system, the critical spectral density of external spatial noise (N_c) is equal to the spectral density of internal noise (N_i). The N_c can be estimated by plotting contrast sensitivity as a function of spectral density of external noise (N_e), and finding the value of N_e at which sensitivity has reduced by a factor of $\sqrt{2}$ from the maximum.

Contrast sensitivity (S) in external spatial noise was modelled by fitting equation:

$$S^{-2} = S_{max}^{-2} (1+N_e/N_c) \tag{1}$$

to the contrast sensitivity data measured at various levels of N_e. Contrast sensitivity was averaged across areas since the effect of external noise is independent of grating area. S_{max} is the maximum obtainable sensitivity. Parameters S_{max} and N_c were determined by finding the minimum of the following:

$$G = \sum_{j=1}^{n} \left(\frac{S_j^{-2} - k_1 - k_2 N_{ej}}{S_j^{-2}} \right)^2 \tag{2}$$

where $k_1=S_{max}^{-2}$, $k_2=S_{max}^{-2}N_c^{-1}$, and S_j (j=1,2,3,...,n) are contrast sensitivities corresponding to spectral densities N_{ej} (j=1,2,3,...,n). It is necessary to calculate the relative least square curve by minimising the percentage error because the range of S^{-2} is several logarithmic units. Otherwise the deviations of the large values of S^{-2} from the least squares curve would dominate the fitting procedure. In the following text subscript j is left out for brevity. Equation (2) was then transformed to:

$$G = \Sigma(1 - k_1S^2 - k_2S^2N_e)^2 \tag{3}$$

Equation (3) was transformed to:

$$G = \Sigma(1 - k_1x_1 - k_2x_2)^2 \quad (4)$$

where $x_1=S^2$ and $x_2=S^2N_e$. The values of k_1 and k_2 that minimise G were then found by the method described in Mäkelä, Whitaker and Rovamo (1993). Thereafter the critical noise spectral density was calculated as $N_c=k_1/k_2$.

Estimation of the maximum efficiency and the critical number of square cycles:

The maximum efficiency (η_{max}) refers to the highest detection efficiency obtainable with small gratings. The critical number of square cycles (z_c) marks the saturation of spatial integration. The z_c can be estimated by plotting efficiency as a function of grating area expressed as square cycles ($z=Af^2$), and by finding the value of z at which efficiency has reduced by a factor of 2 from the maximum.

The dependence of efficiency (η) on grating area expressed as square cycles (z) was modelled by fitting equation:

$$\eta^{-1} = \eta_{max}^{-1} (1+z/z_c) \quad (5)$$

to the efficiencies obtained with various grating areas. The fitting procedure was as described above but in Equations (2)-(4) S^{-2} was replaced by η^{-1}, and N_e by z, and the constants were $k_1=\eta_{max}^{-1}$, and $k_2=\eta_{max}^{-1}z_c^{-1}$. The maximum efficiency was given by: $\eta_{max}=k_1^{-1}$, and the critical number of square cycles by $z_c=k_1/k_2$.

The estimates of efficiency at various grating areas which were inserted into Equation (5) were calculated for each detection threshold measured according to (Rovamo, Luntinen & Näsänen, 1993&1995):

$$\eta = E_d^{-1} d'^2 (N_e+N_c) \quad (6)$$

where E_d is the contrast energy of the stimulus at detection threshold ($E=c^2A$), and d'^2 is the detectability index squared which was equal to 2 in these experiments.

Estimation of the critical retinal illuminance:

The critical retinal illuminance (I_c) is inversely proportional to the spectral density of the critical quantal noise (N_{qc}) which is equal to the internal noise (N_i) when filterend by the neural modulation transfer function of the visual system (Rovamo, Mustonen & Näsänen, 1994a). The I_c can be estimated by plotting contrast sensitivity as a function of retinal illuminance (I), and finding the value of I at which sensitivity has reduced by a factor of $\sqrt{2}$ from the maximum.

Dependence of contrast sensitivity on retinal illuminance was modelled by fitting equation:

$$S^{-2} = S_{max}^{-2} (1+I_c/I) \qquad (7)$$

to the contrast sensitivity data measured at various levels of retinal illuminance. Contrast sensitivity S was averaged across areas since the effect of retinal illuminance is independent of grating area (Rovamo, Mustonen & Näsänen, 1994a). The I_c was determined using the procedure described above for N_c so that in Equations (2)-(4) N_e was replaced by I^{-1}, and the constants were $k_1=S_{max}^{-2}$, and $k_2=S_{max}^{-2} I_c$. The critical retinal illuminance was calculated as $I_c=k_2/k_1$.

APPENDIX VII

Calculation of the spectral density of quantal noise (N_q) on the basis of the contrast detection model.

The total spectral density of pre-detector noise in the human brain is calculated by:

$$N_{tot}' = H_o^2(f)\, H_n^2(f)\, N_e(f) + H_n^2(f)\, N_q + N_i \qquad (1)$$

where $N_e(f)$, N_q and N_i are respectively the external spatial noise, and the spatial equivalents of quantal and internal noises (for further details see Chapter 4, Section 4.1).

The critical spectral density of external spatial noise (N_c) is equal to the spectral density of the internal noise (N_i) after it has been filtered through the optical and neural modulation transfer functions of the human visual system (Rovamo, Luntinen & Näsänen, 1995):

$$N_i = H_o^2(f)\, H_n^2(f)\, N_c \qquad (2a)$$

From this follows that:

$$N_c = \frac{N_i}{H_o^2(f) H_n^2(f)} \qquad (2b)$$

The critical spectral density of quantal noise (N_{qc}) is equal to the spectral density of the internal noise (N_i) after it has been filtered through the neural modulation transfer function (Rovamo, Mustonen & Näsänen, 1994a):

$$N_i = H_n^2(f)\, N_{qc} \qquad (3a)$$

If we divide Equation (3a) by $H_o^2(f)\, H_n^2(f)$, we can express the N_{qc} in terms of N_c:

$$\frac{N_{qc}}{H_o^2(f)} = \frac{N_i}{H_o^2(f) H_n^2(f)} = N_c \quad \Rightarrow$$

$$N_{qc} = H_o^2(f)\, N_c \qquad (3b)$$

The total spectral density of noise transferred into the visual field from the human brain is calculated by:

$$N_{tot} = \frac{N_{tot}'}{H_o^2(f)H_n^2(f)}$$
$$= N_e + \frac{N_q}{H_o^2(f)} + N_c \qquad (4a)$$
$$= N_c\left(\frac{N_e}{N_c} + \frac{N_q}{H_o^2(f)N_c} + 1\right)$$

We can now insert Equation (3b) into Equation (4a):

$$N_{tot} = N_c\left(\frac{N_e}{N_c} + \frac{N_q}{N_{qc}} + 1\right) \qquad (4b)$$

It is known that $N_q=k/I$, and that $N_{qc}=k/I_c$, where I is the retinal illuminance in trolands, I_c is the critical retinal illuminance marking the transition between DeVries-Rose and Weber's laws, and k is a constant (Rovamo, Mustonen & Näsänen, 1994a). Thus, we can write:

$$N_{tot} = N_c\left(\frac{N_e}{N_c} + \frac{I_c}{I} + 1\right)$$
$$= N_e + N_c\frac{I_c}{I} + N_c \qquad (4c)$$

The total spectral density of noise in the human brain, N_{tot}', can be calculated on the basis of Equation (4c) by multiplying N_{tot} by $H_o^2(f)\,H_n^2(f)$, and by applying Equation (2a). We then get:

$$N_{tot}' = H_o^2(f)H_n^2(f)N_e + N_i\frac{I_c}{I} + N_i \qquad (5)$$

By comparing Equations (1) and (5), it can be seen that the spectral density of quantal noise in the human brain is calculated by multiplying the ratio of the critical retinal illuminance to the retinal illuminance by the spectral density of internal noise:

$$N_q' = N_i\frac{I_c}{I} \qquad (6)$$

APPENDIX VIII

Tables of the experimental data presented in the thesis

Figures 4.5 and 4.6

A Matching contrasts for subject KT at 0.5 c/deg.

C_s	1 component	2 components	3 components	4 components
0.28	0.28015	0.25993	0.29222	0.24090
0.14	0.13463	0.13832	0.14031	0.12633
0.07	0.069163	0.067695	0.070925	0.064636
0.035	0.034502	0.030469	0.034835	0.033671
0.018	0.016605	0.017293	0.019055	0.019293
0.0071	0.0059451	0.0072199	0.0075488	0.0087397
0	0.0021071	0.0031850	0.0039360	0.0042127

B Matching contrasts for subject HK at 2 c/deg.

C_s	1 component	2 components	3 components	4 components
0.28	0.26921	0.23290	0.27466	0.21411
0.14	0.13853	0.11907	0.14109	0.11787
0.07	0.069358	0.061496	0.064187	0.058353
0.035	0.034659	0.029309	0.032347	0.028138
0.018	0.016484	0.015196	0.014697	0.014974
0.0071	0.0060238	0.0063605	0.0059365	0.0067609
0	0.0012630	0.0024272	0.0029183	0.0030803

C Matching contrasts for subject KT at 4 c/deg.

C_s	1 component	2 components	3 components	4 components
0.28	0.26638	0.26311	0.25242	0.2169
0.14	0.12333	0.12638	0.12755	0.1149
0.07	0.062808	0.059844	0.058461	0.06067
0.035	0.029511	0.032404	0.029003	0.03116
0.018	0.015404	0.015012	0.013937	0.01670
0.0071	0.0065810	0.0071124	0.0073180	0.008352
0	0.0021718	0.0026856	0.0027306	0.002666

Figures 4.7 and 4.8

A Matching contrasts for subject HK.

C_s	0.5 c/deg	1 c/deg	2 c/deg	4 c/deg	8 c/deg	16 c/deg
0	0.0041926	0.0023672	0.0016026	0.0013946	0.0030068	0.019560
0.0042	0.0070527	0.0061721	0.0041268	0.0034498	0.0090694	0.051856
0.0085	0.013626	0.010593	0.0086827	0.0069555	0.014662	0.055340
0.017	0.022201	0.018639	0.017018	0.018736	0.023592	0.064141
0.035	0.033406	0.035781	0.033406	0.032966	0.044325	0.10252
0.071	0.073705	0.074970	0.065185	0.075472	0.082599	0.13131
0.28	0.26580	0.23477	0.23587	0.24746	0.29442	0.28929
0.57	0.48475	0.49075	0.51897	0.52233	0.58714	---

B Matching contrasts for subject KT.

C_s	0.5 c/deg	1 c/deg	2 c/deg	4 c/deg	8 c/deg	16 c/deg
0	0.0028716	0.0019783	0.0012187	0.0010582	0.0020592	0.0083213
0.0042	0.0063385	0.0043264	0.0046171	0.0041373	0.0073917	0.032030
0.0085	0.0092652	0.0075670	0.0081079	0.0084882	0.013818	0.043412
0.017	0.022425	0.017811	0.016516	0.016918	0.022174	0.074265
0.035	0.042985	0.037680	0.036370	0.032699	0.044306	0.11811
0.071	0.067383	0.062760	0.058101	0.073881	0.085766	0.14023
0.28	0.29273	0.30783	0.27177	0.27275	0.31120	0.27914
0.57	0.58371	0.58184	0.56082	0.56091	0.58868	---

Figures 4.9 and 4.10

A Matching contrasts for subject RL at 1 c/deg.

C_s	A=4 deg^2	A=16 deg^2	A=64 deg^2	A=256 deg^2
0	0.0053948	0.0034408	0.0024572	0.0019433
0.0071	0.011990	0.0077677	0.0065597	0.0069309
0.014	0.020262	0.014632	0.013728	0.014394
0.027	0.028934	0.026783	0.026358	0.026306
0.053	0.050970	0.048261	0.049295	0.051341
0.11	0.093691	0.094951	0.097153	0.11042
0.21	0.18342	0.19437	0.19934	0.19366
0.42	0.39298	0.39552	0.39268	0.36641

B Matching contrasts for subject KT at 4 c/deg.

C_s	A=0.25 deg^2	A=1 deg^2	A=4 deg^2	A=16 deg^2
0	0.0052633	0.0031775	0.0022985	0.0019967
0.0071	0.013572	0.0075600	0.0070611	0.0062306
0.014	0.019007	0.014846	0.014155	0.012341
0.027	0.027763	0.024699	0.025614	0.025168
0.053	0.053316	0.051045	0.046961	0.050179
0.11	0.10900	0.093883	0.10400	0.10515
0.21	0.18653	0.19138	0.19762	0.17618
0.42	0.40399	0.39800	0.39498	0.38377

Figure 4.13

A Matching contrasts for subject KT.

C_s	0.5 c/deg	1 c/deg	2 c/deg	4 c/deg	8 c/deg
0	0.0167859	0.010598	0.0062304	0.0052477	0.0081340
0.012	0.037992	0.015749	0.010107	0.010091	0.022200
0.025	0.045754	0.030838	0.020780	0.019262	0.035994
0.05	0.077851	0.054960	0.047388	0.055846	0.055846
0.1	0.13485	0.10614	0.096637	0.10074	0.13181

B Matching contrasts for subject PM.

C_s	0.5 c/deg	1 c/deg	2 c/deg	4 c/deg	8 c/deg
0	0.013589	0.0077593	0.0042982	0.005014	0.0081564
0.0086	0.018250	0.012623	0.0080557	0.0067956	0.016600
0.017	0.027414	0.022401	0.0162421	0.014505	0.024372
0.034	0.036968	0.041633	0.030823	0.033720	0.048630
0.068	0.085487	0.068477	0.066781	0.069211	0.094541

Figure 4.14

A Matching contrasts for subject KT.

C_s	0.5 c/deg	1 c/deg	2 c/deg	4 c/deg	8 c/deg
0	0.0069657	0.0071036	0.011121	0.012767	0.028229
0.022	0.0178447	0.018429	0.017454	0.019055	0.034763
0.044	0.047405	0.037281	0.038541	0.036379	0.061651
0.09	0.097491	0.08832	0.078208	0.071803	0.13751
0.18	0.18771	0.15976	0.16028	0.15657	0.20027

B Matching contrasts for subject PM.

C_s	0.5 c/deg	1 c/deg	2 c/deg	4 c/deg	8 c/deg
0	0.0076248	0.0063436	0.0096285	0.022878	0.019812
0.02	0.021440	0.015458	0.017464	0.028694	0.031484
0.04	0.036881	0.025276	0.027339	0.044307	0.052515
0.08	0.062382	0.060089	0.056777	0.079207	0.10826
0.16	0.13619	0.15080	0.13729	0.14042	0.21704

Figure 4.15

A Matching contrasts for subject KT.

C_s	0.5 c/deg	1 c/deg	2 c/deg	4 c/deg
0	0.025936	0.023681	0.037072	0.075972
0.074	0.074245	0.070905	0.071214	0.087482
0.15	0.15239	0.14544	0.13482	0.13041
0.3	0.29054	0.27188	0.24804	0.25977
0.6	0.50038	0.52837	0.54501	0.54441

Figures 5.2 and 5.3

A Contrast increment thresholds for subject OL at 0.5 c/deg.

C_p	A=4 deg^2	A=16 deg^2	A=64 deg^2	A=256 deg^2	A=1024deg^2
0	0.0066669	0.0038819	0.0027801	0.0014640	0.0014939
0.0011	-	-	-	0.0013497	0.00039415
0.0022	-	-	0.0012718	0.00063668	0.00046833
0.0044	0.0039999	0.0013531	0.0006464	0.00056419	0.00045095
0.0088	0.0029740	0.0017223	0.00094109	0.00082194	0.0014294
0.018	0.0034189	0.0022083	0.0034847	0.0029688	0.0030880
0.035	0.0036504	0.0048974	0.0048687	0.0054083	0.0037655
0.071	0.0089139	0.0061812	0.0070376	0.0085447	0.0087535
0.28	0.036800	0.019908	0.031056	0.019351	0.023614

B Contrast increment thresholds for subject KT at 4 c/deg.

C_p	A=0.06 deg^2	A=0.25 deg^2	A=1 deg^2	A=4 deg^2	A=16 deg^2
0	0.015867	0.0071608	0.0034349	0.0023112	0.0016491
0.0011	-	-	-	0.0011468	0.00052716
0.0022	-	-	0.0018667	0.00084871	0.00051439
0.0044	0.0086256	0.0033535	0.0015435	0.0076930	0.00055421
0.0088	0.0060477	0.0025697	0.0017014	0.0010985	0.0011501
0.018	0.00546	0.0023658	0.0020895	0.0019535	0.0021159
0.035	0.0056209	0.005173	0.0038299	0.0035161	0.0033592
0.071	0.0090994	0.0070603	0.0063442	0.005428	0.0056454
0.28	0.017395	0.01975	0.020646	0.017995	0.018720
0.57	0.03492	0.024791	0.027062	0.023039	0.027251

Figures 5.5 and 5.8

A Contrast increment thresholds for subject HR at 1 c/deg with A=16 square cycles.

C_p	C_n=0	C_n=0.038	C_n=0.15	C_n=0.3
0	0.0029952	0.0049461	0.018664	0.040064
0.0044	0.00094681	0.0021819	0.013844	0.026088
0.0088	0.0022782	0.0028157	0.013723	0.031589
0.018	0.0031707	0.0045391	0.0093764	0.017972
0.035	0.0048464	0.0064522	0.0089691	0.017256
0.071	0.0074643	0.008942	0.014837	0.02592

B Contrast increment thresholds for subject HR at 1 c/deg with A=64 square cycles.

C_p	C_n=0	C_n=0.038	C_n=0.15	C_n=0.3
0	0.0017959	0.0036495	0.011416	0.026529
0.0044	0.00088384	0.0016532	0.0063733	0.022791
0.0088	0.0017823	0.00279	0.0085234	0.021049
0.018	0.0031016	0.0044119	0.0049333	0.01566
0.035	0.0037355	0.0064221	0.0065665	0.013149
0.071	0.0090731	0.0081032	0.011840	0.012468

C Contrast increment thresholds for subject HR at 1 c/deg with A=256 square cycles.

C_p	C_n=0	C_n=0.038	C_n=0.15	C_n=0.3
0	0.0018919	0.0022249	0.01088	0.023162
0.0044	0.0012989	0.0024447	0.0070090	0.015454
0.0088	0.0020010	0.0019484	0.003765	0.011151
0.018	0.0030079	0.0055381	0.0028338	0.012323
0.035	0.0045368	0.0080095	0.010075	0.0090082
0.071	0.0094140	0.010354	0.013622	0.015858

Figures 5.6 and 5.9

A Contrast increment thresholds for subject KT at 4 c/deg with A=1 square cycle.

C_p	C_n=0.019	C_n=0.038	C_n=0.075	C_n=0.15	C_n=0.3
0	0.013250	0.014206	0.020143	0.033622	0.071884
0.0044	0.010161	0.010891	0.018111	0.042073	0.067069
0.0088	0.0086508	0.013680	0.015724	0.024547	0.062227
0.018	0.0058038	0.0082346	0.014031	0.027311	0.059576
0.035	0.0057566	0.009193	0.011263	0.030509	0.055339
0.071	0.0013243	0.011753	0.01663	0.024140	0.053682

B Contrast increment thresholds for subject KT at 4 c/deg with A=16 square cycles.

C_p	C_n=0.019	C_n=0.038	C_n=0.075	C_n=0.15	C_n=0.3
0	0.0038783	0.0055933	0.0072980	0.017475	0.031236
0.0044	0.0016892	0.0026394	0.0059047	0.014156	0.023517
0.0088	0.0019316	0.0030015	0.0046154	0.010796	0.019991
0.018	0.00 34951	0.0040102	0.0048713	0.0077414	0.018989
0.035	0.0039096	0.0039462	0.0064906	0.0075308	0.015563
0.071	0.01016	0.0079625	0.0087355	0.012433	0.019449

C Contrast increment thresholds for subject KT at 4 c/deg with A=256 square cycles.

C_p	C_n=0.019	C_n=0.038	C_n=0.075	C_n=0.15	C_n=0.3
0	0.0018405	0.0023622	0.0048923	0.0061641	0.015132
0.0044	0.00080138	0.0016798	0.0017717	0.0046333	0.0086687
0.0088	0.0017961	0.0015572	0.0017106	0.0029755	0.0065418
0.018	0.0029205	0.0027659	0.0030848	0.0034921	0.0053017
0.035	0.0035517	0.0051893	0.0064041	0.0058634	0.0080358
0.071	0.0096491	0.008187	0.010628	0.0095479	0.014447

Figures 5.11 and 5.14

A Contrast increment thresholds for subject SU at 2 c/deg with A=16 square cycles.

C_p	2513 td	157 td	9.8 td	0.6 td
0	0.0067025	0.0071024	0.023812	0.16749
0.018	0.0035678	0.0044074	0.087432	0.11293
0.035	0.0070645	0.0076056	0.0097466	0.20515
0.071	0.011590	0.012233	0.011623	0.055439
0.14	0.016382	0.014463	0.024024	0.032283
0.28	0.017259	0.019896	0.026356	0.039601

B Contrast increment thresholds for subject TK at 2 c/deg with A=256 square cycles.

C_p	2513 td	157 td	9.8 td	0.6 td
0	0.00 20980	0.0050232	0.012830	0.049108
0.0011	0.0011121	-	-	-
0.0022	0.0011190	-	-	-
0.0088	0.0016336	0.0017125	0.007218	0.035924
0.018	0.0050960	0.0034505	0.0055220	0.036234
0.035	0.0069437	0.0061702	0.0068167	0.030383
0.071	0.012508	0.01211	0.013586	0.018586
0.14	0.018687	0.0 31223	0.027891	0.025349
0.28	0.03247	0.036838	0.031096	0.057963

Figures 5.12 and 5.15

A Contrast increment thresholds for subject KT at 8 c/deg with A=1 square cycle.

C_p	2513 td	628 td	157 td	39.3 td	9.8 td
0	0.045911	0.061358	0.11034	0.19869	0.35087
0.018	0.03282	0.046493	0.093842	0.19655	0.34144
0.035	0.02448	0.038395	0.0700535	0.16292	0.35995
0.071	0.019962	0.024458	0.075213	0.17439	0.32149
0.14	0.028592	0.019557	0.037421	0.090948	0.27288
0.28	0.051539	0.054694	0.053455	0.055719	0.16750

B Contrast increment thresholds for subject KT at 8 c/deg with A=4 square cycles.

C_p	2513 td	628 td	157 td	39.3 td	9.8 td
0	0.025337	0.032897	0.061116	0.095105	0.21892
0.018	0.013259	0.020483	0.043753	0.083205	0.21278
0.035	0.0085324	0.012948	0.028397	0.087085	0.18793
0.071	0.01213	0.014257	0.017850	0.044103	0.16312
0.14	0.024601	0.030398	0.042373	0.047629	0.0 91243
0.28	0.031012	0.029991	0.037159	0.04765	0.086343

C Contrast increment thresholds for subject KT at 8 c/deg with A=16 square cycles.

C_p	2513 td	628 td	157 td	39.3 td	9.8 td
0	0.012405	0.019004	0.03203	0.052107	0.12222
0.018	0.0043426	0.0078342	0.01971	0.040161	0.091996
0.035	0.0066209	0.0068574	0.0075382	0.029533	0.082566
0.071	0.010049	0.012772	0.018393	0.028586	0.065309
0.14	0.020135	0.018822	0.018049	0.019206	0.057498
0.28	0.030214	0.026931	0.028741	0.032365	0.047247

D Contrast increment thresholds for subject KT at 8 c/deg with A=64 square cycles.

C_p	2513 td	628 td	157 td	39.3 td	9.8 td
0	0.0095015	0.013169	0.022450	0.045336	0.073266
0.018	0.0035185	0.0050617	0.0074837	0.020799	0.051669
0.035	0.0063672	0.0069297	0.010706	0.015354	0.051780
0.071	0.011366	0.0079463	0.013469	0.014584	0.045266
0.14	0.011414	0.017646	0.015461	0.018646	0.029048
0.28	0.019975	0.021543	0.030341	0.026430	0.054973

E Contrast increment thresholds for subject KT at 8 c/deg with A=256 square cycles.

C_p	2513 td	628 td	157 td	39.3 td	9.8 td
0	0.0059277	0.0078449	0.013217	0.025504	0.051502
0.018	0.0037406	0.0038735	0.0065388	0.0 12320	0.048437
0.035	0.0061654	0.0047280	0.0060228	0.0089315	0.034856
0.071	0.012124	0.01339	0.011226	0.010004	0.017482
0.14	0.023324	0.012594	0.015813	0.013911	0.018387
0.28	0.019447	0.025411	0.021893	0.032085	0.056179